DYNAMIC PROPERTIES
OF AN UNDISTURBED CLAY
FROM RESONANT COLUMN TESTS

By

DAN ZAVORAL

B.A.Sc., University of British Columbia, 1988

A THESIS SUBMITTED IN PARTIAL FULFILLMENT OF
THE REQUIREMENTS FOR THE DEGREE OF
MASTER OF APPLIED SCIENCE

in

THE FACULTY OF GRADUATE STUDIES
DEPARTMENT OF CIVIL ENGINEERING

We accept this thesis as conforming
to the required standard

THE UNIVERSITY OF BRITISH COLUMBIA

December, 1990

In presenting this thesis in partial fulfilment of the requirements for an advanced degree at the University of British Columbia, I agree that the Library shall make it freely available for reference and study. I further agree that permission for extensive copying of this thesis for scholarly purposes may be granted by the head of my department or by his or her representatives. It is understood that copying or publication of this thesis for financial gain shall not be allowed without my written permission.

Department of CIVIL ENGINEERING

The University of British Columbia
Vancouver, Canada

Date December 28, 1990

DE-6 (2/88)

ABSTRACT

The dynamic properties of clay deposits under seismic or wave loading conditions must be well understood to assure dynamic stability of structures founded on such soil. The dynamic shear modulus and damping appear to be a complex function of many variables, and a wide range of values have been reported in the literature. Consequently, considerable uncertainty exists in choosing the appropriate values of shear modulus and damping for a particular problem.

This thesis presents a study of the influence of various factors on the shear modulus and damping of a marine clay using a resonant column/torsional shear device. In particular, the influence of factors such as shear strain amplitude, effective confining stress, stress history, frequency (strain rate), and secondary time-dependent behaviour are examined. The pore pressure response is also studied.

The shear modulus was found to degrade for shear strains above 0.005%. The strain dependency was found to be well represented by a single normalized modulus reduction curve regardless of the confining pressure or overconsolidation ratio. Slower strain rates resulted in smaller values of shear modulus.

Of the variables studied, the duration of sample confinement was found to be the most imporant factor affecting the material damping. Above 0.005% strain, the damping of the marine clay increased with shearing strain amplitude. No significant effect of confining pressure and stress history on damping was observed at any strain level. As well, the material damping was found to be relatively independent of loading frequency.

Both the shear wave velocity and damping obtained in this study were found to be consistent with the in situ values determined using the seismic cone penetration test.

TABLE OF CONTENTS

LIST OF FIGURES

LIST OF FIGURES (CONT.)

LIST OF FIGURES (CONT.)

LIST OF FIGURES (CONT.)

LIST OF FIGURES (CONT.)

LIST OF TABLES

ACKNOWLEDGEMENTS

I wish to express gratitude to my supervisor, Professor R.G. Campanella, for giving me the opportunity to work on this research under his guidance. His advice and encouragement throughout this project are greatly appreciated.

I would like to thank John Sully for his valuable insight and suggestions during the course of this work. Thanks are also due to the technical staff in the Department of Civil Engineering who maintained and modified tha equipment used in this research.

The comments and suggestions of Professor P. Byrne in reviewing this thesis were most usefull and welcome.

1. INTRODUCTION

1.1 PURPOSE

It is generally recognized that local soil characteristics affect the ground response when seismic waves propogate through a soil profile. Advances in earthquake ground response analyses have greatly surpassed the knowledge of the basic dynamic soil properties which are required in order to correctly predict the actual ground response.

In the 1985 Mexico City earthquake, areas underlain by soft Mexico City clay greatly amplified the ground motions causing severe damage (Sun et al., 1988). The low shear modulus and damping values associated with Mexico city clay were key factors in producing the large ground motion amplifications. More knowledge is required of the dynamic properties of undisturbed soft clays and the factors affecting them. This thesis examines the dynamic characteristics of a soft clay near Vancouver, B.C. - an area susceptible to large magnitude earthquakes.

This research addresses the complex effect of various factors upon the shear modulus and damping of an undisturbed clay, including: the effect of shear strain amplitude;

effective confining stress; stress history; frequency (strain rate); and secondary time-dependent behaviour.

To perform these studies a resonant column device was used and later modified in order to perform torsional shear tests on the same sample. The clay used in this research was obtained from the Lower 232nd Street University of British Columbia in situ research site along the Trans-Canada Highway about 40 km east of downtown Vancouver.

1.2 ORGANIZATION

A brief literature review emphasizing the effects of various factors on the shear modulus and damping for cohesive soils is given in Chapter 2.

The resonant column/torsional shear apparatus is described in Chapter 3 and the method of analysis for both types of tests is given in Chapter 4.

Chapter 5 describes the research site, the geotechnical aspects of the soil deposit, and the sampling methods used. In Chapter 6 testing procedure considerations are discussed while the test results themselves are presented in Chapters 7 and 8.

Lastly, Chapter 9 compares the shear modulus and damping obtained in the laboratory with the in situ values as determined from the seismic cone penetration test.

2. LITERATURE REVIEW: DYNAMIC PROPERTIES OF COHESIVE SOILS

Several researchers have published comprehensive reports on dynamic soil properties of cohesive soils (Sun at al., 1988; Kokusho et al., 1982; Hardin and Drnevich, 1972a and 1972b). This chapter reviews their main findings and outlines the key factors affecting dynamic shear modulus and damping of cohesive soils.

2.1 SHEAR MODULUS

Hardin and Black (1968) concluded that shear modulus of soils is a function of:

i/ effective octahedral normal stress
ii/ ambient stress and vibration history
iii/ degree of saturation
iv/ deviatoric component of ambient stress
v/ grain characteristics and mineralogy
vi/ amplitude of vibration
vii/ frequency of vibration
viii/ secondary time effects (aging) and magnitude of load increment
ix/ soil structure, and
x/ temperature.

For sands, the modulus at small strains (10^{-3}% or less) is primarily a function of void ratio and effective confining stress, with an additional small aging effect. For clays, the findings are similar except that secondary time effects (aging) and clay mineralogy also appear to be important. The significant factors affecting the shear modulus of cohesive soils are reviewed in the following sections.

2.1.1 Effect of Shear Strain Amplitude

It is clear that the shear modulus of soils reduces rapidly with increasing strain amplitude as indicated by Fig. 2.1. The modulus versus strain amplitude curves are commonly expressed by a normalized modulus reduction curve in which modulus values at any strain are normalized by the small strain modulus, G_{max} or G_o. The value of G_{max} is approximately constant for strains below the order of 10^{-3} percent where the deformations are linear elastic and recoverable. For higher strains from about 10^{-2}-1%, the soil behaviour becomes nonlinear elasto-plastic and results in irrecoverable permanent deformations. Indeed, the shear modulus at 0.5% strain is typically only one tenth of the initial small strain shear modulus.

Unlike the modulus reduction curves for sands which show a relatively small variation from one sand to another, the

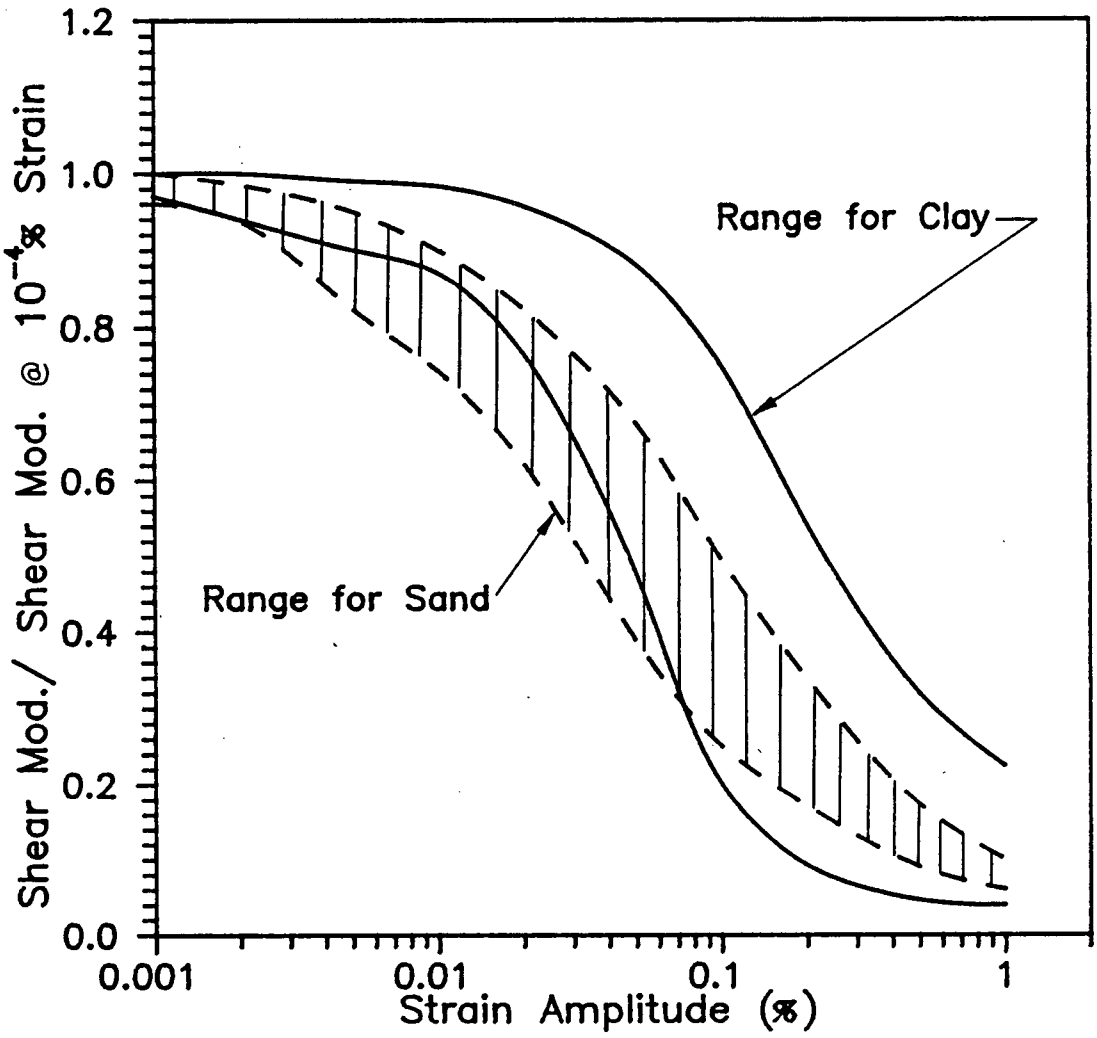

Fig. 2.1 Normalized Modulus Reduction Curves for Sands and Clays

modulus reduction curves for cohesive soils have a much larger scatter (Fig. 2.1). Therefore, certain factors affecting shear modulus - strain relationships for clays must be considered to obtain a more usable modulus reduction relationship.

Kokusho et al. (1982) and Sun et al. (1988) reported that plasticity index, an indirect measure of clay mineralogy, has a marked influence on the form of the normalized modulus reduction curves (Fig. 2.2). Higher plasticity clays show a slower rate of modulus reduction as well as a gradual shift of the curve to the right.

2.1.2 Effect of Void Ratio

It is not possible to independently vary both the void ratio and confining pressure for normally consolidated samples. Hence, it is difficult to separately determine the effect of these two parameters on the small-strain shear modulus. However, a linear variation of shear wave velocity with void ratio enables the void ratio effect to be examined (Hardin and Richart, 1963). This observation allowed Hardin and Black (1968) to show that a void ratio factor, F(e), can be used in an equation of the form

$$G_{max} = K*F(e)(P_a)^{1-n}(\sigma_{3C}')^{n} \qquad (2.1)$$

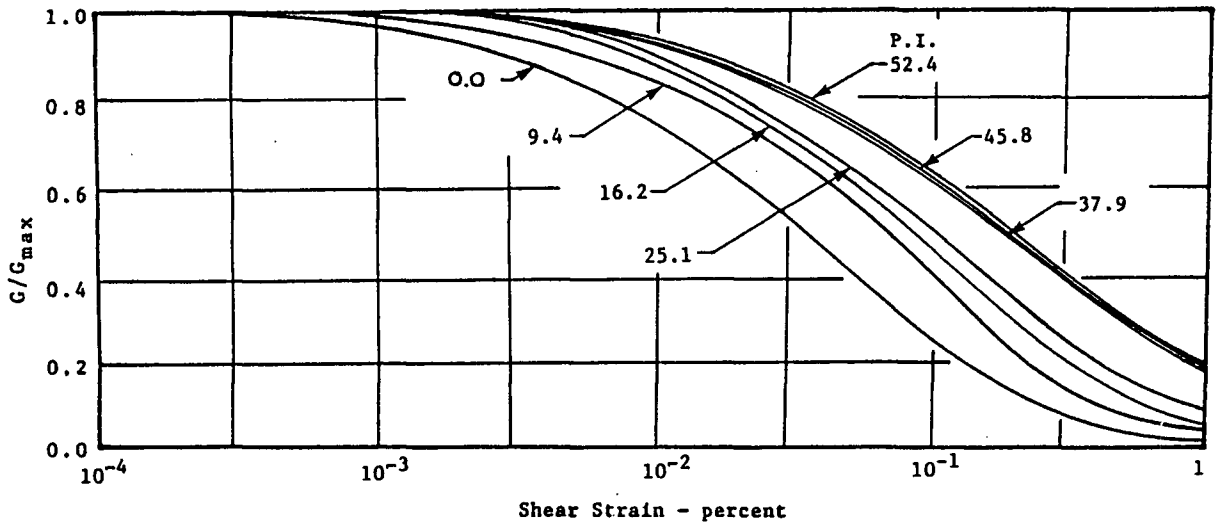

Fig. 2.2 Effect of Plasticity Index (PI) on Normalized Modulus Reduction Curves of Cohesive Soils (from Zen et al., 1978)

in which K is a dimensionless constant, σ_{3c}' is the effective isotropic confining pressure in the same units as the atmospheric pressure (P_a) and G_{max}, and in which the void ratio factor is

$$F(e) = (2.973 - e)^2/(1 + e) \qquad (2.2)$$

Although widely used, Equation 2.2 is based on tests on laboratory-prepared kaolinite and been found to be applicable only for low plasticity clays or relatively stiff clays with void ratio smaller than 1.5 (Ishihara, 1982).

For clays with high plasticity index, Marcuson and Wahls (1972) defined the void ratio factor as

$$F(e) = (4.4 - e)^2/(1 + e) \qquad (2.3)$$

Undisturbed alluvial clay samples are more compressible than laboratory samples on which Eqns. 2.2 and 2.3 are based. To evaluate such soils, Kokusho et al. (1982) performed tests on undisturbed samples of soft alluvial clay from Teganuma, Japan, and proposed the following formula:

$$F(e) = (7.32 - e)^2/(1 + e) \qquad (2.4)$$

Equation 2.4 is based on tests using laboratory-prepared bentonite clay in which time and overconsolidation effects were

not eliminated. It applies to clays with void ratios between 1.5 and 2.5. The PI of this clay varied from 40 to 100 and the void ratio values ranged from 1.5 to 4.0.

Equations 2.2, 2.3, and 2.4 are all of the same form. The different constants in each of the equations are derived from a regression analysis of the respective data sets which also provides the value of K in Eq. 2.1. These equations are plotted in Fig. 2.3 for three different confining pressures. The above three formulae give approximately the same shear modulus for void ratios of about 1.5 but otherwise large differences exist. Considerable judgement is therefore required in choosing the appropriate void ratio relationship.

2.1.3 Effect of Confining Stress

Increased confining stress results in higher shear modulus. For equations employing a void ratio factor as in Eq. 2.1, the modulus exponent, n, for a variety of clays ranges from 0.5 to 0.6 (Kokusho et al., 1982, Marcuson and Wahls, 1978, Hardin and Black, 1968). To overcome the uncertainty in choosing the correct void ratio factor, shear modulus is often simply reported as

$$G_{max} = K(P_a)^{1-n}(\sigma_{3C}')^{n} \qquad (2.5)$$

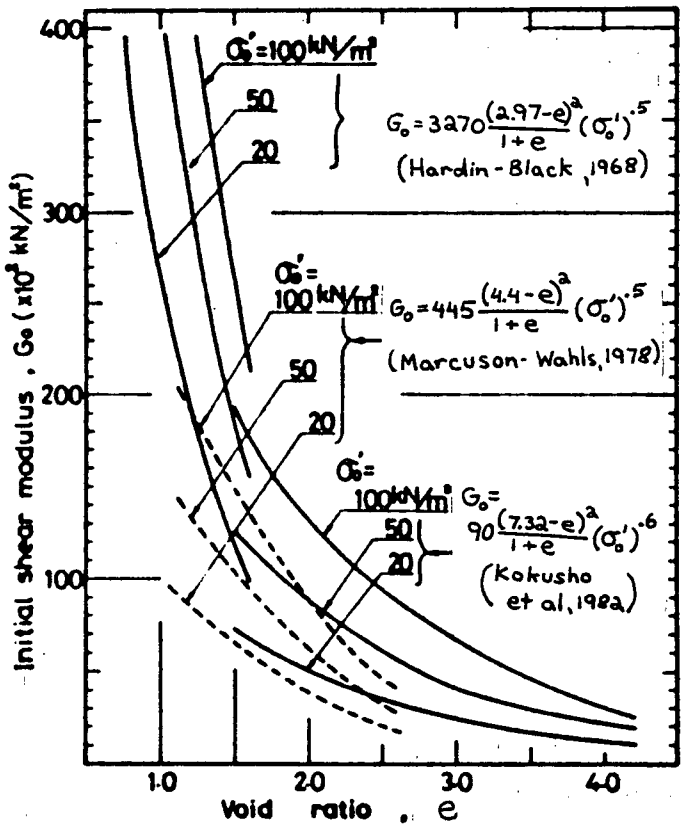

Fig. 2.3 Comparison of Three Experimental Formulas on Modulus vs. Void Ratio Diagram (from Ishihara, 1982)

in which K and n vary according to the type of clay. An equation of the form of Eq. 2.5 may be convenient when the void ratio of the clay is not accurately known. However, both the modulus multiplier (K) and the modulus exponent (n) vary with clay type.

Weiler (1988) gathered data found in the literature on shear modulus-confining pressure relationships for normally consolidated, naturally-deposited clays. The shear modulus-confining pressure equations for the respective data sets are presented in table and graph form in Fig. 2.4. Also included in Fig. 2.4 is the shear modulus-confining pressure relationship for Teganuma Clay (Kokusho et al., 1982).

It appears that the modulus multiplier values shown in Fig. 2.1 decrease with increasing plasticity index, while the modulus exponent values increase. This is intuitively satisfying since a more plastic clay would be expected to be softer (lower modulus) than a lean clay, and should therefore have a lower modulus multiplier. Since a higher plasticity clay generally undergoes a more rapid void ratio reduction with increasing confining pressure (higher compressibility), the shear modulus increase (modulus exponent) would be expected to be greater. The modulus exponent values for all natural clays reported in the literature fall in the range 0.8-1.2. The range in shear modulus values for the various clays shown in Fig. 2.4 is almost an order of magnitude. However, the trend

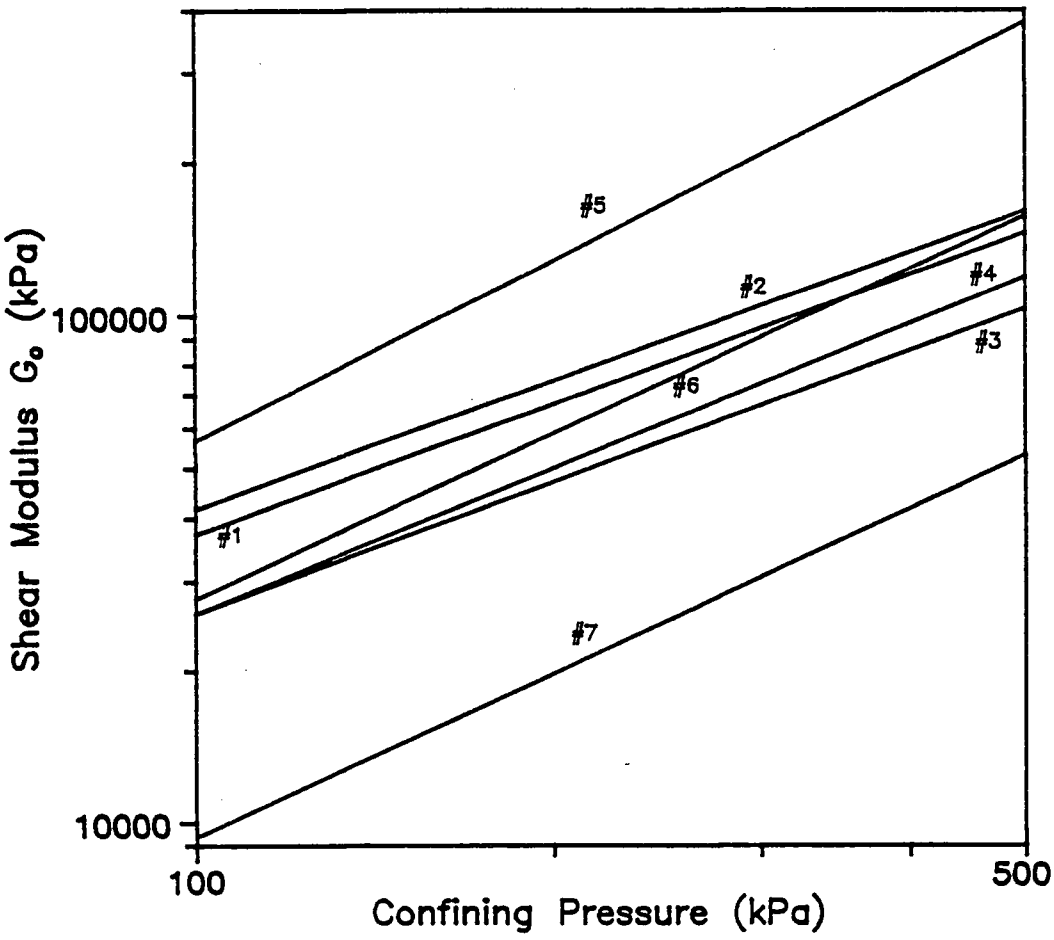

#	CLAY	PI	G_{max}	REFERENCE
1	Gulf of Alaska	14-15	$372.1P_a^{.15}(\sigma_{3C}')^{.85}OCR^{.59}$	Weiler (1988)
2	AGS CL Clay	16-22	$436.3P_a^{.16}(\sigma_{3C}')^{.84}OCR^{.27}$	"
3	Boston Blue Clay	19-23	$248.2P_a^{.14}(\sigma_{3C}')^{.86}OCR^{.60}$	"
4	San Fran. Bay Mud	43	$164.6P_a^{.05}(\sigma_{3C}')^{.95}OCR^{.51}$	"
5	AGS CH Clay	32-38	$126.2P_a^{-.18}(\sigma_{3C}')^{1.18}OCR^{.69}$	"
6	Leda Clay	37-44	$97.4P_a^{-.08}(\sigma_{3C}')^{1.08}OCR^{.69}$	"
7	Teganuma Clay	40-103	$53.6P_a^{-.08}(\sigma_{3C}')^{1.08}OCR^{.59}$	Kokusho et al (1982)

Fig. 2.4 Small Strain Shear Modulus Equations for Seven Naturally Deposited Clays

in the curves is predictable based on the plasticity index of the clay as suggested by the table in Fig. 2.4.

2.1.4 Consolidation Stress History

The effect of overconsolidation on the small strain shear modulus of naturally deposited cohesive soils is to increase the modulus as compared to the normally consolidated condition. The shear modulus increase due to stress history is often expressed by an overconsolidation ratio (OCR) term incorporated into Eq. 2.5 such that

$$G_{max} = K(P_a)^{1-n}(\sigma_{3C}')^{n}OCR^{m} \qquad (2.6)$$

The table in Fig. 2.4 presents equations of this form for six natural clays. The influence of OCR on small-strain shear modulus for five of the clays examined by Weiler (1988) is illustrated in Fig. 2.5. The slope of this plot (m) is the OCR exponent. Almost all of the data falls within a range of m of 0.3 to 0.7, with an average of about 0.6. Although there is some variation between the various clays, no trend of OCR exponent with clay plasticity is evident.

However, if an equation employing the void ratio factor is used, then

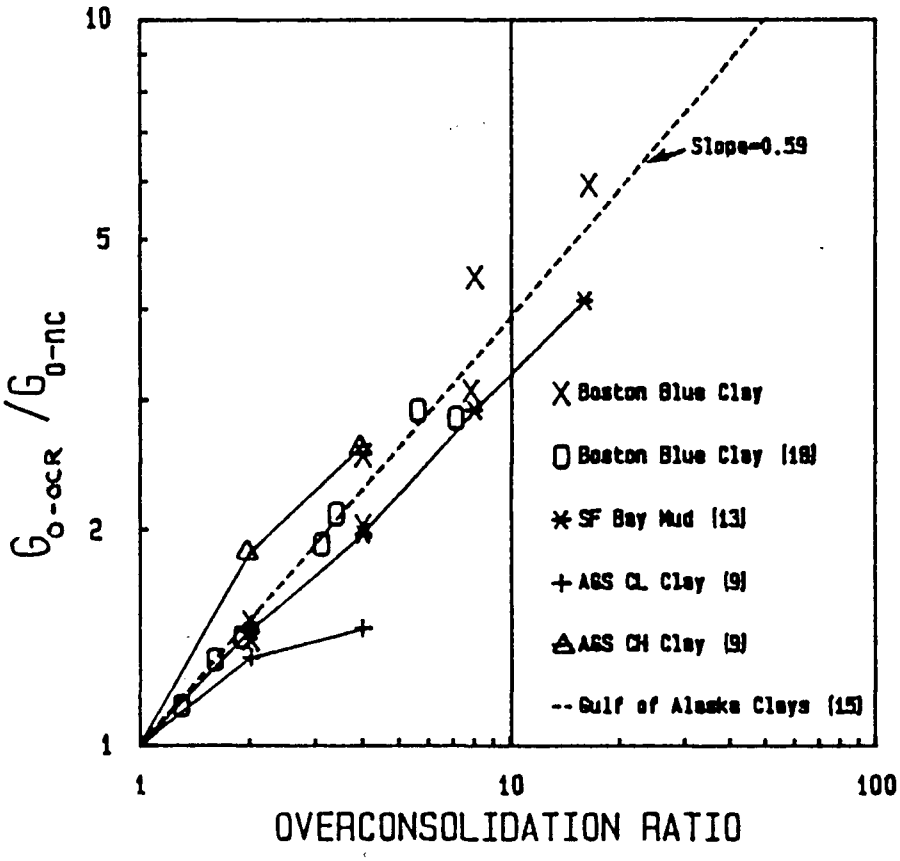

Fig. 2.5 Effect of Overconsolidation Ratio on the Small Strain Shear Modulus of Five Naturally Deposited Clays (from Weiler, 1988)

$$G_{max} = K*F(e)(P_a)^{1-n}(\sigma_{3C}')^{n}OCR^{k} \qquad (2.7)$$

and k varies with plasticity index (PI) as shown in Table 2.1.

2.1.5 Frequency Effect

Aggour et al. (1987) applied random vibrations with varying cut-off frequencies to study the effect of loading frequency on the shear modulus reduction curves for cohesive soils. From these tests, it was found that random loading with different frequency content affects the shear modulus reduction curve (Fig. 2.6). The soil modili in the case of random loading were found to increase with higher frequency content and were lower than the moduli obtained from sinusoidal testing. The differences increased with increasing strain amplitude. However, the different frequency cut-off values are higher than the frequencies in the 0.1 Hz to 30 Hz range of interest for most earthquakes (Sun et al., 1988).

2.1.6 Secondary Time Effects

Several investigators have shown that time-dependency is a significant parameter affecting the dynamic properties of soils

Table 2.1 Values of k

PI	k
0	0
20	0.18
40	0.30
60	0.41
80	0.48
>100	0.50

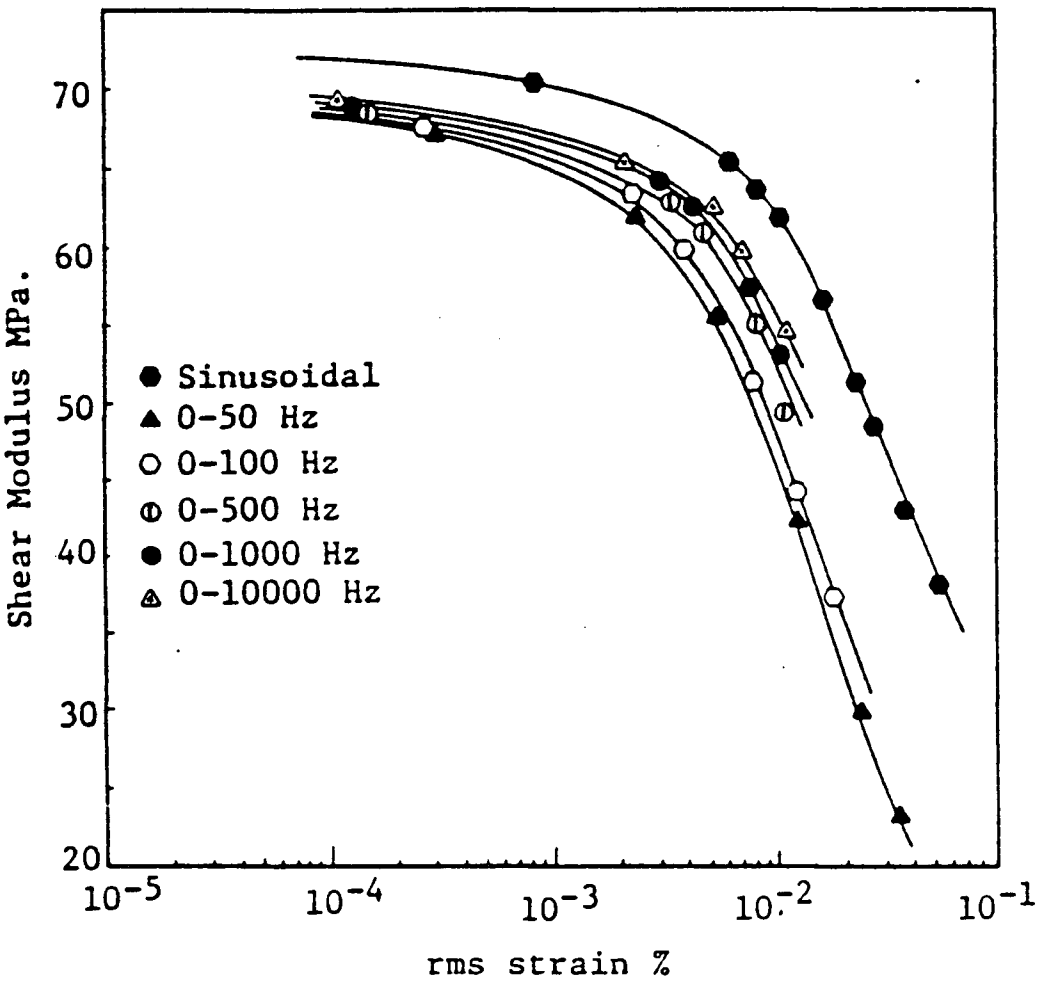

Fig. 2.6 Effect of Varying Frequency Content on the Shear Modulus vs. Strain Curves for Cohesive Soils (after Aggour et al., 1987)

(Hardin and Black, 1968; Marcusson and Wahls, 1972; Anderson and Woods, 1976; Anderson and Stokoe, 1978; Kokusho et al., 1982). The results of these investigations confirm that small strain dynamic shear moduli of both sands and clays increase with time of confinement under sustained pressures.

Results of these studies suggest that time-dependent change in shear modulus can be separated into a period of primary behaviour and a period of secondary behaviour. The primary behaviour has been shown (Fig. 2.7) to coincide with the period of primary consolidation (Kokusho et al., 1982; Anderson and Stokoe, 1978).

During the long-term time effect the values of shear modulus generally increase with the logarithm of time. Figure 2.7 indicates that this secondary increase is much larger than that predicted from the secondary decrease in void ratio estimated by Eq. 2.1. A time or thixotropic effect is therefore seen as being responsible for this behaviour.

The rate of secondary modulus increase has been quantified by the ratio $\Delta G/G_{1000}$ in which ΔG is the increase in shear modulus per logarithmic cycle of time, and G_{1000} is the modulus measured 1000 minutes after the start of primary consolidation. Generally, the rate of secondary modulus increase becomes greater with decreasing mean grain size (Afifi and Richart, 1973). However, Kokusho et al. (1982) suggest that a

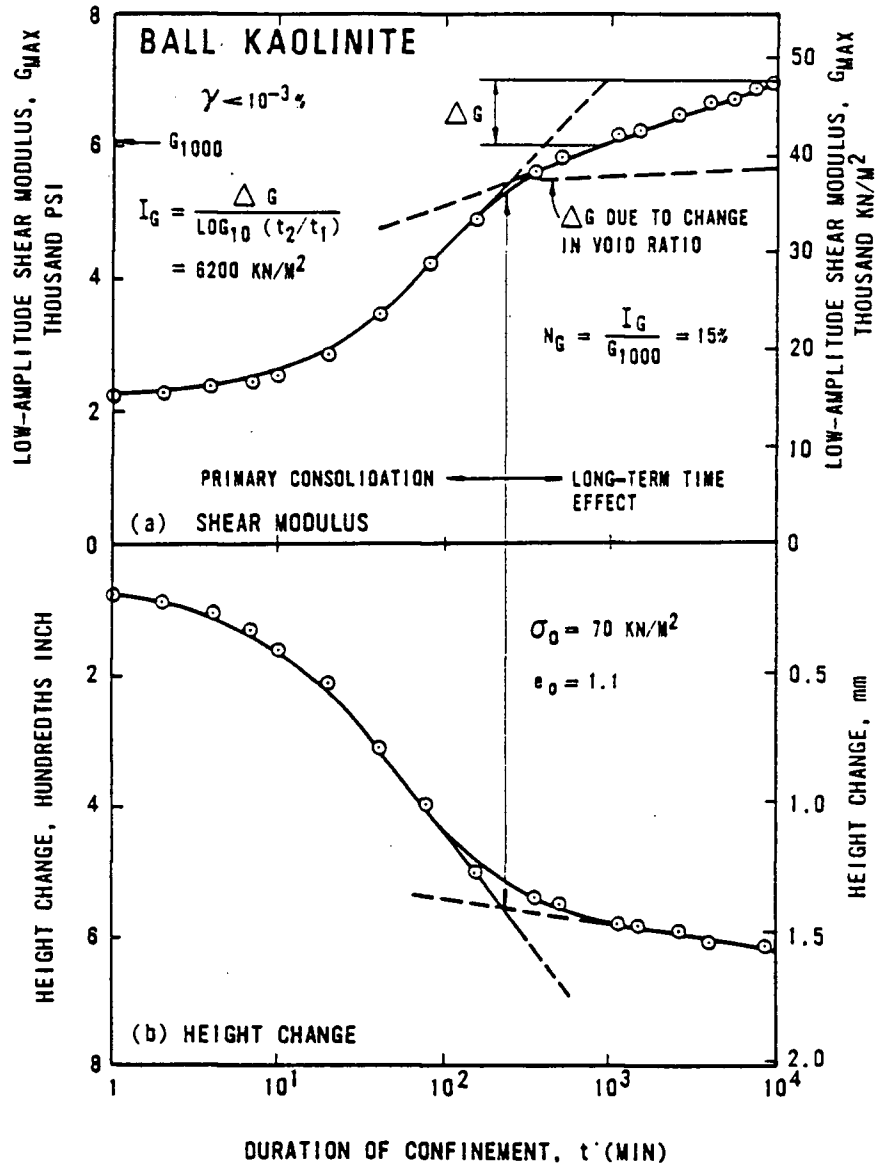

Fig. 2.7 Typical Time-Dependent Increase in Low Amplitude Shear Modulus for Clay at Constant Confining Pressure (after Anderson and Stokoe, 1978)

relationship involving plasticity index (PI) may be more logical since PI is a parameter which reflects the chemical activity of clay minerals (Fig. 2.8). The rate of secondary modulus increase becomes larger as PI increases, with values as large as 25% per log cycle of time. Clearly, time effects must be considered when conducting laboratory tests for shear modulus or when extrapolating laboratory tests to field conditions.

2.2 DAMPING RATIO

Damping exists in all vibrating systems. It serves to remove energy from the oscillating system. The energy loss can be determined from the vibrating system response. This loss in energy results in the decay in amplitude during free vibration. For steady state forced vibration, the energy loss is balanced by the energy input of the driving force.

Damping is commonly distinguished as being either viscous or hysteretic in nature. The damping is said to be viscous when the dissipated energy per cycle increases proportionally with frequency. This is the assumption in determination of damping from the amplitude decay method in the resonant column test. The damping is said to be hysteretic when the dissipated energy per cycle is independent of the frequency of loading. This is the assumption when the damping is determined from the

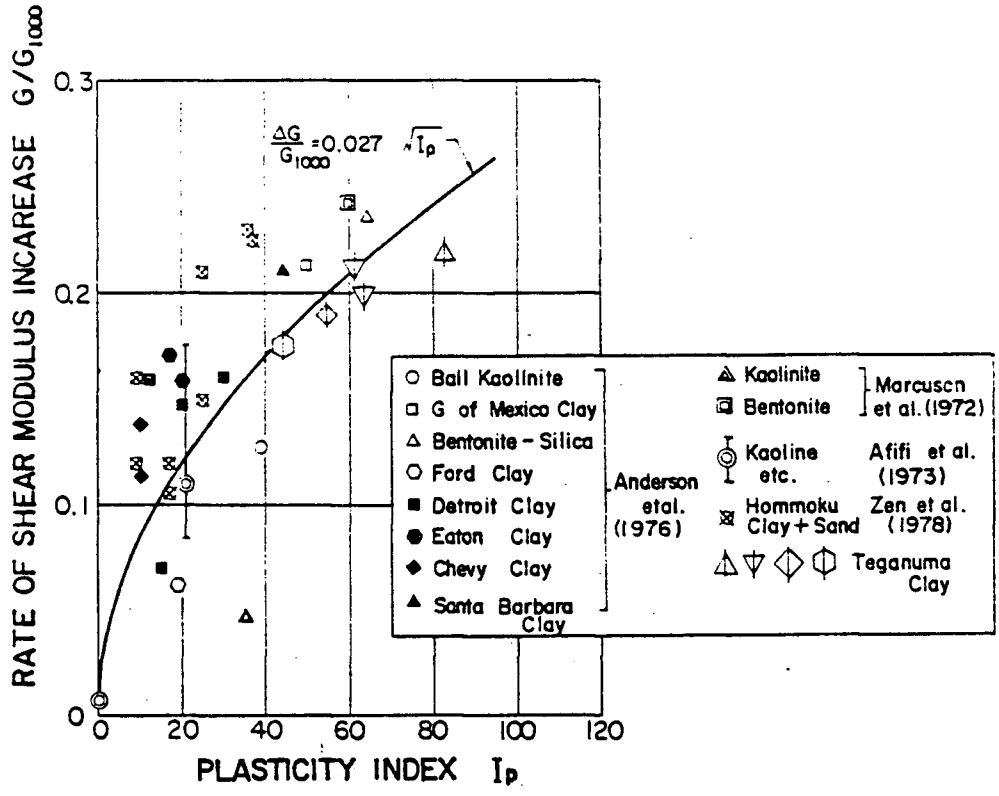

Fig. 2.8 Relationship Between Rate of Modulus Increase and Plasticity Index (from Kokusho et al., 1982)

stress strain response curves. Details on damping calculations are given in Chapter 4.

The damping of a particular soil has been found to depend primarily on:

i/ the strain amplitude of vibration
ii/ the ambient state of effective stress
iii/ vibration frequency
iv/ void ratio, and
v/ confining time

as well as other, less significant factors. These variables are essentially the same as those affecting the shear modulus (section 2.1) and are discussed in the following sections.

2.2.1 Effect of Shear Strain Amplitude

There is not an abundance of data reported in the literature on the variation of damping ratio with shear strain amplitude. The limited data suggest that the damping ratio curves for cohesive soils have a wider range than those for sands. Much of the early work during the 1960's was summarized by Seed and Idris (1970). Figure 2.9 shows the range in damping values summarized by Seed and Idris as well as the

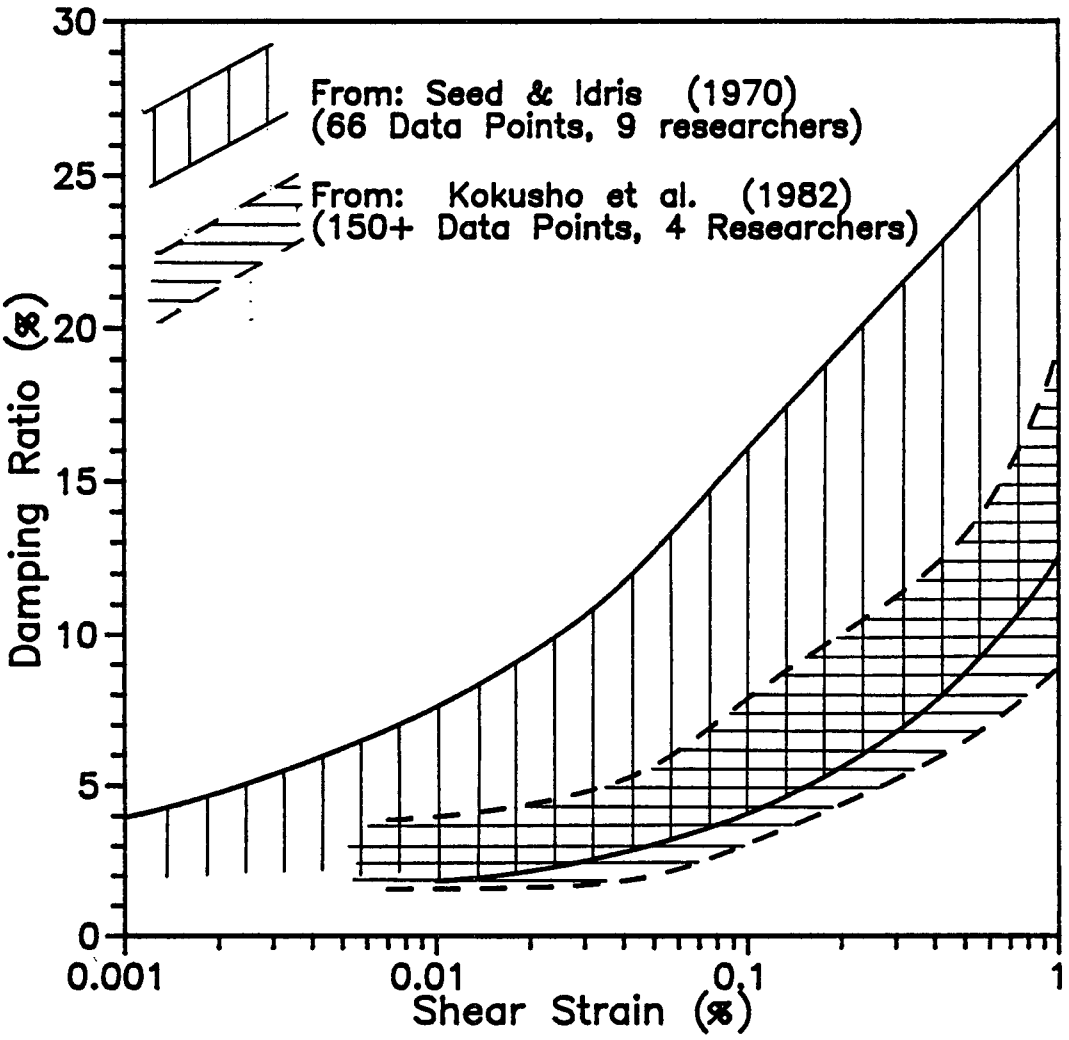

Fig. 2.9 Range of Damping Ratios vs. Shear Strain for Cohesive Soils

range in damping curves identified by Kokusho et al. (1982) from studies performed in the 1970's and early 1980's.

It is quite likely that the smaller range in damping ratio presented by Kokusho et al. (1982) reflects the improvement in dynamic testing equipment and procedures since the early studies in the 1960's. Nevertheless, it can be seen that the damping ratio for cohesive soils increases from a minimum value less than 5% at a shear strain of about 0.01% to a value greater than 8% at a shear strain of 1.0%.

It is well known that a strong correlation exists between damping ratio and shear modulus; in particular, the damping ratio decreases as shear modulus increases. Hardin and Drnevich (1972b) suggested the following simple equation to relate damping ratio (D) to shear modulus:

$$D = D_{max}(1-G/G_{max}) \qquad (2.8)$$

where D_{max} is the maximum damping at large strain.

2.2.2 Secondary Time Effects

The effect of duration of confinement of cohesive soils is to decrease the damping logarithmically as a function of time. This behaviour has been observed in laboratory-prepared clays

(Marcusson and Wahls, 1978) as well as naturally deposited clays (Kokusho et al., 1982; Hardin and Drnevich, 1972a).

Due to the relationship between damping ratio and shear modulus (Eq. 2.8), it is reasonable that the damping ratio should decrease with duration of confinement since shear modulus increases with confining time (see section 2.1.6). Unlike the two time-dependent stages of behaviour (primary and secondary) of shear modulus, a consistent linear logarithmic decrease of the damping ratio exists with no kink apparent at the completion of primary consolidation (Fig. 2.10).

The rate of damping ratio decrease has been found to be as high as 25% per logarithmic cycle of time for bentonitic clay (Marcusson and Wahls, 1978).

2.2.3 Frequency Effects

A series of random vibration tests with varying cut-off frequencies were performed by Aggour et al. (1987) to study the effect of loading frequency on dynamic properties of clay. These tests suggest that higher frequencies are associated with lower values of damping (Fig. 2.11), though the chosen cut-off frequencies were well above the frequency range of interest for most earthquakes (0.1-30 Hz). As well, the damping curve for conventional sinusoidal loading does not appear to fit this

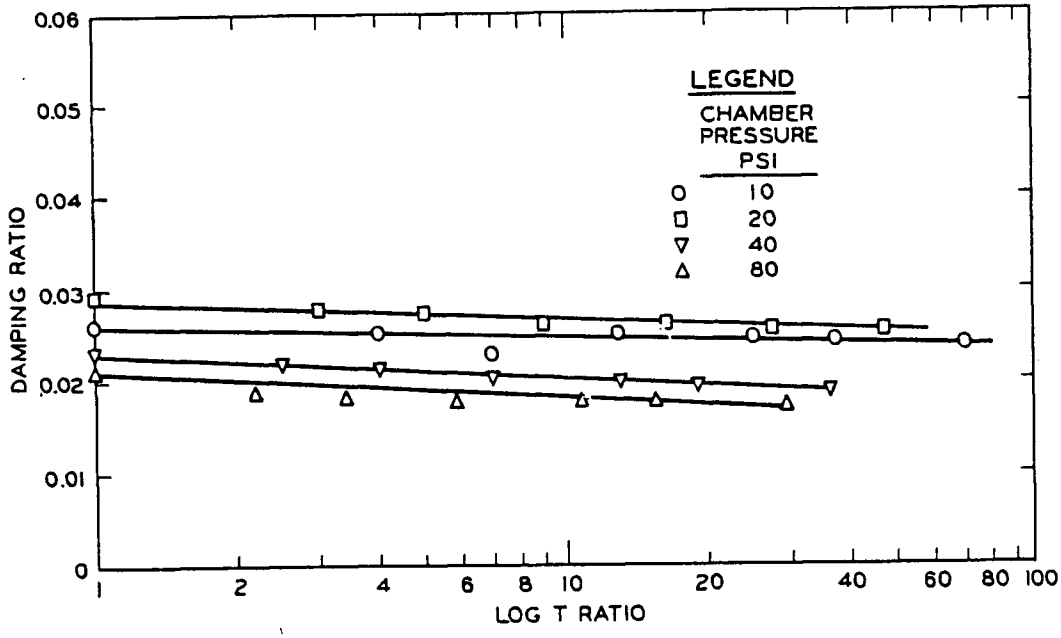

Fig. 2.10 Typical Time Dependent Decrease in Damping Ratio at Constant Effective Stress for Clay (from Marcuson and Wahls, 1978)

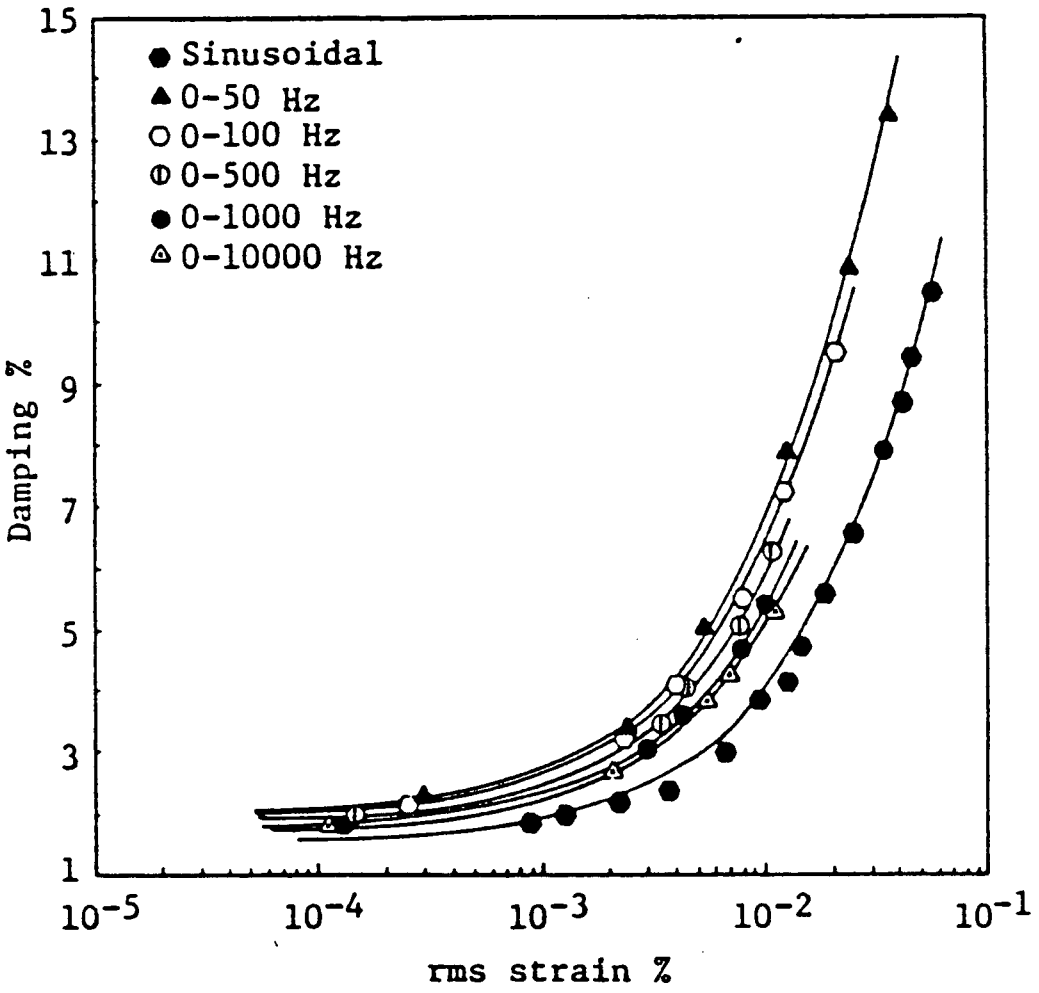

Fig. 2.11 Effect of Varying Frequency Content on the Damping vs. Strain Curves for Clay (after Aggour et al., 1987)

trend since it lies below the damping curve with the highest frequency content.

Hardin and Drnevich (1972a), in their tests on Lick Creek Silt, suggested that frequencies above 0.1 Hz have only a minor effect on damping. However, this finding requires more study since it is based on only a few data points.

2.2.4 Confining Pressure

The effect of confining pressure on damping in cohesive soils has not been conclusively established in the literature. Kokusho et al. (1982) presented data on small strain damping for clay with PI ranging from 40 to 100 which, despite large variations, appear to show only a slightly decreasing damping with increasing confining pressure (Fig. 2.12). Furthermore, the differences in the damping for OCR values up to 15 were found to be insignificant, on the average.

Hardin and Drnevich (1972b) proposed that damping decreases with the square root of confining stress, but the large variation in damping values at low strain makes their finding questionable.

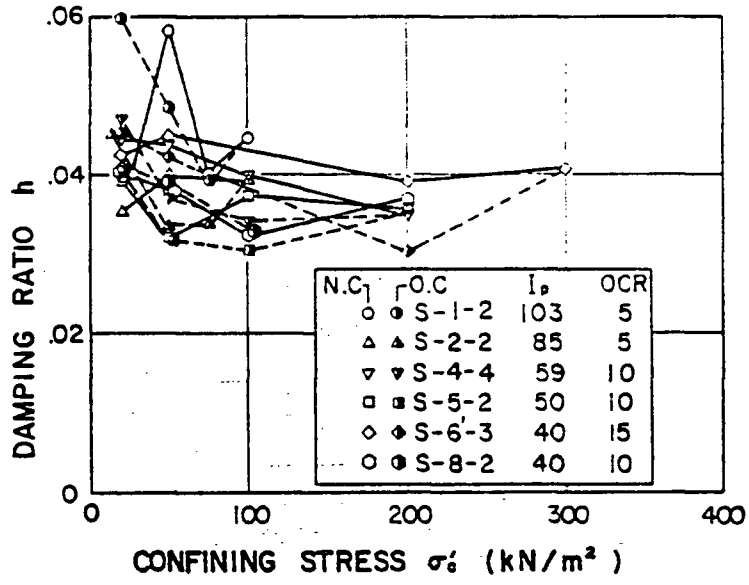

Fig. 2.12 Effect of Confining Stress, PI, and OCR on the Small Strain Damping of Clay (from Kokusho et al., 1982)

2.3 NEEDS FOR RESEARCH

It is well known that the shear strain amplitude affects both the shear modulus and damping of cohesive soils. However, since the dynamic properties appear to be a complex function of many variables, there is considerable uncertainty in choosing the correct values of shear modulus and damping for a particular problem. There is a need to establish more thoroughly the manner in which shear modulus and damping vary with factors such as confining pressure, stress history, loading frequency, and aging. The plasticity index may offer a guide since it is a reflection of the clay chemistry.

This research addresses some of the aforementioned concerns.

3. RESONANT COLUMN/TORSIONAL SHEAR APPARATUS

3.1 INTRODUCTION

The resonant column apparatus used in this study is known as a Drnevich Long-Tor Resonant Column Apparatus. It was purchased from Soil Dynamics Instruments Inc. in 1981 for use in the Graduate Soil Mechanics Laboratory at the Civil Engineering Department of UBC. The term Long-Tor denotes the capability of the apparatus to vibrate specimens in either a longitudinal or torsional mode of vibration. For this research, however, only the torsional aspect of the equipment was used since the focus of this study was primarily on shear modulus and shear damping characteristics. Young's modulus and longitudinal damping are not examined herein as they are usually of secondary importance in analyses of earthquake response.

3.2 RESONANT COLUMN APPARATUS

Several modifications were made to the apparatus in order to allow for testing of saturated samples and to enable torsional shear tests to be performed. The basic theory behind this equipment is introduced in Chapter 4.

The resonant column apparatus is bolted securely to a heavy steel base which stands 80 cm high. This is necessary to ensure that the base of the sample is relatively free of ambient vibration (Drnevich Long-Tor Resonant Column Apparatus Operating Manual, 1981). The apparatus in position for either resonant column or torsional shear testing is shown in Fig. 3.1. Except for the bottom aluminum pedestal or platen, all components are made of stainless steel.

3.2.1 Confining Chamber

The confining chamber encloses the soil sample and the mechanical components of the resonant column device so that a confining pressure can be applied to the soil sample. The chamber, which is designed for a maximum safe working pressure of 700 kPa, essentially consists of a cast acrylic tube which is secured between the bottom base plate and top chamber lid by four long stainless steel bolts. The chamber lid contains a port connecting the chamber to a regulated air pressure supply and also houses the connections which join the interior and exterior electronic component cables. The sample pedestal, which is attached to the rigid bottom chamber base plate, is designed to accommodate 3.5 cm diameter samples.

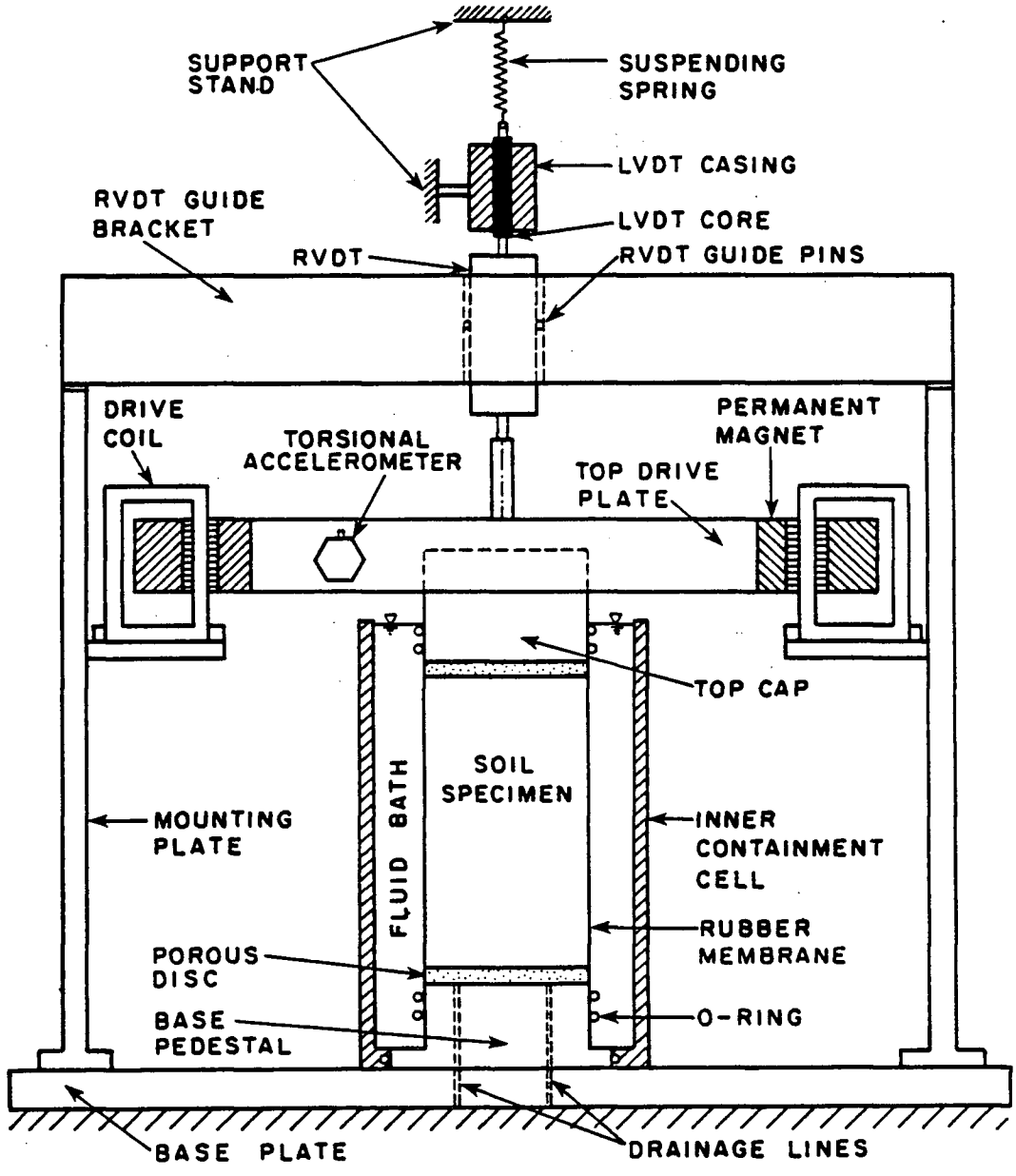

Fig. 3.1 Resonant Column/Torsional Shear Apparatus

3.2.2 Drive Mechanism

The 1.27 kg top drive platen consists of the top sample cap, four permanent magnets, one horizontally and one vertically oriented accelerometer, and a support rod which allows a vertical displacement transducer core and suspending spring to be attached. This counterbalancing spring is suspended from a bracket at the top of a support stand, and is necessary to counteract the weight of the top drive platen which would otherwise be acting as an axial force on the specimen. Isotropic confining pressures are thus maintained. During resonant testing, the top drive platen is essentially floating and able to rotate in the horizontal plane so that forced torsional excitation can be applied at the top of the specimen.

The drive mechanism consists of four drive coils which are encircled by the permanent magnets located at the four corners of the top drive platen (Fig. 3.2). This configuration is superior to that found in some other resonant column devices in that it can accommodate fairly large torsional rotations without mechanical interference between the magnets and coils. Such a configuration allows testing at a much wider range of strains (approximately .0005-2%) than is possible for some other device types. In addition, this configuration can allow for approximately a 1.5 cm decrease in sample height during consolidation or testing.

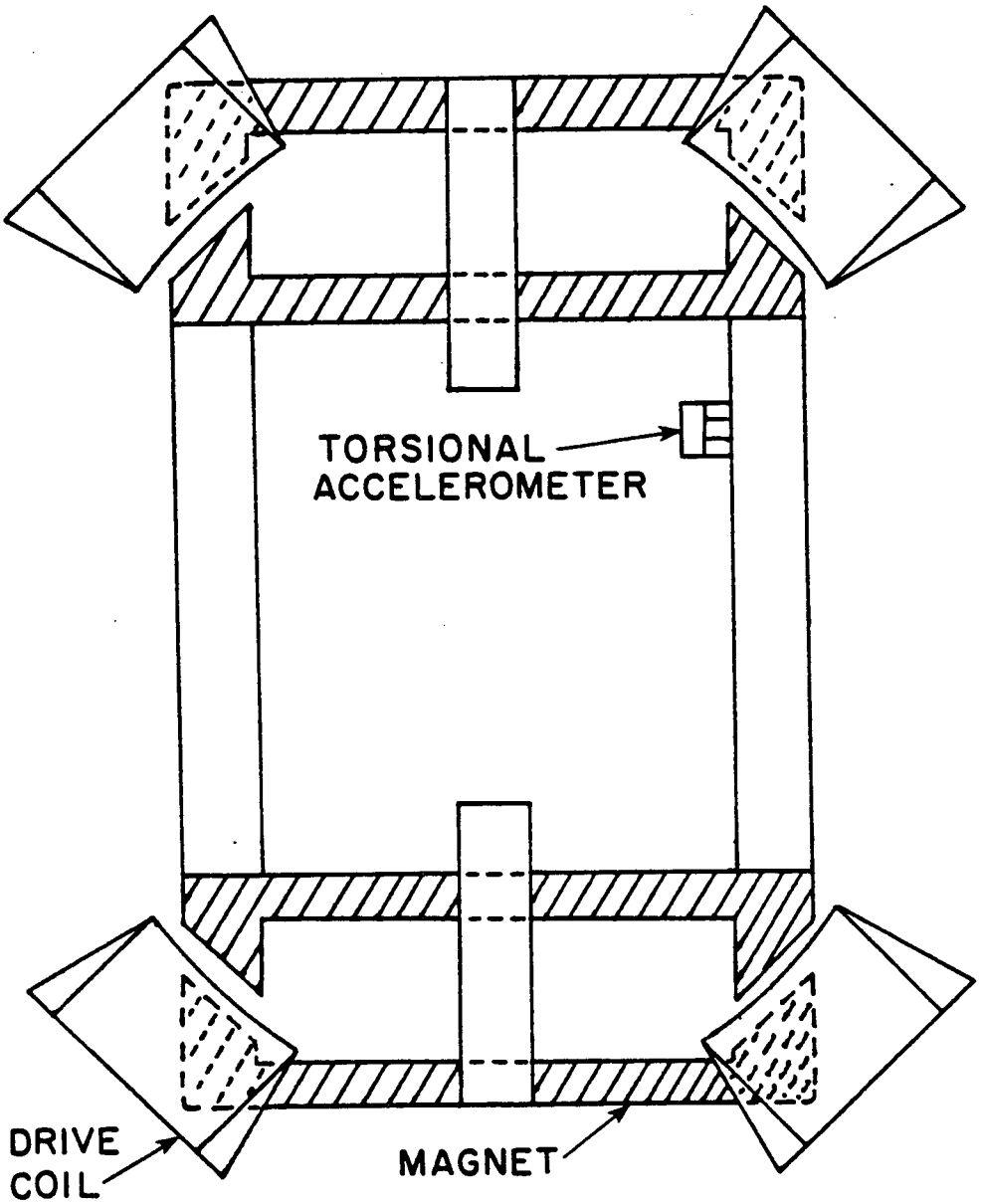

Fig. 3.2 Plan View of Resonant Column Top Drive Plate

The oscillating torsional rotation force is created by the interaction of magnetic fields; specifically, the interaction of magnetic fields generated by the sinusoidally varying drive coil input current with those caused by the permanent magnets of the drive plate.

Complete coupling between the specimen and the end platens is ensured by using bronze porous discs with embedded razorblade vanes which protrude about 1.5 mm. The discs themselves are securely attached to the top and bottom platens by means of machine screws.

3.2.3 Torsional Accelerometer

The torsional motion of the top platen is monitored by a horizontally oriented accelerometer (Columbia Research Labs, Model 200-1-H) bolted to the top platen. The accelerometer is mounted at a distance of 3.16 cm from the axis of rotation. An acceleration sensitivity range of 0.01 g-10k g is specified by the manufacturer.

3.2.4 Height-Change Measurement

Changes in specimen height during consolidation and shearing are determined using a linear variable displacement transducer (LVDT-Schaevitz 300-HR) which is mounted between the top drive plate and the suspending spring (Fig. 3.1). The LVDT coil casing is mounted on the support stand which provides a fixed reference for the relative displacements of the LVDT core.

3.2.5 Volume-Change and Pore Pressure Monitoring Equipment

Provision for drainage and pore pressure measurement is made by means of two drainage lines which connect to the bottom pedestal; no drainage is provided through the top end of the sample. The other ends of the drainage lines are attached to a volume change device which consists of several valves and a volume-calibrated pipette through which a back pressure can be applied to the sample. This is precisely the same system commonly used for triaxial tests.

Pore pressures are measured with a 150 psi capacity pore pressure transducer (Data Sensors Inc. PB519A) mounted on the volume change device.

3.2.6 Air Pressure Transducer

The confining pressures applied to the sample are measured with a 200 psi capacity air pressure transducer (Statham TP-A-1064-EX) mounted on the confining chamber lid.

3.3 RESONANT COLUMN ELECTRONIC COMPONENTS

The electronic components used for resonant column testing are described in this section, except for the pressure transducers, accelerometers, and LVDT which are described in the preceding section as part of the resonant column apparatus. A wiring schematic is shown in Fig. 3.3. The switch and control boxes enable the operator to switch between torsional and longitudinal modes of vibration as well as channelling the accelerometer output and drive coil input currents to the oscilliscope.

3.3.1 Function Generator

The sinusoidal signal which is input to the drive coils is generated by an EXACT Model 508 Function Generator. It is capable of generating a wide range of frequencies (0.001 Hz-20,000 Hz). The logarithmic frequency scanning feature proved to be convenient as it allowed for rapid location of the

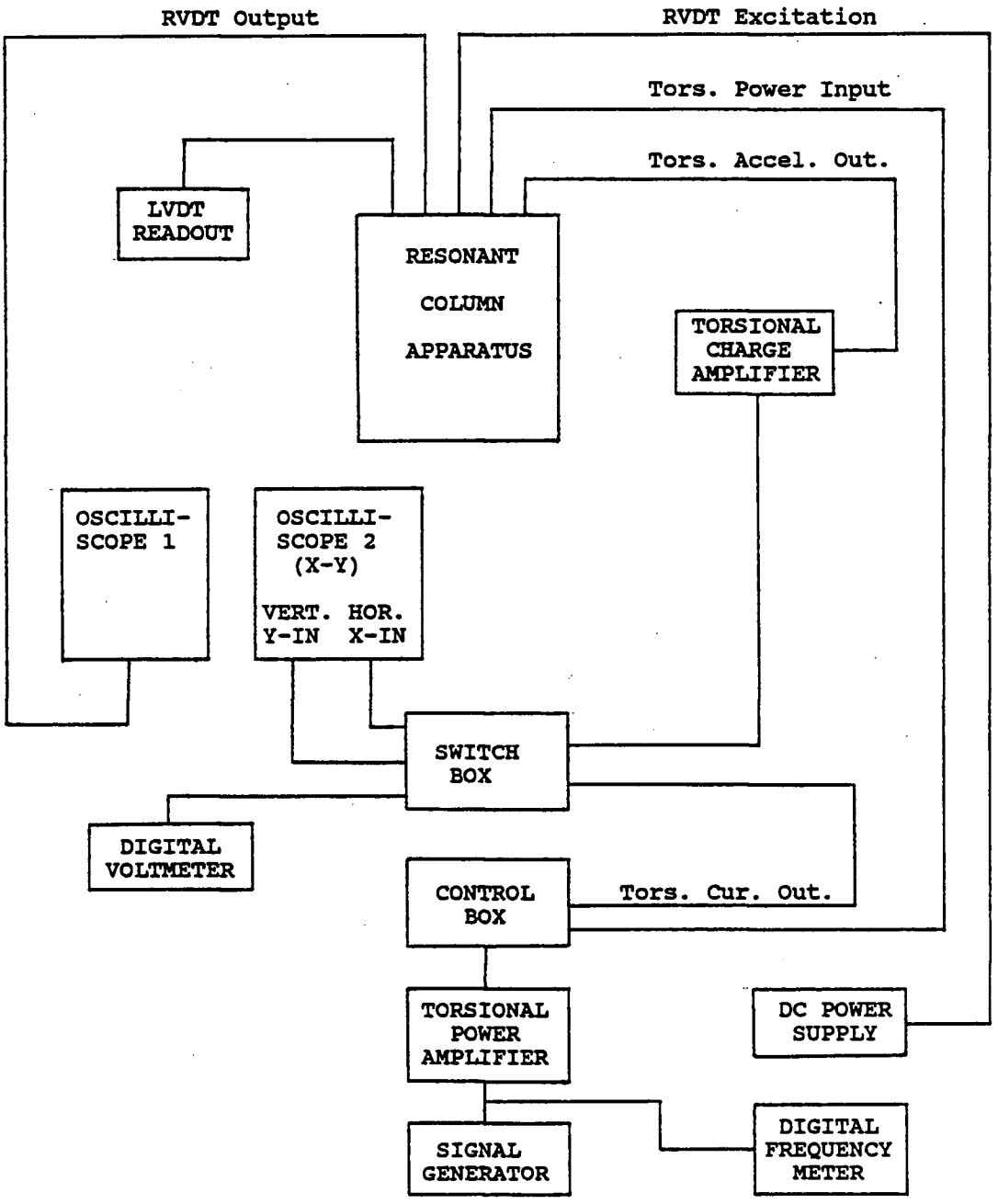

Fig. 3.3 Resonant Column/Torsional Shear Wiring Schematic

resonant frequency. For low amplitude tests, the output level of the function generator was sufficient to power the drive coils. High amplitude and torsional shear testing required an amplifier to magnify the signal to the specified amplitude.

3.3.2 Signal Amplifier

For high amplitude resonant column testing, the sinusoidal output signal from the function generator is amplified by a power amplifier (Phase Linear 300 Series Two) before being input to the drive coils. The frequency response of the amplifier is from 10Hz-190kHz necessitating the use of a different amplifier for torsional shear tests which are run at much lower frequencies.

3.3.3 Charge Amplifier

The torsional accelerometer output signal is conditioned by a charge amplifier (Columbia model 4102) prior to being measured and recorded. A transducer sensitivity control permits balancing of the amplifier to the accelerometer sensitivity.

3.3.4 Storage Oscilliscope

A two channel digital storage oscilliscope (Nicolet N 310) is used to monitor the sinusoidal drive coil input and accelerometer output. The X-Y feature of the oscilliscope provides an on-screen display of one channel as the X-ordinate and the other channel as the Y-ordinate. This yields an ellipse - known as a Lissajous figure - when both channels have sinusoidal signals. The resonant condition of the vibrating column can be readily identified because the on-screen figure rotates to a vertical position and stretches as the column comes to resonance.

The storage capability of the oscilliscope was used primarily to capture the decay in accelerometer response during free vibration from which damping was determined.

3.3.5 Frequency Counter

Resonance frequencies are read from the frequency counter (FLUKE 1900A) when the column comes to resonance - as determined from the Lissajous figure on the oscilliscope screen. The frequency counter displays frequency values to 0.1 Hz accuracy.

3.3.6 Digital Multimeter

At resonance, a digital multimeter (Fluke 8000A) is used to read the rms voltages associated with the drive coil input current and the conditioned accelerometer output current. The multimeter is also useful in checking that the maximum current capacity of the drive coils (about 1 amp) is not exceeded during high amplitude testing.

3.3.7 LVDT Readout Unit

An LVDT readout unit (Schaevitz LPM-210) converts the LVDT output signal directly into a relative displacement (millimeters) if the LVDT is zeroed prior to testing. Seperate phase and gain adjustments on the readout unit enable the unit to be calibrated.

3.3.8 Strain Indicator

The pore pressure and air pressure transducer outputs are read with a strain indicator box (Budd P-350). This device requires manual balancing with a dial in order to obtain a reading. The output readings are given in units of microstrain and must be multiplied by the respective pore pressure or air

pressure transducer calibration factors for a conversion to units of pressure.

The manual balancing procedure was simple for setting cell pressures and back pressures for consolidation. However, during high amplitude testing in which pore pressure changes can be rapid, the manual balancing and recording procedure required considerable skill since simultaneous adjustments of the input current frequency were necessary to keep the column in resonance.

3.4 TORSIONAL SIMPLE SHEAR EQUIPMENT

Torsional shear testing employed essentially the same equipment used for resonant tests (section 3.2, 3.3) although some apparatus modifications and additional electronic equipment were required. In these tests, the torsional accelerometer and charge amplifier were not required. However, since resonant column testing was always run in conjunction with the torsional shear tests, the full complement of equipment was needed. A description of the required additional equipment follows.

3.4.1 Rotary Transducer

A rotary differential displacement transducer (RVDT, Pickering & Co., Inc., Model 23384) is used for measuring rotational displacements during torsional shear tests. Since the angular acceleration during these lower-frequency tests is below the sensitivity of the torsional accelerometer, the accelerometer could not be used to calculate torsional displacements.

The RVDT has a range of motion of $\pm 10^{o}$ and a maximum non-linearity of 0.01%. By using a digital low-pass filter to eliminate high frequency noise from the recorded RVDT signal, it was found that angles as small as 0.018 degrees (typically 0.005% strain) could be accurately and repeatably measured. Calibration of the RVDT for such small rotations was done by mounting the RVDT on the axis of rotation of a highly accurate theodolite.

A special guide bracket and RVDT casing (Fig. 3.1) were needed to allow the RVDT to move down with the top platen during specimen consolidation. This was achieved by using a fixed cross-beam with a carefully machined cylindrical bore containing two vertical guide slots in which the guide pins of the RVDT casing could descend as the sample consolidated. The guide slots and pins enabled the RVDT to remain aligned with the sample axis and at the same time constrained the RVDT

casing from rotating thereby providing a fixed reference for the rotating RVDT core.

A RVDT was used instead of proximity sensors since the RVDT is able to measure a larger range of motion (0 to $\pm 10^{o}$) and does not require such a careful setup procedure.

3.4.3 DC Power Supply

The regulated ± 6 volt excitation required by the RVDT was supplied by a DC tracking power supply (Leader model LPS-151).

3.4.5 Power Amplifier

In order to supply the high voltage and driving current needed during torsional shear tests, a DC to 20 KHz power amplifier with a 50 volt, 1.0 amp peak output was employed (HP Model 6824A). The maximum 1.0 amp output is precisely the limiting current of the torsional drive coils.

The sinusoidal driving signal was produced by the Exact Model 508 Function Generator which was then amplified and adjusted by means of a variable gain control on the power amplifier. The amplified output signal has virtually no phase shift.

3.4.6 Storage Oscilliscope

In addition to the storage oscilliscope used for resonant column tests, a second digital oscilliscope was used for torsional shear tests. This second oscilliscope (Nicolet 4094) is equipped with two disk drives which allow storage of recorded signals on computer disks for subsequent conditioning and analysis. This feature was used for recording the drive coil input and RVDT output signals from which stress-strain loops are determined. Also, the second storage oscilliscope was used occassionally during resonant column tests to check and compare strains calculated from the torsional accelerometer response with those determined from the RVDT.

4. THEORETICAL BACKGROUND

The dynamic shear modulus and damping can be determined either from resonant testing or from slow torsional testing. The specific methods and theory for each type of test are presented in this chapter.

4.1 SHEAR STRESS AND STRAIN DISTRIBUTION

The variation of shear displacement in the soil specimen as a result of forced torsional rotation of the top cap is shown in Fig. 4.1. The torsional displacement varies from zero at the fixed base to a maximum of r_{max} at the top of the sample. A linear variation of displacement from the top to the bottom of the sample implies that there is no vertical variation in shear strain. This has been experimentally verified (Drnevich, 1972a). Radially, displacements vary from zero along the longitudinal axis of the specimen to a maximum at the sample radius. Therefore, there exists a radial strain gradient since the shear strain (γ) at any point depends on the distance, r, from the center of rotation according to:

$$\gamma = r\theta/l \qquad (4.1)$$

where l is the sample length

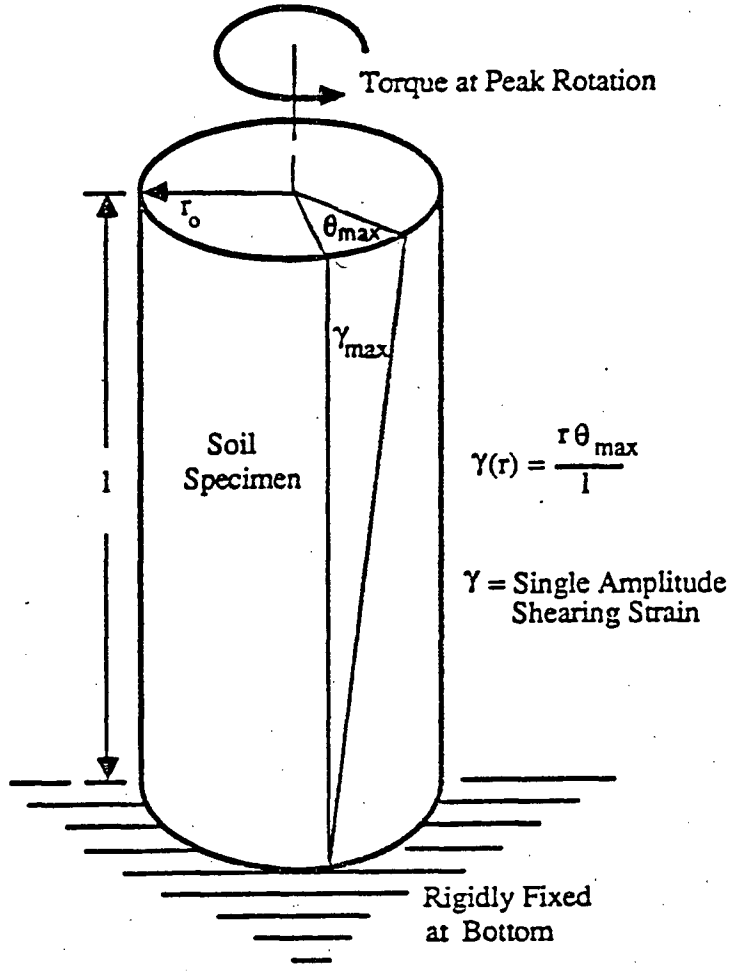

Fig. 4.1 Shear Strain in Sample

θ is the angular displacement

The fact that stress and strain vary with radius in such a specimen does not create a serious error. Hardin and Drnevich (1972a) reported no significant differences in the behaviour of hollow and solid cylindrical samples when compared on the basis of average strain (γ_{av}) in the specimen. It can be easily shown that the average strain is given by

$$\gamma_{av} = 2/3*(r_{max}\theta_{max}/l) \qquad (4.2)$$

In order to avoid the confusion arising from inadequately defined shear strains found in the literature, it should be noted that all resonant column and torsional shear strains reported herein are based on the average shear strain defined by Eq. 4.2. Shear strains are reported as single amplitude values. These are the average strains determined at peak rotational displacement with respect to the original null position. Although Eq. 4.2 is strictly applicable only in the elastic range where a linear relationship exists between stress and strain, no attempt has been made in this research to determine a nonlinear equivalent radius. Ni (1987) reported that an equivalent radius of $3/4*r_{max}$ may be appropriate for shear strains up to 0.1 percent.

4.2 RESONANT COLUMN TEST

The determination of dynamic soil properties from the resonant column test is based on linear vibration theory. The fundamental aspects of the theory and the equations used to calculate shear modulus and damping are outlined in the following sections.

4.2.1 Linear Vibration Theory

The analysis of the resonant column test in terms of linear vibration theory was given by Hardin (1965), Drnevich (1967), and Ni (1987). The analytical solution assumes a Kelvin-Voigt soil model having constant stiffness, G, and constant viscous damping, c (amplitude independent). Also, it is assumed that the shear strain does not vary with height in the specimen. The equation of motion for torsional vibration of the resonant column is:

$$\partial^2\theta/\partial t^2 = G/\rho\ (\partial^2\theta/\partial x^2) + c/\rho\ (\partial^3\theta/\partial x^2\partial t) \qquad (4.3)$$

or $\theta_{tt} = V_s{}^2\theta_{xx} + \nu\theta_{xxt}$

where V_s = shear wave velocity = $(G/\rho)^{0.5}$

θ = angle of twist, ρ = mass density of soil

ν = dynamic viscosity = c/ρ

with subscripts x and t corresponding to derivatives with respect to length and time, respectively.

Using the separation of variables procedure, and by applying the appropriate boundary conditions, the frequency equation of motion is obtained:

$$I/I_o = (\omega l/V_s)\tan(\omega l/V_s) \qquad (4.4)$$

where I_o represents the mass moment of inertia of the top cap and drive plate, I is the mass moment of inertia of the assembled soil column, and ω is the undamped natural frequency.

The frequency equation (Eq. 4.4) can be routinely used to calculate the shear wave velocity of the elastic homogeneous soil column. The equation applies to the case of steady-state vibration and is also valid for the case of decaying free vibration. While Eq. 4.4 is rigorously correct only for soil exhibiting linear visco-elastic behaviour (strains less than about 0.001%), much of the non-linear behaviour can be described by performing the linear dynamic analysis incrementally at various strains thereby approximately establishing the non-linear strain amplitude dependent dynamic soil properties.

4.2.2 Shear Modulus

The methods of dynamic modulus and damping determination are covered by Drnevich et al. (1978) and the details of the apparatus calibration procedure are given in the resonant column operating manual (Soil Dynamics Instruments Inc., 1981).

Knowing the resonant frequency of the soil column, sample length, and mass moment of inertia of the sample, the shear wave velocity can be calculated from the frequency equation (Eq. 4.4). A system calibration procedure gives the value of the mass moment of inertia (I_o) of the top cap and drive plate.

Solution of Eq. 4.4 was facilitated through the use of a Fortran data reduction computer program modified from Drnevich et al. (1978). Nomographs for solving Eq. 4.4 are also available and were used to check the computer generated values.

Shear modulus (G_{max}) can be obtained from the shear wave velocity (V_s) since they are related through the theory of elasticity:

$$G_{max} = \rho V_s^2 \qquad (4.5)$$

where ρ is the soil density. The shear modulus determined from the resonant column test is the secant modulus since only the points of peak response are measured.

4.2.3 Damping Ratio

As mentioned in section 4.2.1, the theory underlying the resonant column test assumes a viscous dashpot to represent the soil damping. Two methods can be employed to determine the damping ratio: the amplitude-decay method and the steady state method.

4.2.3.1 Amplitude Decay Damping

Energy loss in a freely vibrating system results in a decaying vibration amplitude. The response of a single degree of freedom (linear) soil column is described by the solution of Eq. 4.3:

$$\theta(x,t) = Ce^{-D\Omega t}\sin(\omega_d t + \phi)\sin(\omega x/V_s) \qquad (4.6)$$

where
θ = rotational angle
C = a constant
D = damping ratio = $c\omega/2G$
ϕ = phase angle
ω_d = damped natural frequency = $(1-D^2)^{0.5}$
Ω = natural frequency

Considering the ratio of two successive peaks of vibration gives:

$$\theta_n/\theta_{n+1} = e^{D\omega T} \qquad (4.7)$$

where T is the period of vibration = $2\pi/\omega_d$

The logarithmic decrement, d, is defined as the natural logarithm of Eq. 4.7:

$$\begin{aligned} d = \ln(\theta_n/\theta_{n+1}) &= D\Omega T \\ &= 2\pi\Omega D/\omega_d \\ &= 2\pi D/(1-D^2)^{0.5} \end{aligned} \qquad (4.8)$$

Rearranging the terms in Eq. 4.8 gives the damping ratio which can be readily determined from the free vibration response:

$$D = [d^2/(4\pi^2 + d^2)] \qquad (4.9)$$

4.2.3.2 Steady State Damping

During steady state resonant vibrations the effect of transient vibrations becomes insignificant, and the damping can be determined from the system resonant response. The dynamic amplification of the viscously damped system at resonance is given by:

$$X/X_o = 1/(2D) \qquad (4.10)$$

where X is the peak dynamic displacement, X_o is the peak static displacement, and D is the viscous damping ratio. The damping can be calculated using Eq. 4.10 and the magnification factor (X/X_o) which is determined from the system response and the apparatus constants.

4.3 TORSIONAL SHEAR TEST

The resonant column device can also be used as a torsional shear test device by applying a slow sinusoidal torque to the sample cap and measuring the resulting rotation angle. Apparatus modifications and additional equipment required to be perform such tests are described in section 3.4. The torque-twist response can be readily converted to a stress-strain loop from which shear modulus and visco-elastic damping can be determined. The methods and calculations involved in determining these parameters from the torsional shear test have been given previously by Isenhower (1979) and Ni (1987), and are briefly outlined below.

4.3.1 Shear Modulus

The shear modulus is measured as the secant shear modulus joining the end points of the stress-strain hysteresis loop (Fig. 4.2). Mathematically, the secant shear modulus is expressed by:

$$G = \tau/\gamma \tag{4.10}$$

The shear stress, which is determined from the applied torque, is based on the theory of elasticity of a circular bar in torsion. Assuming a linearly varying shear stress with radius, the average shear stress (τ_{avg}) is given by:

$$\tau_{avg} = r_{eq}T/J \tag{4.11}$$

where T is the applied torque, r_{eq} is the equivalent radius ($2/3r_{max}$), and J is the polar moment of inertia given by:

$$J = \pi r^4/4 \tag{4.12}$$

The applied torque is determined from the applied voltage to the drive coils, V_t, and the linear torque calibration factor, K_t. Thus, the average shear stress relation is:

$$\tau_{avg} = r_{eq}K_tV_t/J \tag{4.13}$$

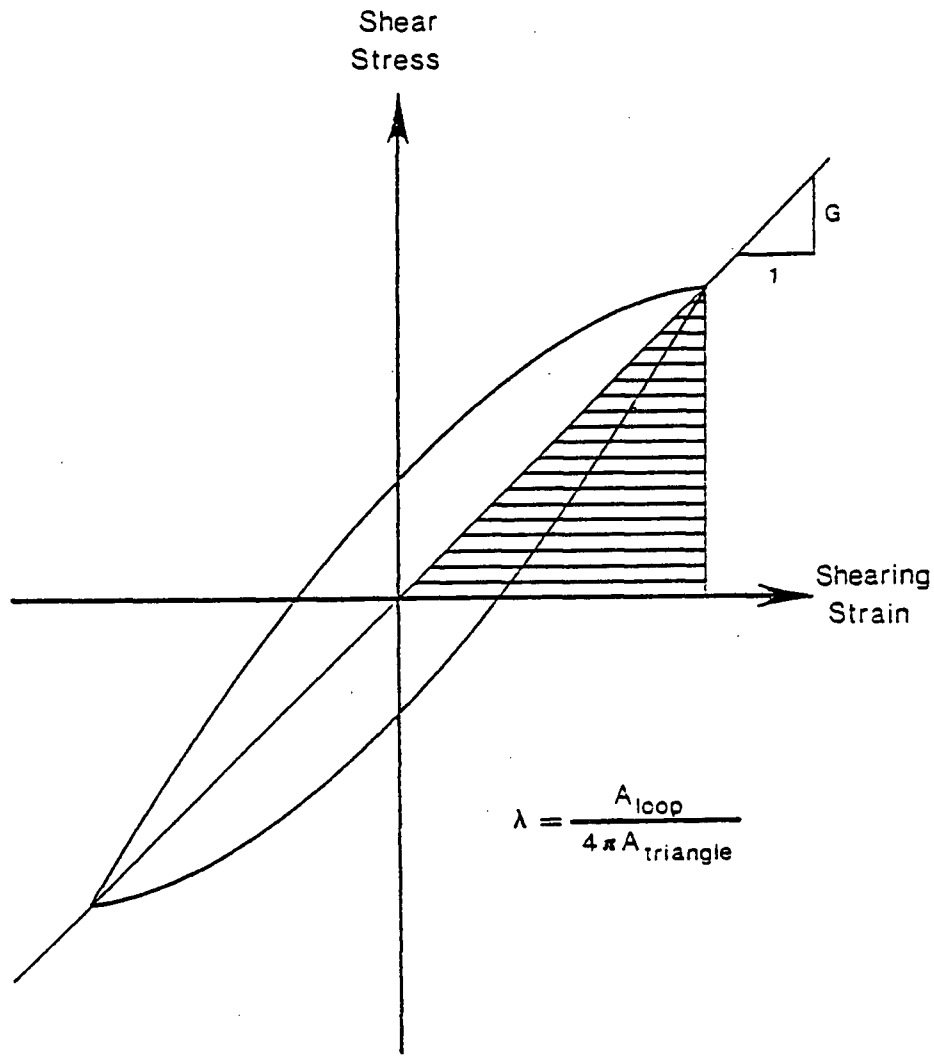

Fig. 4.2 Secant Modulus and Hysteretic Damping Ratio From Torsional Shear Test (from Isenhower, 1979)

The shear strain (γ), on the other hand, is calculated from Eq. 4.2 with the rotation angle determined from the rvdt calibration factor, K_r (radians/volt), multiplied by the RVDT output voltage ,Vr:

$$\gamma_{eq} = r_{eq}K_rV_r/l \qquad (4.14)$$

The limitation of non-linear soil behaviour in the resonant column discussed in section 4.1 similarly applies to equations 4.13 and 4.14. That is to say, the equations are strictly applicable in the low range of strain (0.001% or less) where soil behaviour is elastic. As such, both the stress and the strain defined by equations 4.13 and 4.14 tend to be slightly underestimated at high strains.

4.3.2 Damping Ratio

The hysteretic damping ratio can be determined from the stress-strain hysteresis loop for a cycle of loading (Fig. 4.2). By relating the work done (hysteresis loop area), W_d, to the stored elastic energy (area of triangle), W_s, a simple expression for damping can be developed. For a single degree of freedom system it can be proven that

$$W_d = 2\pi Dkx^2 \qquad (4.15)$$

where D is the damping ratio, k is the Kelvin-Voigt spring constant, and x is the peak displacement. As well, it is easily shown that the stored elastic energy is

$$W_S = kx^2/2 \qquad (4.16)$$

Combining equations 4.15 and 4.16 and solving for the damping term results in the damping expression

$$D = W_d/(4\pi W_S) \qquad (4.17)$$

Equation 4.17 enables the calculation of damping for any cycle of loading from the measured stress-strain response. The disadvantage of Eq. 4.17 is that it provides a method of calculating damping which requires the system to be at resonance. However, since the effect of frequency on damping is relatively minor (Ni, 1987), the method can be extended to other loading frequencies.

5. TESTING PROCEDURE

5.1 RESONANT COLUMN TEST

The procedure followed to measure dynamic soil properties from the resonant column was similar to that outlined in Drnevich et al. (1978) and Novak and Kim (1981). Since dynamic soil properties are significantly dependent on the testing procedures and methods used, a summary of the testing procedures used in this research is given in the following.

The setup of RCTS tests entailed a number of steps. First, the apparatus pore pressure system was saturated, the specimen prepared, and the entire system assembled. At this point, initial readings and baselines were taken of the various monitoring equipment.

The sample setup procedure is similar to that used in conventional triaxial testing, though two notable differences exist. For one, filter paper strips were used around the entire surface of the sample to facilitate rapid consolidation. As well, double silicone-greased membranes were used to limit air diffusion (see section 5.3.2).

Prior to consolidation, the pore water pressure coefficient, B, was checked using Skempton's equation

$B=\Delta u/\Delta\sigma_{3C}'$, where Δu is the pore pressure increase. The sample was assumed to be saturated if the value of B was greater than 0.95.

Consolidation was initiated by opening the drainage valves connecting the sample to the volume change device. To monitor the consolidation, readings were frequently taken of the water level in the volume change device as well as of the LVDT output. During the consolidation period, low amplitude vibrations were applied to the specimen to determine the change in shear modulus and damping with time which can be very significant in cohesive soils.

For all tests, consolidation was allowed to proceed at least until the end of primary consolidation which was always less than 1000 minutes when radial filter paper drains were used. Then, the drainage valves were closed and pore pressures in the sample were allowed to equalize before high amplitude dynamic testing was performed.

The high amplitude testing sequence commenced at a low strain amplitude (about 0.001 percent) and progressed to a high strain level (usually 0.5 to 1 percent). For some tests, pore pressures were monitored during and after each level of dynamic testing - commonly conducted at twice the strain amplitude of the previous increment.

The procedure for conducting a high amplitude test was to first increase the drive coil input power to the pre-selected level. Then, the frequency of the sinusoidal input current was varied until resonance was established. Since the ratio between power and resonance frequency is not linear, a simultaneous adjustment for both the power and input frequency is necessary to achieve resonance at a particular strain amplitude (Novak and Kim, 1981). Resonance was identified by adjusting the frequency to obtain a vertically oriented ellipse on the x-y oscilliscope display of input current versus accelerometer output. At this time readings were taken of the frequency, input signal voltage, output signal voltage, and lvdt output.

Damping by the amplitude decay method was determined from the decaying free vibrations measured by the torsional accelerometer response after power was cut off to the drive coils. This usually required the capture of at least twenty cycles of accelerometer response on the digital oscilliscope. The entire procedure described above was performed for each strain level of a high amplitude test.

Lastly, to minimize the effect of the number of cycles on the dynamic soil behiour, the duration of resonance was generally maintained at about 60 seconds.

5.2 TORSIONAL SHEAR TEST

Since torsional shear tests could be performed on the same samples as resonant column tests, the sample setup procedure was identical. The testing procedure, however, was entirely different since the theory underlying the torsional shear test is psuedo-static whereas the resonant column test is based on linear vibration theory.

Contrary to the resonant column test, the stresses and strains for the torsional shear test were measured in a relatively direct manner. That is, the stress and strain were determined from a linear calibration for torque and rotational displacement, respectively.

Prior to commencing a torsional shear test sequence the shear modulus at small strain (about 0.001%) was measured in the resonant column mode. This was done so that the shear modulus from the resonant column test sequence which immediately followed the torsional shear testing could be corrected for pre-straining.

First, the testing frequency was selected and the amplitude of the drive coil input current was adjusted to give the estimated torque required. From a trial run it was found that the maximum frequency at which the torsional shear test could be run without significant dynamic effects was about

1 Hz; therefore, the torque calibration was valid only for psuedo-static conditions. After the frequency and amplitude were selected, the torsional shear test was conducted with the sinusoidal drive coil input and RVDT output digitally recorded for the vibration cycles of interest. These two data records were later modified to give the stress-strain response by means of a digital data processing program (VU-POINT, Maxwell Laboratories, Inc.) on a personal computer. The progam also allowed for integration of the stress-strain loops thereby enabling quick calculation of the hysteretic damping ratio.

The pore pressure response was monitored both during and after the torsional shear testing, and significant pore pressure changes were recorded. Equalization of pore pressures was allowed before the next increment of testing was performed. Commonly, testing was done at three or four shear strain levels before the maximum capacity of the drive coils was reached.

After the strain-dependent response was determined from the torsional shear test, the strain-dependent response was also determined using the resonant column test which allowed testing to a somewhat higher maximum strain.

5.3 PORE PRESSURE MEASUREMENT CONSIDERATIONS

5.3.1 Pore Pressure Measurement

It is well known that sufficient time is required to measure pore pressures in laboratory tests on fine grained soils because of the time lag involved in registering pore pressure changes - even when small volume compliance transducers are used (Bishop and Henkel, 1962, Sangrey et al., 1978). This is an important consideration in the case of resonant column testing since the specimen is subjected to very fast rates of cyclic strain. However, no pore pressures are developed until a sufficiently high strain amplitude is surpassed.

The radial distribution of stress within the sample is not uniform (see section 4.1), resulting in a nonuniform pore pressure distribution within the specimen. Thus, the maximum value of pore pressure occurring within the sample will not be measured, even if enough time is allowed for pore pressure equalization. The problem of high pore pressure gradients will only be important in high shear strain amplitude tests since shear-induced pore pressures are presumably not significant at very low strains.

During high strain amplitude staged tests, pore pressures were allowed to come to equilibrium before the next level of strain was applied. This was done to minimize the nonhomogenous state of stress in the sample resulting from pore pressure gradients generated during high amplitude testing.

5.3.2 Air Diffusion Effects

Several researchers have reported the problem of air diffusion through the membrane and its effect on pore pressure measurements (Novak and Kim,1981, Sangrey et al., 1978, Marcuson and Wahls, 1978, Pollard et al., 1977). Due to the presence of an air-water interface within the testing chamber, air is forced into solution with the water and progressively diffuses through the rubber membrane. After passing through the membrane the air can come out of solution in the form of air bubbles resulting in erroneous volume change readings and inaccurate excess pore pressure measurements. Pollard et al. (1977) examined the pore pressure change within a triaxial sample and concluded that the process could be described by

$$P_S = P_C[1-e^{-d(T-Ti)}] \qquad (5.4)$$

where

P_s = specimen pore pressure

P_c = cell pressure, and

T = time.

The value d is an empirical diffusion parameter which is approximately constant but varies somewhat with pressure, degree of cell fluid saturation by air, and several secondary factors (Sangrey et al., 1978). The variable T_i is an initial reference time depending primarily on the degree of air saturation in the cell and pore fluids. Pore pressures are not affected by air diffusion until time T_i when the partial pressure gradient of air becomes sufficient to establish significant diffusion through the membrane. However, the pore pressure errors become prominent as continued air diffusion causes the pore pressures to increase.

Figure 5.1 shows the result of an air diffusion test. The test was performed in a standard triaxial cell using precisely the same sample dimensions and setup details as used in all resonant column and torsional shear tests in this research. Deaired water was used as the confining fluid and silicone-greased double prophylactic memranes were used around the sample. The zero hour time in Fig. 5.1 corresponds to the time after isotropic consolidation and pore pressure equalization of the sample. At that time an air water interface was introduced into the cell by draining all the cell water leaving water only in the small inner plexiglass containment cell directly around

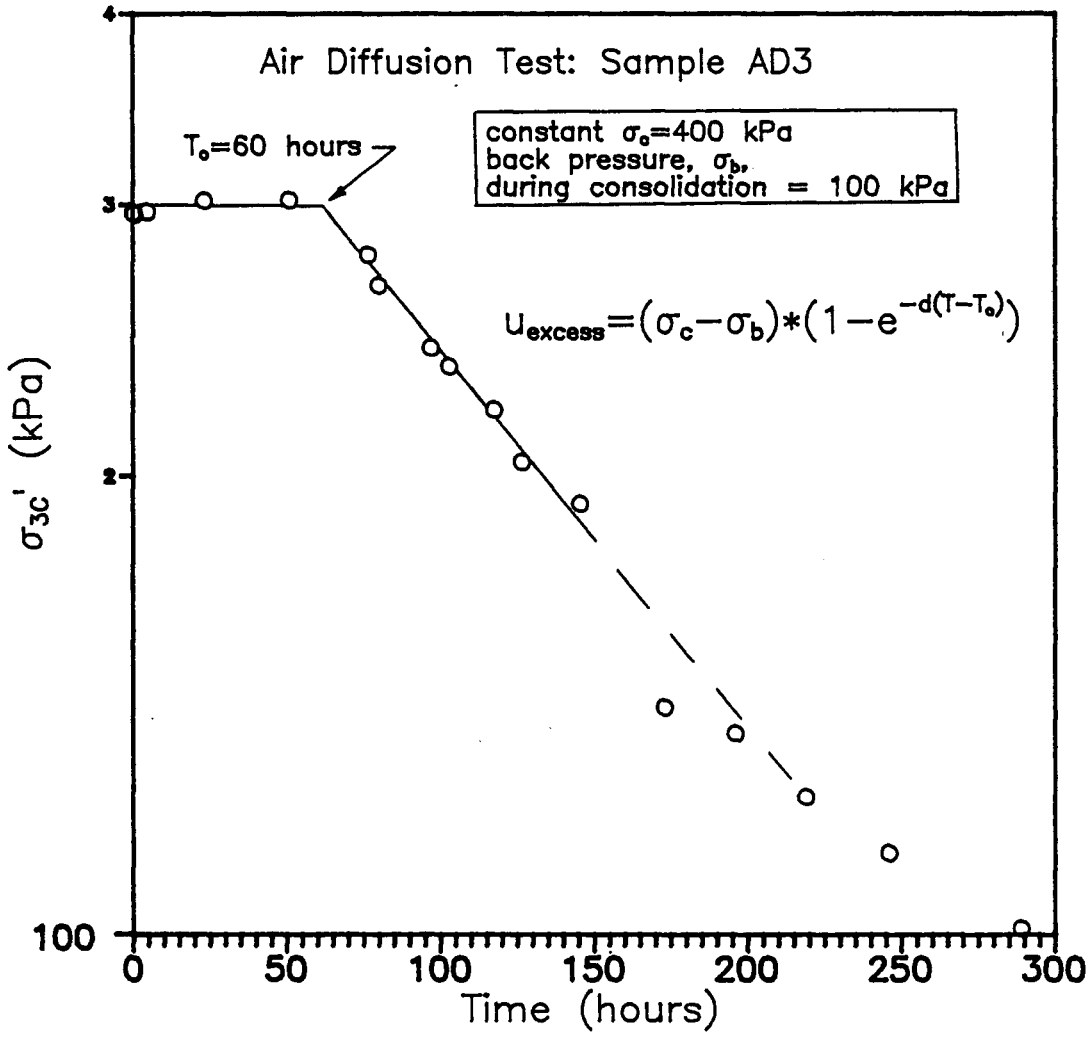

Fig. 5.1 Effect of Air Diffusion on Effective Stress In Sample

the specimen. The jacket of water around the specimen was required to avoid direct contact of pressurized air with the sample memrane.

Under a constant applied cell pressure, no effect of air diffusion on the measured pore pressure is evident for about the first 60 hours. Thereafter, continued air diffusion and pore pressure increase causes the effective confining pressure to decrease to 50 percent of the initial value after only 170 hours (Fig. 5.1).

To circumvent these difficulties, some researchers have successfully used mercury as a containment fluid because air does not readily dissolve in mercury, even under high pressures (Novak and Kim, 1981, Marcuson and Wahls, 1978). The apparatus modifications and special safety precautions required to use a mercury jacket precluded its use in the UBC Soil Mechanics Laboratory.

A testing program constraining all tests involving pore pressure measurements to 60 hours duration was therefore undertaken. This was considered to be a safe time limit since most tests were performed at lower cell pressures than the 400 kPa cell pressure used for the air diffusion test of Fig. 5.1. Lower cell pressures delayed onset of air diffusion effects (i.e. longer T_i) in tests performed by Pollard et al. (1977).

However, in order to be able to complete staged tests within the 60 hour time limit, it was necessary to use filter paper drains around the specimen to shorten the drainage path thereby decreasing the time required for consolidation. Based on the theory of consolidation, the use of radial drains offers a greater than 70-fold decrease in the time required for completion of primary consolidation (Bishop and Henkel, 1962). The actual consolidation time decrease using radial drains was somewhat less - a 28-fold decrease at a consolidation stress of 70 kPa (Fig. 5.2). At higher consolidation stresses, the effectiveness of the filter drains was reduced, presumably as a result of the decreasing permeability of the filter paper with increasing confining stress. Nevertheless, the reduction in consolidation times was sufficient to enable any test to be completed within the 60 hour limit.

The degree of saturation of the specimen was checked immediately following every stage of testing by determining the Skempton B-parameter. A B-value of 0.95 or greater was considered sufficiently high to indicate that saturation of the specimen was maintained. Pore pressures generated during testing were considered accurate only if such a high B-value was determined following the test stage.

For tests requiring consolidation stresses greater than about 150 kPa, the decrease in sample volume as a result of consolidation caused the water level in the confining jacket

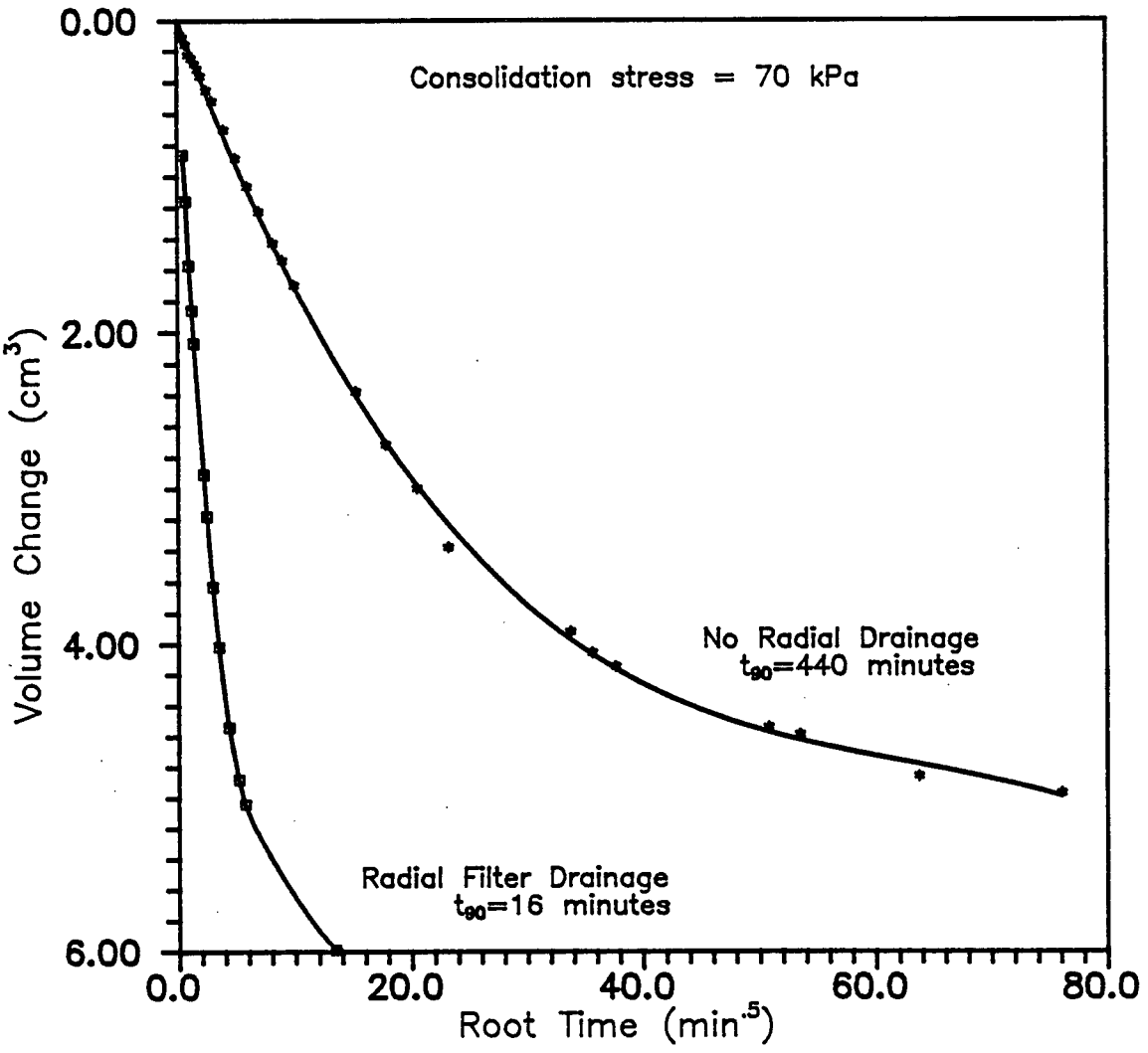

Fig. 5.2 Comparison of Consolidation Rate with and without Radial Drains

surrounding the specimen to drop low enough to directly expose the uppermost portion sample memrane to the pressurized air in the confining chamber. This led to an earlier onset of air diffusion effects for these higher-pressure tests as indicated by the more rapid decrease in B-value (Fig. 5.3). For tests performed at effective consolidation stresses less than 150 kPa, Fig. 5.2 shows that B-values of about 0.95 were maintained for a time period greater than 60 hours. Thus, information on generated pore pressures had to be obtained shortly after consolidation (several hours) for high pressure tests.

In future testing, it is recommended that a method be developed to eliminate this problem. A telescoping containment cell with a method to periodically flush the containment cell with deaired water is suggested.

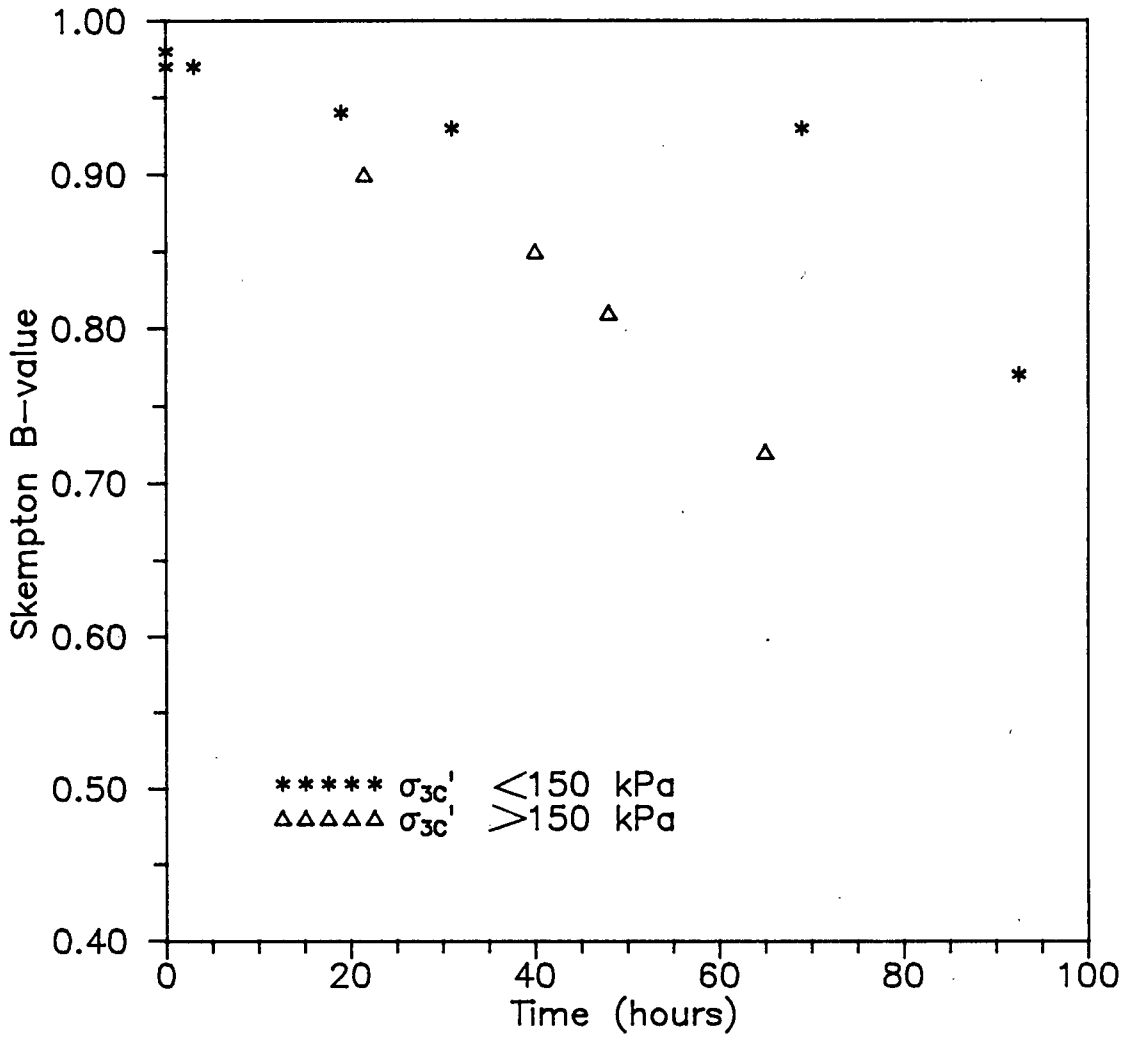

Fig. 5.3 Increased Air Diffusion Effect at High Confining Stress

6. SITE DESCRIPTION

6.1 GEOLOGY AND GEOTECHNICAL SITE DESCRIPTION

The Lower 232nd St. research site is located at the 232nd St. interchange of the Trans Canada Highway, about 40 km east of downtown Vancouver (Fig. 6.1). The Quaternary sequence at the site is part of the Fort Langley Formation consisting of marine silt to clay with occasional sand lenses, deposited during the glacial regression (Armstrong, 1978). These fine grained soils have become slightly sensitive as a result of leaching subsequent to deposition. The silts and clays are slightly organic and are underlain by dense sands and gravels. Due to dessication, the soil is overconsolidated at the surface, becoming normally consolidated below a depth of about 5 m.

Numerous Atterberg limit tests and hydrometer tests indicate that the soil below 3 m is reasonably uniform, except for occasional sandy layers (Fig. 6.2). Above 2.5 m depth, the surficial soil is of higher plasticity (PI=40) while the soil below 3 m is of lower plasticity (PI=20).

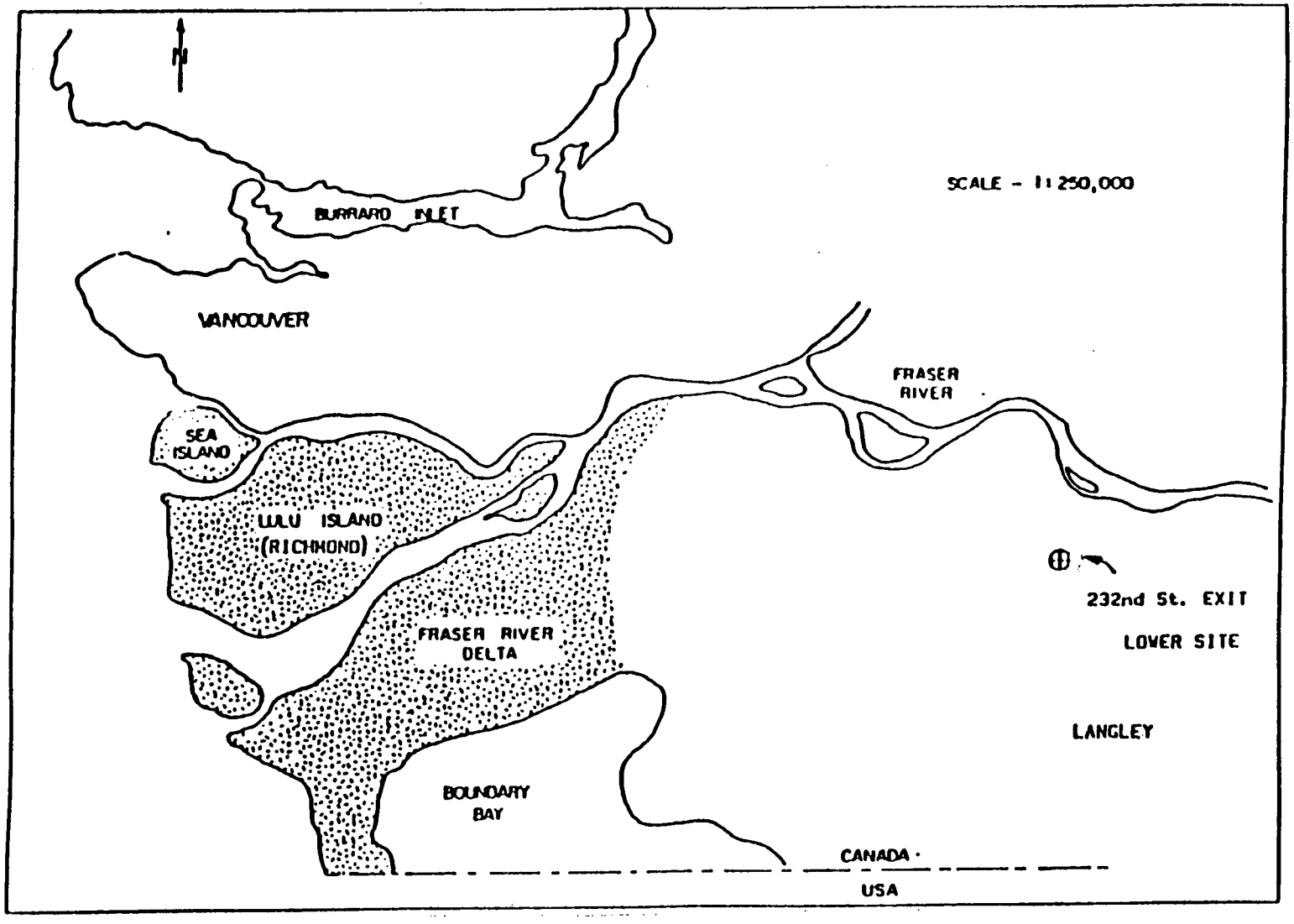

Fig. 6.1 Lower 232nd St. Site Location

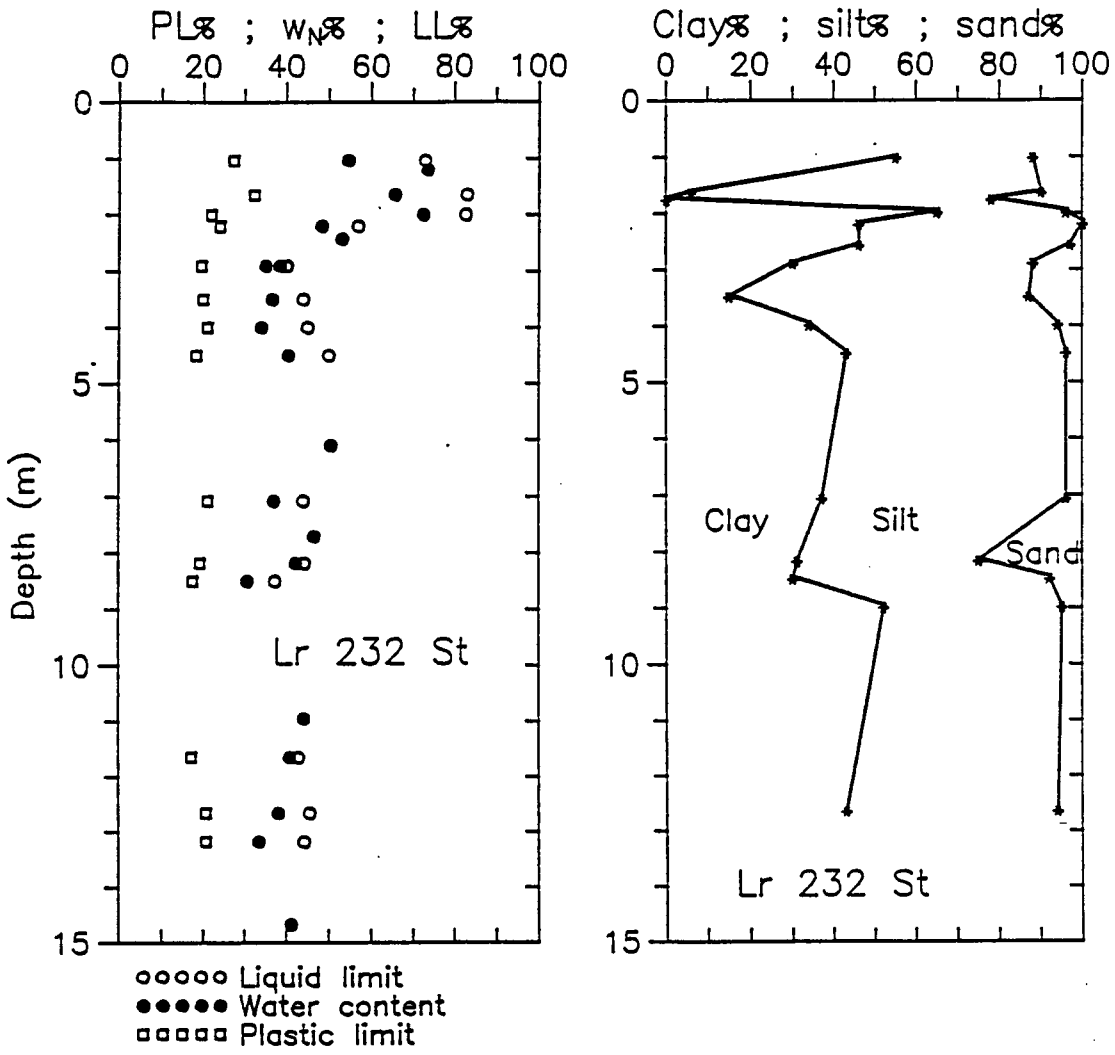

Fig. 6.2 Profiles of Atterberg Limits and Grain Size

6.2 LABORATORY SOIL SAMPLES

Two types of undisturbed soil samples were obtained; block samples and 2.6" inner diameter tube samples. The block samples were carefully trimmed at a depth of 2 m from an excavated pit whereas the wireline tube samples continuously sampled the soil to a depth of 16 m. Both types of samples were sealed and stored in a humidity room until needed.

The block samples were obtained in order to have a large number of identical samples from the same horizon which could be used to study the effects of various parameters on the dynamic soil properties. On the other hand, only a few tube samples were tested since they were used mainly to compare the dynamic properties determined in the laboratory with those derived from in situ techniques. The difference in plasticity index (PI) between the two types of samples also enabled the comparison of dynamic properties on the basis of PI.

7. RESONANT COLUMN RESULTS

7.1 LOW AMPLITUDE SHEAR MODULUS

It is natural to examine separately the effects on low amplitude and high amplitude shear modulus of various parameters such as confining pressure and duration of confinement.

7.1.1 Effect of Confining Pressure and Void Ratio

As mentioned in section 2.1.2, the effects of confining pressure and void ratio on shear modulus of normally consolidated cohesive soils are difficult to examine independently since these two factors are intimitely linked. When considered together, however, their individual effects can be distinguished.

From fourteen undisturbed block samples taken from a depth of 2.0 m, 19 normally consolidated determinations of low amplitude shear modulus (G_{max}) were made at effective confining pressures ranging from 70 to 500 kPa. These low amplitude dynamic shear modulus values are plotted against the respective isotropic effective confining stresses in Fig. 7.1. Despite some data scatter, the shear modulus increases almost in direct

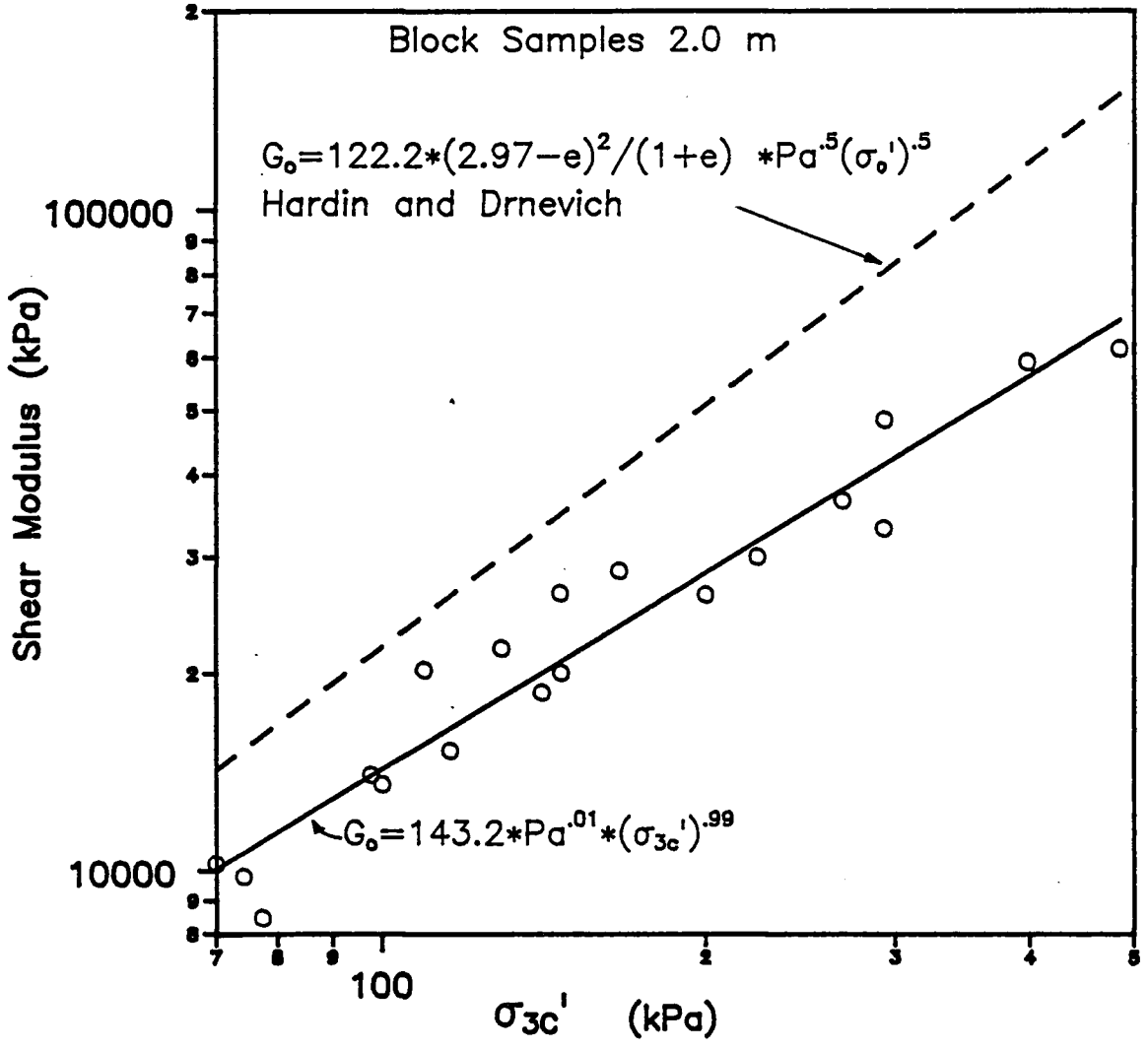

Fig. 7.1 Shear Modulus vs. Confining Pressure Relationship for Block Samples

proportion to the increase in effective confining stress. The relationship between G_{max} and confining pressure can be approximated as

$$G_{max} = 143.2P_a^{.01}(\sigma_{3c}')^{.99} \qquad (7.1)$$

where is σ_{3c}' the effective confining pressure and P_a is the atmospheric pressure in the same units as G_{max} and σ_{3c}'. No attempt to separate the influence of void ratio is made in Eq. 7.1.

The standard error in estimating shear modulus using Eq. 7.1 is 3900 kPa. Due to the change in the profile of soil characteristics (Fig. 6.2) at the 2.0m depth from which the block samples were obtained, some of the scatter in shear modulus values may be the result of sample differences. Indeed, vertical variation in final water content within some block samples were found to be as high as 15% suggesting that specimens were non-uniform.

Low amplitude shear modulus (G_{max}) was also determined for several tube samples obtained from 8-14m and tested at effective confining pressures ranging from 70 to 400 kPa. Once again, the shear modulus values clearly increase with confining pressure for the normally consolidated tests in Fig. 7.2. The least squares best fit line describing the relationship is given by

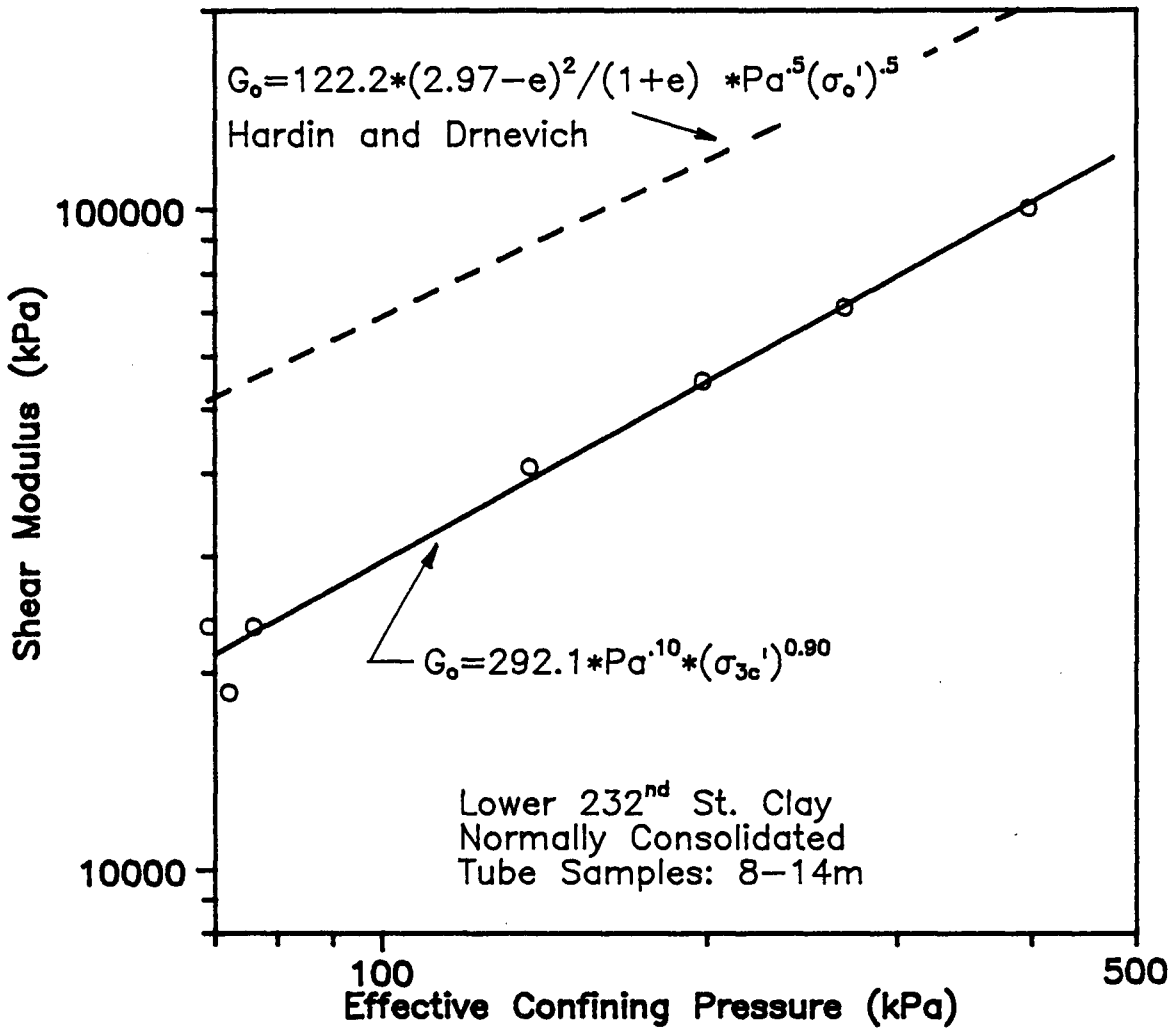

Fig. 7.2 Shear Modulus vs. Confining Pressure Relationship for Tube Samples

$$G_{max} = 292.1 * P_a^{.10} (\sigma_{3C}')^{.90} \qquad (7.2)$$

with a sample standard error of 2000 kPa. Void ratio effects are not separated from Eq. 7.2. The soil index properties (PI and grain size) in the 8-14m depth range from which these tube samples were obtained is relatively uniform; the standard error is about half that of the block samples.

The dimensionless modulus multiplier values, K, for the block samples and tube samples - 143.2 and 463.6, respectively - fit the trend of increasing modulus multiplier with decreasing PI identified in Fig. 2.4 for seven undisturbed clays of varying plasticity. These are shown graphically in Fig. 7.3 which provides a first estimate of K on the basis of PI.

The respective modulus exponent values for the block samples and tube samples are 0.99 and 0.90. These values are shown plotted against PI in Fig. 7.4 along with the modulus exponents for the clays presented in Fig. 2.4. The modulus exponents of all the clays lie in a fairly narrow range between 0.84 and 1.18 with the less plastic clays generally having smaller modulus exponents.

The trend of increasing modulus exponent and decreasing modulus multiplier with increasing plasticity index might be

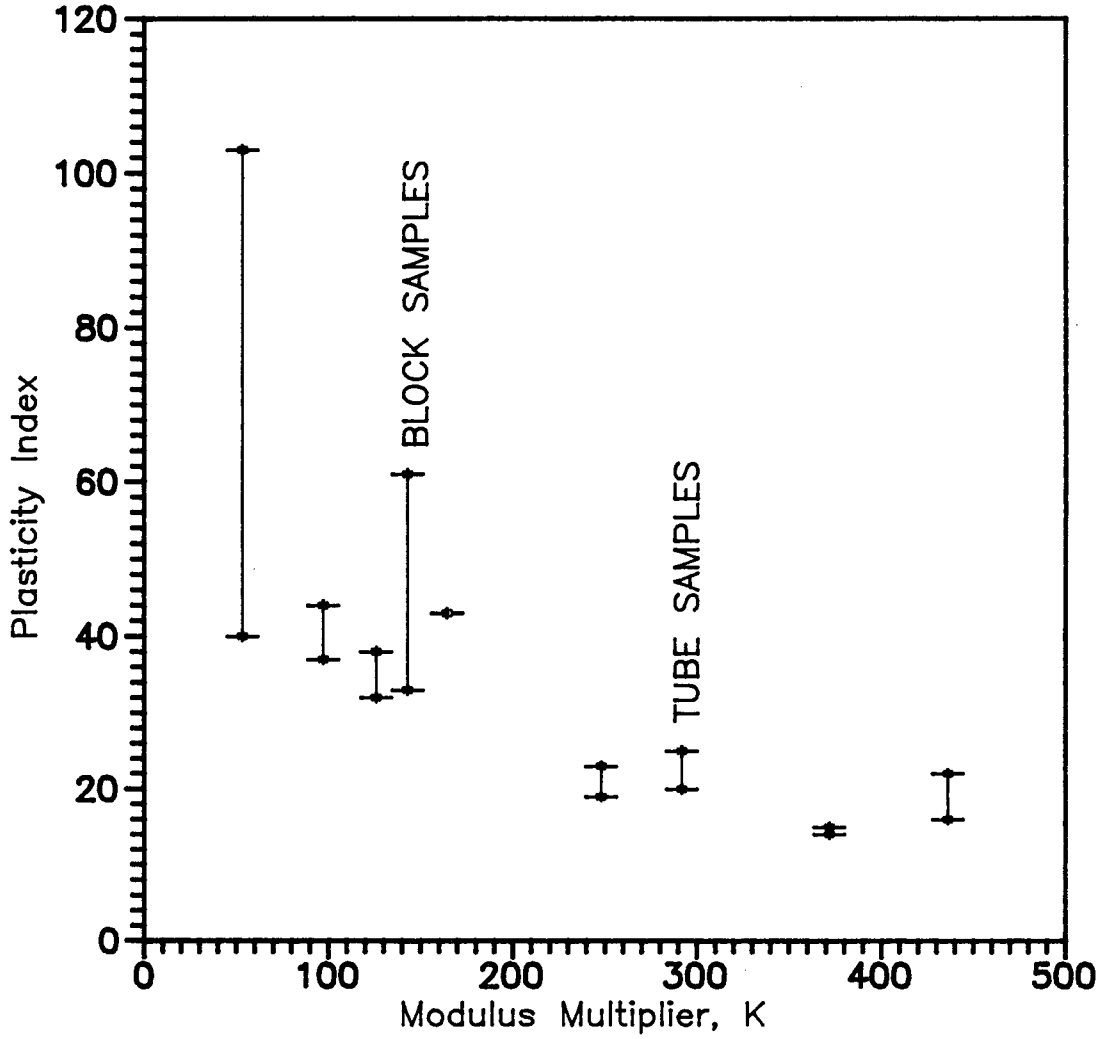

Fig. 7.3 Variation of Modulus Multiplier with Plasticity Index

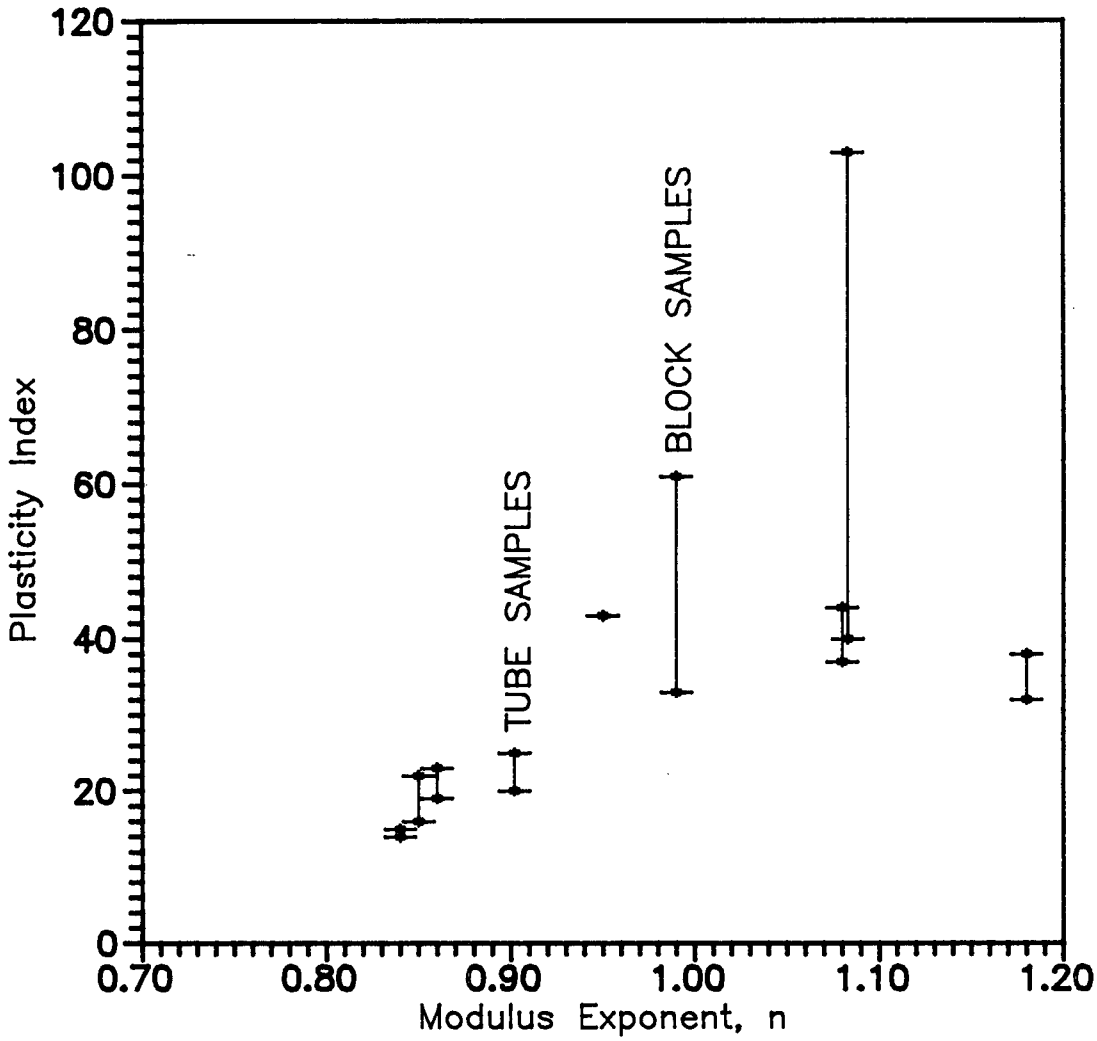

Fig. 7.4 Variation of Modulus Exponent with Plasticity Index

intuitively predicted; since higher plasticity clays are generally softer (lower modulus) than less plastic clays, a lower modulus multiplier would be expected. Higher plasticity clays would also be expected to have a higher modulus exponent than less plastic clays since they generally undergo a more rapid reduction in void ratio with increasing confining pressure.

In order to examine the effect of void ratio on shear modulus of both the tube and the block samples, a void ratio factor in the form of Eq. 2.1 was employed. The form of the equation is derived from the assumption of a linear relationship of shear wave velocity with void ratio which appears to be valid for the block samples (Fig. 7.5) as well as for the tube samples (Fig 7.6). Much of the scatter in the data is the result of sample differences since only small variations from a linear relationship were observed for individual samples tested at more than one normally consolidated state.

For the normally consolidated block samples tested, the combined effect of void ratio (e) and confining pressure (σ_{3C}') on low amplitude shear modulus (G_{max}) is shown in Fig. 7.7 with a best fit line given by

$$G_{max} = 29.3*F(e)P_a^{.40}(\sigma_{3C}')^{.60} \qquad (7.3)$$

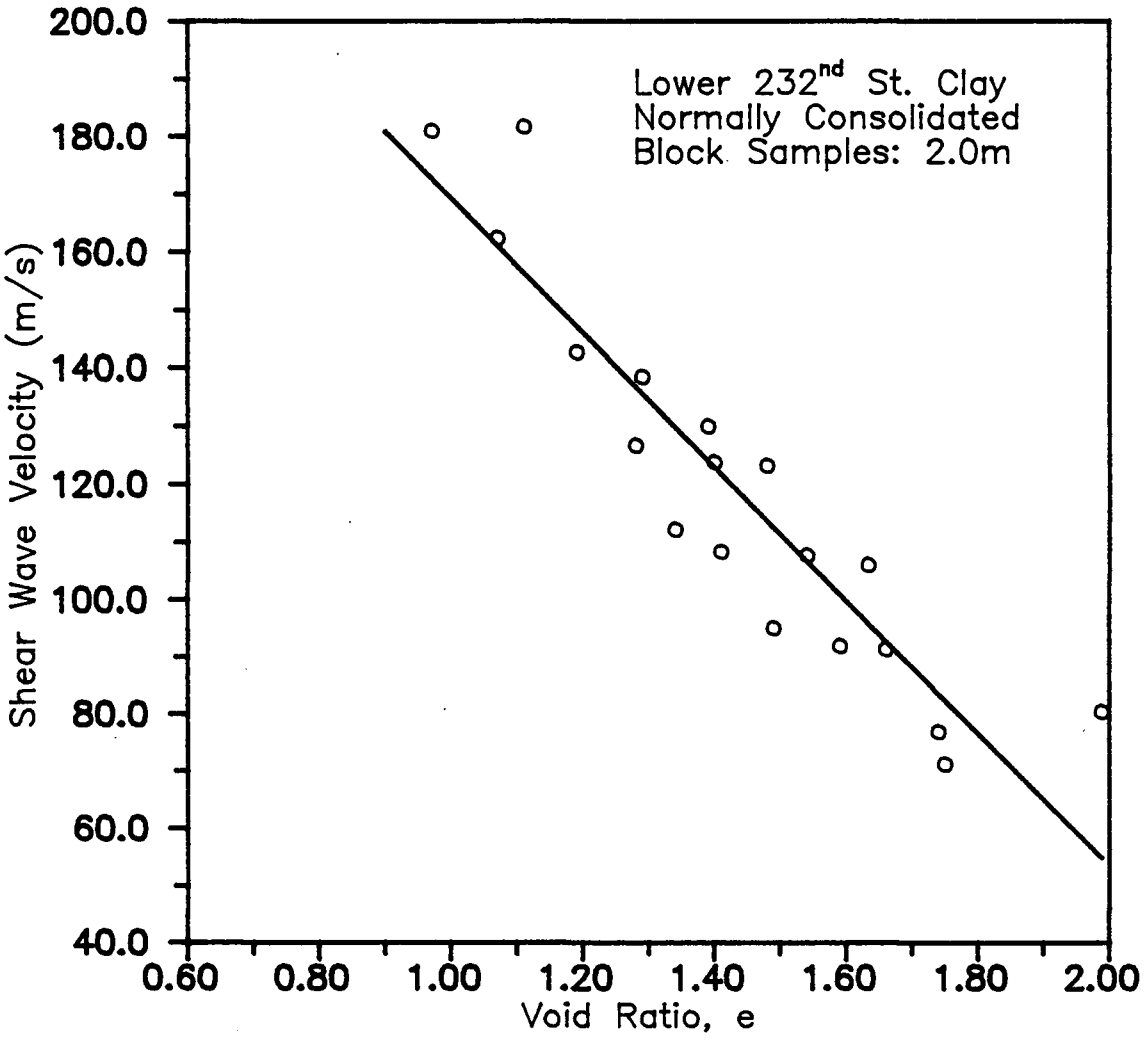

Fig. 7.5 Variation of Shear Wave Velocity with Void Ratio for Normally Consolidated Block Samples

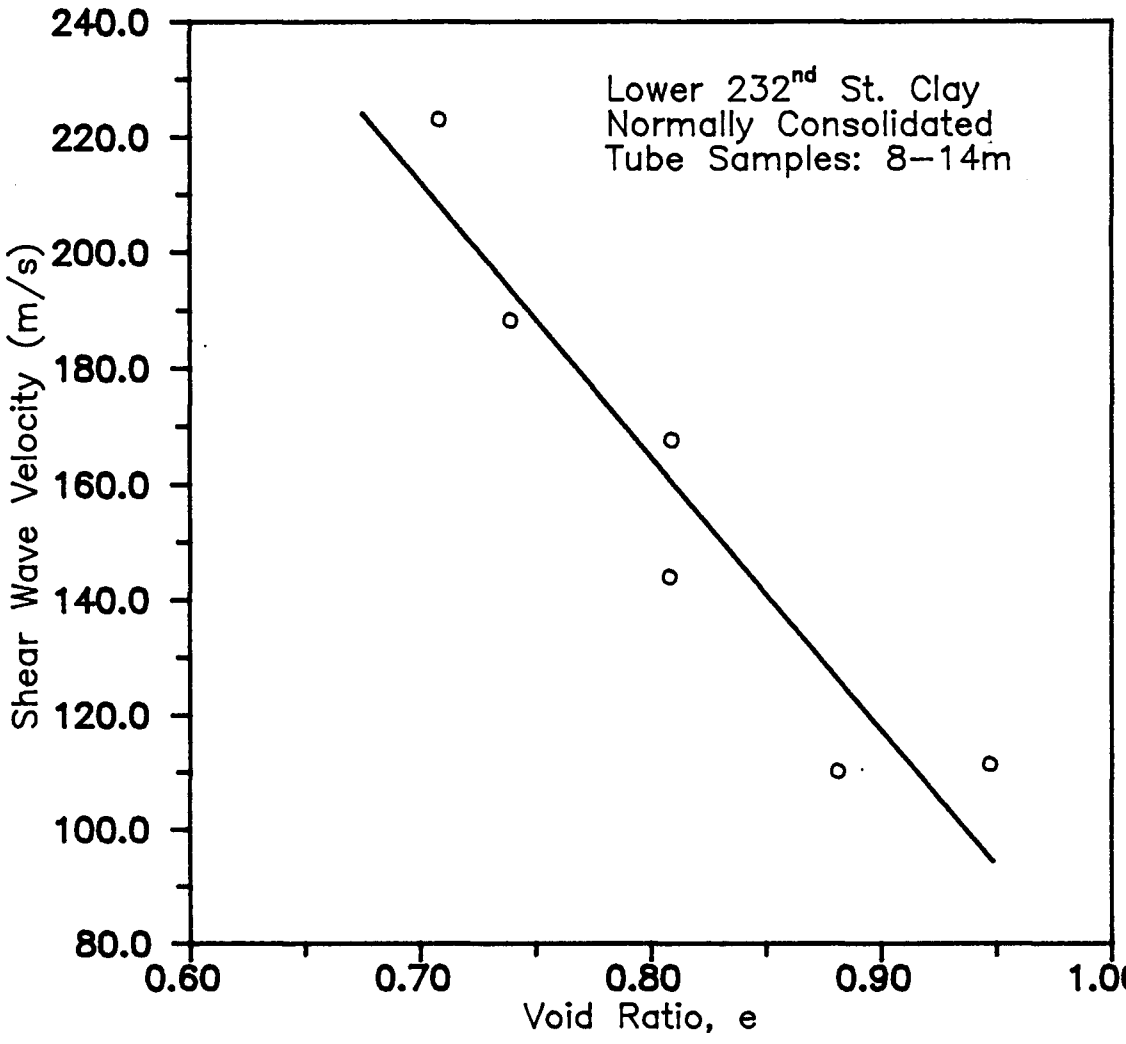

Fig. 7.6 Variation of Shear Wave Velocity with Void Ratio for Normally Consolidated Tube Samples

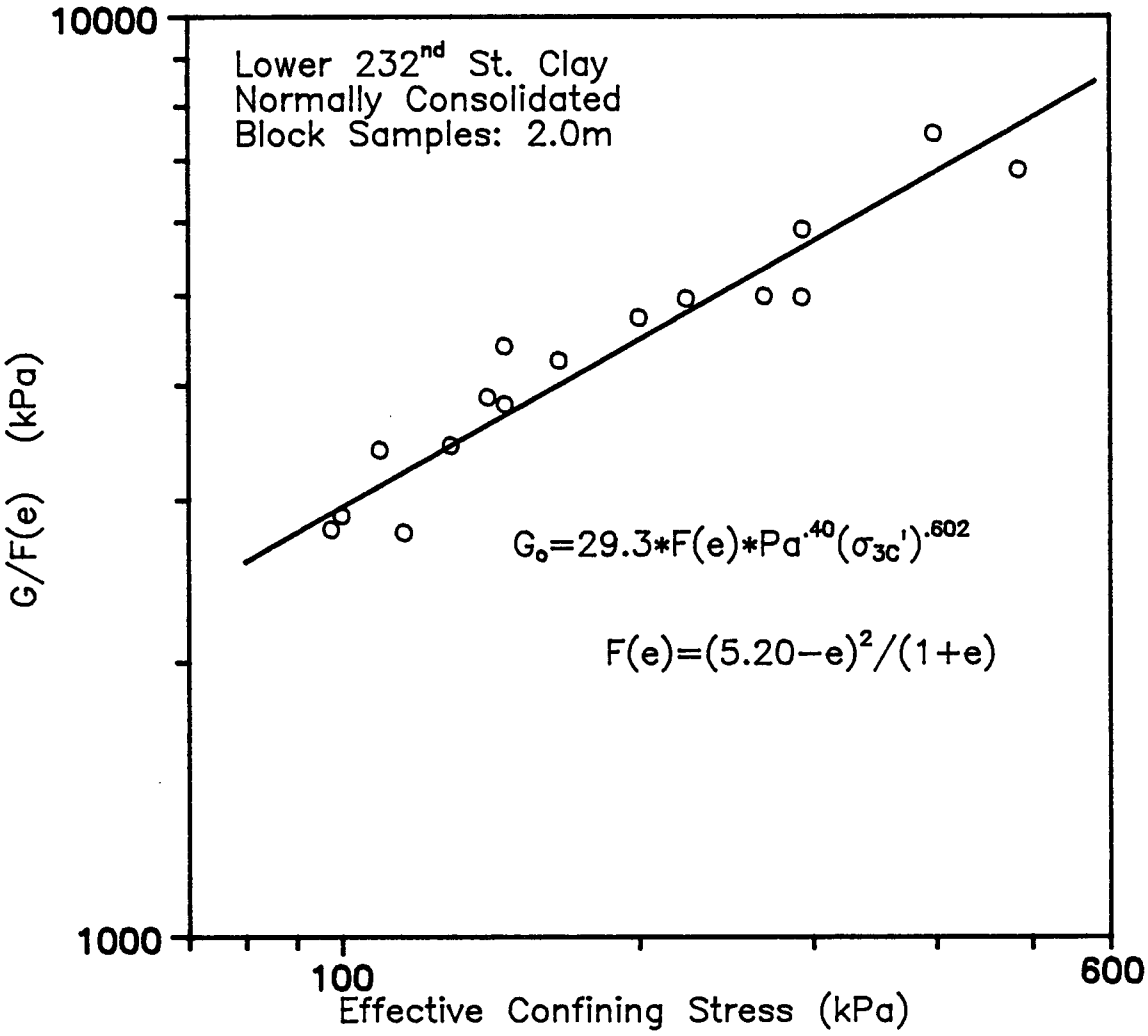

Fig. 7.7 Void Ratio Modified Shear Modulus vs. Confining Pressure for Normally Consolidated Block Samples

where P_a = atmospheric pressure in the same units as σ_{3c}' and G_{max}

and $F(e) = (5.2-e)^2/(1+e)$

Equation 7.3 has the atmospheric pressure term, Pa, included to make the equation valid for any system of units and to make the modulus multiplier (29.3) dimensionless. The constant of 5.2 in the numerator of the void ratio function, F(e), was determined by regession analysis which involved varying the constant until the linear log $G_{max}/F(e)$ versus log σ_{3c}' relationship with the smallest standard error was identified. This constant appears to be dependent on the clay type as values ranging from 2.97 to 7.32 have been identified in the literature (Kokusho et al., 1982). If the commonly used form of F(e) with a constant of 2.97, as suggested by Hardin and Drnevich (1972b) is used, a poor fit to the block sample data is observed and the shear modulus exponent for the best fit line is only 0.27. Data presented by Zen et al. (1978) indicates that the Hardin and Drnevich expression with F(e) constant of 2.97 does not yield a good agreement to the experimental results for clays with PI greater than about 25.

The best fit line described by Eq. 7.3 has a standard error in shear modulus of 3000 kPa which is not a very large improvement on Eq. 7.1 with a standard error of 3900 kPa. Shown in Fig. 7.8 are the measured values of shear modulus which compare reasonably well to the predicted values based on Eq. 7.3.

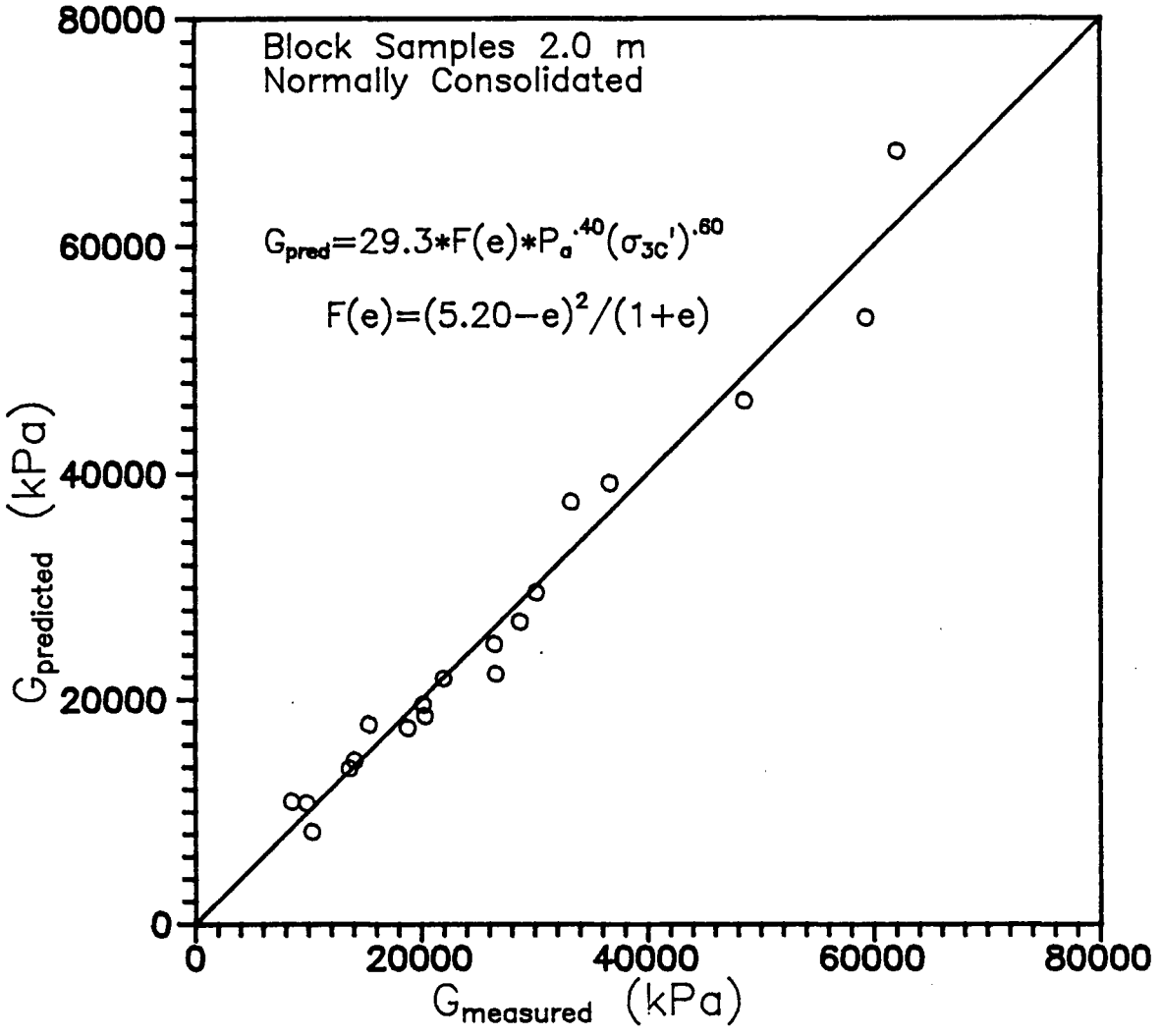

Fig. 7.8 Comparison of Predicted and Measured Shear Moduli for Normally Consolidated Block Samples

For the normally consolidated tube samples tested, the combined effect of void ratio and confining pressure is shown in Fig. 7.9 with best fit line given by

$$G_{max} = 137.2*F(e)P_a^{.384}(\sigma_{3C}')^{.616} \qquad (7.4)$$

where P_a = atmospheric pressure in the same units as G_{max} and σ_{3C}'

and $F(e) = (2.97-e)^2/(1+e)$

The void ratio factor with a constant of 2.97 is that given by Hardin and Drnevich (1972b) to be applicable for all soils. However, data presented by Zen et al. (1978) suggests that it is only valid for clays with PI less than 25. The predicted shear moduli based on Eq. 7.4 and the measured shear moduli show good agreement (Fig. 7.10), with a standard error in shear modulus of 2700 kPa.

Seperating out the void ratio influence by means of F(e) in equations 7.3 and 7.4 makes the shear modulus exponent 0.6 for both the block samples and tube samples. This is the same value of modulus exponent given by Kokusho et al. (1982) for Teganuma Clay, though the shear modulus multiplier and void ratio factor values are different since they appear to depend on the characteristics of the particular soil.

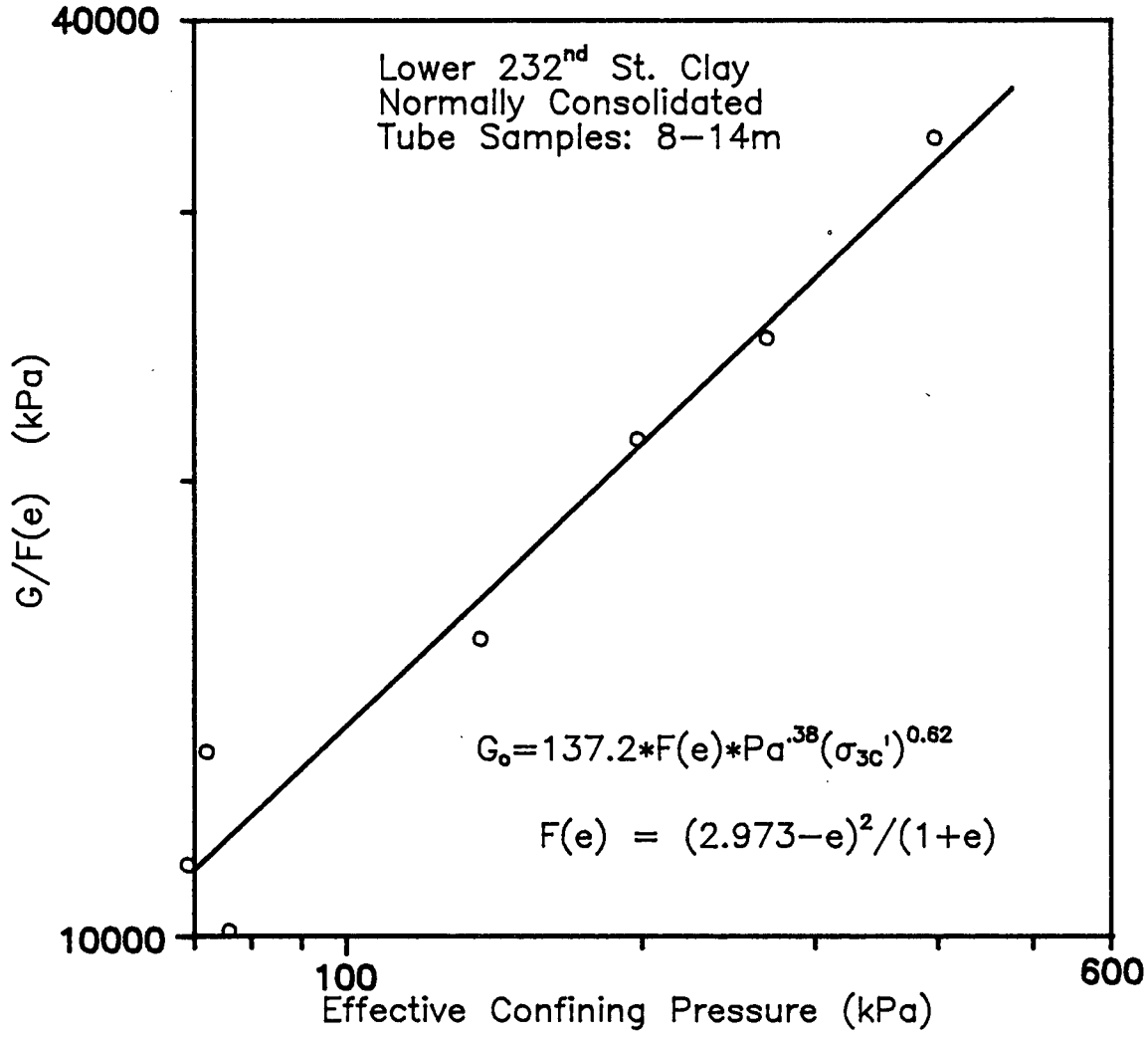

Fig. 7.9 Void Ratio Modified Shear Modulus vs. Confining Pressure for Normally Consolidated Tube Samples

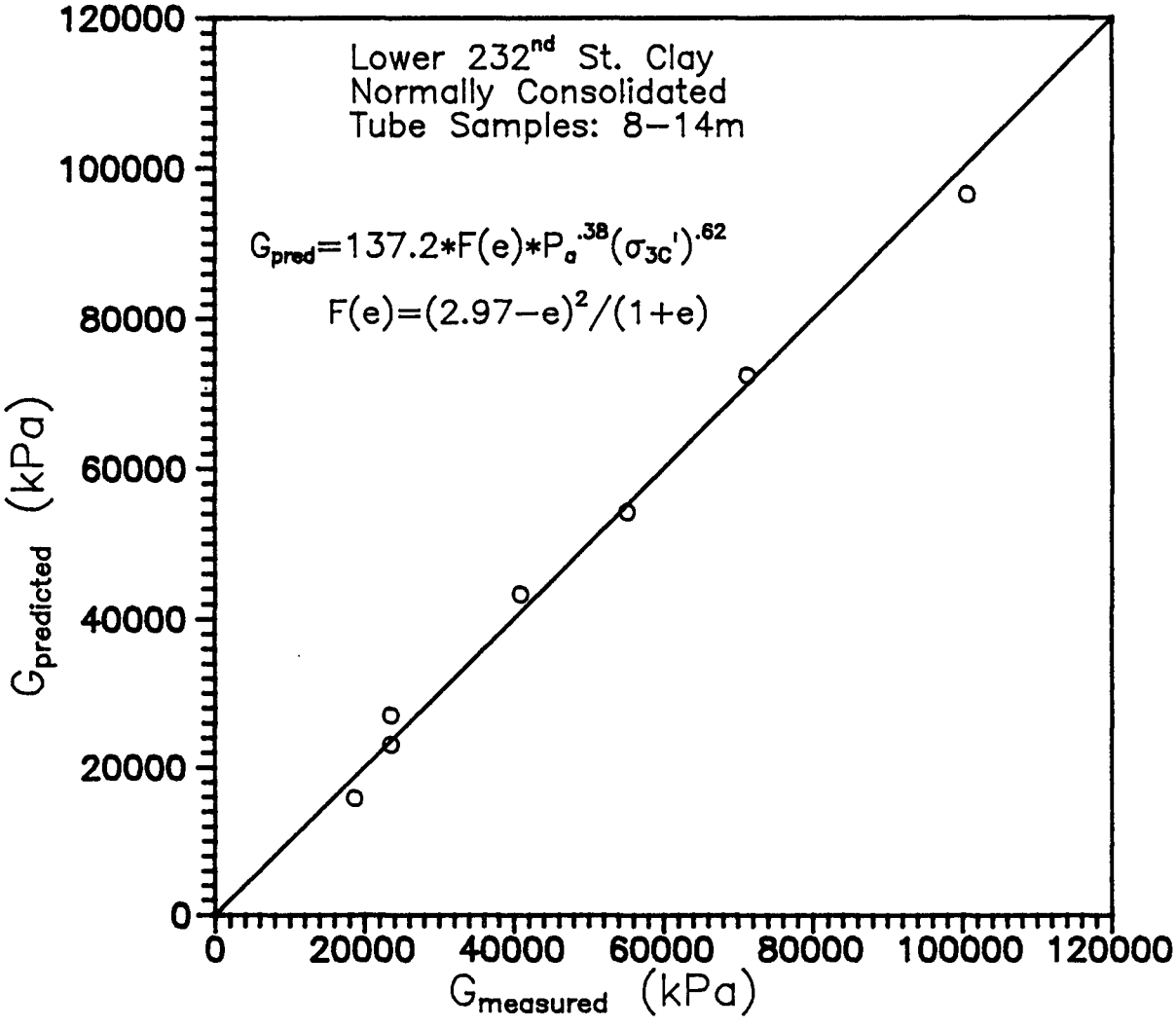

Fig. 7.10 Comparison of Predicted and Measured Shear Moduli for Normally Consolidated Tube Samples

As can be seen in figures 7.1 and 7.2, the well-known equation for shear modulus (Eq. 2.1, 2.2) given in Hardin and Drnevich (1972b) significantly overpredicts the shear modulus values for both the block samples and tube samples of Lower 232nd St. Clay. This finding confirms data presented by Zen et al. (1978) which suggests that the Hardin and Drnevich equation should not be used with higher plasticity clays (PI>25).

7.1.2 Stress History

To study the effect of stress history on the low amplitude shear modulus for Lower 232nd St. Clay, block samples were tested at various states of overconsolidation. In general, the shear modulus increases with increasing overconsolidation ratio (OCR).

The normalized small strain shear modulus values for overconsolidated block samples are shown in Fig. 7.11 for various OCR. The normalized shear modulus is the shear modulus measured in the overconsolidated (OC) condition divided by the shear modulus for normally consolidated (NC) samples given by Eq. 7.1. Despite some data scatter, the shear modulus can be expressed as

$$G_{max} = (G_{max})_{nc} OCR^{.55} \qquad (7.5)$$

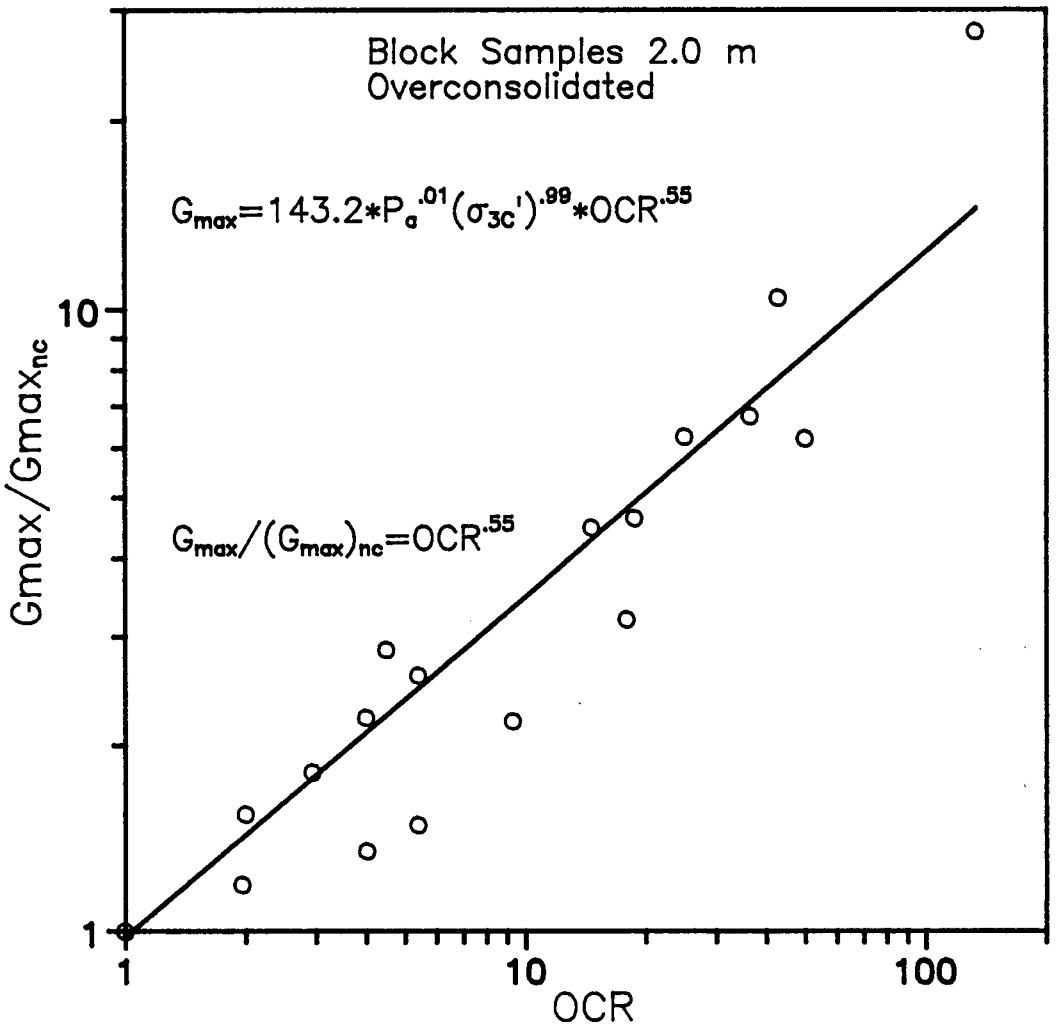

Fig. 7.11 Effect of OCR on Shear Modulus for Block Samples

where G_{max} is the measured shear modulus and $(G_{max})_{nc}$ is the shear modulus for a normally consolidated sample measured at the same effective confining stress. Substituting Eq. 7.1 for normally consolidated shear modulus in Eq. 7.5 gives the shear modulus expression valid for both normally consolidated and overconsolidated block samples

$$G_{max} = 143.2*P_a^{.01}(\sigma_{3C}')^{.99}OCR^{.55} \qquad (7.6)$$

The OCR exponent of .55 in Eq. 7.6 is in the range of 0.5-0.7 identified for all but one of the seven undisturbed cohesive soils listed in Fig. 2.4.

Alternatively, if Eq. 7.4 is used to represent the normally consolidated soil with F(e) to account for void ratio changes, then the expression for shear modulus is

$$G_{max} = (G_{max})_{nc}OCR^{.26} \qquad (7.7)$$

As can be seen in Fig. 7.12, a relatively large scatter exists which suggests that the same void ratio factor, F(e), does not apply to both NC and OC clay, though some of the data scatter may be the result of errors in void ratio measurement. The reason for the reduced OCR exponent in Eq. 7.7 as compared to Eq. 7.5 is that the effect of overconsolidation on G_{max} is partially accounted for by the void ratio function, F(e).

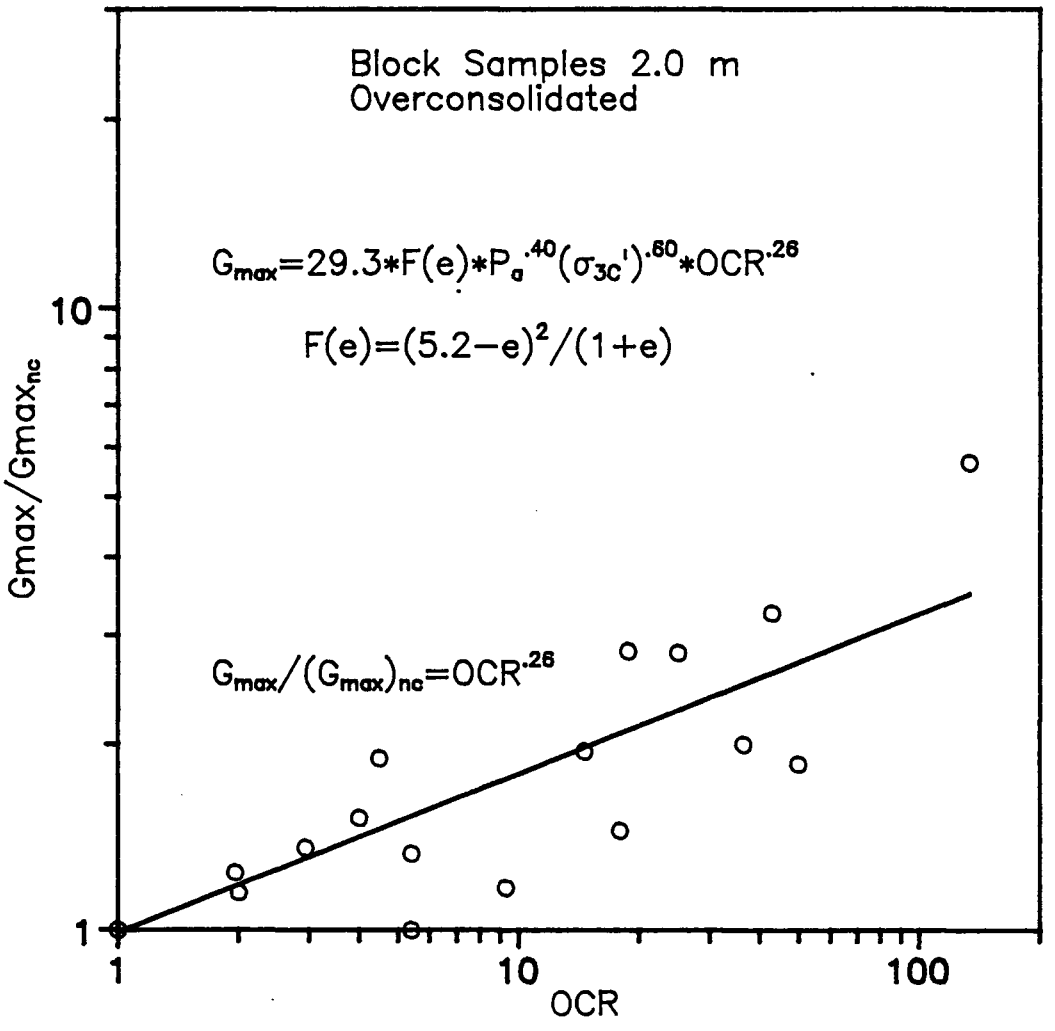

Fig. 7.12 Effect of OCR on Void Ratio Modified Shear Modulus for Block Samples

The OCR exponent, however, agrees with the 0.18-0.30 range specified by Hardin and Drnevich (1972b) for clays with PI between 20 and 40 (Table 2.1). The void ratio modified shear modulus expression for both NC and OC block samples is

$$G_{max} = 29.3*F(e)P_a^{.40}(\sigma_{3C}')^{.60}OCR^{.26} \qquad (7.8)$$

where $F(e) = (5.2-e)^2/(1+e)$

Tube samples were not tested at overconsolidated states as the focus of the tests was on normally consolidated behaviour since the insitu soil is normally consolidated at the depths tube samples were obtained. Furthermore, only a limited number of samples were available for testing.

7.1.3 Secondary Time Effects

To study the time dependent increase in low amplitude shear modulus discussed in section 2.1.6, the shear modulus for some samples was monitored at various times during the consolidation period. This generally involved taking measurements well beyond the time required for completion of primary consolidation in order to establish the time dependent increase at constant effective stress.

The time dependent increase in shear modulus for a normally consolidated block sample of Lower 232nd St. Clay is shown for three effective confining pressures in Fig. 7.13. After about the first ten minutes, the modulus versus log T relationship may be approximated by two straight lines corresponding to the primary and secondary consolidations. Good agreement exists between the kink in the curve and the completion of primary consolidation determined from the consolidation curve (not shown) for each confining pressure which is represented by the arrow on each curve. Modulus values determined prior to the end of primary consolidation correspond to an unknown effective stress since excess pore water pressures still exist within the specimen.

The rate of secondary increase in shear modulus per log cycle of time, ΔG, increases with confining pressure (Fig. 7.13). The normalized rate of shear modulus increase, N_G, as defined by Anderson and Stokoe (1978) is given by

$$N_G = \Delta G / G_{1000} \qquad (7.9)$$

where $v\lambda$ = secondary increase in G per log cycle of time

G_{1000} = G measured at 1000 minutes of confinement

The values of N_G for the tests shown in Fig. 7.13 range from about 18-22%. Although the duration of each test in Fig. 7.13 was less than 2000 minutes, two tests (B14C2 and

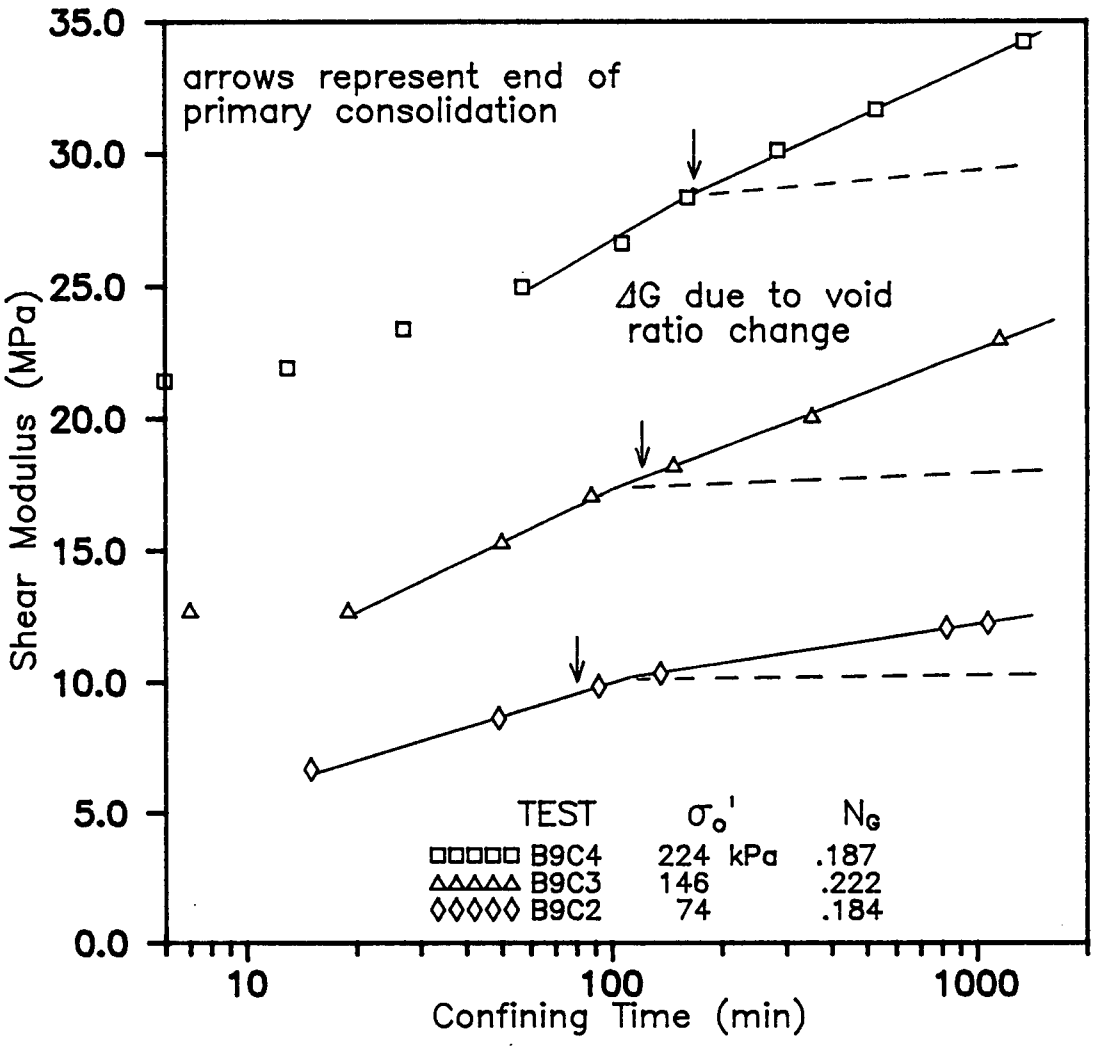

Fig. 7.13 Time-Dependent Increase in Shear Modulus for Normally Consolidated Block Sample

B8C2) were continued to 6000 minutes with no deviation from the linear semi-log relationship. Anderson and Stokoe (1978) report a similar modulus-time response for periods as long as 20 weeks.

For comparison, the time dependent shear modulus increase for a tube sample obtained from a depth of 11.75m is shown in Fig. 7.14 for three effective confining pressures. The behaviour is very similar to that shown by the block samples (Fig. 7.13). Once again, the kink in the curve corresponds closely to the end of primary consolidation represented by the arrow on each curve and the value of ΔG increases with confining pressure. The normalized rate of shear modulus increase, N_G, given by Eq. 7.9 ranges from 15-21% - slightly less than the 18-22% range determined for the block samples.

The secondary increase in shear modulus is not unique to positive confining pressure increments such as those shown in Figs. 7.13 and 7.14. Figure 7.15 shows the shear modulus versus time relationship for two unloading confining pressure increments to overconsolidation ratios of 2.9 and 9.3. After the initial modlus reduction as a result of swelling to equilibrium with a lower confining pressure, a secondary increase in shear modulus is again observed. The values of N_G are about 12% and 18% for unloading to OCR of 2.9 and 9.3, respectively.

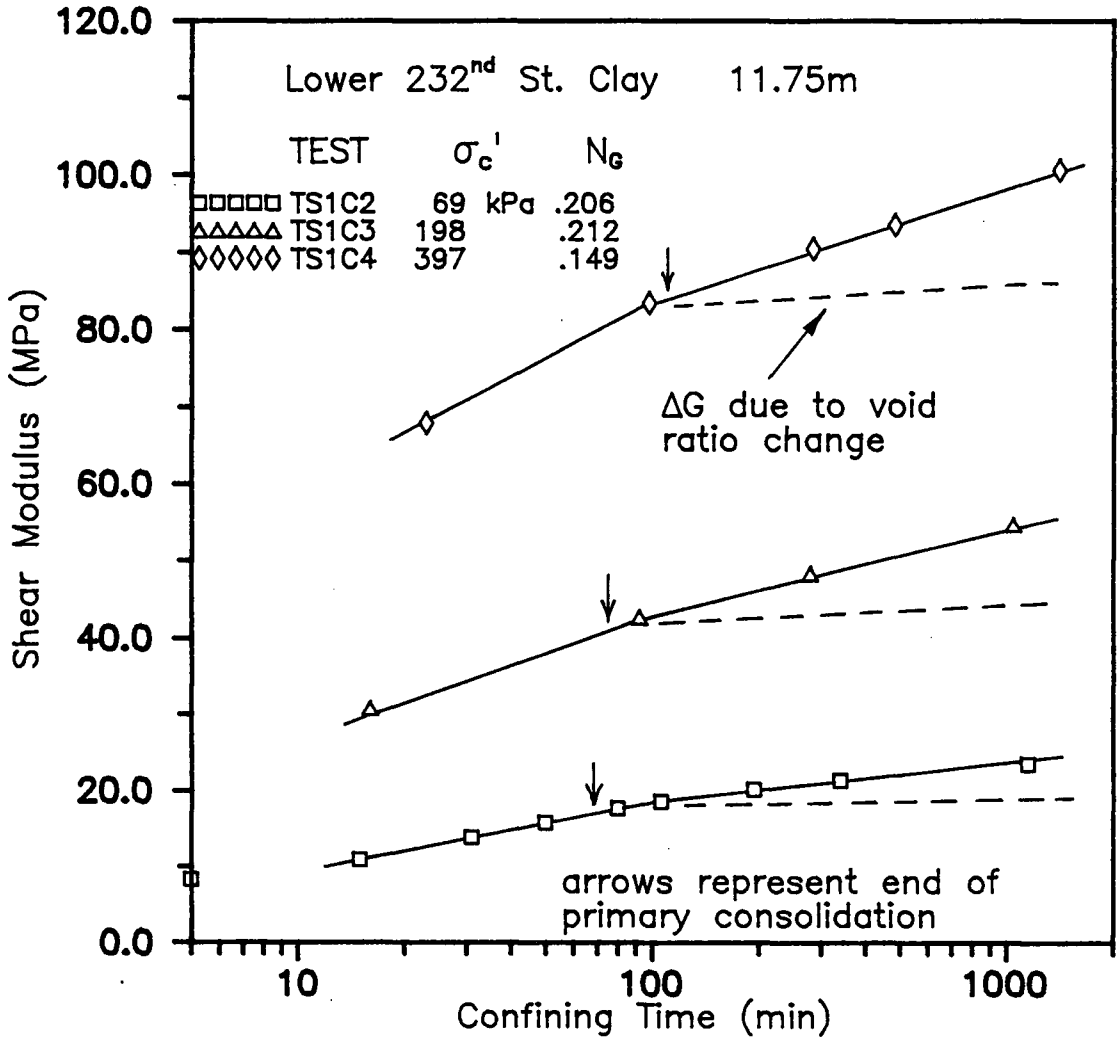

Fig. 7.14 Time-Dependent Increase in Shear Modulus for Tube Sample of Lower 232nd St. Clay

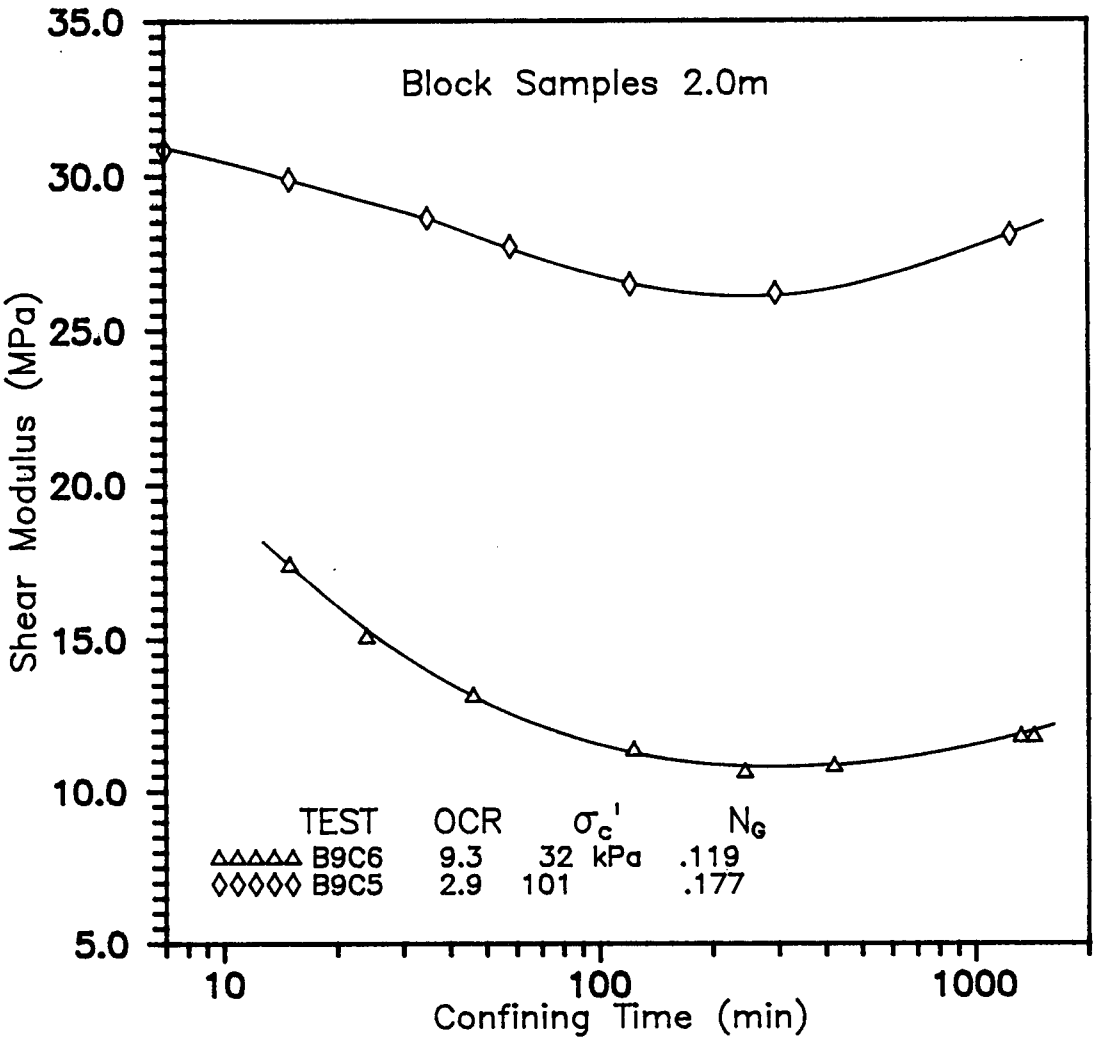

Fig. 7.15 Time-Dependent Increase in Shear Modulus for Overconsolidated Block Sample

Values of N_G determined for a number of tests are listed in Table 7.1. Values for normally consolidated tests range from 13.8 to 23.4% with an average of 18.4%. Time, therefore, must be considered when interpreting laboratory tests since the shear modulus is time dependent. Unless otherwise stated, the shear moduli reported herein are those values measured at approximately 1000 minutes of confining time.

The rate of secondary modulus increase, N_G, is such that it can not be accounted for by changes in void ratio during secondary consolidation. When these void ratio changes are considered, the increase in shear modulus estimated from Eqns. 7.3 and 7.4 is much less than that observed. This predicted increase is shown by the dashed lines in Figs. 7.13 and 7.14. Some time-dependent physio-chemical bonding may be the cause of the large secondary shear modulus increase.

Insight into the aging effect can be obtained by examining Fig. 7.16. The normalized modulus reduction curves for a block sample are shown for two different confining times (3 and 93 hours) by the open symbols. Correspondingly, the solid symbols represent the low amplitude shear modulus measured immediately after each increment of high amplitude cycling. The solid symbols therefore reflect the amount of degredation or disturbance of the soil structure bonds. No significant decrease in the low amplitude shear modulus occurs for strains less than about 0.005%. Thereafter, the degredation increases

Table 7.1 Values of N_G for Normally Consolidated Samples

TEST	σ_{3C}' (kPa)	N_G
B8C2	77.4	.234
B9C2	74.3	.184
B9C3	146.4	.222
B9C4	223.5	.187
B12C3	292.5	.138
B14C2	70.0	.164
B18C2	146.2	.197
B19C2	109.3	.145
TS1C2	69.0	.206
TS1C3	198.0	.212
TS1C4	397.0	.149

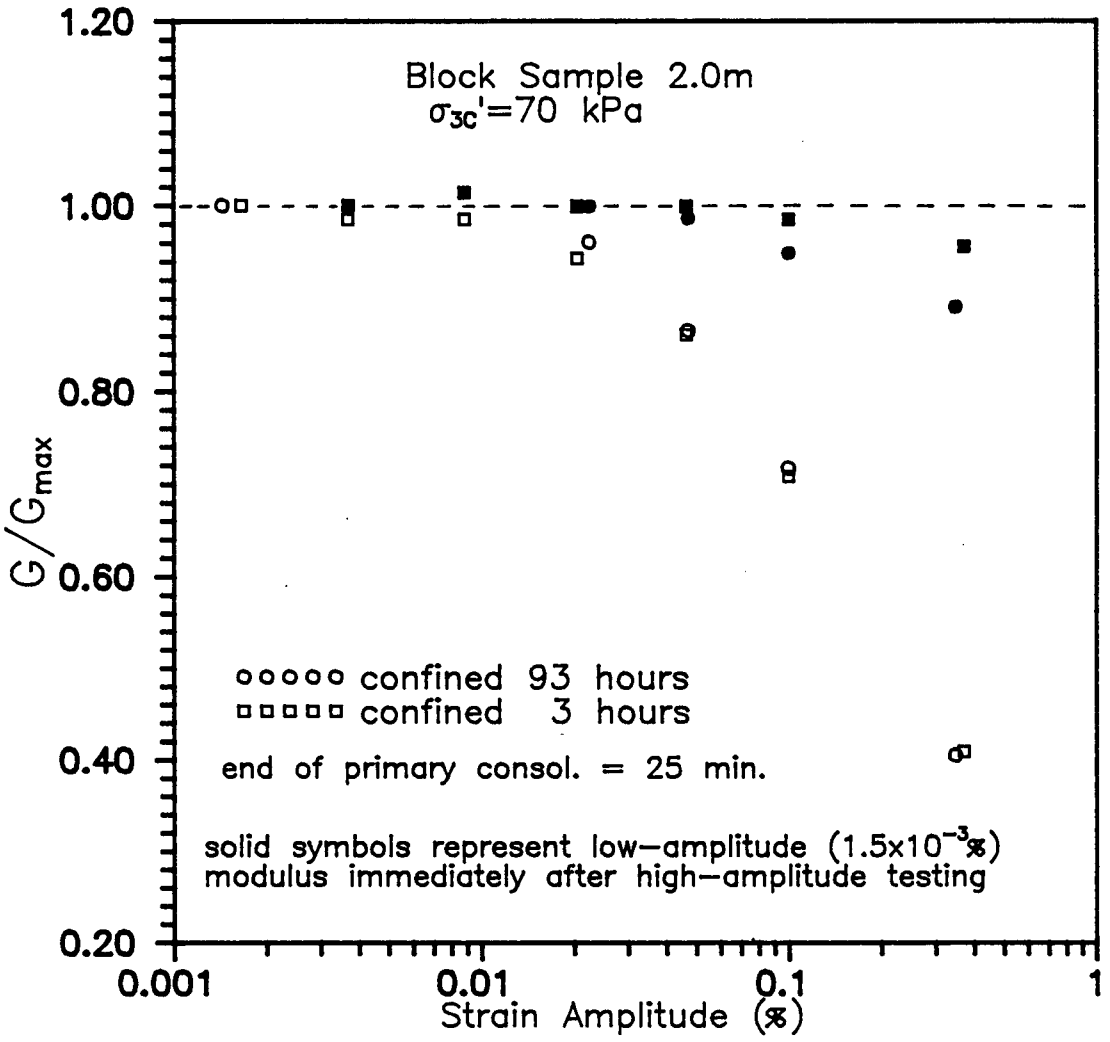

Fig. 7.16 Effect of Aging on Normalized Modulus Reduction Curves and on Low Amplitude Shear Modulus Measured After High Amplitude Testing

with shear strain amplitude. However, the amount of degredation is considerably larger for the longer confining time suggesting that proportionately more physio-chemical bonding has taken place.

It should be mentioned that the low amplitude shear modulus always recovered to its original value given a sufficient period of time after high amplitude testing, although the length of time required for recovery increased for longer confining times. The low amplitude modulus regain behaviour was also observed by Isenhower (1979) in his tests on San Francisco Bay Mud and is consistent with a time dependent physio-chemical bonding mechanism.

7.2 HIGH AMPLITUDE SHEAR MODULUS

The high amplitude shear modulus is the shear modulus corresponding to shear strains greater than about 0.005%, where the shear modulus becomes strain dependent. The factors affecting high amplitude shear modulus are discussed in the following sections.

7.2.1 Nonlinear Behaviour

In resonant column testing the method used to establish the resonant frequency of the soil sample involves sweeping a range of frequencies in order to identify the peak vibration response. A typical low-strain frequency response curve is shown by the lowermost curve in Fig. 7.17. The curve is symmetrical about the resonant frequency implying that the soil behaviour is linear elastic at small strains.

With increasing strain the frequency response curves become increasingly asymmetrical and shift to the left. The strain dependency is shown in Fig. 7.18 where the frequency response curves at three strains have been normalized by the peak amplitude. Since the shear modulus is calculated from the resonant frequency (section 4.2.1), the decrease in the resonant frequency with strain amplitude implies that the soil stiffness is non-linear. The strain softening characteristics of soils are best illustrated on a semi-logarithmic plot, known as a modulus reduction curve.

7.2.2 Effect of Shear Strain

A typical shear modulus reduction curve for a block sample of Lower 232nd St. Clay at 2.0m depth is shown in Fig. 7.19. The curve was obtained from a high amplitude test sequence in

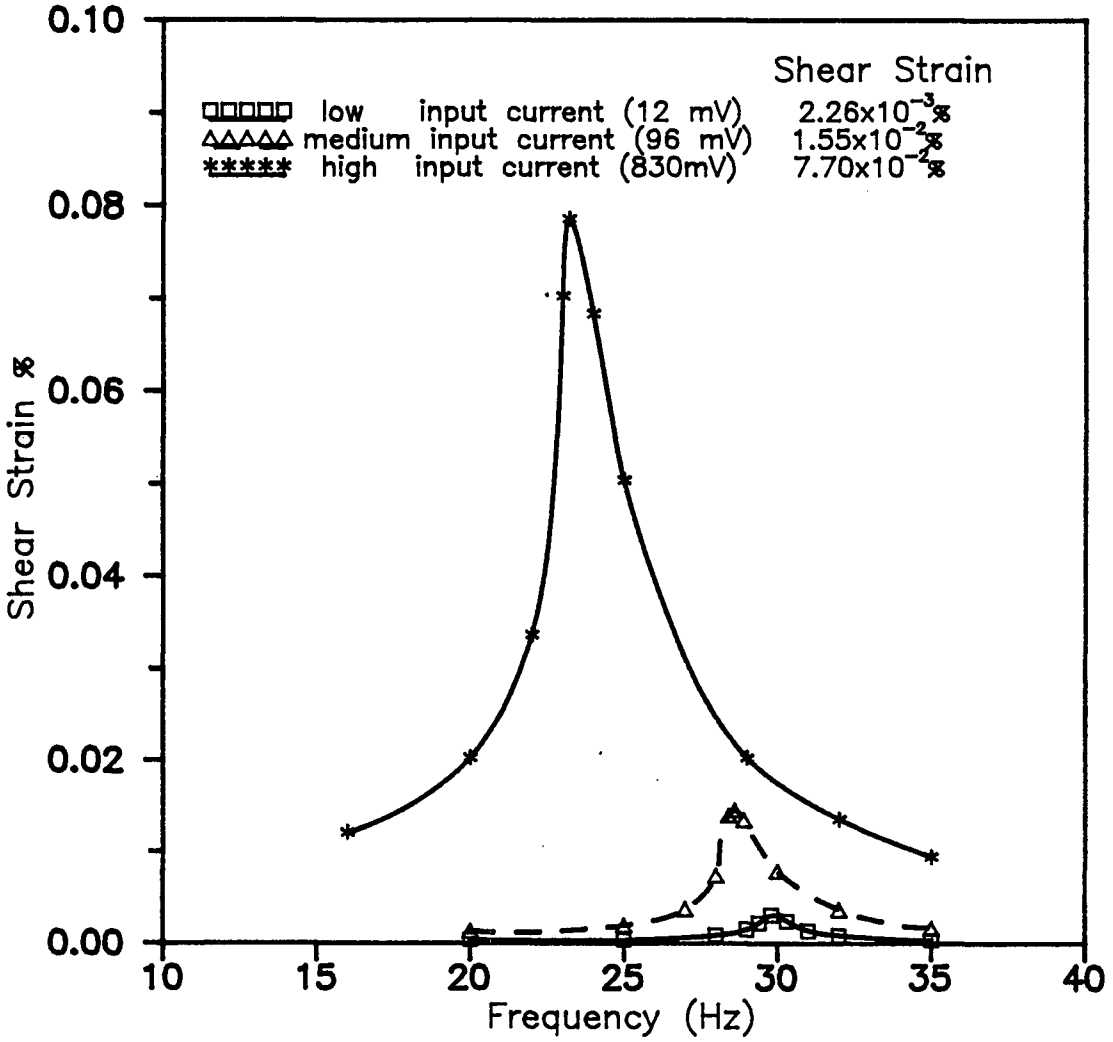

Fig. 7.17 Frequency Response Curves for Lower 232nd St. Clay for Three Strain Levels

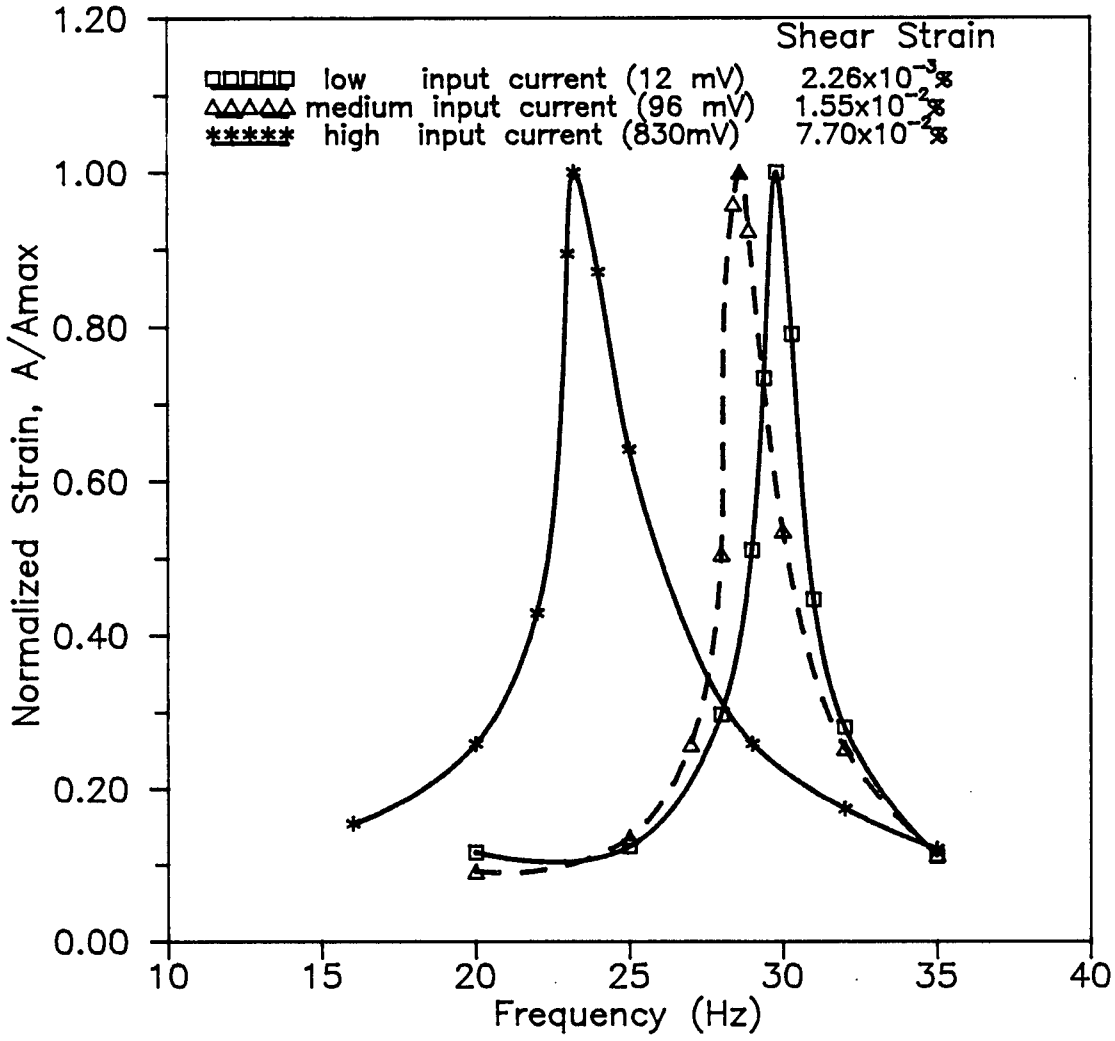

Fig. 7.18 Normalized Frequency Response Curves

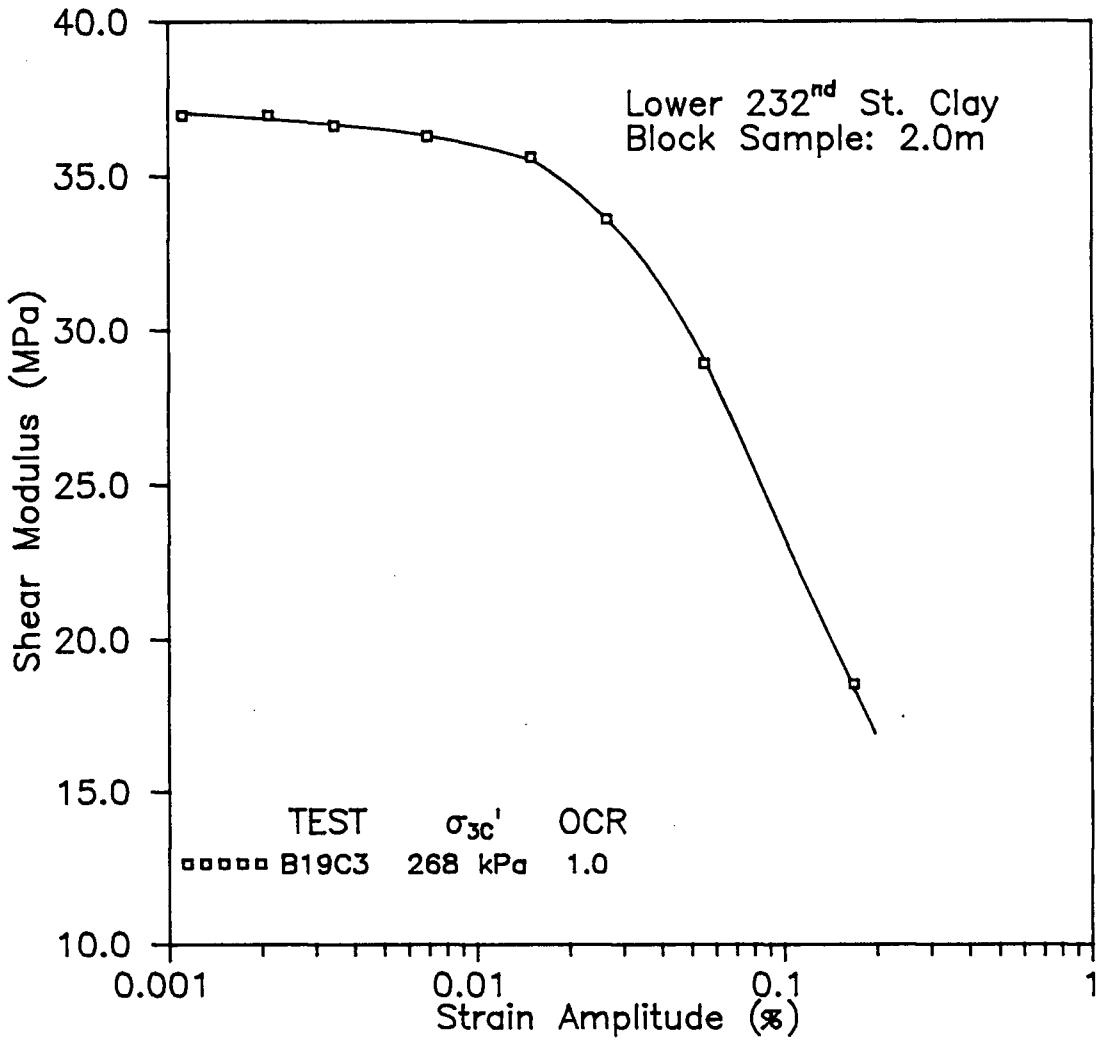

Fig. 7.19 Typical Shear Modulus vs Strain Curve for Lower 232nd St. Clay

which the shear modulus is determined first at a low strain (about 0.001%) and then at progressively larger strains. The shear modulus is approximately constant for strains less than 0.005% suggesting linear elastic behaviour in that range. For shear strains greater than 0.01%, the clay stiffness exhibits a large strain softening behaviour; indeed, the shear modulus at 0.4% strain is less than half of the constant small strain shear modulus, usually termed G_{max} or G_o. It should be noted that beyond the linear elastic threshold of 0.005%, both the frequency and strain rate vary along the curve. These effects are further discussed in section 8.1.

The shear modulus reduction curves for all successful high amplitude tests are given in Appendix A. These include the tests performed on the clay-silt from block samples at 2.0 m depth as well as tests on 2.6" diameter tube samples from various depths to 14m.

When comparing modulus reduction curves, it is often desireable to present the results in the form of a normalized modulus reduction curve in which the shear modulus at a given strain is normalized by G_{max}. Such a curve is shown in Fig. 7.16. The percent reduction in shear modulus at any strain is readily apparent since the low amplitude shear modulus has a ratio of one. Also shown in Fig. 7.16 is the small strain shear modulus (measured at 0.0015% strain) measured immediately after each increment of high amplitude

testing. The G_{max} values remain essentially the same when measured after high amplitude tests up to 0.07% strain and only a small (<5%) reduction in G_{max} occurs after the highest strain tested (about 0.4%).

This finding suggests that very little structural breakdown occurs in the clay for the range of strains tested in the resonant column. An important implication to testing procedure is that more than one high amplitude test can be carried out on the same sample without significant deterioration of the clay structure. This serves to reduce the number of samples required as well as to enable the comparison of high amplitude non-linear behaviour for various stress and time conditions on the same sample, therby eliminating some problems with sample differences.

7.2.3 Effect of Confining Pressure and Stress History

For the block samples obtained from a depth of 2.0 m with PI ranging from 33 to 61, there is essentially no influence of effective confining stress (50 to 500 kPa) and overconsolidation ratio (1.0 to 9.3) on the normalized modulus reduction curve. This can be seen in Fig. 7.20 where the normalized modulus values for a wide range of stress states fall on a single curve. Thus, knowing the shape of the normalized modulus reduction curve allows the high amplitude

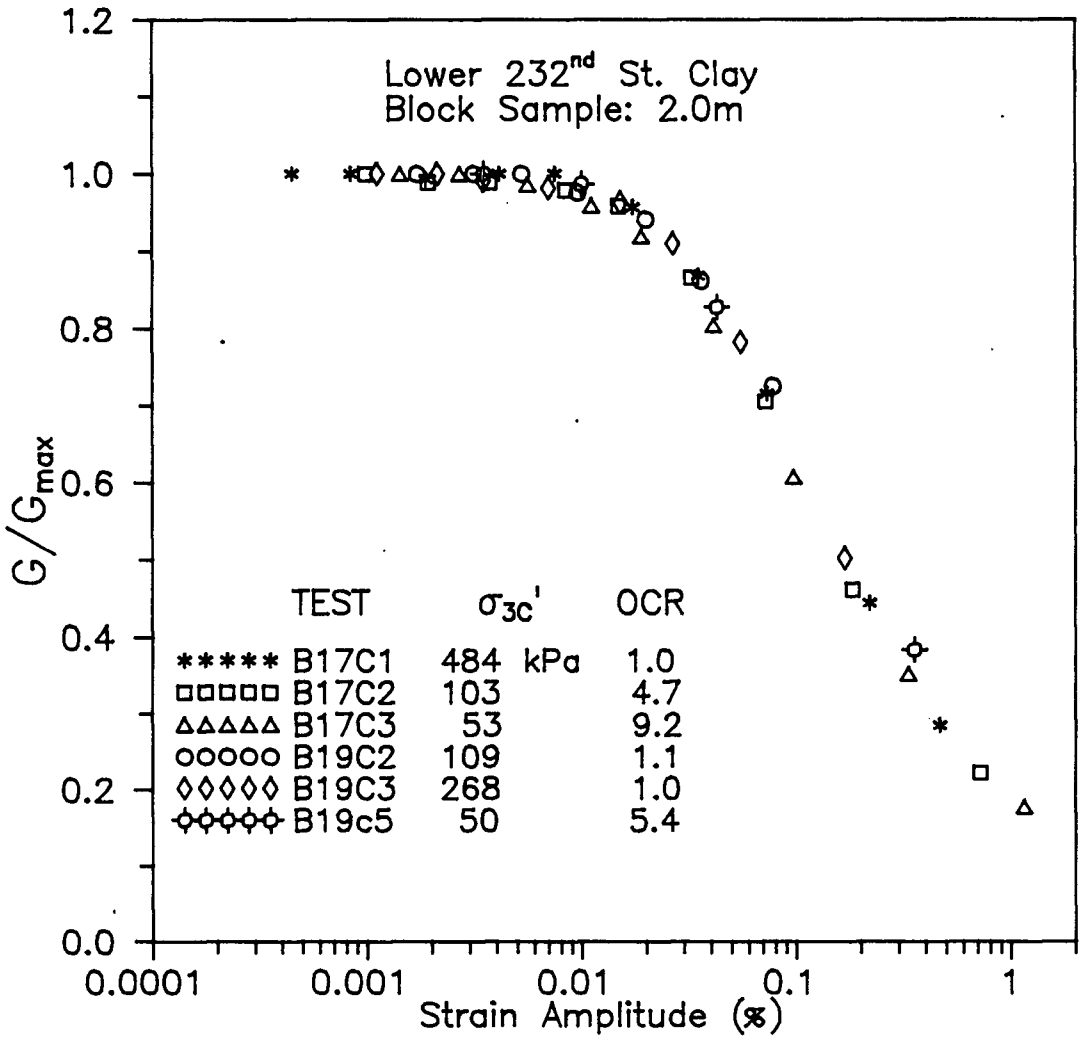

Fig. 7.20 Normalized Modulus Reduction Curves for Block Samples

shear modulus to be predicted for a wide range of effective confining stress and OCR values if the low amplitude shear modulus for the particuluar stress state is known.

The normalized modulus reduction curves for samples from depths of 11.75 and 13.2 m are shown for several effective confining pressures in Figs. 7.21 and 7.22, respectively. These samples have PI's between 20 and 25. A small effect of confining pressure is seen for both depths in the 0.01-0.1% range of strain amplitudes where the strain amplitude values are still fairly accurate. Above 0.1% strain, differences in the number of cycles shift the G/G_{max} values so as to obscure the effect of confining pressure. Nevertheless, it can be seen that higher confining pressures in the 0.01%-0.1% range shift the modulus reduction curve to the right. Also shown in Fig. 7.21 is the modulus reduction curve for an overconsolidated sample (OCR=3.9) which suggests little effect of stress history on the normalized modulus values.

It appears that the differences in plasticity between the block samples and the tube samples affect the normalized modulus curves. These results agree with those summarized by Sun et al. (1988) in which the influence of confining pressure on the normalized modulus reduction curve was shown to gradually diminish with increasing plasticity index.

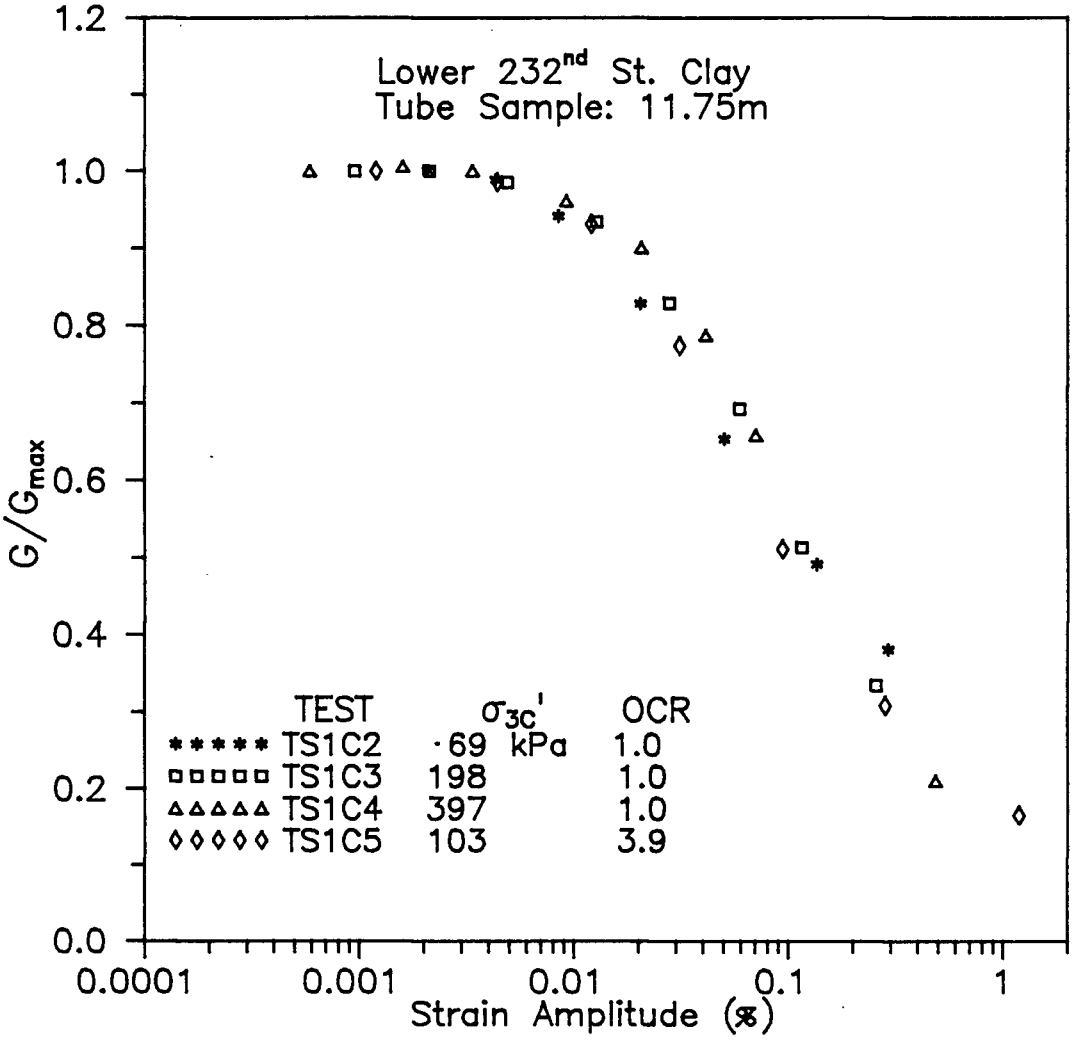

Fig. 7.21 Normalized Modulus Reduction Curves for Tube Samples from 11.75m

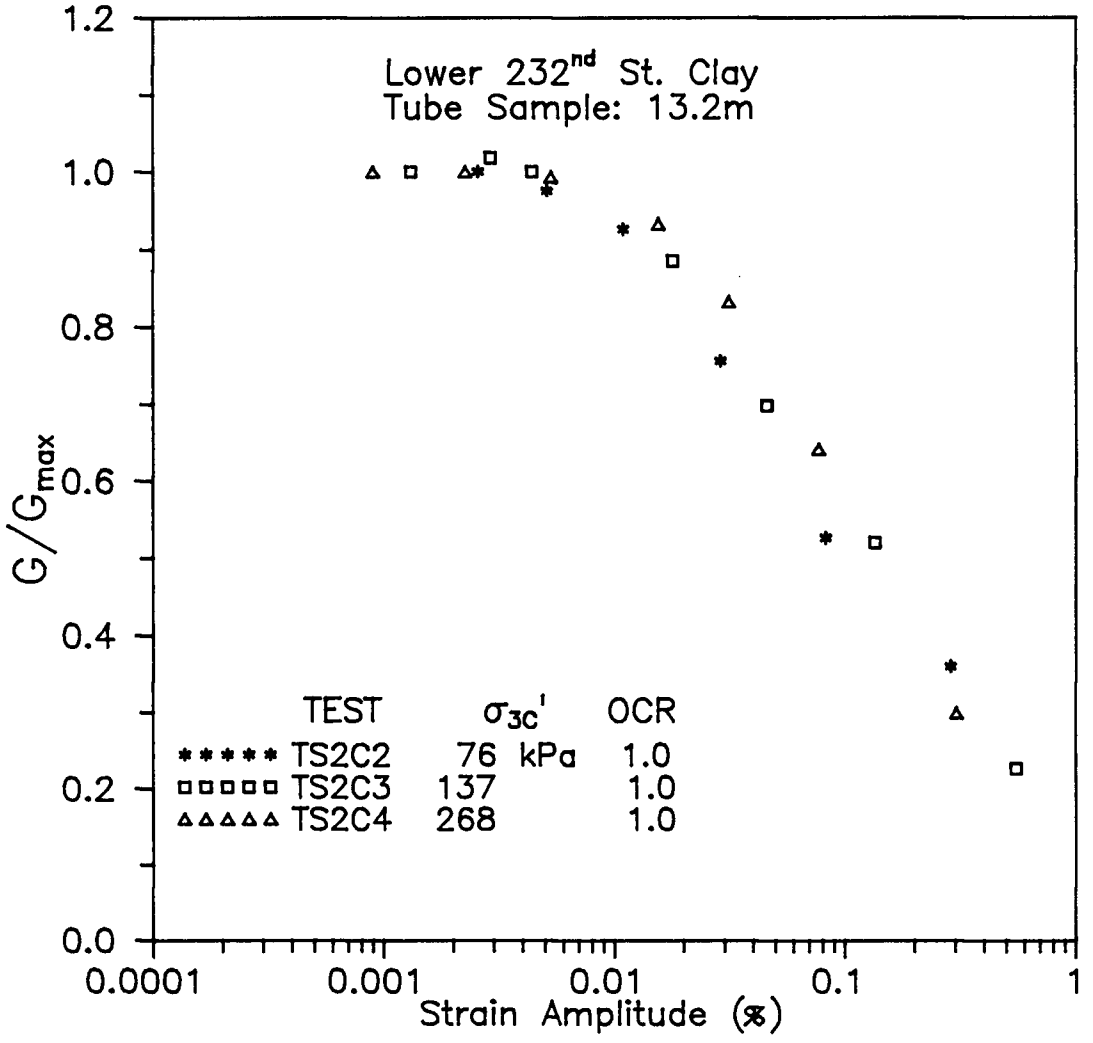

Fig. 7.22 Normalized Modulus Reduction Curves for Tube Samples from 13.2m

7.2.4 Secondary Time Effects

Based on Fig. 7.16 it may be concluded that the duration of confinement has virtually no effect, within the range investigated, on the normalized modulus reduction curve. The reason for this can be seen from Fig. 7.23 where the normalized rate of shear modulus increase, N_g, defined in Eq. 7.9 is essentially independent of strain amplitude. Thus, both the small strain and large strain amplitude moduli increase at about the same rate leaving their ratio (G/G_{max}) unchanged.

In summary, for the Lower 232nd St. Clay studied there is relatively little influence of confining stress, stress history, and secondary time effects on the normalized shear modulus reduction curves, especially for the higher plasticity block samples obtained from a depth of 2.0m. For the tube samples, a small shift of the curves to the right occurs with increasing confining stress.

7.3 LOW-AMPLITUDE DAMPING RATIO

As with the shear modulus presented in sections 7.1 and 7.2, damping ratio is presented seperately in terms of low amplitude and high amplitude results.

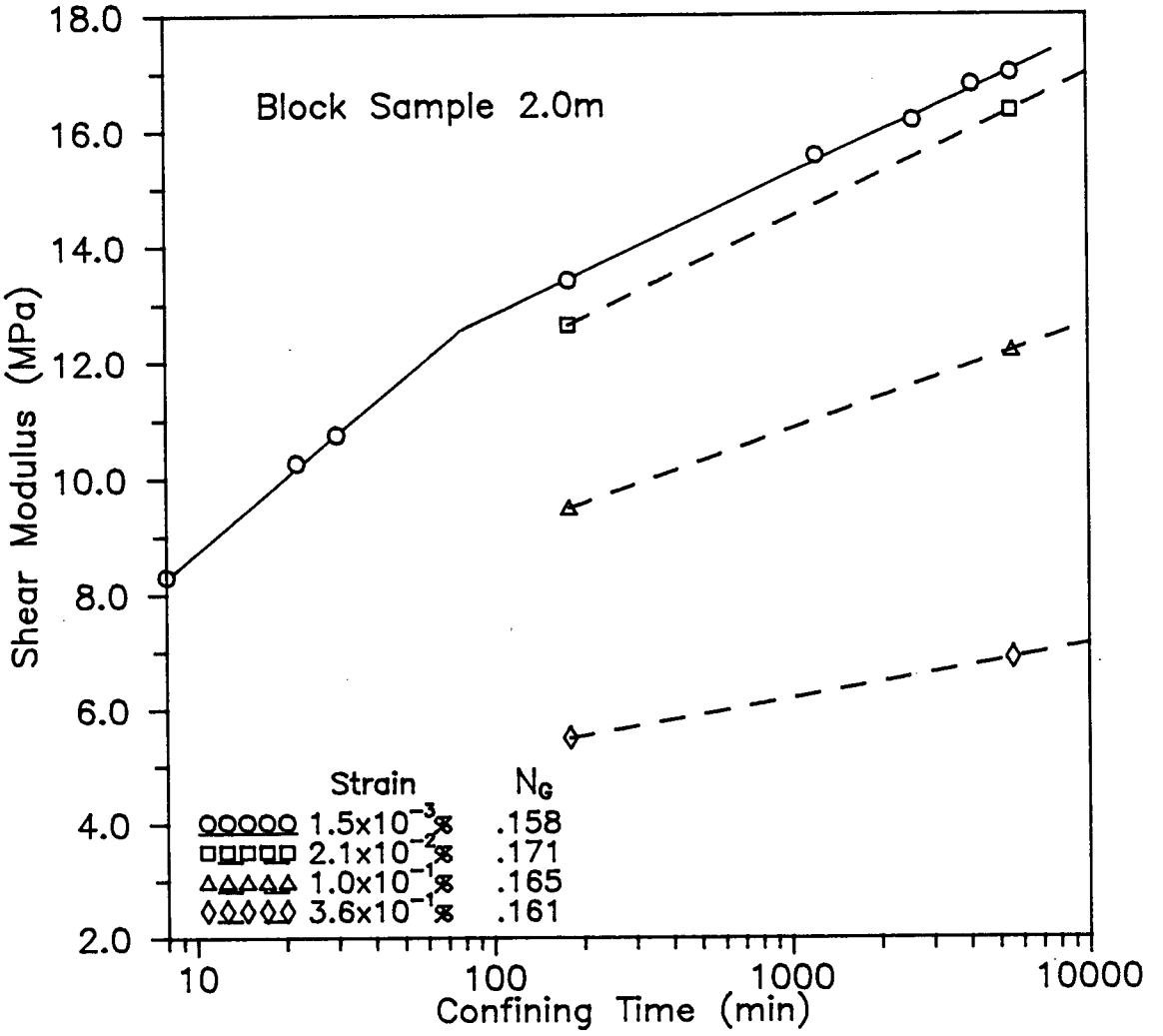

Fig. 7.23 Time-Dependent Increase in Shear Modulus for Various Strain Levels

7.3.1 Effect of Confining Pressure and Stress History

The low amplitude damping ratio for three block samples of Lower 232nd St. Clay are shown in Fig. 7.24 for a wide range of effective confining stress and OCR values. Very little influence of confining stress or stress history is seen on the low amplitude damping ratio, which is determined at a strain of 0.001% by the amplitude decay method. Regardless of the state of stress, the damping ratio for all tests shown is between 1.0 and 1.7%.

On the other hand, the damping ratio values determined from the tube samples, which are of lower plasticity, decrease with confining pressure (Fig. 7.25). Based on the limited data, it appears that the damping ratio decreases in direct proportion to the increase in confining stress. However, damping ratio differences between individual samples are greater than the effect of confining pressure over the range tested. Considering the range in confining pressure and OCR values, the 0.9% to 2.4% range in damping for the tube samples is relatively narrow. The damping ratios presented herein are those values determined at approximately 1000 minutes of confinement.

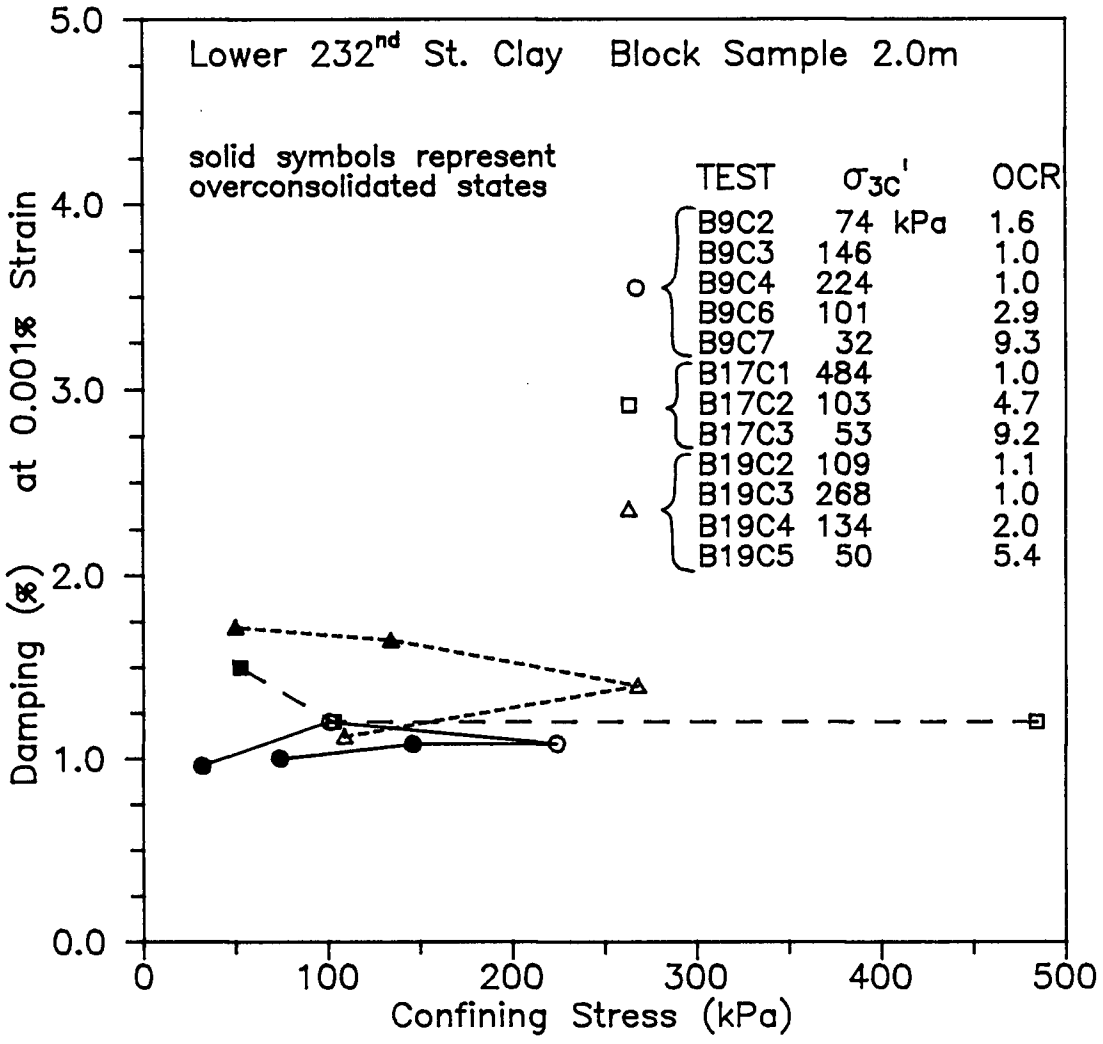

Fig. 7.24 Variation of Low Amplitude Damping Ratio with Effective Confining Stress for Block Samples

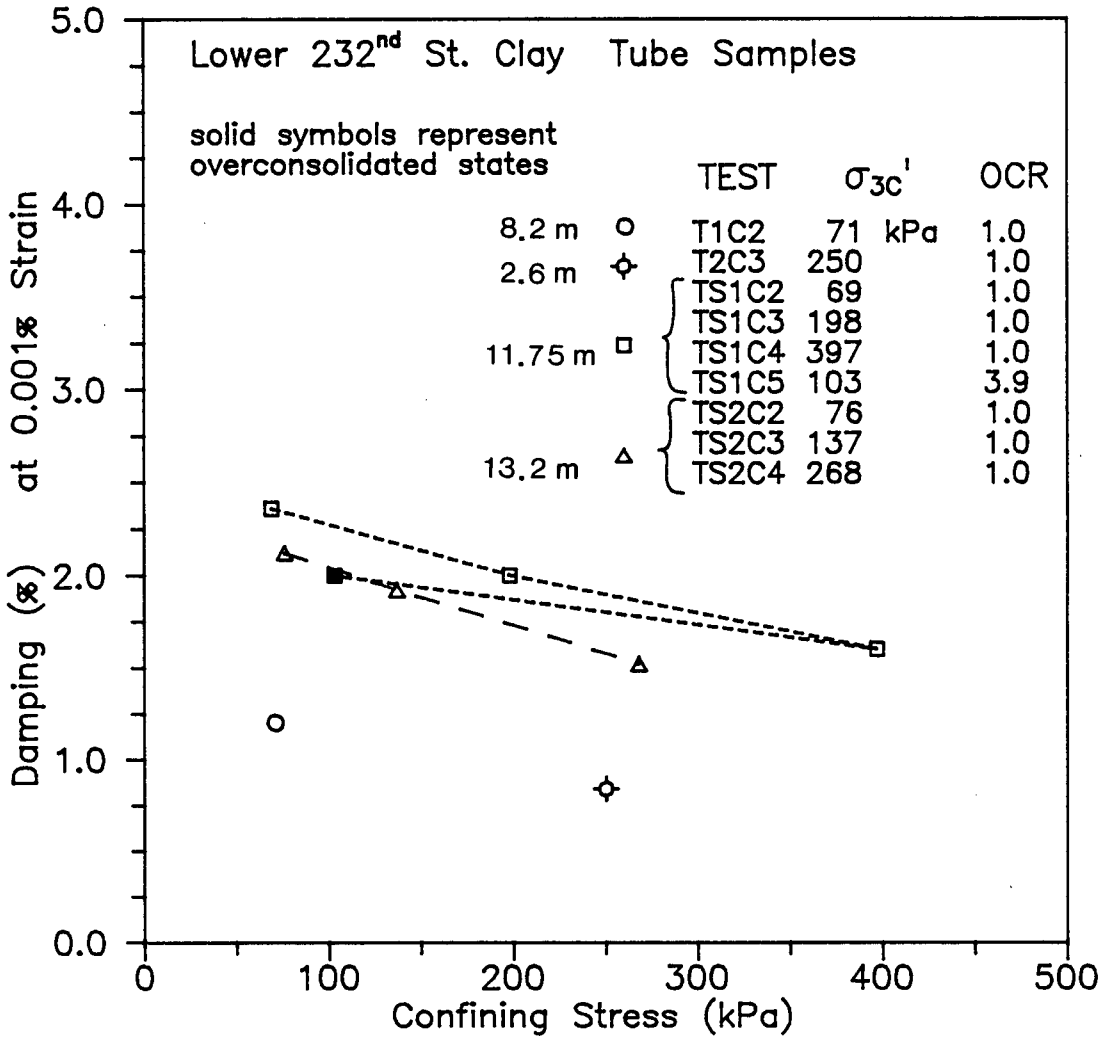

Fig. 7.25 Variation of Low Amplitude Damping Ratio with Effective Confining Stress for Tube Samples

7.3.2 Secondary Time Effects

To study the time dependent decrease in damping ratio modulus at constant effective confining stress, damping measurements for a number of tests were taken well beyond the time required for completion of primary consolidation.

The decrease in damping ratio with the logarithm of time is shown in Fig. 7.26 for a block sample of Lower 232nd St. Clay from a depth of 2.0 m. For all five stress states shown, the damping ratio determined by the steady state method decreases linearly with the logarithm of time. However, for the two unloading increments shown, the damping ratio remains constant until the completion of swelling and decreases thereafter. In all cases, swelling or consolidation was complete before 250 minutes.

The rate of secondary decrease in damping ratio, N_d, can be quantified by

$$N_d = \Delta D / D_{1000} \qquad (7.10)$$

where ΔD = secondary decrease in damping ratio per log cycle of time

D_{1000} = damping ratio determined at 1000 minutes of confinement

The value of N_d is shown in Fig. 7.26 for each stress state. Values range from 39-60% which suggests that the damping has an

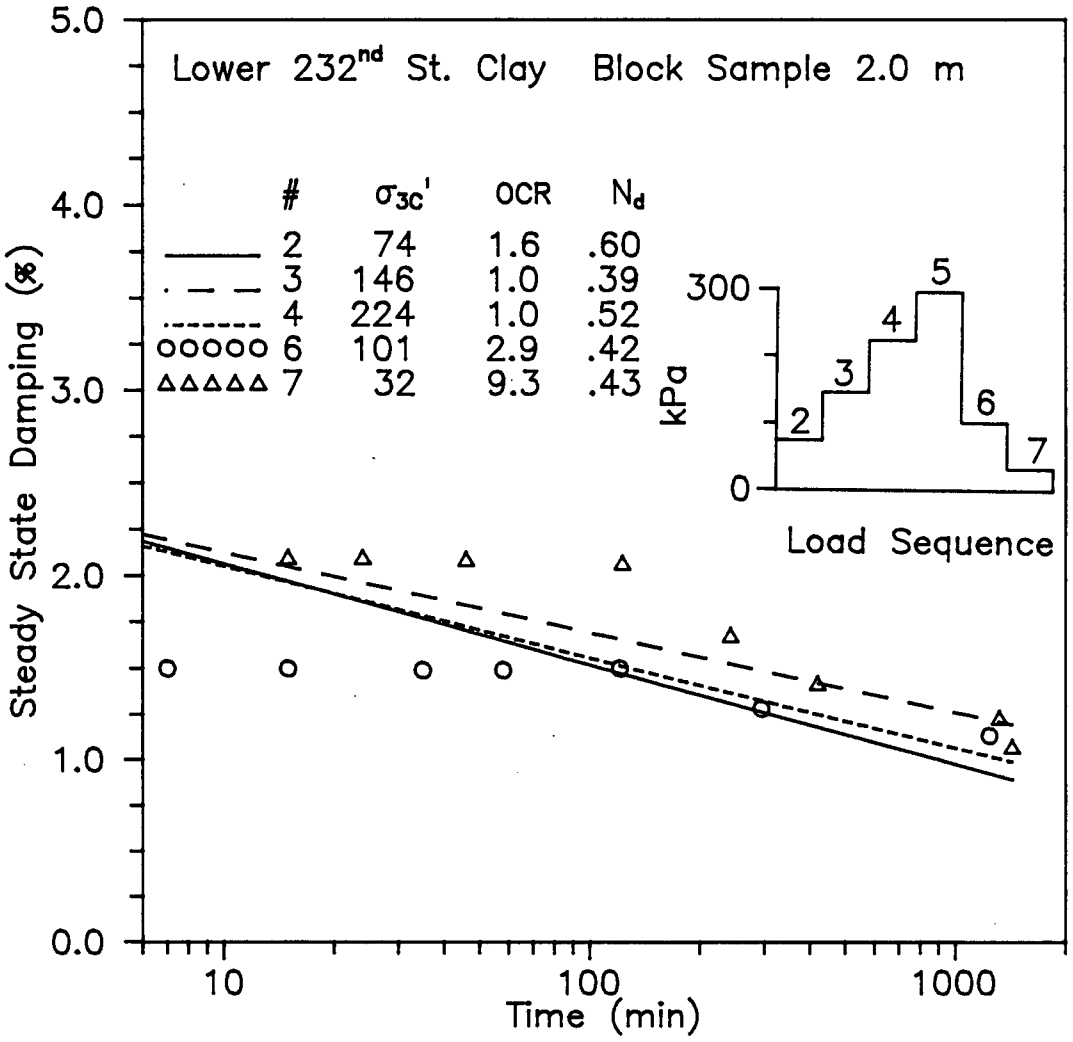

Fig. 7.26 Decrease in Damping Ratio with Time for Block Samples

even greater relative time dependency than the 14-23% determined for shear modulus.

For tube samples, the time dependent damping response is much the same as that identified for the block samples. Referring to Fig. 7.27, the normalized rate of damping decrease, N_d, ranges from about 35-43% per log cycle of time.

The N_d values determined from a number of tests are shown in Table 7.2 along with the respective OCR and effective stress values. The range in N_d values is 15-60% with an average of 38%. This corresponds to a decrease in damping ratio of approximately 0.5% per log cycle of time (in minutes) which compares quite well to the 0.4-0.7% decrement of damping ratio identified by Kokusho et al. (1982) in their tests on Teganuma Clay.

Applying an increment of confining pressure erases much of the aging effect of the previous confining pressure. This is evident from Figs. 7.26 and 7.27 where the damping ratio always increases after a change in confining pressure and decreases with time thereafter.

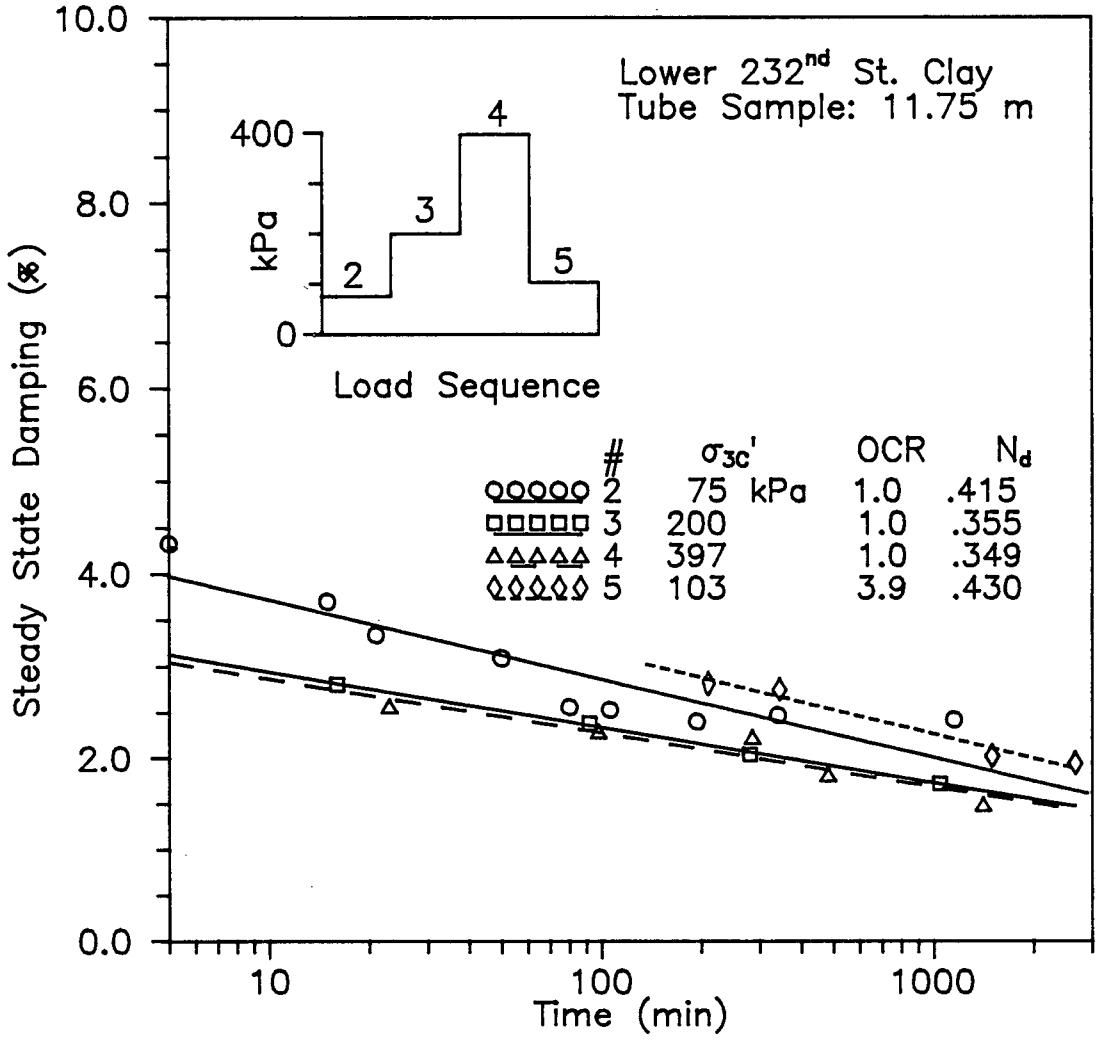

Fig. 7.27 Decrease in Damping Ratio with Time for Tube Samples

Table 7.2 Values of N_d for Samles at Various σ_{3C}' and OCR

TEST	σ_{3C}' (kPa)	OCR	N_d
B8C2	77.4	1.0	.350
B9C2	74.3	1.6	.600
B9C3	146.4	1.0	.388
B9C4	223.5	1.0	.515
B9C6	101.0	2.9	.421
B9C7	32.0	9.3	.429
B12C3	292.5	1.0	.152
B14C2	70.0	1.7	.207
B19C2	109.3	1.0	.515
TS1C2	75.0	1.0	.415
TS1C3	198.0	1.0	.355
TS1C4	397.0	1.0	.349
TS1C5	103.0	3.9	.430

7.4 HIGH-AMPLITUDE DAMPING RATIO

7.4.1 Effect of Strain and Nonlinearity

A typical high amplitude damping curve for lower 232nd St. Clay is given in Fig. 7.28 with values given by both the steady state and amplitude decay methods. The strain amplitude reported for tests employing the amplitude decay method is that immediately prior to power cutoff (ie. the maximum value). At shear strains less than 0.01%, both methods give essentially the same constant low amplitude damping value. But, with increasing strain the steady state method gives a smaller damping attenuation than the amplitude decay method. This high amplitude discrepancy occurred in virtually all high amplitude tests conducted in this study as well as in tests previously performed on sand. Since the steady state method assumes a symmetrical frequency response curve which is not a good assumption for high amplitude tests, the amplitude decay method is preferable.

As discussed in section 7.2.1, the frequency response of a soil sample becomes nonlinear as the strains exceed a threshold value of approximately 0.005%. Similarly, the calculation of damping ratio will be affected by the nonlinear response.

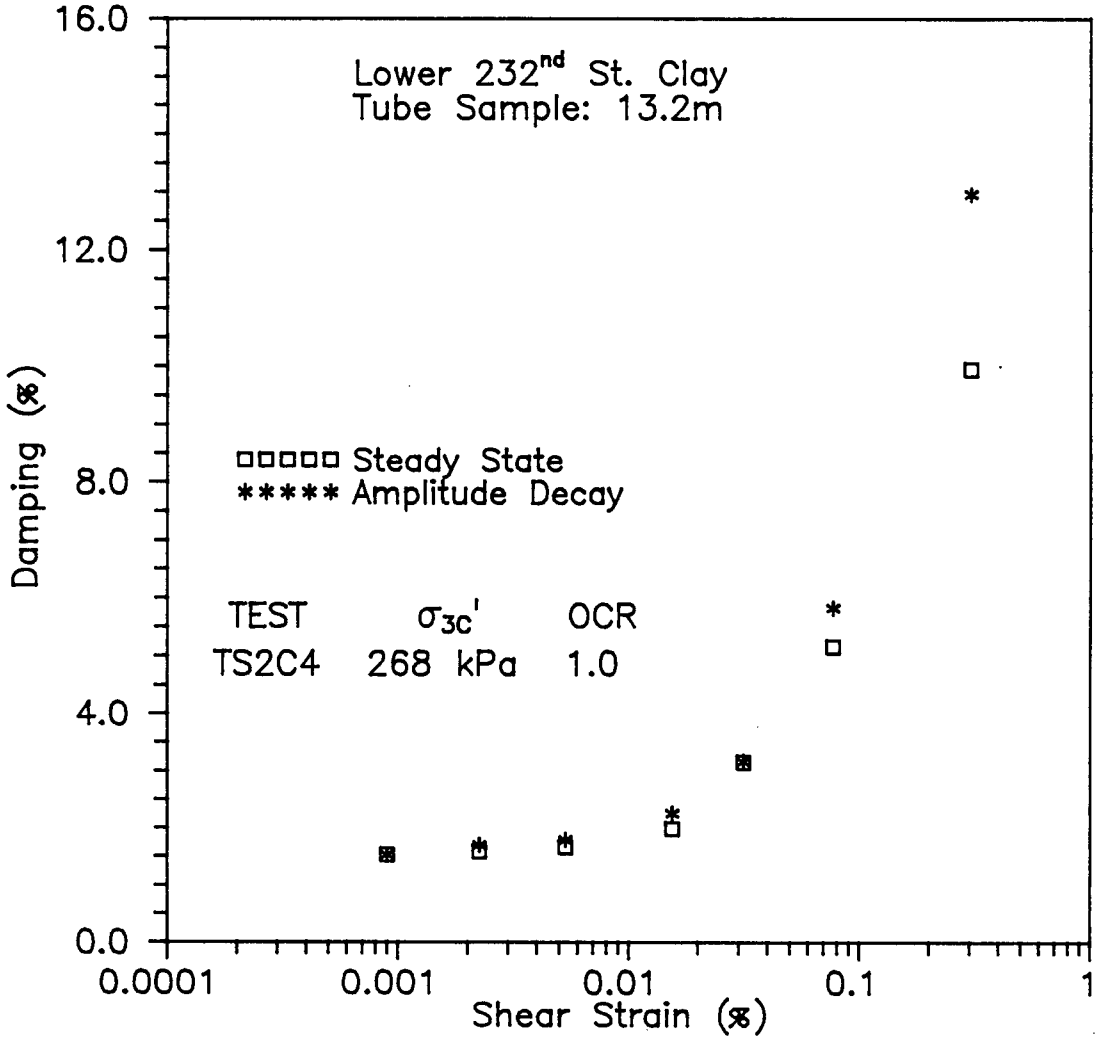

Fig. 7.28 Steady State and Amplitude Decay Damping vs. Shear Strain

In the amplitude decay of free vibrations method discussed in section 4.3.2.1, the damping ratio is calculated from the logarithmic decrement of free vibrations monitored after the driving current is turned off. The damping ratio is calculated from Eq. 4.9 in which the logarithmic decrement, d, is assumed to be constant in order to yield a unique value of damping ratio. However, for strains in excess of the threshold value the logarithmic decrement will not be unique but will vary with the number of free vibration cycles selected. This effect can be seen in Fig. 7.29 where the normalized amplitude is plotted on a logarithmic axis against the number of free vibration cycles. The normalized amplitude is the peak accelerometer output for a particular cycle divided by the peak accelerometer output prior to drive current cutoff. The logarithmic decrement becomes increasingly nonlinear with number of cycles as the shear strain increases. In order to minimize the effect of such nonlinearity on the calculated damping ratio, the logarithmic decrement for all tests was established at a normalized amplitude of 0.2 to 0.3 where the deviation from the initial linear logarithmic decrement is negligible for all strains, within the range tested (Fig. 7.29).

Since the decay of free vibrations is determined from the accelerometer response, it is not the true displacement response required by Eq. 4.8 in the calculation of damping. However, this introduces only a small error as the displacement and acceleration are essentially related by a constant for any

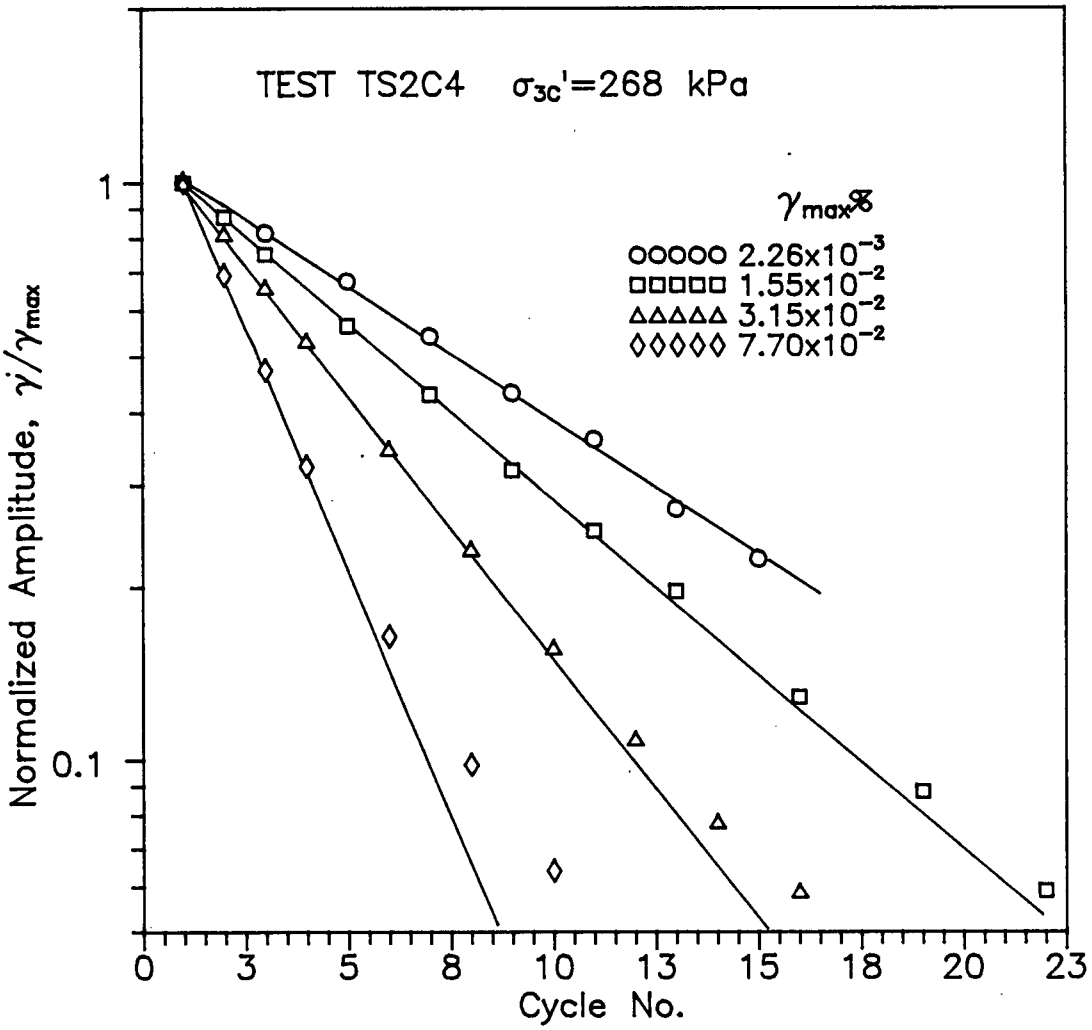

Fig. 7.29 Effect of Non-Linearity on determination of Amplitude Decay Damping

particular test. As can be seen in Fig. 7.30 the shapes of the accelerometer decay and rotational displacement (RVDT) decay curves are virtually identical. In tests where the rotational transducer was used, very good agreement between the curves was observed for both high strain and low strain tests confirming that the use of the accelerometer decay curve to determine the material damping ratio is a valid procedure.

7.4.2 Effect of Confining Pressure and Stress History

The influence of confining pressure and stress history on the high amplitude material damping can be evaluated by comparing the damping attenuation curves at different stress states. Damping attenuation curves for all high amplitude tests are includes in Appendix B.

For block samples stage tested, there is no noticeable inluence of effective confining pressure and stress history on the damping attenuation curves, within the range tested. This is clearly evident in Fig. 7.31 where the damping data from different samples and testing conditions fall on the same curve. Thus, a single damping attenuation curve can be extended to apply to a wide range of confining stress and OCR values. Since the corresponding normalized modulus reduction values formed a unique curve (Fig. 7.20), the use Eq. 2.8 to relate high amplitude shear modulus and damping appears

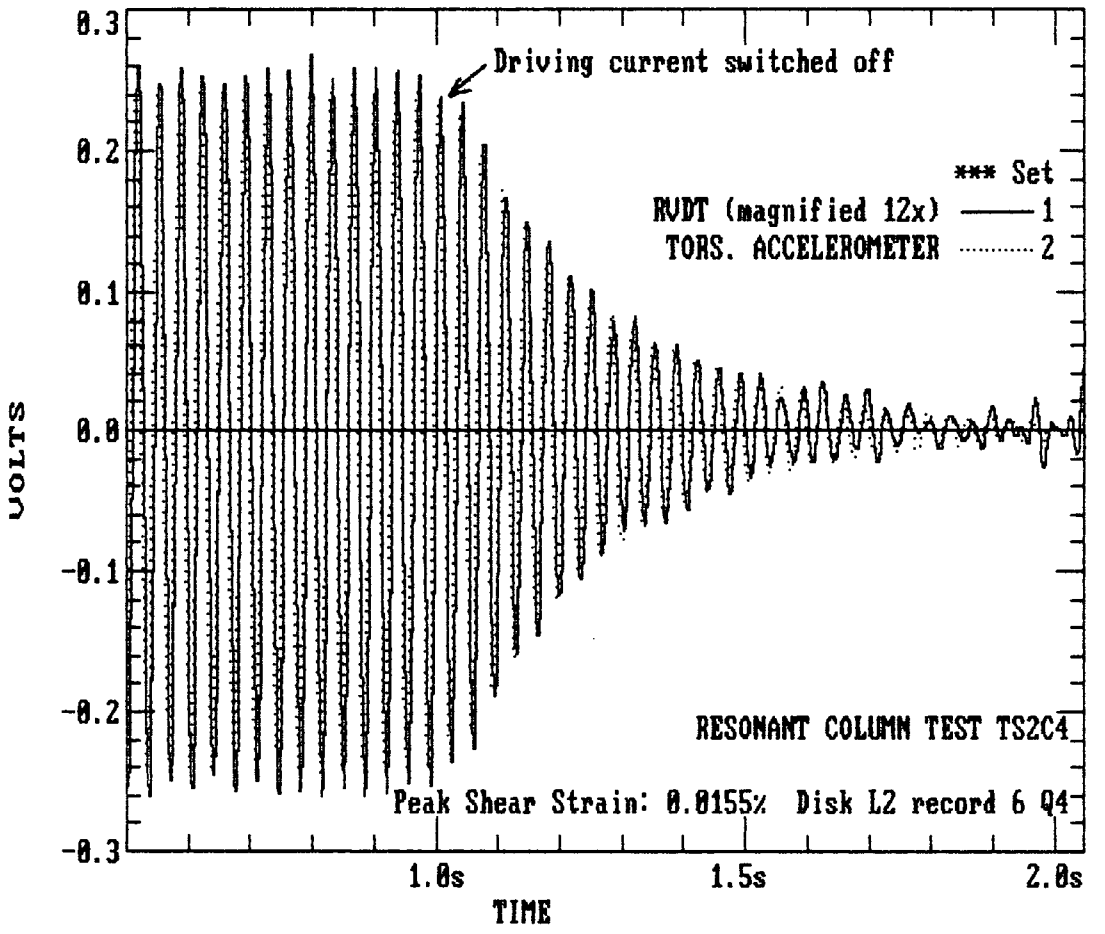

Fig. 7.30 Comparison of Accelerometer and RVDT Decay Response

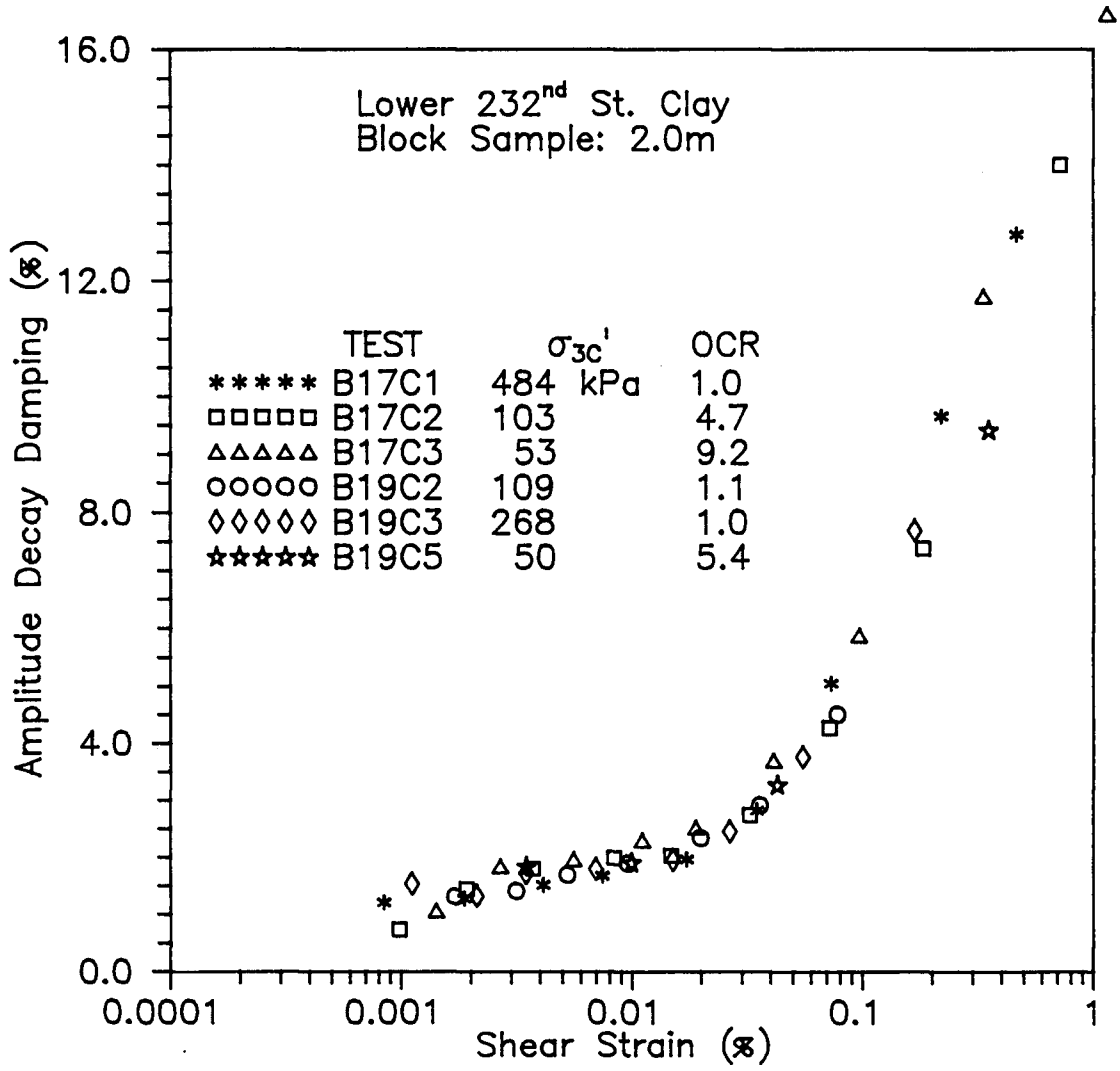

Fig. 7.31 Damping vs. Shear Strain for Block Samples at Various Confining Pressures and OCR

reasonable, though Eq. 2.8 incorrectly suggests a low amplitude damping of zero when $G=G_{max}$.

However, stage tested tube samples obtained from depths of 11.75 m and 13.2 m show some dependence of damping ratio on the effective confining stress (Fig. 7.32). Generally, the higher the confining pressure the lower the damping attenuation curve; this effect is masked by differences in the number of loading cycles for strains greater than about 0.1%.

Also shown in Fig. 7.32 is the damping attenuation curve identified for the tests on block samples in Fig. 7.31. The comparison indicates that the higher plasticity block samples have a lower damping ratio for the entire range of strains tested. The shape of the modulus attenuation curves for both types of samples, however, is essentially the same. These findings are very similar to those established by Kokusho et al. (1982) in their tests on Teganuma Clay.

7.4.3 Secondary Time Effect

Although a comprehensive series of tests to establish the effect of confinement time on the high amplitude damping ratio were not performed, it nevertheless appears that aging has an effect on the high amplitude damping. Based on the limited data it appears that the duration of confinement influences not

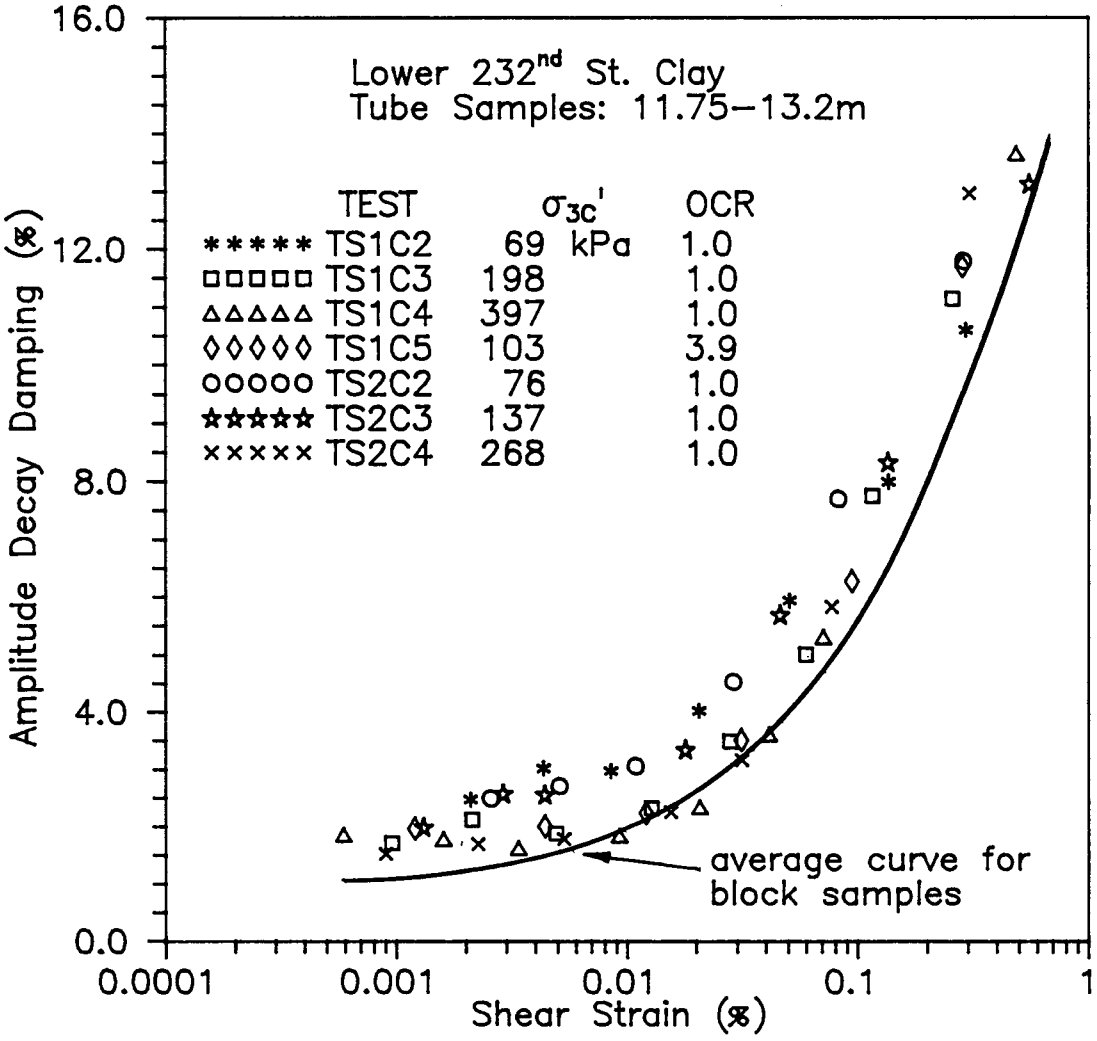

Fig. 7.32 Damping vs. Shear Strain for Tube Samples at Various Confining Pressures and OCR

only the low amplitude damping ratio (section 7.3.2) but also the high amplitude values (Fig. 7.33); longer confining times decrease the damping ratio over the entire strain range tested. Therefore it may be possible to use the "unaged" damping attenuation curve along with the "aged" low amplitude damping value in order to establish the aged high amplitude damping ratio.

7.5 PORE PRESSURE RESPONSE

In saturated soil subjected to a cyclic stress-strain history, excess pore pressures may develop thereby reducing the shear resistance of the soil. It is therefore of interest to examine the relationship between excess pore pressures and factors such as confining pressure and shear strain amplitude.

During resonant column testing, dynamic pore pressures are rarely reported because of the fast rate of torsional loading which results in a non-uniform pore pressure distribution within the specimen. However, if pore pressures are allowed to equalize between vibration intervals, an indication of the magnitude of the pore pressure response may be obtained from the residual excess pore pressure.

For several tests the excess pore pressure was monitored both during and after the usual one minute vibration interval,

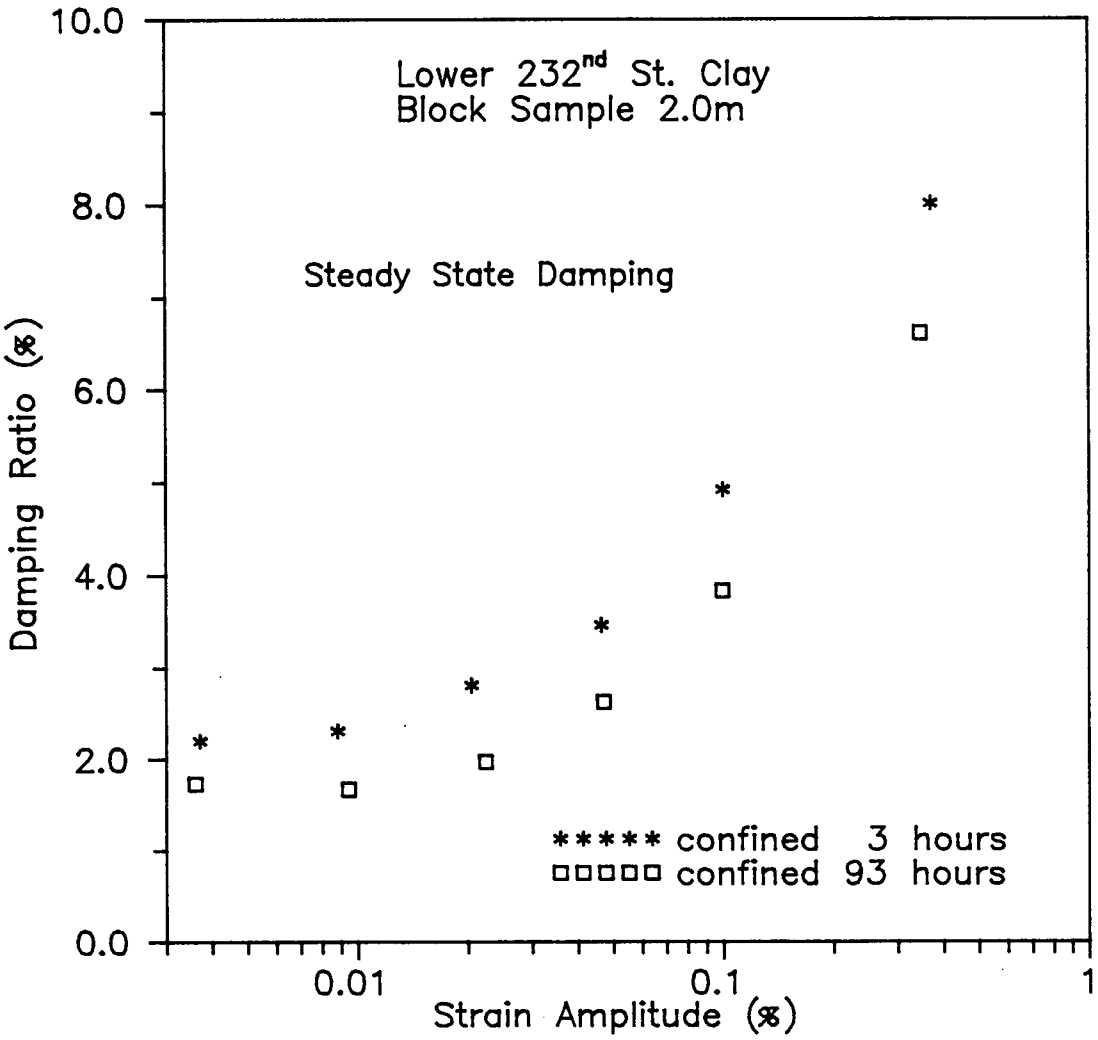

Fig. 7.33 Effect of Duration of Confinement on High Amplitude Damping

until a steady value was obtained. One minute of vibration corresponds to 600 to 1800 cycles, depending on the resonant frequency which in turn depends primarily on the strain amplitude and confining pressure. The pore pressure response for a block sample of Lower 232nd St. Clay is shown in Fig. 7.34 for four levels of shear strain. For each strain level, some time beyond the end of the vibration interval is required for the pore pressures to reach a steady value. This was generally achieved within five minutes after cycling was terminated. The residual value of excess pore pressure increases with increasing strain amplitude. Precisely the same behaviour is seen for a tube sample from a depth of 8.2m (Fig. 7.35). Overconsolidated samples, however, displayed a dilatent behaviour showing increasingly negative excess pore pressures with strain amplitude (Fig. 7.36).

Six specimens normally consolidated at effective confining pressures ranging from 72 kPa to 486 kPa were subjected to shear strains as high as 1.0%. Figure 7.37 shows the relationship between the shear strain and the residual excess pore pressure, u, normalized by the effective confining pressure. Again, it should be noted that the residual pore pressures are those resulting from about 600 to 1800 vibration cycles (one minute of vibration), depending on the resonant frequency of the sample which in turn depends primarily on the confining pressure and shear strain amplitude. All six specimens show essentially the same behaviour with very little

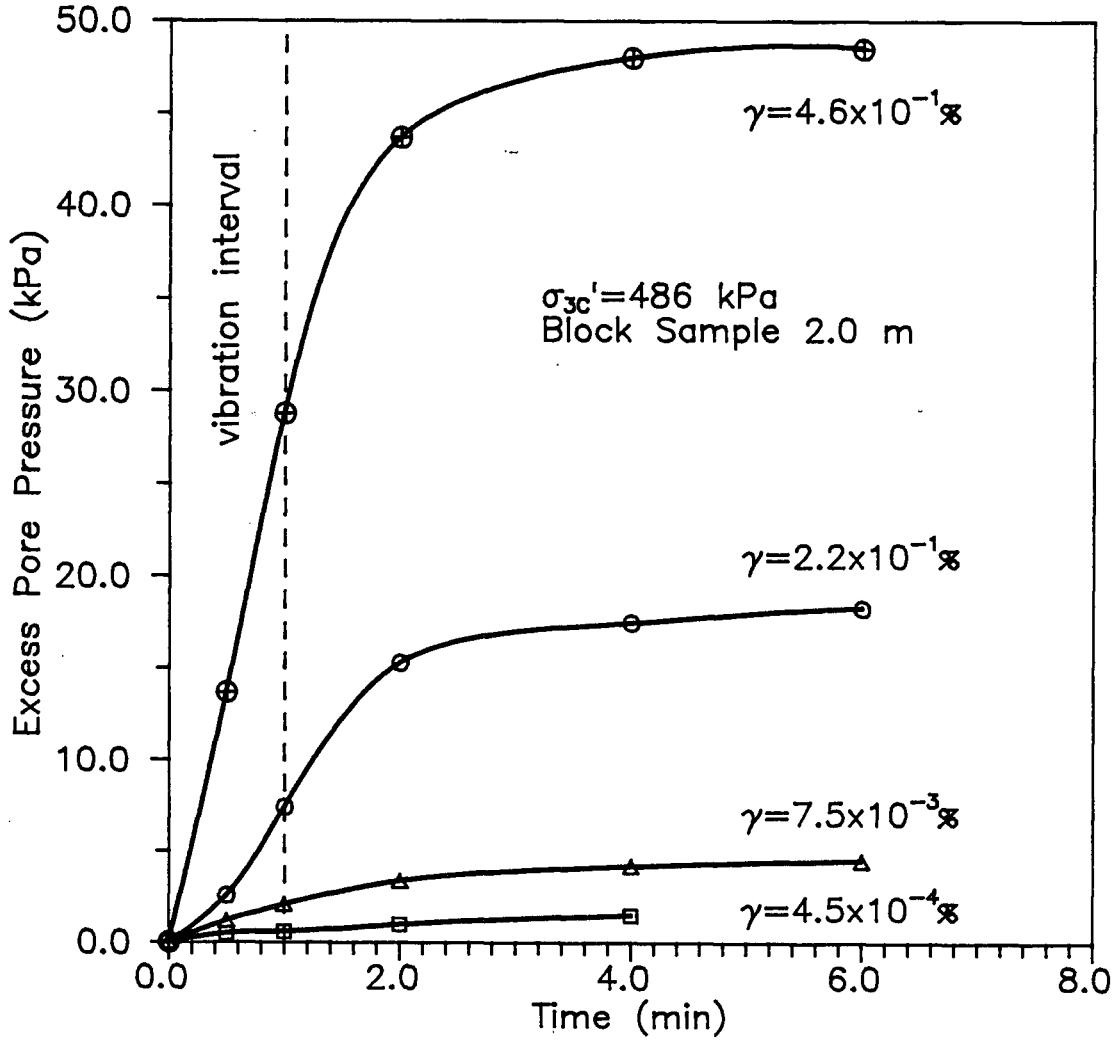

Fig. 7.34 Pore Pressure Response for Normally Consolidated Block Samples in Resonant Column Test

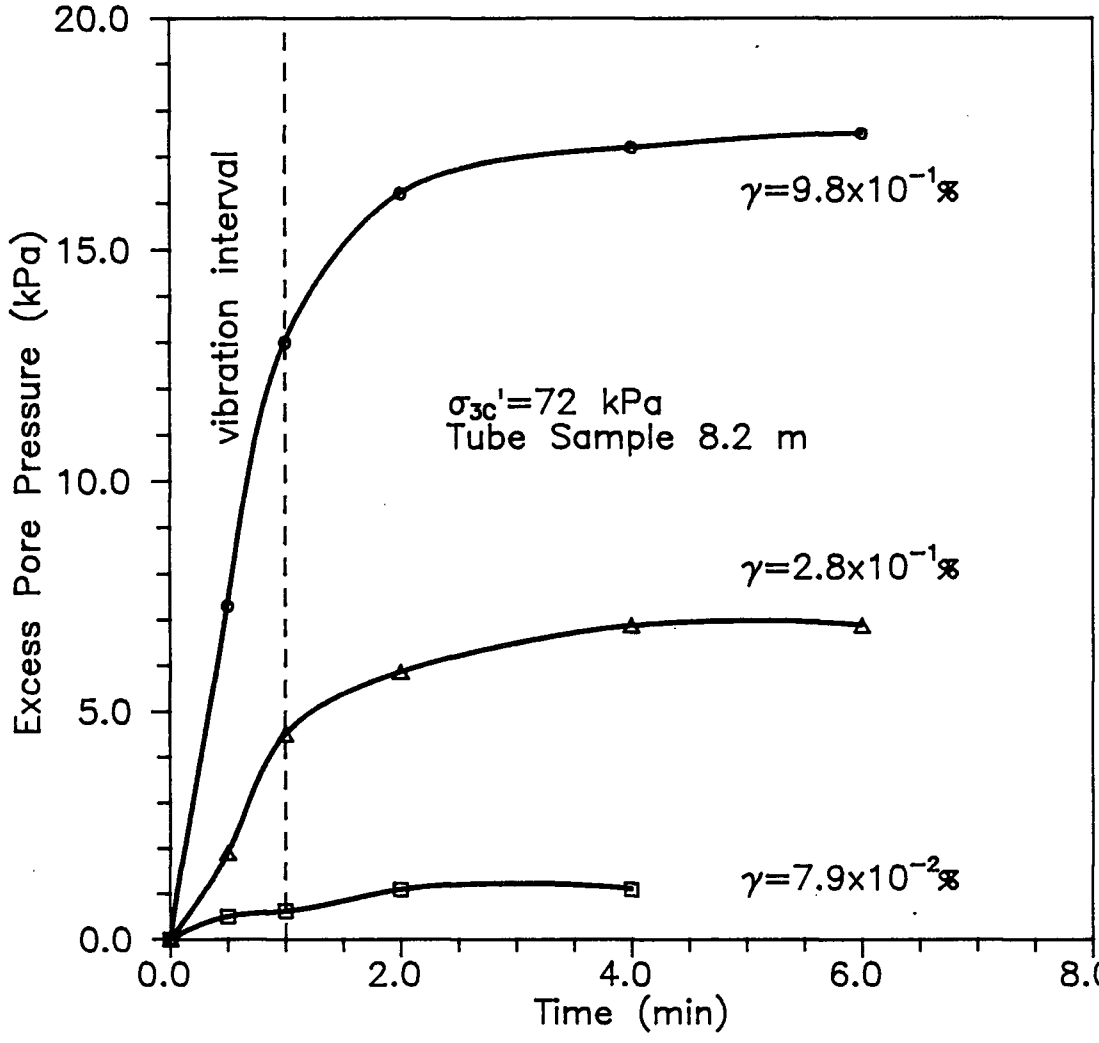

Fig. 7.35 Pore Pressure Response for Normally Consolidated Block Samples in Resonant Column Test

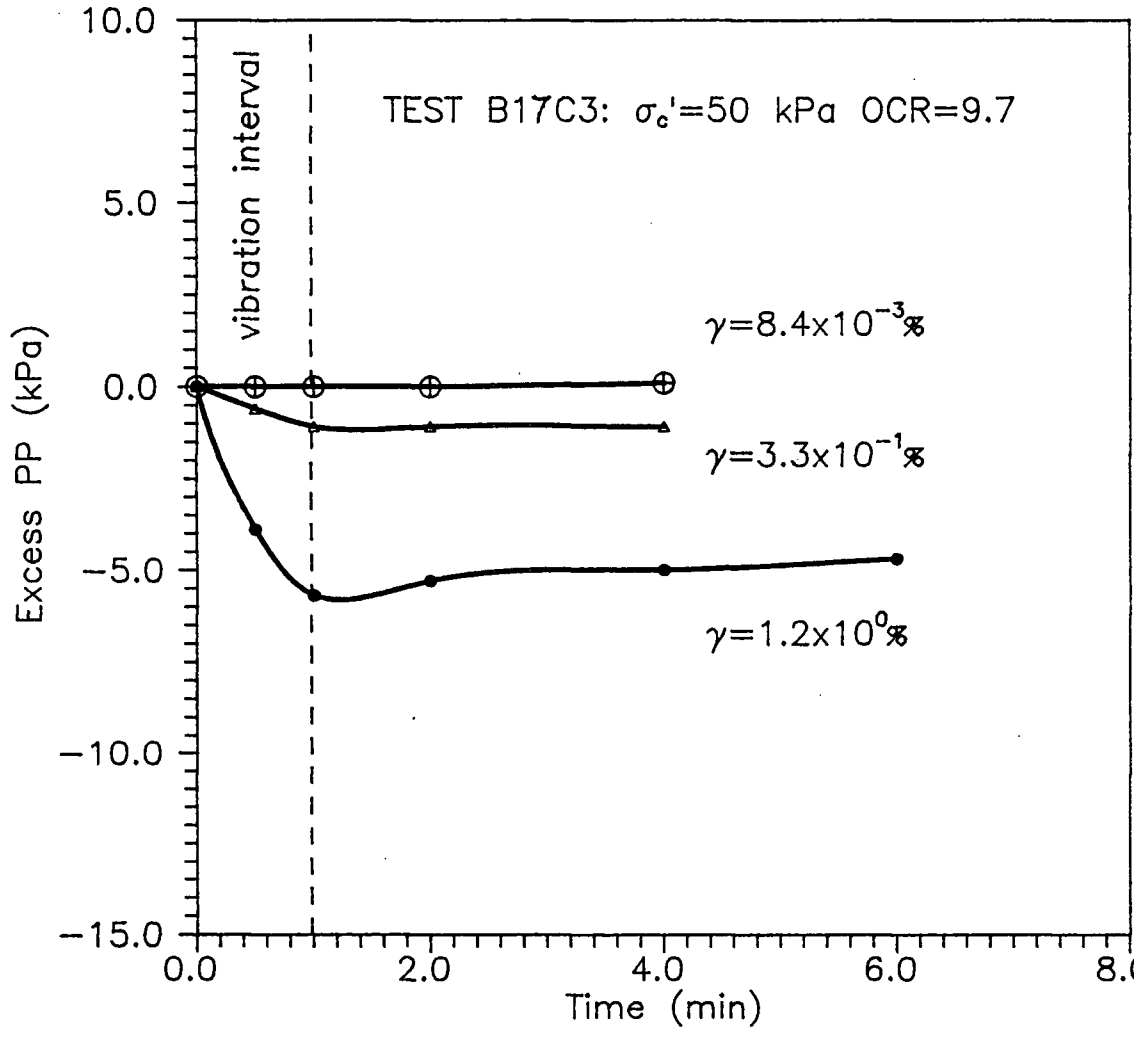

Fig. 7.36 Pore Pressure Response for Overconsolidated Block Sample in Resonant Column Test

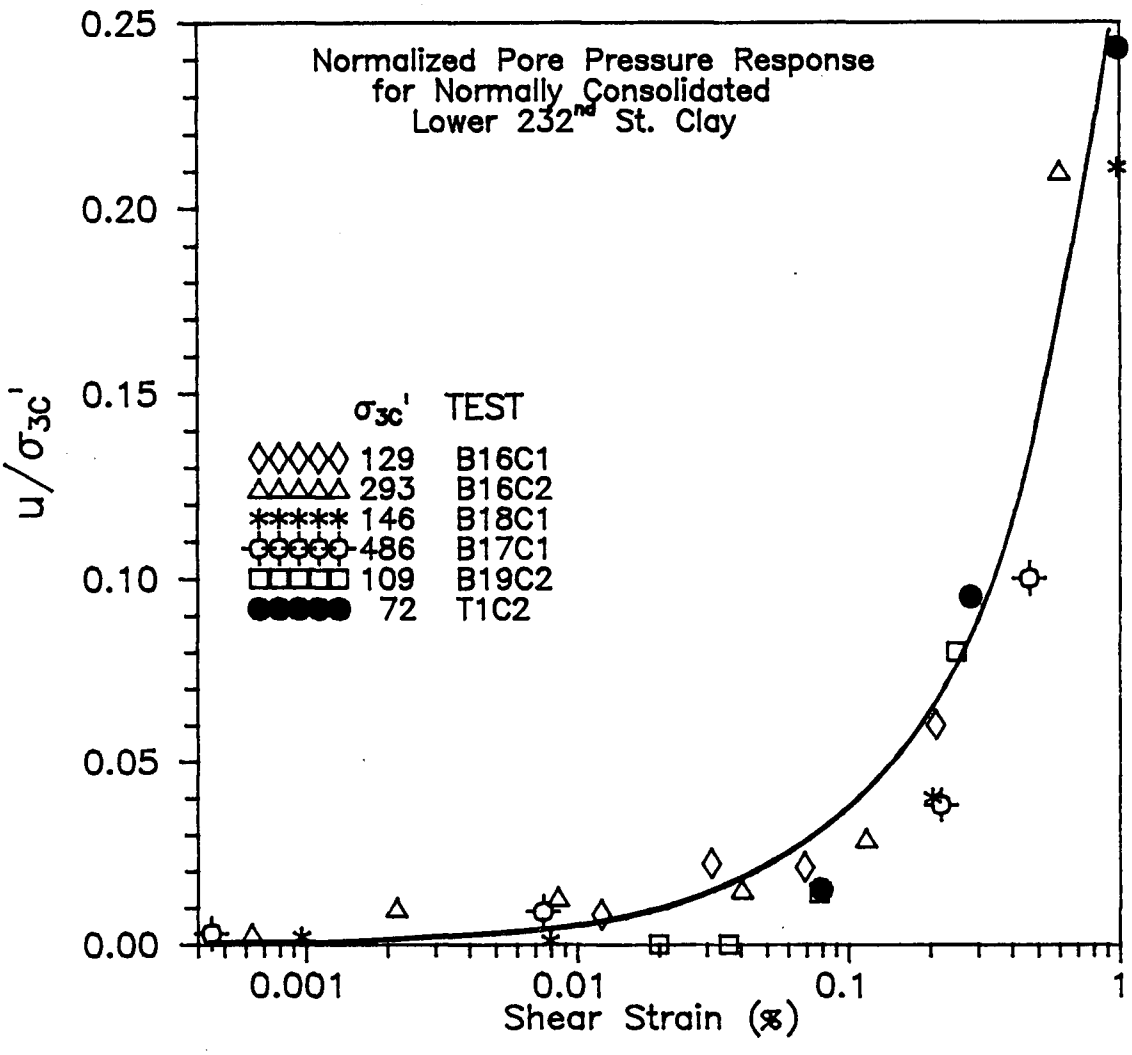

Fig. 7.37 Normalized Pore Pressure Response for Normally Consolidated Clay in Resonant Column

pore pressure generation below 0.01% strain. Above 0.1% strain, the normalized residual pore pressure rises rapidly with shear strain suggesting the onset of large plastic strains. Included in Fig. 7.37 is the pore pressure response for a tube sample from 8.2m represented by the solid circles which shows essentially the same behaviour as the block samples. The resonant vibration frequencies for shear strains greater than 0.1% were between 8 Hz and 19 Hz, depending on the confining pressure. Due to the rapid rise in pore pressure, failure of the samples would have occurred for strains much in excess of 1.0%.

When compared to the damping attenuation curves shown in Fig. 7.38, the normalized pore pressures respond in a very similar fashion with strain. Also, it appears that the onset of pore pressure development and, hence, plastic strains at about 0.01% corresponds to the start of strain softening in shear modulus. Thus, for saturated normally consolidated samples the normalized residual excess pore pressure, the damping ratio, and the normalized shear modulus are similarly related to shear strain.

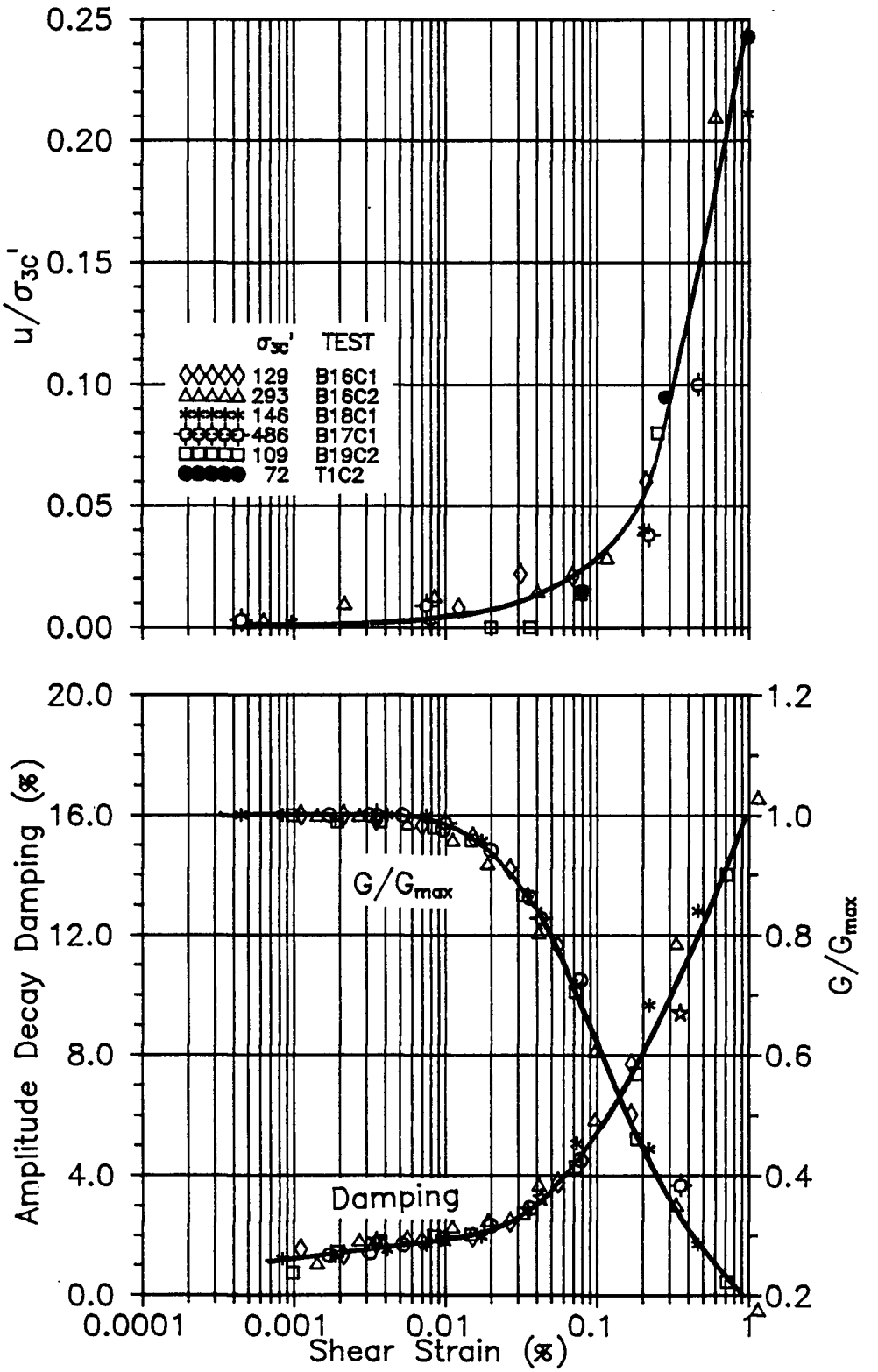

Fig. 7.38 Comparison of Pore Pressure, Damping, and Shear Modulus vs. Strain Curves for Normally Consolidated Clay

8. COMPARISON OF TORSIONAL SHEAR & RESONANT COLUMN RESULTS

Towards the end of the research program, the resonant column apparatus was modified to enable tests to be performed at any chosen frequency while maintaining the capability of performing resonant tests on the same sample. The apparatus modifications are discussed in section 3.4 and the theory underlying the torsional shear test is given in section 4.3. These changes enable the comparison of dynamic properties obtained at various testing frequencies by means of the combined resonant column/torsional shear method. Specifically, the shear modulus, damping ratio, and pore pressure response are considered in the following sections.

8.1 SHEAR MODULUS

Shear modulus values from both resonant column and torsional shear tests for two tube samples from depths of 11.75 and 13.2m are shown in Figs. 8.1 and 8.2, respectively. The resonant column tests, shown by open symbols, and the 0.1 Hz torsional shear tests, represented by solid symbols, show good agreement at the low confining pressures. As the effective confining pressure increases, the difference between shear modulus values obtained by the two methods also increases. In addition, the discrepency between resonant column and torsional shear values generally decreases with increasing strain

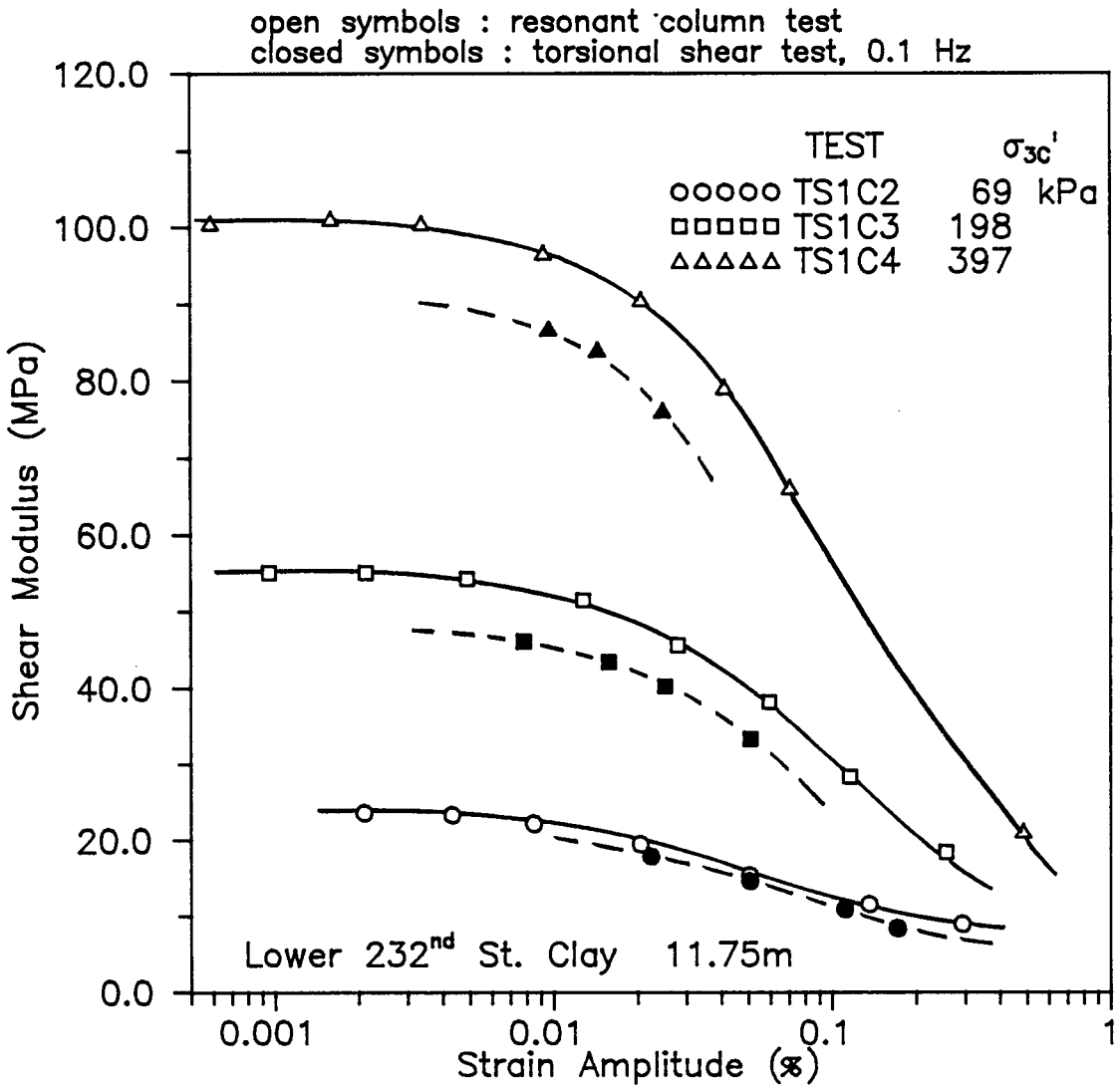

Fig. 8.1 Shear Modulus vs. Strain Curves from Resonant Column and Torsional Shear Tests for Sample from 11.75m

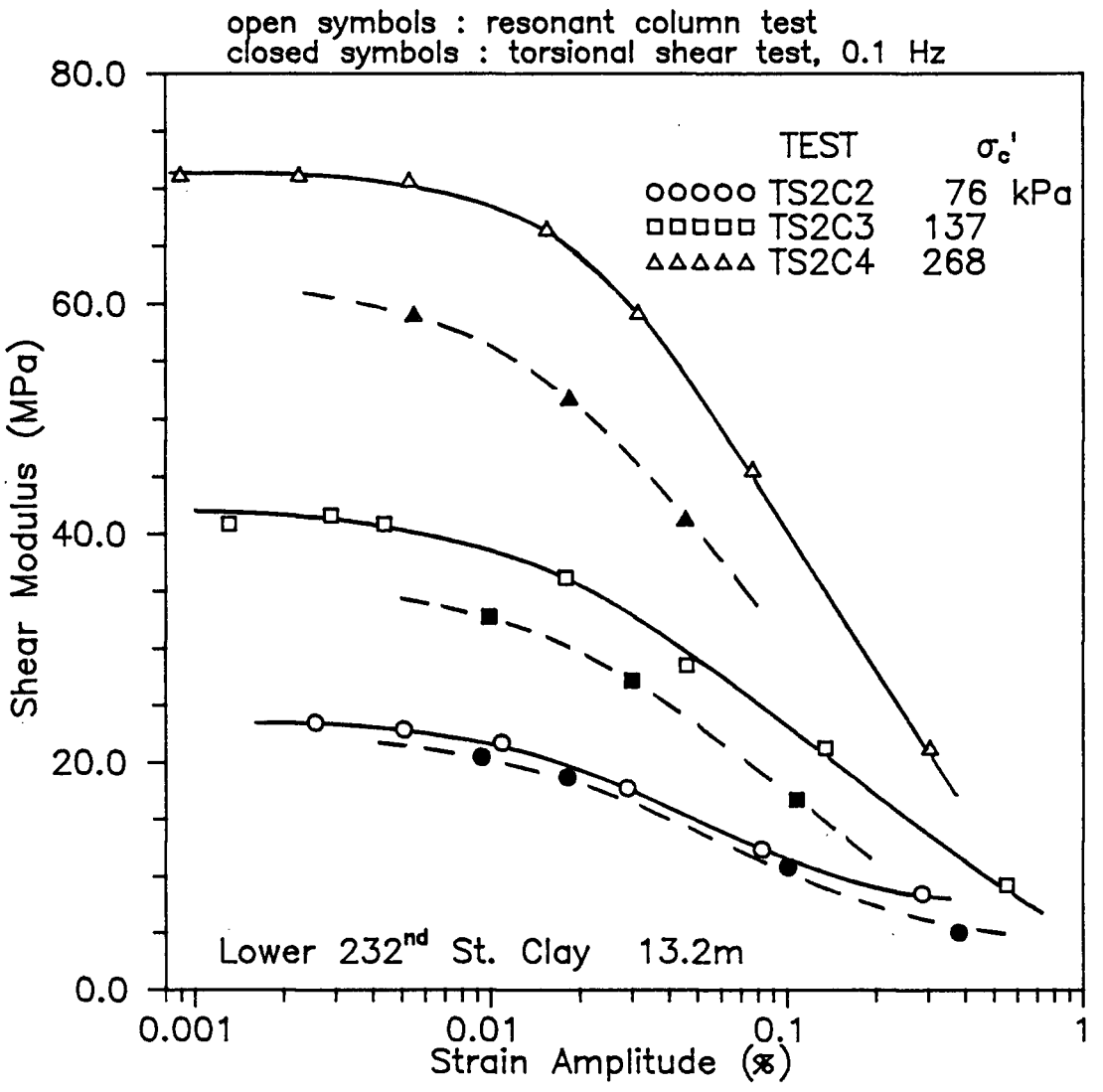

Fig. 8.2 Shear Modulus vs. Strain Curves from Resonant Column and Torsional Shear Tests for Sample from 13.2m

amplitude. The disparity in shear modulus values appears to be largely due to differences in the oscillation frequencies which represent differences in strain rate between torsional shear and resonant column tests.

Figures 8.3 and 8.4 show the shear modulus values from torsional shear tests conducted at frequencies of 0.01, 0.1, and 1.0 Hz as well as the shear modulus values obtained from the resonant colunm. For the torsional shear tests it is evident that the shear modulus increases with increasing frequency, and hence, with increasing strain rate. The higher shear modulus values obtained in the resonant column test might be expected since the resonant column tests are run at higher frequencies.

In order to extend the torsional shear results to frequencies greater than about 1.0 Hz, a torque cell would have to be built into the apparatus to measure the applied dynamic shear stress. For frequencies of about 1 Hz or less, a static calibration was found to be sufficient. On average it was found that the rotational transducer (RVDT) gave shear strains which were about 15% lower than those given by the accelerometer calibration in the resonant column test. However, the differences in observed shear modulus values between resonant column and torsional shear tests cannot be accounted for by such a small difference in shear strains. In fact the shear strain difference is such that the discrepency

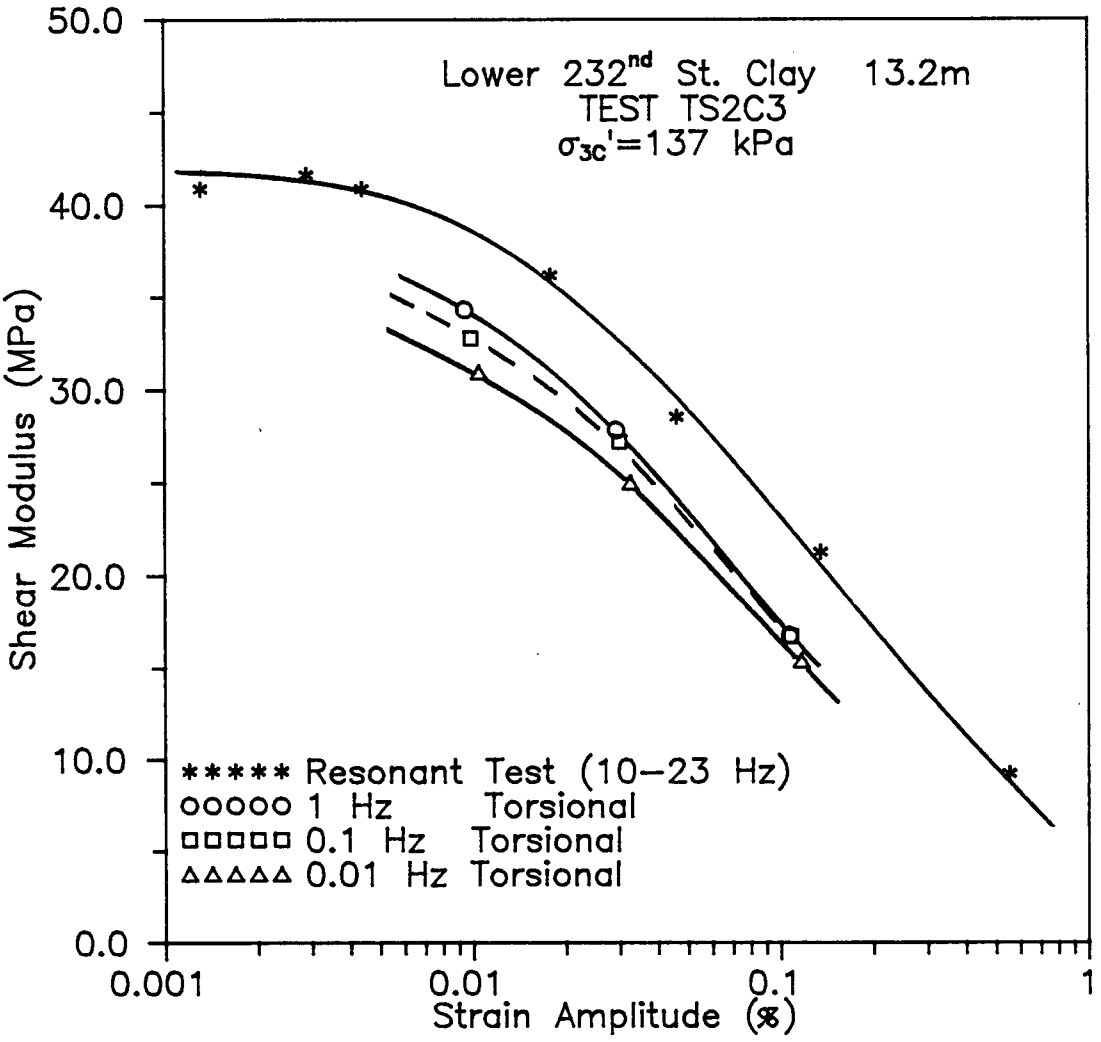

Fig. 8.3 Frequency (Strain Rate) Dependency of Shear Modulus vs. Strain Curves

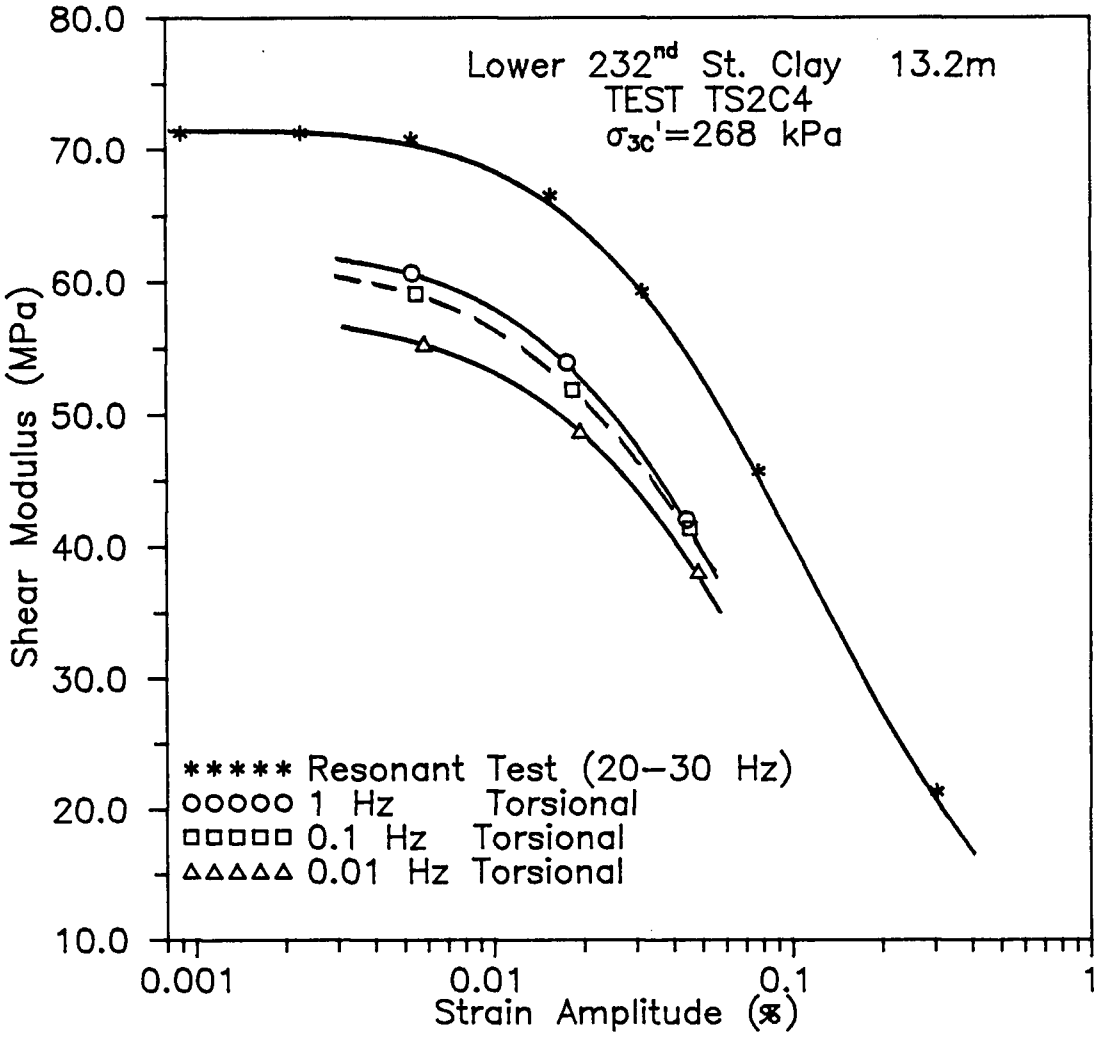

Fig. 8.4 Frequency (Strain Rate) Dependency of Shear Modulus vs. Strain Curves

between resonant column and torsional shear values would be slightly greater if shear strain corrections were to be made. Since it is not known which method yields a more accurate value of strain, no corrections were made.

Based solely on the results of torsional shear tests, a 100-fold increase in frequency from 0.01 to 1.0 Hz results in an increase in shear modulus of only 10% at a strain of 0.01%. The effect of strain rate therefore appears to be fairly minor, in the range investigated.

It should be mentioned that no frequency effect was observed in a torsional shear/resonant column test conducted on a dry sand sample. Dynamic and static torsional shear tests performed by Bolton and Wilson (1989) confirm that the dynamic response of dry sand is independent of frequency.

8.2 DAMPING RATIO

The damping attenuation curves for tube samples from 11.75 and 13.2m consolidated to the in situ octahedral stress are shown in Figures 8.5 and 8.6, respectively. Regardless of whether the torsional shear or resonant column method is used, the damping is approximately the same for any particular shear strain. For the resonant column tests, the amplitude decay method was used to determine the damping whereas the damping

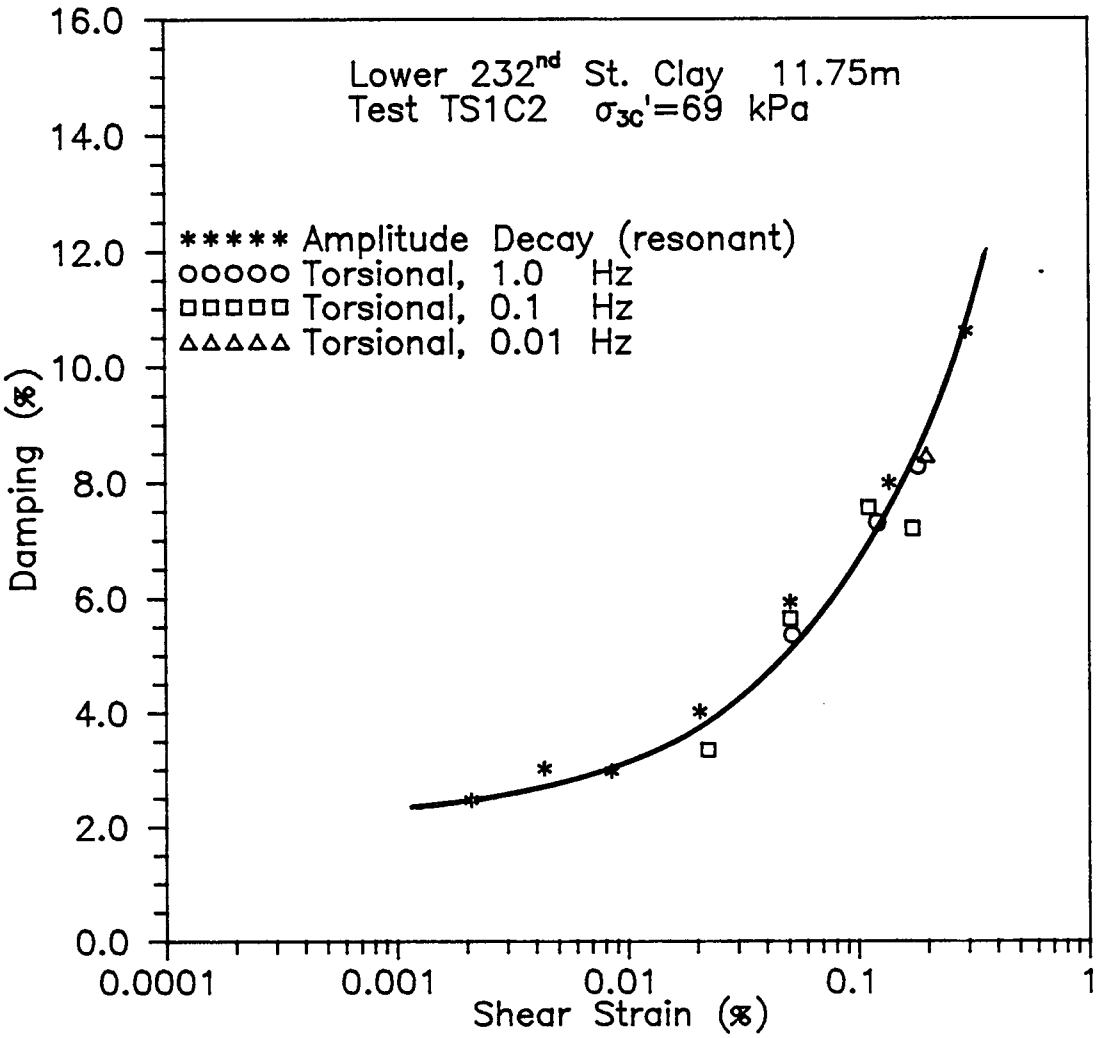

Fig. 8.5 Damping Attenuation Curves Determined at Various Frequencies for Clay from 11.75m

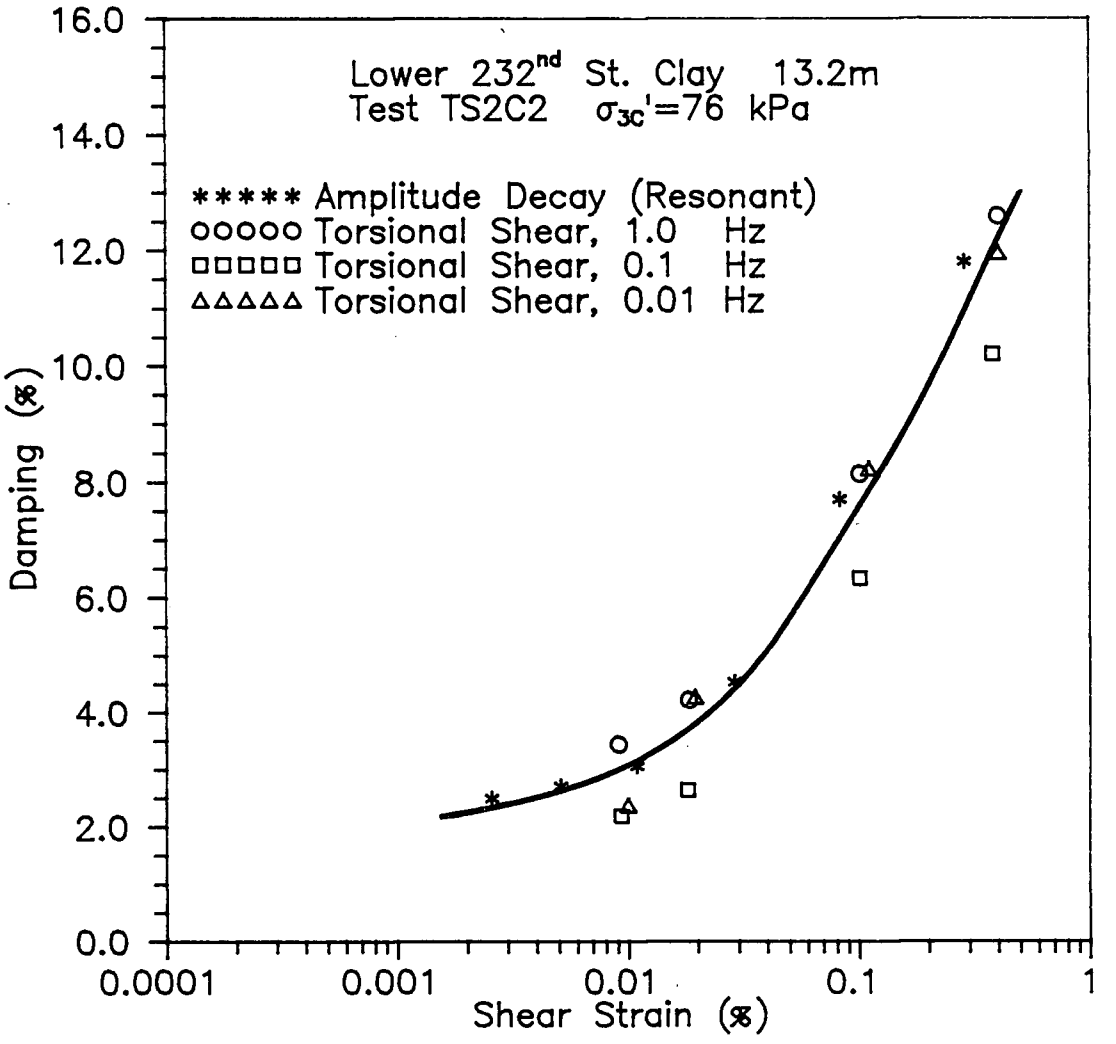

Fig. 8.6 Damping Attenuation Curves Determined at Various Frequencies for Clay from 13.2m

ratio from the torsional shear tests was determined from the measured stress-strain hysteresis loops.

Based on the limited data, the damping ratio appears to be unaffected by frequency, and hence strain rate, since the torsional shear tests conducted at 0.01, 0.1, and 1.0 Hz and the resonant column tests give essentially the same result. Since the dissipated energy per cycle seems to be independent of the frequency of loading, the damping ratio can be considered to be hysteretic. Viscous damping, on the other hand, would require the dissipated energy to increase proportionally with frequency.

8.3 PORE PRESSURE RESPONSE

For the torsional shear tests conducted, final excess pore pressures were monitored only for tests at a frequency of 1.0 Hz. In order to compare results of torsional shear and resonant column tests at a comparable number of loading cycles, at least 300 cycles of loading were performed in the torsional shear test before the pore pressures were allowed to equalize. This large number of cycles would require too long a vibration interval at 0.01 Hz or 0.1 Hz to be completed in a reasonable period of time. Thus, only the 1.0 Hz values are considered herein.

The normalized residual excess pore pressures versus strain for both block samples and tube samples in the resonant column was given in Fig. 7.37. This data is shown in Fig. 8.7 along with the data from torsional shear tests conducted on tube samples at a frequency of 1.0 Hz. Clearly, the normalized residual pore pressures are significantly higher for the torsional shear tests than for the resonant column tests which, depending on confining pressure, have vibration frequencies of 8 to 22 Hz in the 0.1 to 1% shear strain range. Though the tests are such that they are stress controlled as opposed to strain controlled, the threshold strain below which no excess pore pressures are generated appears to be about 0.01% - the same as for resonant column tests.

The results are consistent with those reported for cyclic simple shear tests (Ansal and Erken, 1989) as well as those for cyclic triaxial tests (Matsui et al., 1980), both of which report a dependence of excess pore pressures on loading frequency in addition to a threshold stress ratio below which no excess pore pressures are generated.

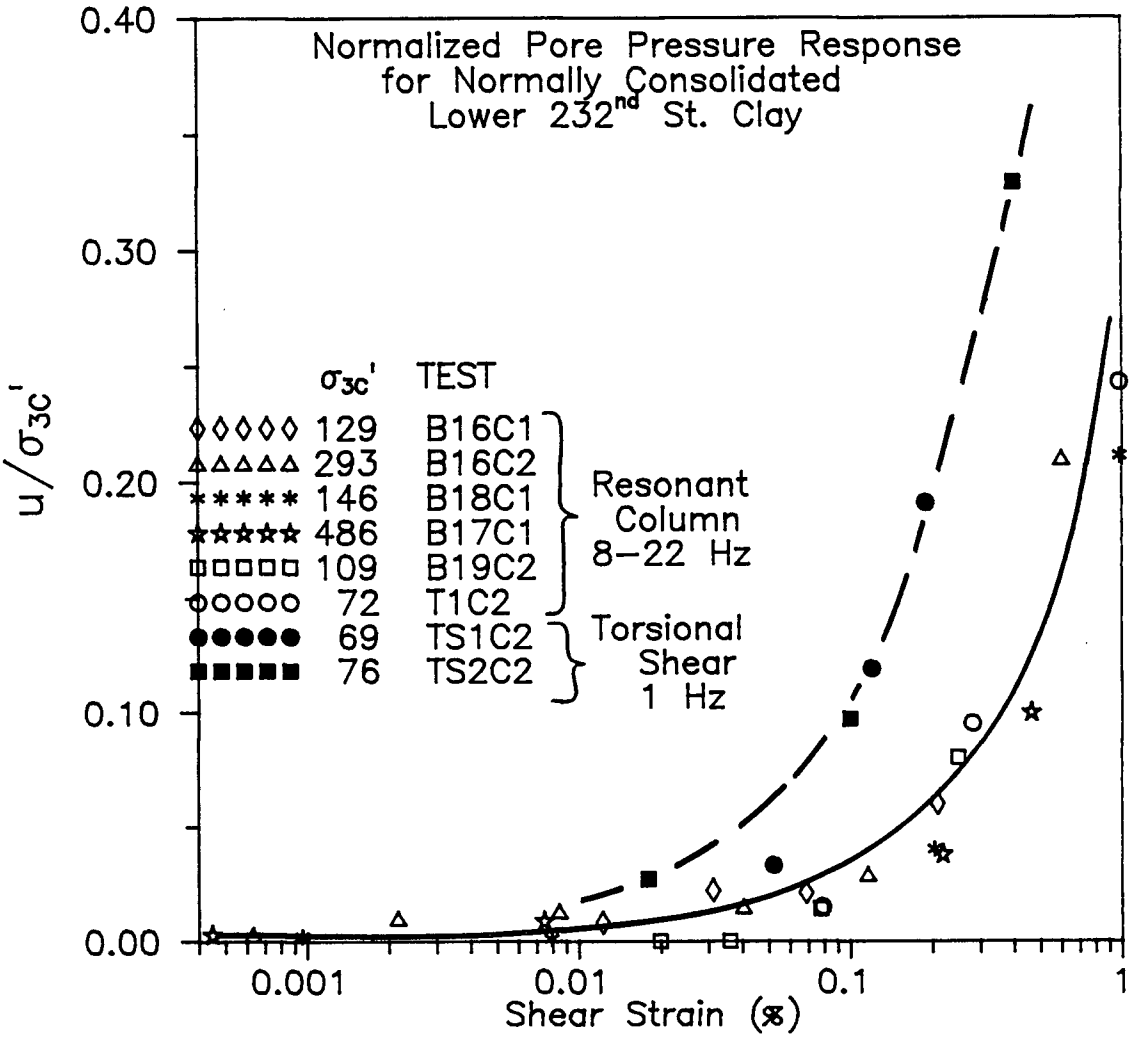

Fig. 8.7 Comparison of Normalized Residual Pore Pressure Response for Samples from Resonant Column and Torsional Shear Tests

9. COMPARISON TO FIELD RESULTS

9.1 INTRODUCTION

It is often desireable to determine the dynamic properties of soil in situ since laboratory tests may not always be representative of field conditions. One of the best in situ techniques is the seismic cone penetration test (SCPT) which has been used extensively at UBC since 1980 (Robertson et al., 1986). At first, research was focused on determining the in situ small strain shear wave velocity from which the shear modulus can be easily calculated. These methods are now well established (Campanella and Stewart, 1990). More recently, emphasis has been placed towards determination of the in situ damping characteristics (Stewart and Campanella, 1990).

The SCPT method involves horizontally striking a weighted beam at the ground surface thereby producing a polarized shear wave which travels through the ground and is sensed at depth by a horizontally oriented accelerometer located near the tip of the cone. This procedure is repeated as the cone is advanced in one meter depth increments. Comparison of the successive accelerometer records is the basis on which the shear wave velocity and damping characteristics are determined.

9.2 SHEAR WAVE VELOCITY

The shear wave velocity profiles determined from two SCPT soundings are shown in Fig. 9.1. The shear wave velocities from both tests increase almost linearly with depth from a value of about 85 m/s at a depth of 3m to a value of approximately 140 m/s at a depth of 20m. The shear strains associated with the in situ shear wave velocities are in the range 0.001% to 0.0001% where the soil behaviour is linear elastic.

In order to compare laboratory and insitu properties, the stresses in laboratory tests should correctly model those in the field. However, the isotropic confining pressures applied to laboratory specimens are rarely representative of the anisotropic in situ stresses. Resonant column tests on anisotropically consolidated clay have shown that the deviatoric component of stress has no effect on the shear wave velocity for stress ratios less than 2.5 (Hardin and Black, 1968). Only the octahedral normal stress was found to control the shear wave velocity.

In situ and laboratory tests performed by Sully (1990) indicate that: the soil at the Lower 232nd St. site is essentially normally consolidated below a depth of 6m; the lateral coefficient at rest pressure (K_o) for the normally consolidated clay is 0.55; and the soil can be considered as

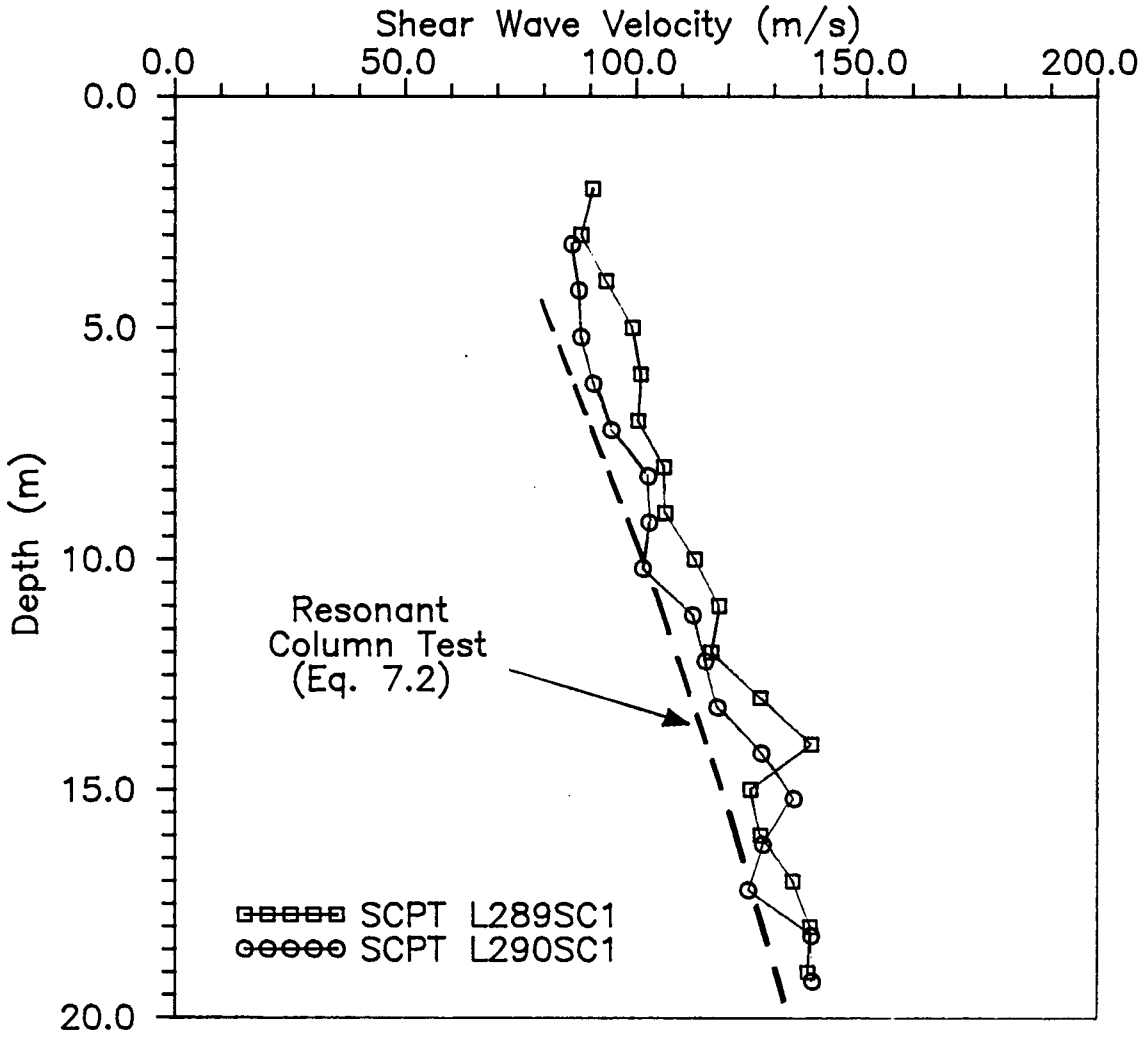

Fig. 9.1 Comparison of Shear Wave Velocities Determined from Resonant Column and SCPT Methods

being in a cross-anisotropic state of stress. These findings coupled with the aforementioned findings by Hardin and Black suggest that it is reasonable to compare the shear wave velocities from the isotropically consolidated resonant column tests with the normally consolidated SCPT in situ velocities at the same effective octahedral stress. The in situ octahedral stress for the normally consolidated clay was calculated based on a cross-anisotropic state of stress with a K_o value of 0.55.

The variation of shear wave velocity with depth for the resonant column tests on tube samples is shown by the thick dotted line in Fig. 9.1. This relationship was derived by substituting Eq. 7.2 into Eq. 4.5 and solving for the shear wave velocity. On average, the laboratory derived velocities are about 10 m/s lower than the in situ velocities and the rate of velocity increase with depth is the same. Lower laboratory values might be expected since they were generally determined after 1000 minutes of sample confinement, with no aging effects considered; aging, as exists in situ, always increases stiffness response or modulus. Nevertheless, the agreement between laboratory and in situ results is quite good. Lastly, it should be noted that while the shear strains corresponding to the resonant column velocities are slightly greater than those in situ, they are still in the linear elastic range and should therefore give the same result.

9.3 DAMPING RATIO

Several methods are available to calculate the in situ damping ratio from the SCPT. Experience at UBC (Stewart and Campanella, 1990) suggests that only the spectral slope method developed by Redpath et al. (1982) gives consistently meaningful results.

The spectral slope method is based on the equation

$$d[\ln(A2/A1)]/(df*dR) = -z \qquad (9.1)$$

where A2/A1 = ratio of signal amplitudes in frequency domain from successive depths

dR = depth derivative

df = frequency derivative

z = a/f, where a is an attenuation coefficient

which has its development given in Stewart and Campanella (1990). The solution of Eq. 9.1 requires a signal processing computer program. The coefficient z is determined by first calculating the fast Fourier transform (FFT) of one signal at a given depth, then for each deeper signal computations are made of the FFT, the ratio of the FFT's, and the negative of the natural logarithm (ln) of the ratio. Next, the slope of the ln(ratio) versus frequency plot (spectral ratio slope) for each depth is plotted against depth. Such a plot is given in Fig. 9.2 for the Lower 232nd St. site between 5 m and 20 m.

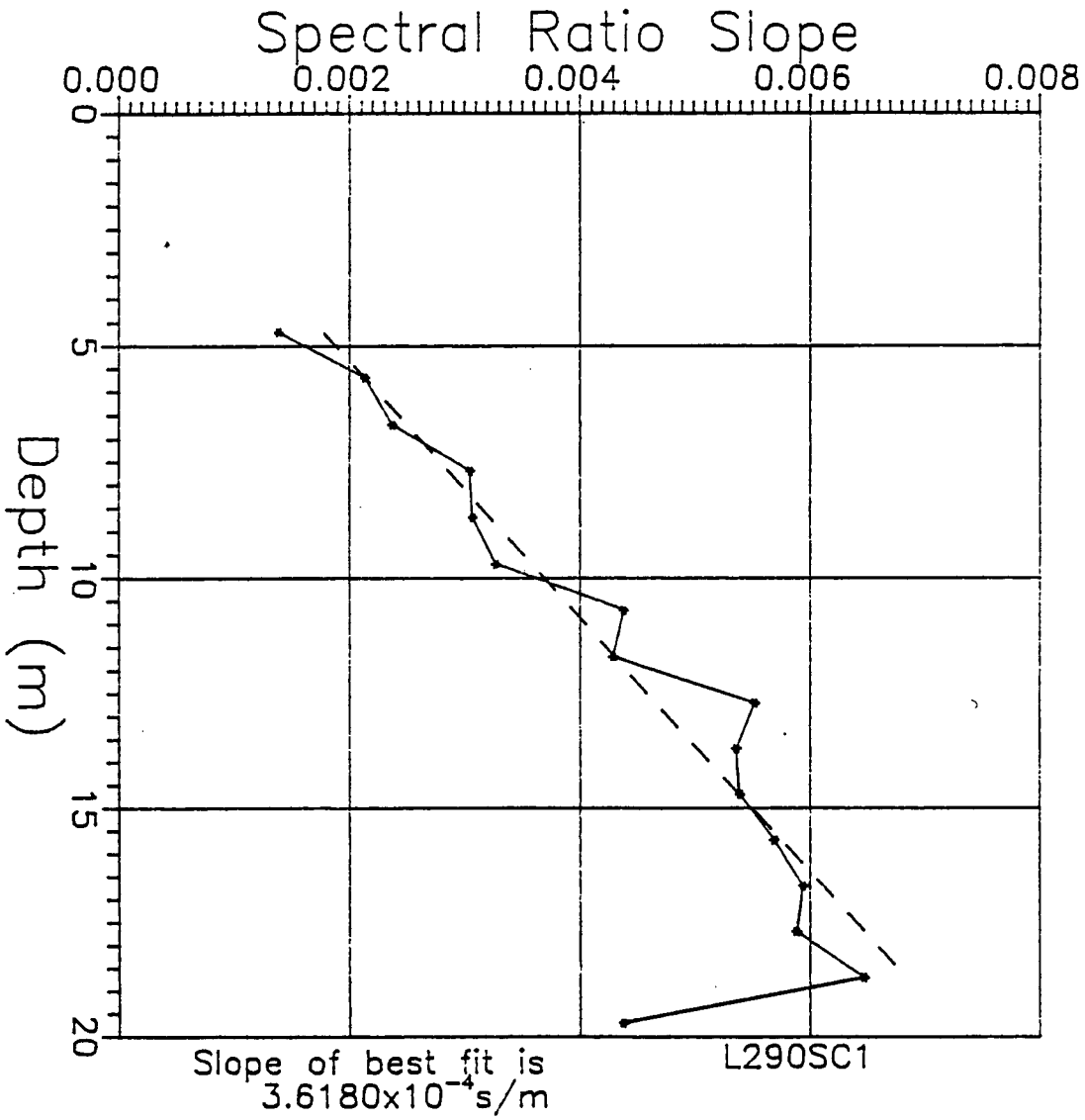

Fig. 9.2 Spectral Ratio Slope Method for Calculation of In Situ Damping

The slope of this depth plot gives the z coefficient for the particular soil layer. Finally, the fraction of critical damping (D) can be computed from

$$D = (zV_S)/(2\pi) \qquad (9.2)$$

where V_S is the shear wave velocity.

Using eqn. 9.2, the spectral slope method yields a damping ratio of 0.6% for the soil between 5 and 20 m. Analysis of two other SCPT soundings gave damping ratios of 1.2% and 1.9%, respectively. These values compare well with the 0.9% to 2.4% range of unaged damping ratio values determined from resonant column tests on normally consolidated samples from 8-14 m (section 7.3.1). As discussed in section 7.3.2, the aging effect on damping in resonant column tests appears to be very significant with the damping ratio decreasing about 0.5% per log cycle of time (minutes) at constant effective stress. If the aging effect were considered the damping ratio from resonant column tests would be lower. However, since the length of time to which the laboratory aging effect can be extended is not known, a time extrapolation of resonant column results to field conditions is difficult to make at this time.

10. CONCLUSIONS

The following is a summary of the dynamic characteristics and response of Lower 232nd St. clay, based on the results of resonant column and torsional shear tests performed for this study.

LOW AMPLITUDE SHEAR MODULUS (Gmax)

Under isotropic confinement, a linear log-log relationship exists between dynamic shear modulus (G_{max}) and effective isotropic confining pressure (σ_{3C}'). For the higher plasticity block samples (PI=40) the relationship can be expressed as

$$G_{max} = 29.3*F(e)P_a\ (\sigma_{3C}')^{.60}OCR^{.26} \qquad (10.1)$$

where $F(e) = (5.2-e)^2/(1+e)$

in which P_a is the atmospheric pressure in the same units as G_{max} and σ_{3C}', and e is the void ratio.

For normally consolidated tube samples having Plasticity index of 20-25, the relationship is given by

$$G_{max} = 137.2*F(e)P_a^{.38}(\sigma_{3C}')^{.62} \qquad (10.2)$$

where $F(e) = (2.97-e)^2/(1+e)$

The commonly used Hardin and Drnevich equation for shear modulus significantly overpredicts the value of G_{max} for both clay types. Although it is widely used, it appears that the Hardin and Drnevich void ratio factor with constant of 2.97 is valid only for clays with PI less than 25.

Overconsolidated samples generally have higher shear modulus than normally consolidated specimens. The effect of stress history on G_{max} is expressed by the OCR term in equation 11.1 with exponent 0.26. This agrees with the range in OCR exponents suggested by Hardin and Drnevich for clays with PI between 20 and 40.

Increasing duration of confinement at constant effective stress was found to result in a significant increase in shear modulus. Typically, the rate of shear modulus increase normalized by the 1000 minute value was found to range from 14-23% per log cycle of time (minutes).

From torsional shear tests, it was found that increasing the torsional frequency from 0.01 Hz to 1.0 Hz resulted in a 10% increase in shear modulus. Shear modulus values from the resonant column test were always higher than torsional shear tests since they were always run at higher frequencies (strain rate).

The resonant column shear wave velocities, and hence shear moduli, were found to be slightly lower than the in situ values determined from the seismic cone penetration test. The difference can be explained due to the increased stiffness of the in situ soil as a result of aging (5,000 to 10,000 years).

HIGH AMPLITUDE SHEAR MODULUS

The shear modulus decreases with increasing shear strain for strains greater than about .005%. Regardless of the confining pressure or overconsolidation ratio, normalized modulus reduction relationship (G/G_{max} vs. shear strain) can be represented by a single curve for the higher plasticity (PI=40) clay. A slight shift of the G/G_{max} curve towards higher values occurs with increasing effective confining pressure for the lower plasticity (PI=20) clay. Thus, the influence of confining pressure diminishes with increasing plasticity.

Based on limited data it appears that duration of confinement causes both the small strain and large strain amplitude moduli to increase at about the same rate thereby leaving the normalized modulus reduction curve unaffected.

LOW AMPLITUDE DAMPING RATIO

Very little influence of confining pressure or stress history was observed on the small strain (.001%) damping ratio for the higher plasticity clay (PI=40). Damping ratios obtained from resonant column tests ranged from 1.0-1.7%. For the lower plasticity samples (PI=20) the damping ratio was found to decrease slightly with effective confining pressure. Damping ratios ranging from 0.9-2.4% were obtained.

The damping ratio was found to significantly decrease with increasing time at constant effective stress. On average, the damping ratio decreased about 0.5% per log cycle of time (minutes).

The damping ratio appears to be unaffected by frequency, and hence, strain rate, since the torsional shear tests conducted at various frequencies and the resonant column tests gave essentially the same result.

The range of damping ratios determined from the seismic cone penetration test using the spectral slope method yielded damping values from 0.6-1.9%. This range compares well with the 1.2-2.4% identified from unaged resonant column tests.

HIGH AMPLITUDE DAMPING

There is no effect of confining pressure or stress history on the high amplitude damping for the clay with PI of 40. For the lower plasticity (PI=20) clay, there is a slight decrease in damping with confining pressure. The higher PI clay was found to have slightly lower damping for the entire strain range tested. This implies that sites with higher plasticity soils would tend to have higher ground motion amplifications.

Based on results from resonant column and torsional shear tests, there appears to be no significant effect of frequency (strain rate) on the high amplitude damping ratio.

Limited data indicates that the increased duration of confinement at constant effective stress decreases the damping ratio over the entire strain range tested.

PORE PRESSURE RESPONSE

In the resonant column test, no significant excess pore pressure is generated until shear strains of 0.05-0.1% are surpassed. Pore pressures increase rapidly thereafter.

Results of torsional shear tests indicate that the magnitude of the residual excess pore pressure increases significantly with slower frequency.

BIBLIOGRAPHY

Afifi, S.S. and Richart, F.E., Jr. (1973), "Stress-History Effects on Shear Modulus of Soils", Soils and Foundations, Japan, Vol. 13, No. 1, March, pp. 77-95.

Aggour, M.S., Tawfiq, K.S. and Amini, F. (1987), "Effects of Frequency Content on Dynamic Properties for Cohesive Soils", Proceedings, Third International Conference on Earthquake Engineering and Soil Dynamics, Princeton, June, Vol. 42, pp. 31-39.

Anderson, D.G. and Stokoe, K.H., II, (1978), "Shear Modulus: A Time Dependent Soil Property", Dynamic Geotechnical Testing, ASTM STP 654, American Society for Testing and Materials, pp. 66-90.

Anderson, D.G. and Woods, R.D. (1976), "Time-Dependent Increase in Shear Modulus of Clay", Journal of the Geotechnical Engineering Division, ASCE, Vol. 102, GT5, May, pp. 525-537.

Ansal, A.M. and Erken, A. (1989), "Undrained Behavior of Clay Under Cyclic Shear Stresses", Journal of Geotechnical Engineering, ASCE, Vol. 115, No. 7, July, pp. 968-983.

Armstrong, J.E. (1978), "Post Vachon Wisconsin Glaciation, Fraser River Lowland, British Columbia", Goelogical Survey of Canada, Bulletin 332.

Bolton, M.D. and Wilson, M.R. (1989), "An Experimental and Theoretical Comparison Between Static and Dynamic Torsional Soil Tests", Geotechnique, Vol. 39, No. 4, pp. 585-599.

Bishop, A.W. and Henkel, D.J. (1962). The Measurement of Soil Properties in the Triaxial Test. 2nd Ed., William Clowes and Sons, London.

Campanella, R.G. and Stewart, W.P. (1990), "Seismic Cone Analysis Using Digital Signal Proccessing for Dynamic Site Characterization", Proceedings, 43rd Canadian Geotechnical Conference, Quebec, Canada.

Drnevich, V.P. (1967), "Effect of Strain on the Dynamic Properties of Sand", Ph.D. Thesis, University of Michigan, at Ann Arbor.

Drnevich Long-Tor Resonant Column Apparatus Operating Manual (1981), Soil Dynamics Instruments, Inc., Lexington, Kentucky.

Drnevich, V.P., Hardin, B.O. and Shippy, D.J. (1978), "Modulus and Damping of Soils by the Resonant Column Method", Dynamic Geotechnical Testing, ASTM STP 654, American Society for Testing and Materials, pp. 91-125.

Hardin, B.O. (1965), "Nature of Damping in Sands", Journal of the Soil Mechanics and Foundations Division, ASCE, Vol. 91, No. SM1, Jan., pp. 63-97.

Hardin, B.O. and Black, A.M. (1968), "Vibration Modulus of Normally Consolidated Clay", Journal of the Soil Mechanics and Foundations Division, ASCE, Vol. 94, No. SM2, March, pp.353-369.

Hardin, B.O. and Drnevich, V.P. (1972a), "Shear Modulus and Damping in Soils: Measurement and Parameter Effect", Journal of the Soil Mechanics and Foundations Division, ASCE, Vol. 98, SM6, June, pp. 603-624.

Hardin, B.O. and Drnevich, V.P. (1972b), "Shear Modulus and Damping in Soils: Design Equations and Curves", Journal of the Soil Mechanics and Foundations Division, ASCE, Vol. 98, No. SM7, July, pp. 667-692.

Hardin, B.O. and Richart, F.E. Jr. (1963), "Elastic Wave Velocities in Granular Soils", Journal of the Soil Mechanics and Foundations Division, ASCE, Vol. 89, No. SM1, pp. 33-65.

Isenhower, W.M. (1979), "Torsional Simple Shear/Resonant Column Properties of San Fransisco Bay Mud", MASc Thesis. Civil Engineering Department, University of Texas at Austin, Austin, Texas, 307 p.

Ishihara, K. (1982), "Dynamic Response Analysis", Proceedings, Int. Symposium on Numerical Models in Geomechanics, Zurich, September, pp. 237-259.

Kokusho, T., Yoshida, Y. and Esashi, Y. (1982), "Dynamic Properties of Clay for Wide Strain Range", Soils and Foundations, Vol. 22, No. 4, December, pp. 1-18.

Marcuson, W.F., III, and Wahls, H.E. (1972), "Time Effect on Dynamic Shear Modulus of Clays", Journal of the Soil Mechanics and Foundations Division, ASCE, Vol. 98, No. SM12, pp. 1359-1373.

Marcuson, W.F., III, and Wahls, H.E. (1978), "Effect of Time on Damping Ratio of Clays", Dynamic Geotechnical Testing, ASTM STP 654, American Society for Testing and Materials, pp. 126-147.

Matsui, T., Ohara, H. and Ito, T. (1980), "Cyclic Stress-Strain History and Shear Characteristics of Clay", Journal of Geotechnical Engineering, ASCE, Vol.106, No. GT10, October, pp. 1101-1120.

Ni, Sheng-Huoo (1987), "Dynamic Properties of Sand under True Triaxial Stress States from Resonant/Column Torsional Shear Tests. Ph.D. Thesis. Civil Engineering Department, University of Texas at Austin, Austin, Texas, 421 p.

Novak, M. and Kim, T.C. (1981), "Resonant Column Technique for Dynamic Testing of Cohesive Soils", Canadian Geotechnical Journal, Vol. 18, pp. 448-455.

Pollard, W.S., Sangrey, D.A. and Poulos, S.J. (1977), "Air Diffussion Through Membranes in Triaxial Tests", Journal of the Geotechnical Engineering Division, ASCE, Vol. 103, No. GT10, pp.1169-1173.

Redpath, B.B., Edwards, R.B., Hale, R.J. and Kintzer, F.C. (1982), " Development of Field Techniques to Measure Damping Values for Near-Surface Rocks and Soils. Prepared for NSF Grant No. PFR-7900192.

Robertson, P.K., Campanella, R.G., Gillespie,D. and Rice, A., (1986), "Seismic CPT to Measure In-Situ Shear Wave Velocity. Journal of Geotechnical Engineering Division, ASCE, Vol. 112, No. 8, pp. 791-804.

Sangrey, D.A., Pollard, W.S. and Egan, J.A. (1978), "Errors Associated with Rate of Undrained Cyclic Testing of Clay Soils", Dynamic Geotechnical Testing, ASTM STP 654, American Society for Testing and Materials, pp. 280-294.

Seed, H.B. and Idris, I.M. (1970), "Soil Moduli and Damping Factors for Dynamic Response Analysis", Report No. UCB/EERC-70/10, University of California, Berkeley, December.

Stewart, W.P. and Campanella, R.G. (1991), "Insitu Measurement of Damping in Soils", Proc. 2nd International Conference on Geotechnical Earthquake Engineering and Soil Dynamics, St. Louis, March.

Sully, J.P. (1990), "Evaluation of In Situ Lateral Stress From Full Displacement Tests", Ph.D. Thesis, Civil Engineering Department, University of British Columbia.

Sun, J.I., Golesoskhi, R. and Seed, B.H. (1988), "Dynamic Moduli and Damping Factors for Cohesive Soils", Report No. UCB/EERC-88/15, University of California, Berkeley, August.

Weiler, W.A, Jr. (1988), "Small-Strain Shear Modulus of Clay", Earthquake Engineering and Soil Dynamics II - Recent Advances in Ground-Motion Evaluation, ASCE Geotechnical Special Publication, No. 20, pp. 331-345.

Zen, K., Umehara, Y. and Hamada, K. (1978), "boratory Tests and In-Situ Seismic Survey on Vibratory Shear Modulus of Clayey Soils with Various Plasticities", Fifth Japan Earthquake Engineering Symposium, pp. 721-728.

APPENDIX A:

Shear Modulus vs. Strain Curves

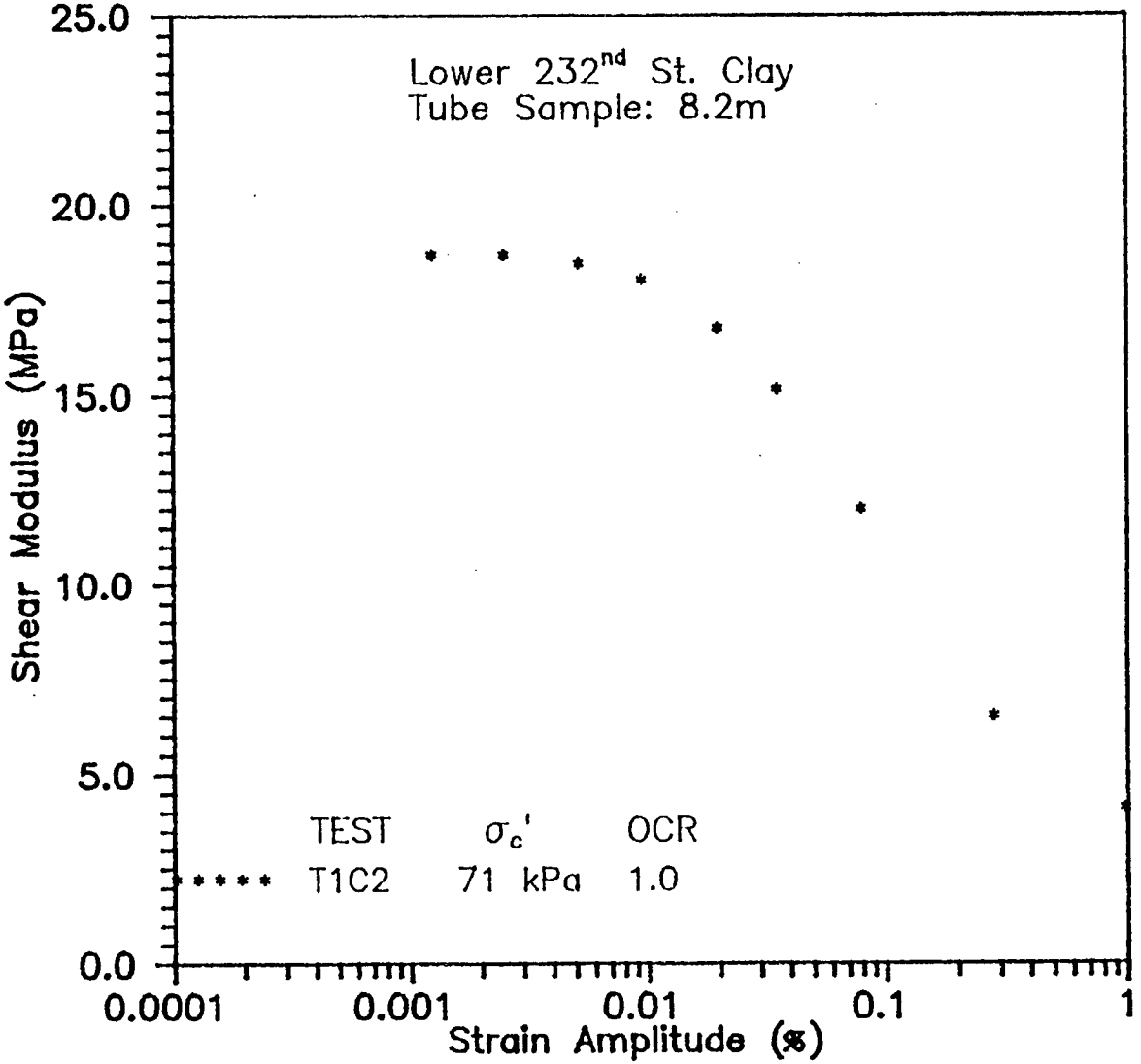
Lower 232nd St. Clay
Tube Sample: 8.2m
Shear Modulus (MPa)
25.0
20.0
15.0
10.0
5.0
0.0
0.0001
0.001
0.01
0.1
1
Strain Amplitude (%)
TEST
σc'
OCR
T1C2
71 kPa
1.0

Shear Modulus (MPa)
60.0
50.0
40.0
30.0
20.0
10.0
0.0
0.0001
0.001
0.01
0.1
1
Strain Amplitude (%)
Lower 232nd St. Clay
Tube Sample: 8.2m
TEST σc' OCR
21C3 250 kPa 1.0

Shear Modulus (MPa)
30.0
25.0
20.0
15.0
10.0
5.0
0.0
0.0001
0.001
0.01
0.1
1
Strain Amplitude (%)
Lower 232nd St. Clay
Tube Sample: 13.2m
TEST σc' OCR
TS2C2 76 kPa 1.0

Shear Modulus (MPa)
50.0
40.0
30.0
20.0
10.0
0.0
0.0001
0.001
0.01
0.1
1
Strain Amplitude (%)
Lower 232nd St. Clay
Tube Sample: 13.2m
TEST σo' OCR
TS2C3 137 kPa 1.0

Shear Modulus (MPa)
0.0
20.0
40.0
60.0
80.0
Strain Amplitude (%)
0.0001
0.001
0.01
0.1
1
Lower 232nd St. Clay
Tube Sample: 13.2m
TEST σc' OCR
TS2C4 268 kPa 1.0

Shear Modulus (MPa)
30.0
25.0
20.0
15.0
10.0
5.0
0.0
0.0001
0.001
0.01
0.1
1
Strain Amplitude (%)
Lower 232nd St. Clay
Tube Sample: 11.75m
TEST
σc'
OCR
TS1C2
69 kPa
1.0

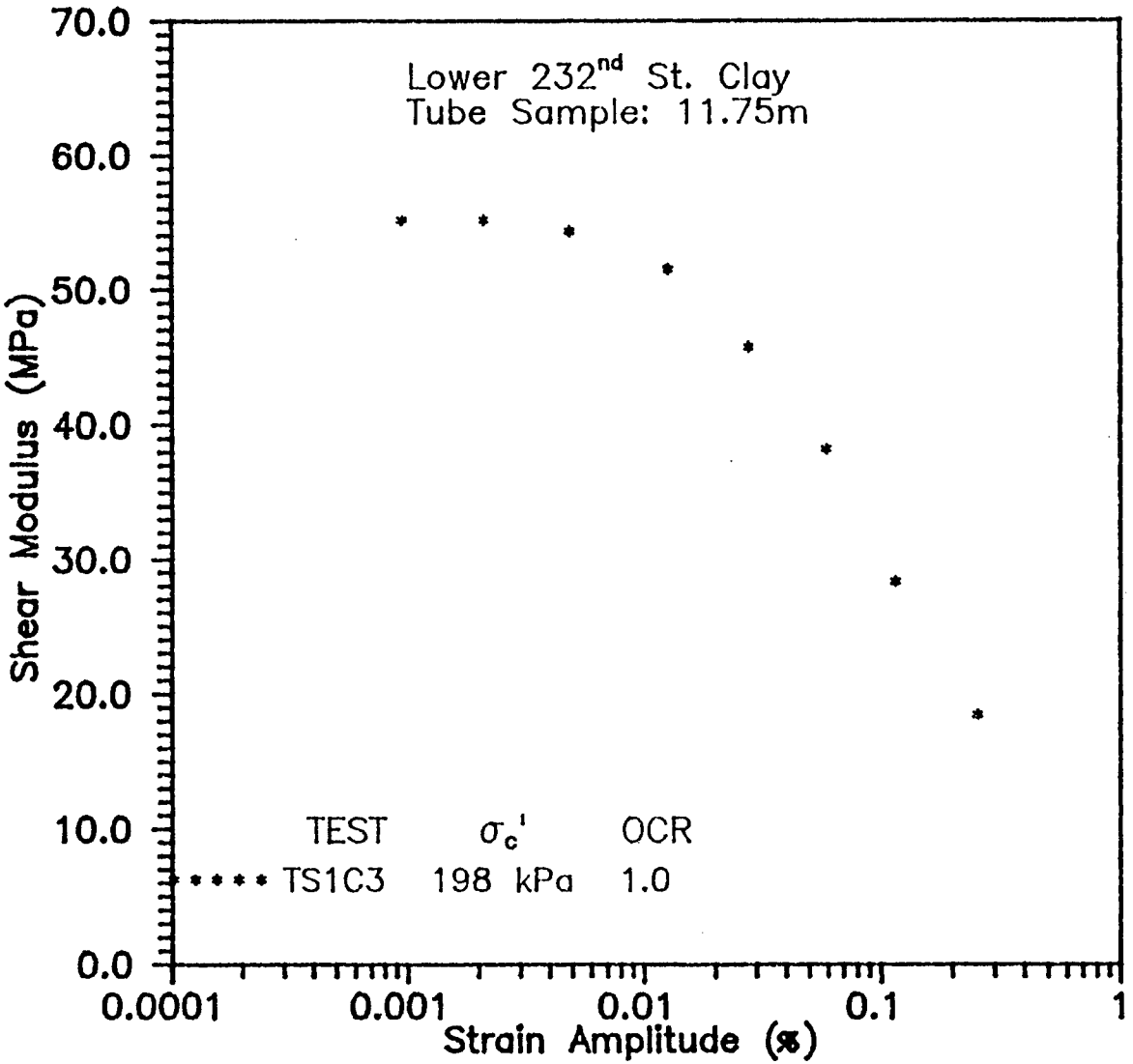
Lower 232nd St. Clay
Tube Sample: 11.75m
Shear Modulus (MPa)
70.0
60.0
50.0
40.0
30.0
20.0
10.0
0.0
0.0001
0.001
0.01
0.1
1
Strain Amplitude (%)
TEST σc' OCR
TS1C3 198 kPa 1.0

Shear Modulus (MPa)
120.0
100.0
80.0
60.0
40.0
20.0
0.0
0.0001
0.001
0.01
0.1
1
Strain Amplitude (%)
Lower 232nd St. Clay
Tube Sample: 11.75m
TEST σc' OCR
TS1C4 397 kPa 1.0

Shear Modulus (MPa)
60.0
50.0
40.0
30.0
20.0
10.0
0.0
0.0001
0.001
0.01
0.1
1
Strain Amplitude (%)
Lower 232nd St. Clay
Tube Sample: 11.75m
TEST
σc'
OCR
TS1C5
103 kPa
3.9

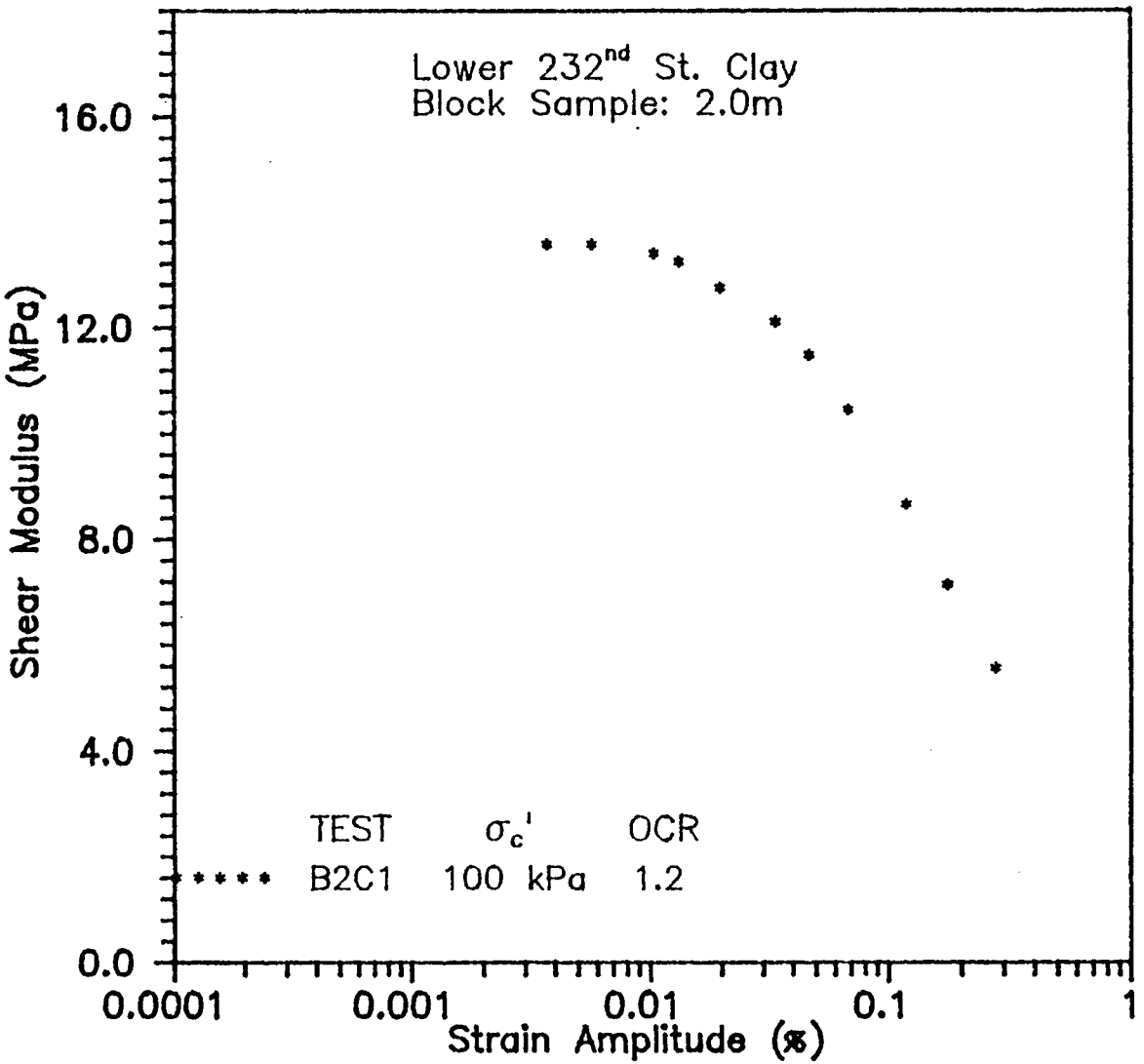
Lower 232nd St. Clay
Block Sample: 2.0m
16.0
12.0
8.0
4.0
0.0
Shear Modulus (MPa)
0.0001
0.001
0.01
0.1
1
Strain Amplitude (%)
TEST
σc'
OCR
B2C1
100 kPa
1.2

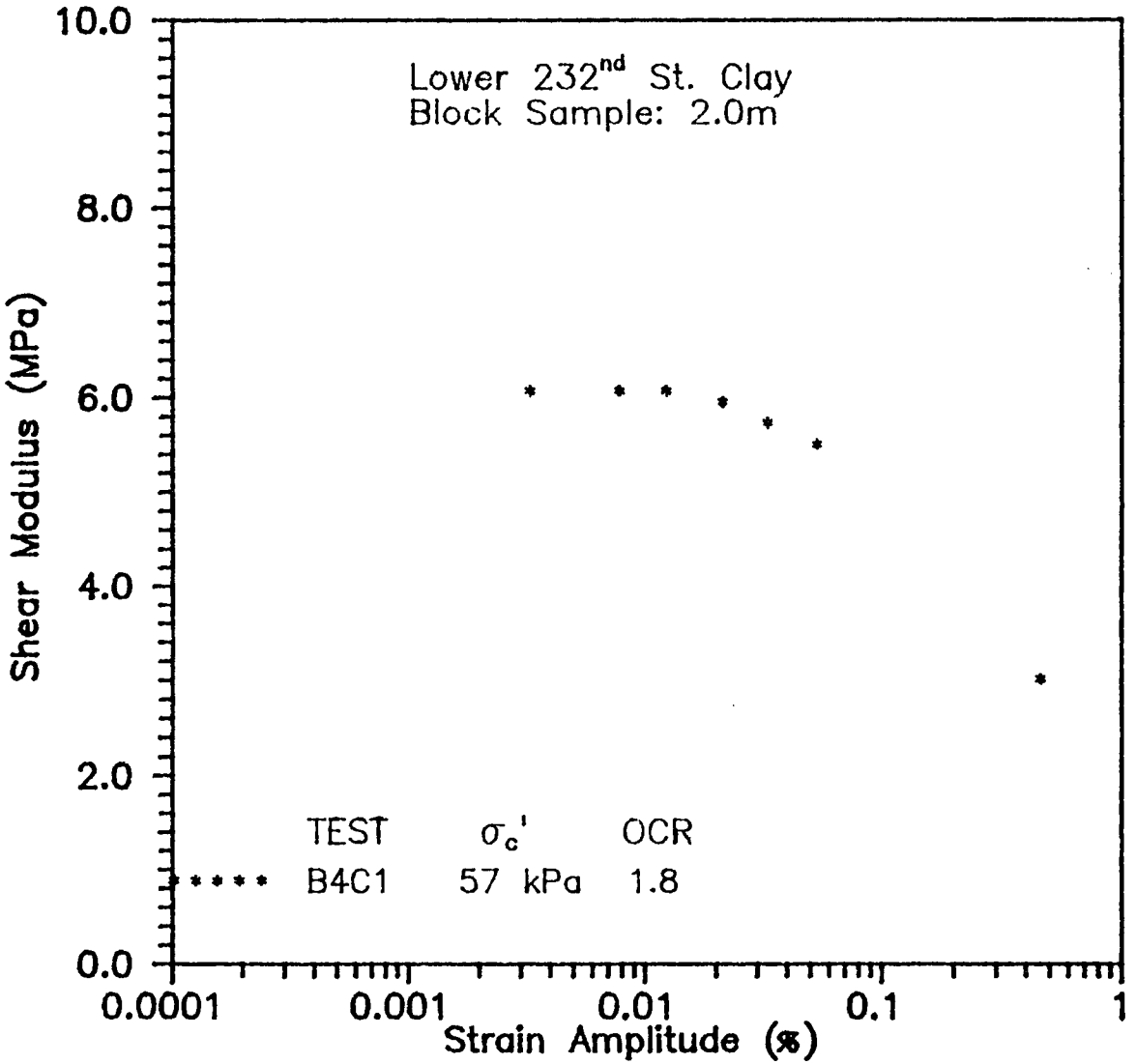
Lower 232nd St. Clay
Block Sample: 2.0m
Shear Modulus (MPa)
10.0
8.0
6.0
4.0
2.0
0.0
0.0001
0.001
0.01
0.1
1
Strain Amplitude (%)
TEST
σc'
OCR
B4C1
57 kPa
1.8

Shear Modulus (MPa)
35.0
30.0
25.0
20.0
15.0
10.0
Strain Amplitude (%)
0.0001
0.001
0.01
0.1
1
Lower 232nd St. Clay
Block Sample: 2.0m
TEST σc' OCR
B5C1 166 kPa 1.0

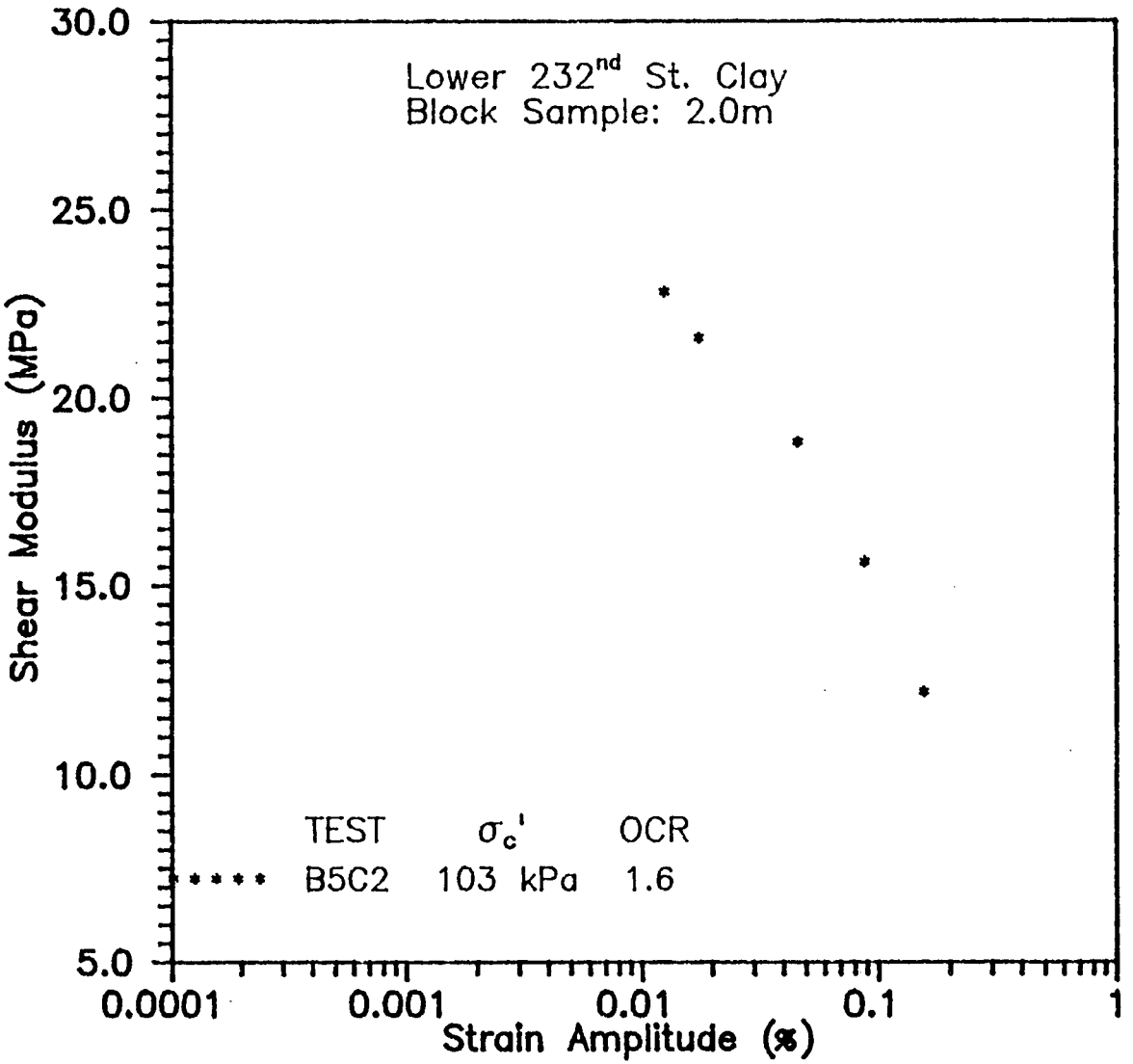
Lower 232nd St. Clay
Block Sample: 2.0m
30.0
25.0
20.0
15.0
10.0
5.0
Shear Modulus (MPa)
TEST σc' OCR
B5C2 103 kPa 1.6
0.0001
0.001
0.01
0.1
1
Strain Amplitude (%)

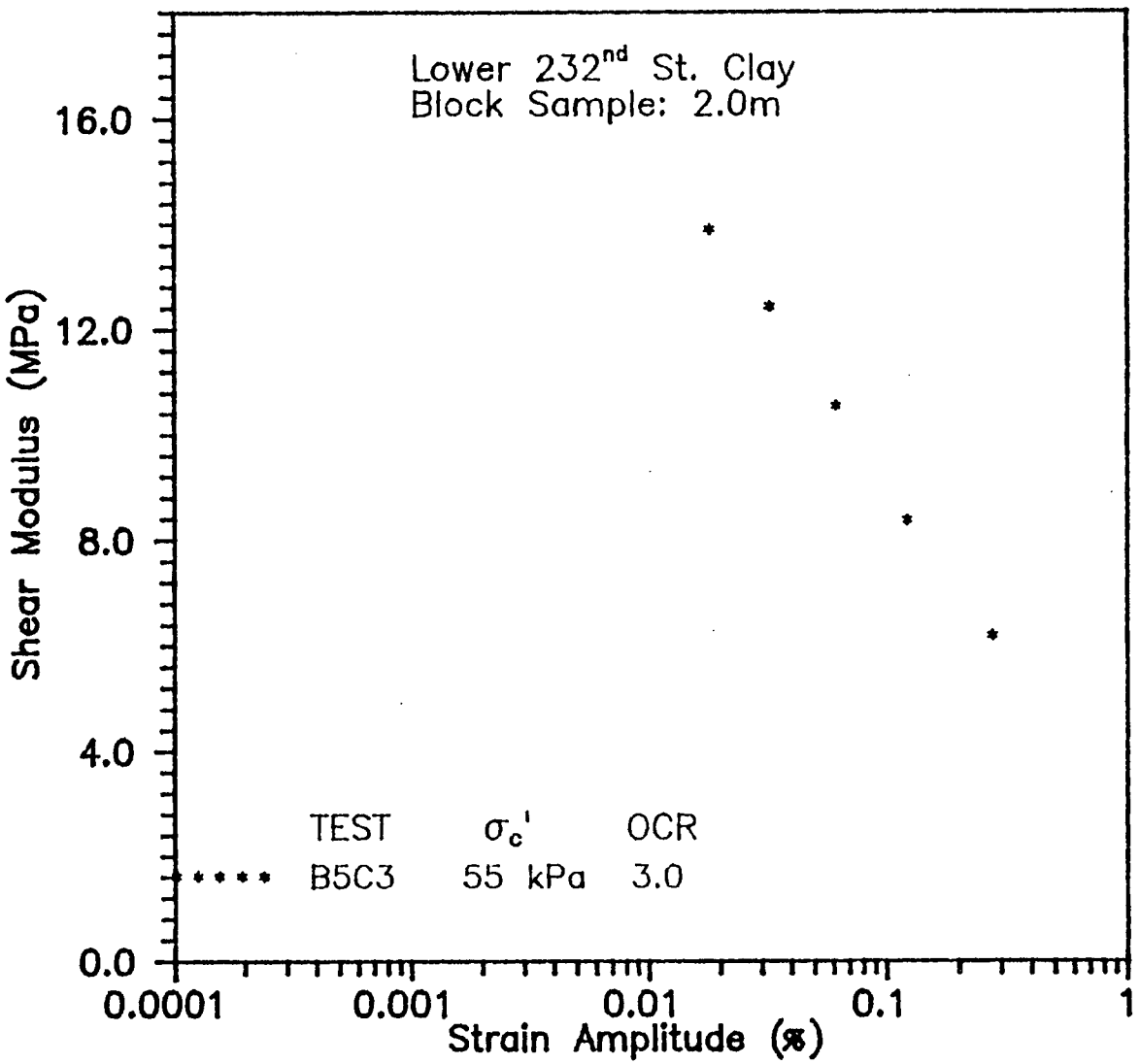
Lower 232nd St. Clay
Block Sample: 2.0m
16.0
12.0
8.0
4.0
0.0
Shear Modulus (MPa)
TEST
σc'
OCR
B5C3
55 kPa
3.0
0.0001
0.001
0.01
0.1
1
Strain Amplitude (%)

Shear Modulus (MPa)
18.0
17.0
16.0
15.0
14.0
13.0
12.0
0.0001
0.001
0.01
0.1
1
Strain Amplitude (%)
Lower 232nd St. Clay
Block Sample: 2.0m
TEST σc' OCR
B6C1 116 kPa 1.0

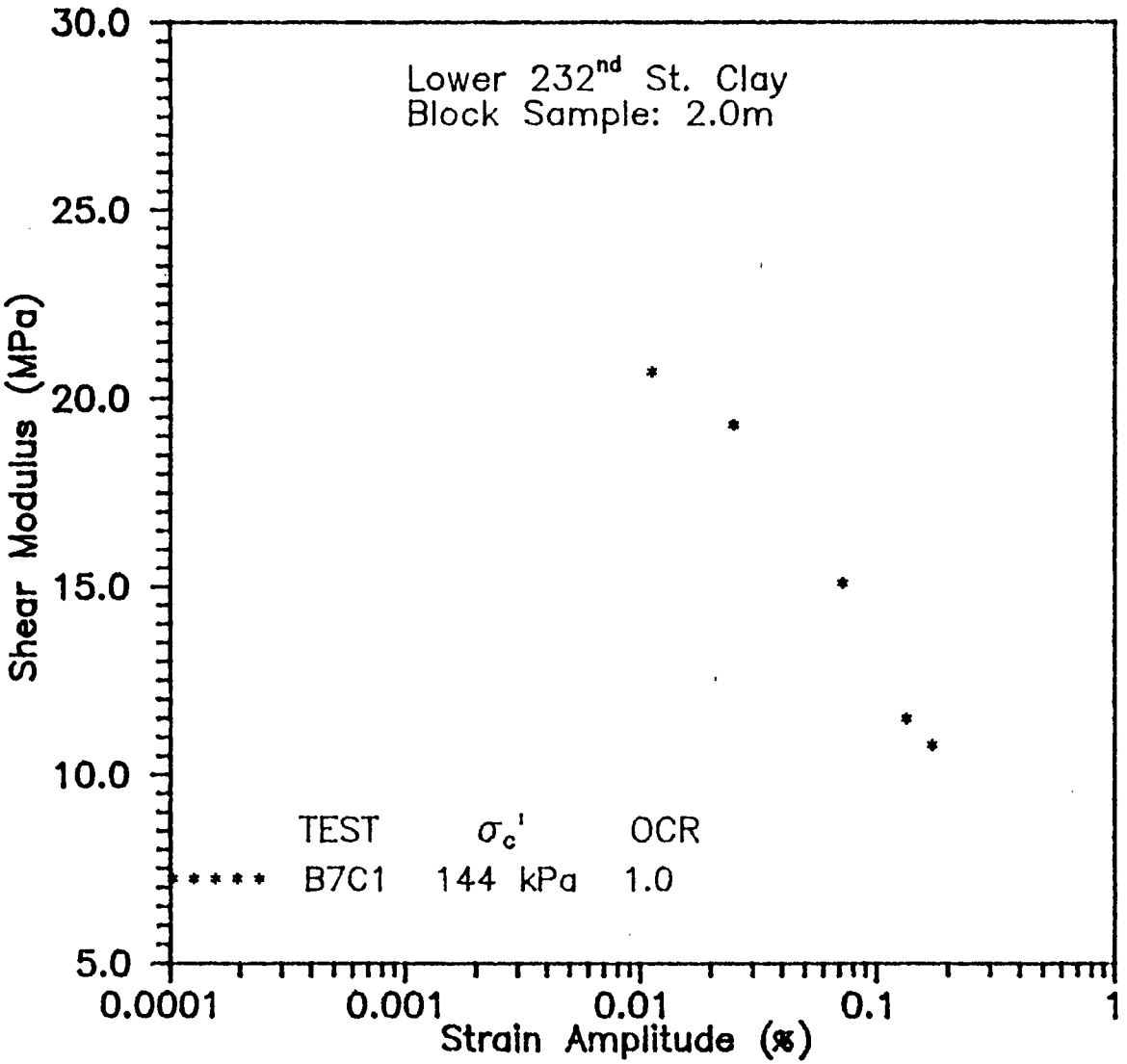
Lower 232nd St. Clay
Block Sample: 2.0m
30.0
25.0
20.0
15.0
10.0
5.0
Shear Modulus (MPa)
TEST
σc'
OCR
B7C1 144 kPa 1.0
0.0001
0.001
0.01
0.1
1
Strain Amplitude (%)

Shear Modulus (MPa)
0.0
2.0
4.0
6.0
8.0
10.0
12.0
14.0
Strain Amplitude (%)
0.0001
0.001
0.01
0.1
1
Lower 232nd St. Clay
Block Sample: 2.0m
TEST σc' OCR
***** B8C2 144 kPa 1.0

Shear Modulus (MPa)
20.0
18.0
16.0
14.0
12.0
10.0
8.0
0.0001
0.001
0.01
0.1
1
Strain Amplitude (%)
Lower 232nd St. Clay
Block Sample: 2.0m
TEST σc' OCR
B9C2 74 kPa 1.6

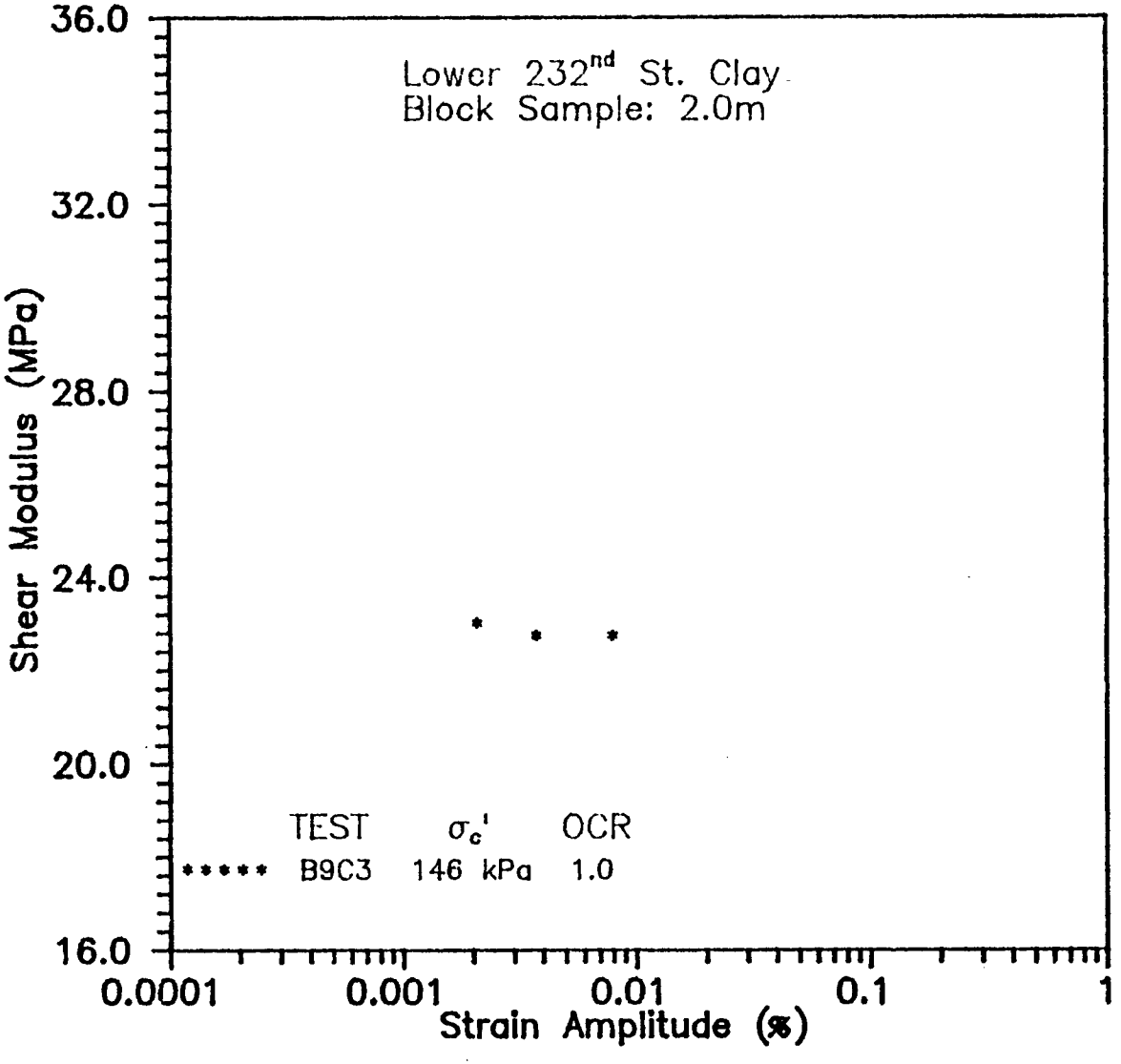
Lower 232nd St. Clay
Block Sample: 2.0m
36.0
32.0
28.0
24.0
20.0
16.0
Shear Modulus (MPa)
TEST
σc'
OCR
***** B9C3 146 kPa 1.0
0.0001
0.001
0.01
0.1
1
Strain Amplitude (%)

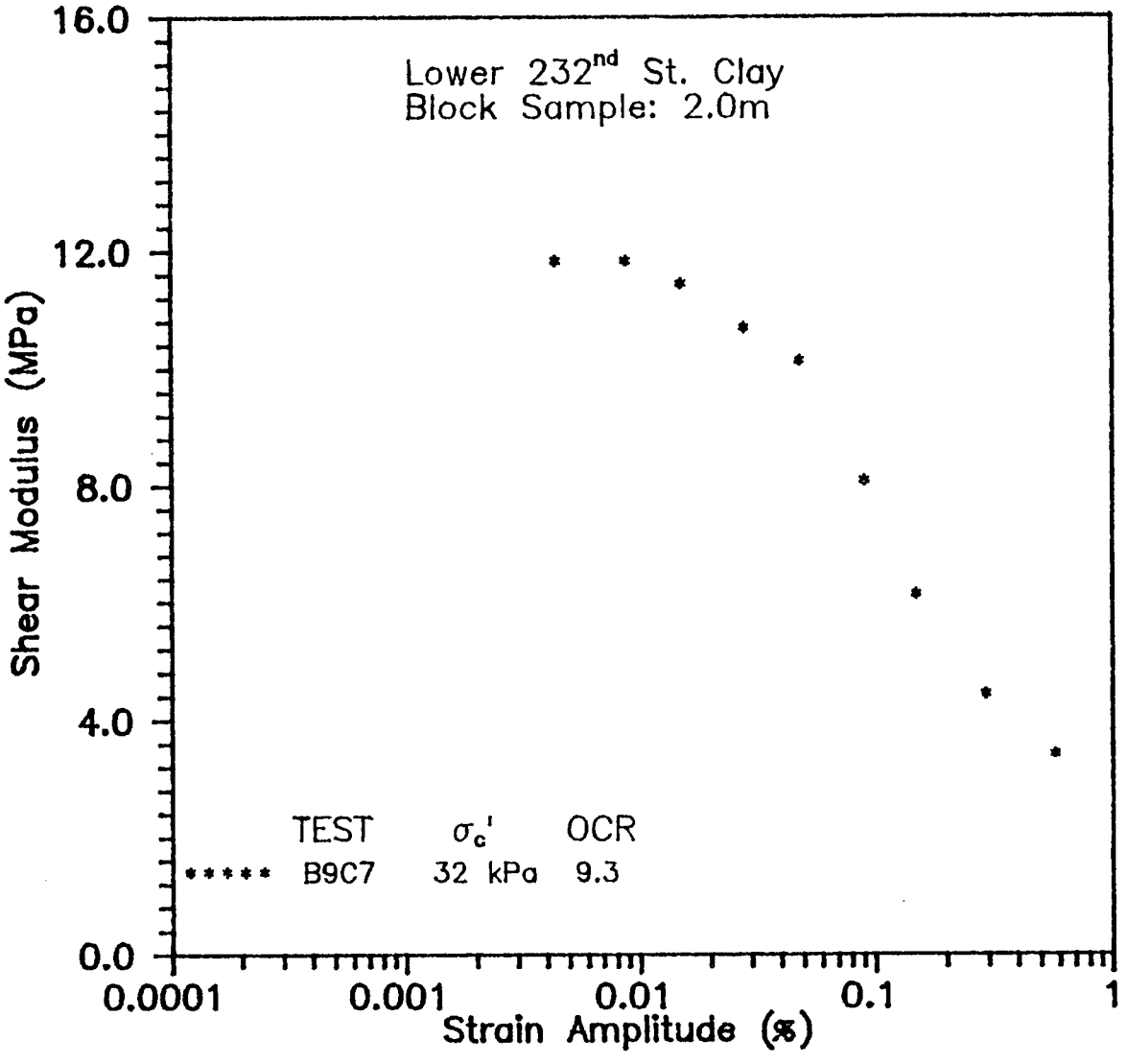
Lower 232nd St. Clay
Block Sample: 2.0m
16.0
12.0
8.0
4.0
0.0
Shear Modulus (MPa)
TEST
σc'
OCR
***** B9C7 32 kPa 9.3
0.0001
0.001
0.01
0.1
1
Strain Amplitude (%)

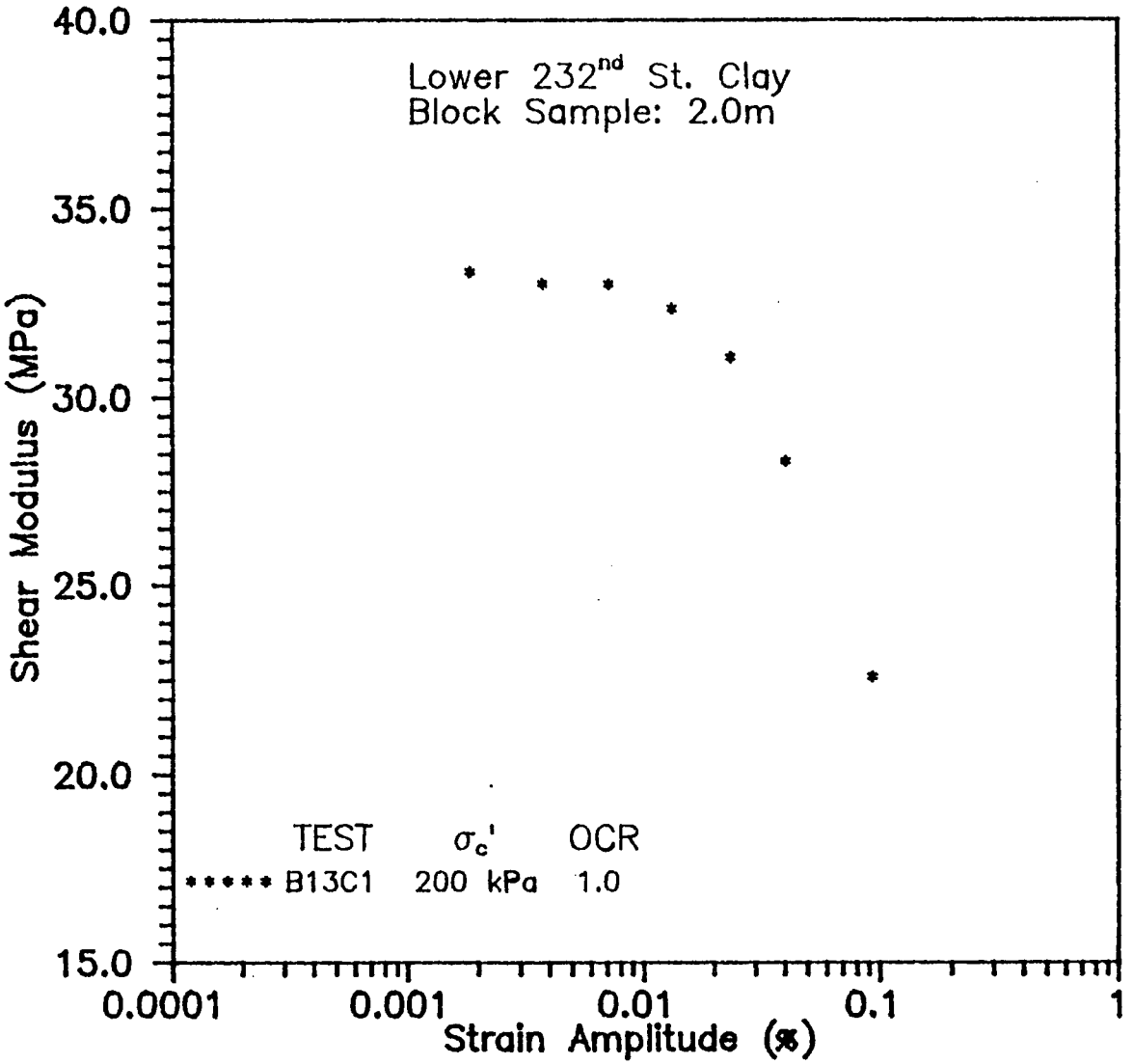
Lower 232nd St. Clay
Block Sample: 2.0m
Shear Modulus (MPa)
40.0
35.0
30.0
25.0
20.0
15.0
TEST σc' OCR
***** B13C1 200 kPa 1.0
0.0001
0.001
0.01
0.1
1
Strain Amplitude (%)

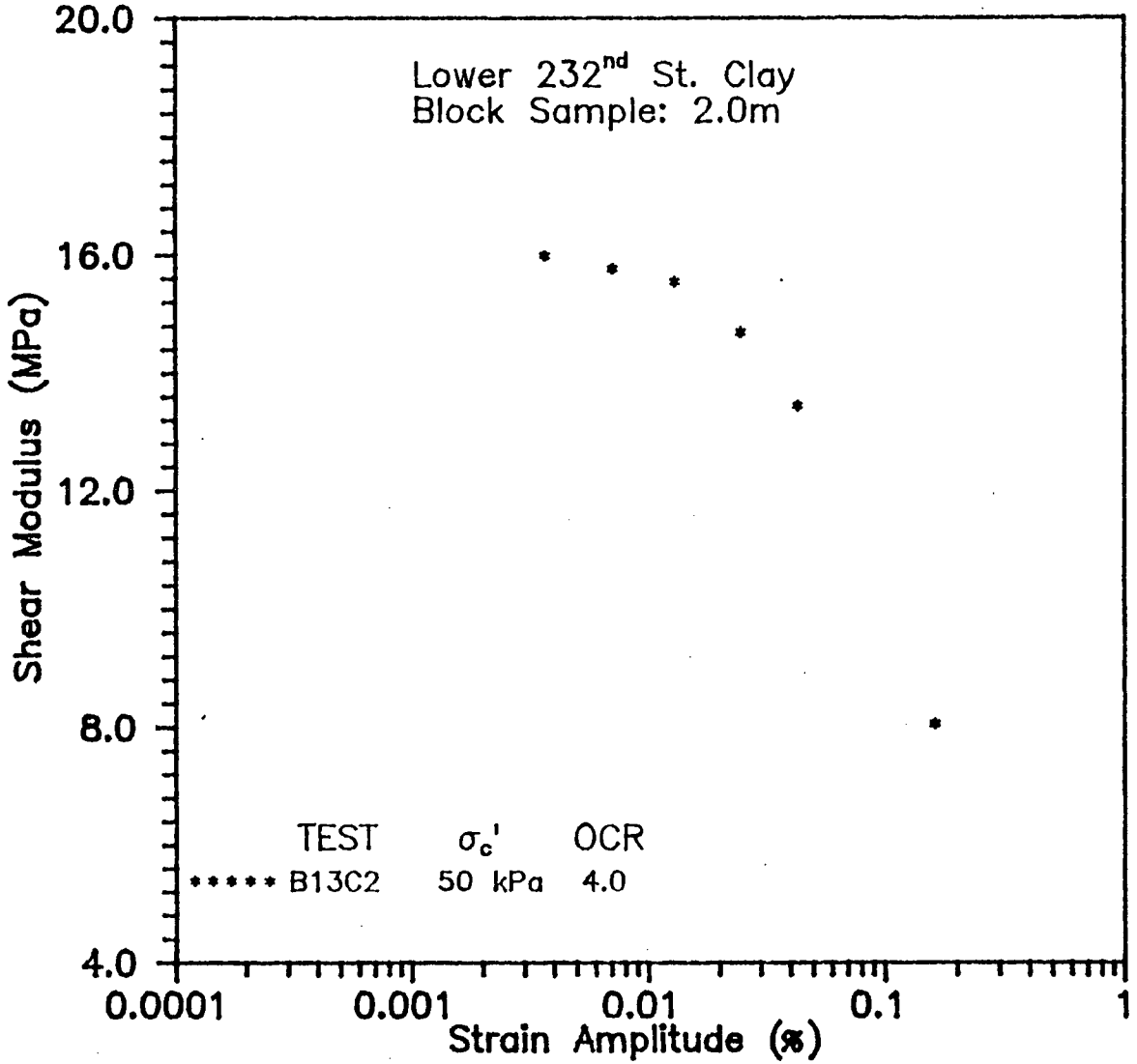
Lower 232nd St. Clay
Block Sample: 2.0m
20.0
16.0
12.0
8.0
4.0
Shear Modulus (MPa)
TEST
σc'
OCR
***** B13C2
50 kPa
4.0
0.0001
0.001
0.01
0.1
1
Strain Amplitude (%)

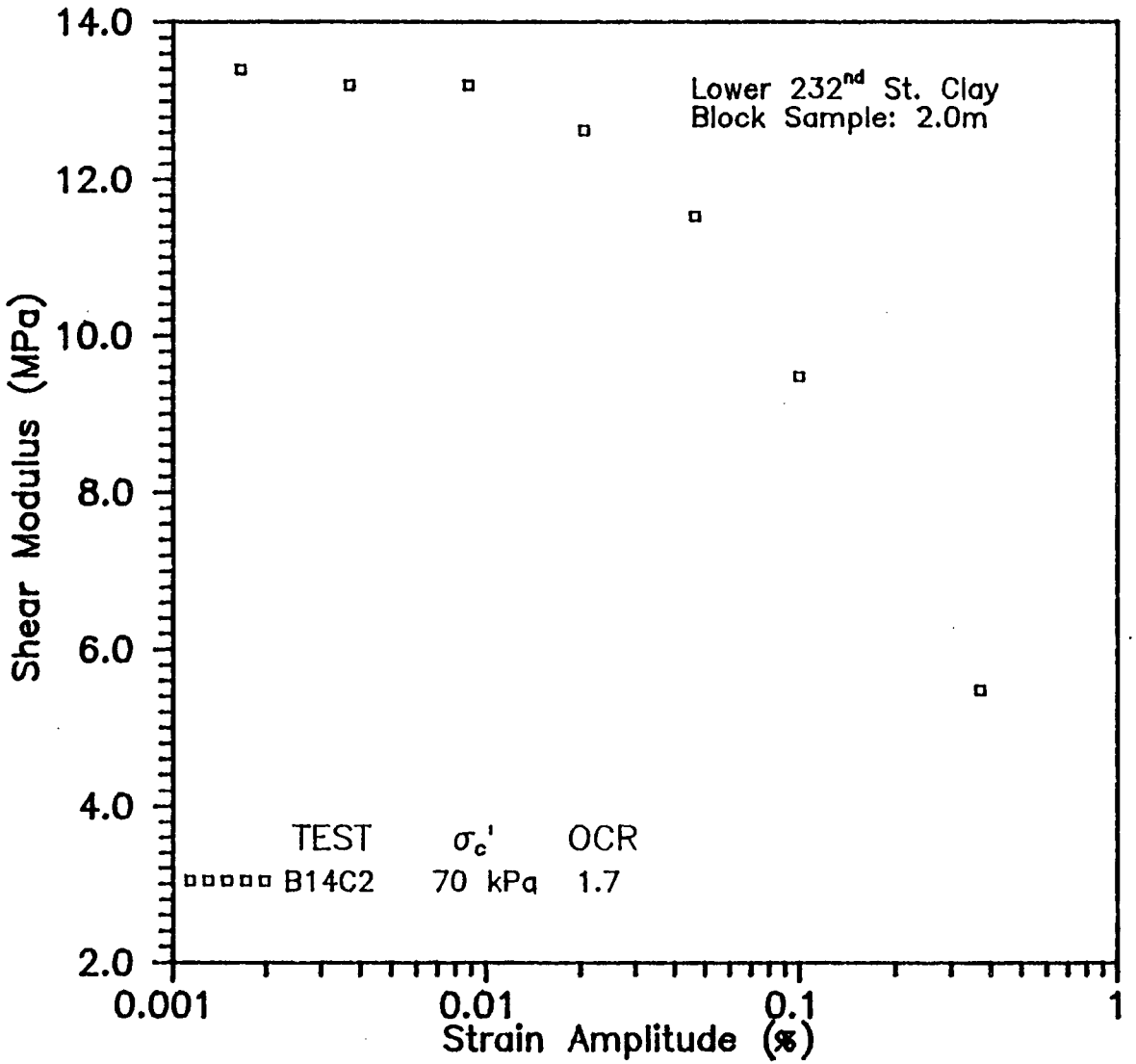
Lower 232nd St. Clay
Block Sample: 2.0m
TEST
σc'
OCR
B14C2
70 kPa
1.7
Shear Modulus (MPa)
14.0
12.0
10.0
8.0
6.0
4.0
2.0
0.001
0.01
0.1
1
Strain Amplitude (%)

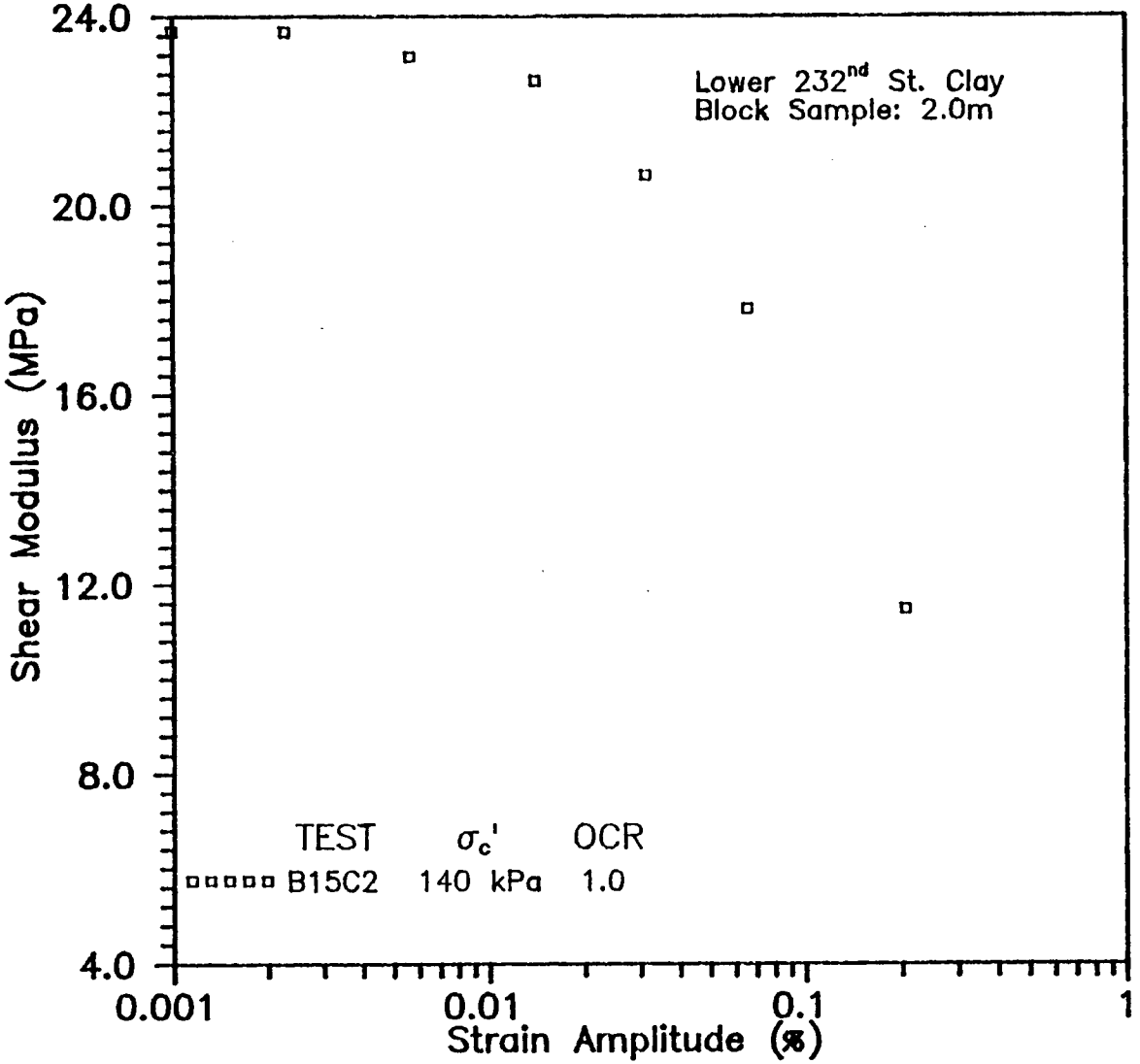
Lower 232nd St. Clay
Block Sample: 2.0m
TEST σc' OCR
B15C2 140 kPa 1.0
Shear Modulus (MPa)
24.0
20.0
16.0
12.0
8.0
4.0
0.001
0.01
0.1
1
Strain Amplitude (%)

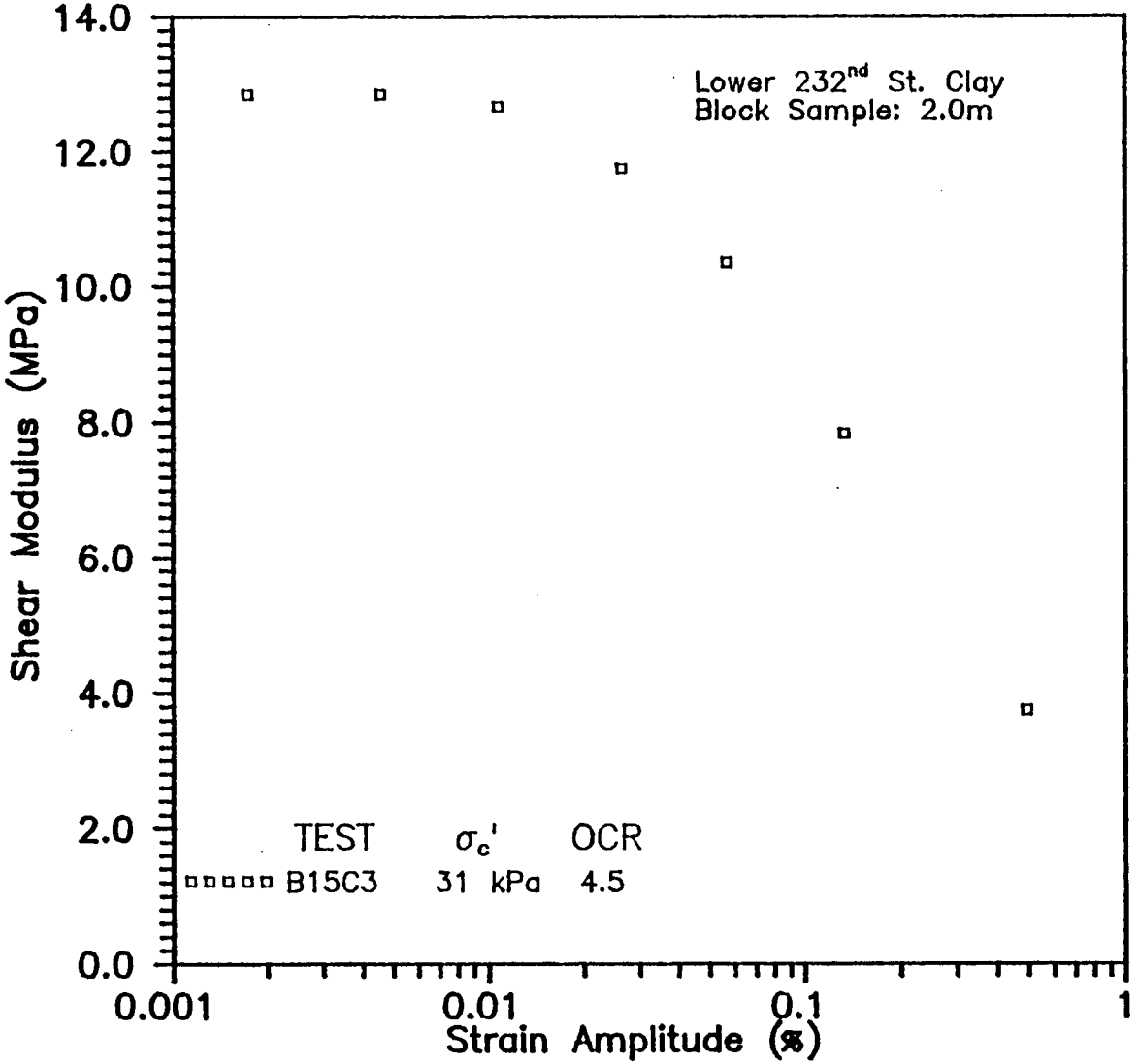
Lower 232nd St. Clay
Block Sample: 2.0m
TEST
σc'
OCR
B15C3
31 kPa
4.5
Shear Modulus (MPa)
Strain Amplitude (%)
14.0
12.0
10.0
8.0
6.0
4.0
2.0
0.0
0.001
0.01
0.1
1

Shear Modulus (MPa)
22.0
20.0
18.0
16.0
14.0
12.0
10.0
8.0
Strain Amplitude (%)
0.01
0.1
1
Lower 232nd St. Clay
Block Sample: 2.0m
TEST σc' OCR
B16C2 130 kPa 1.0

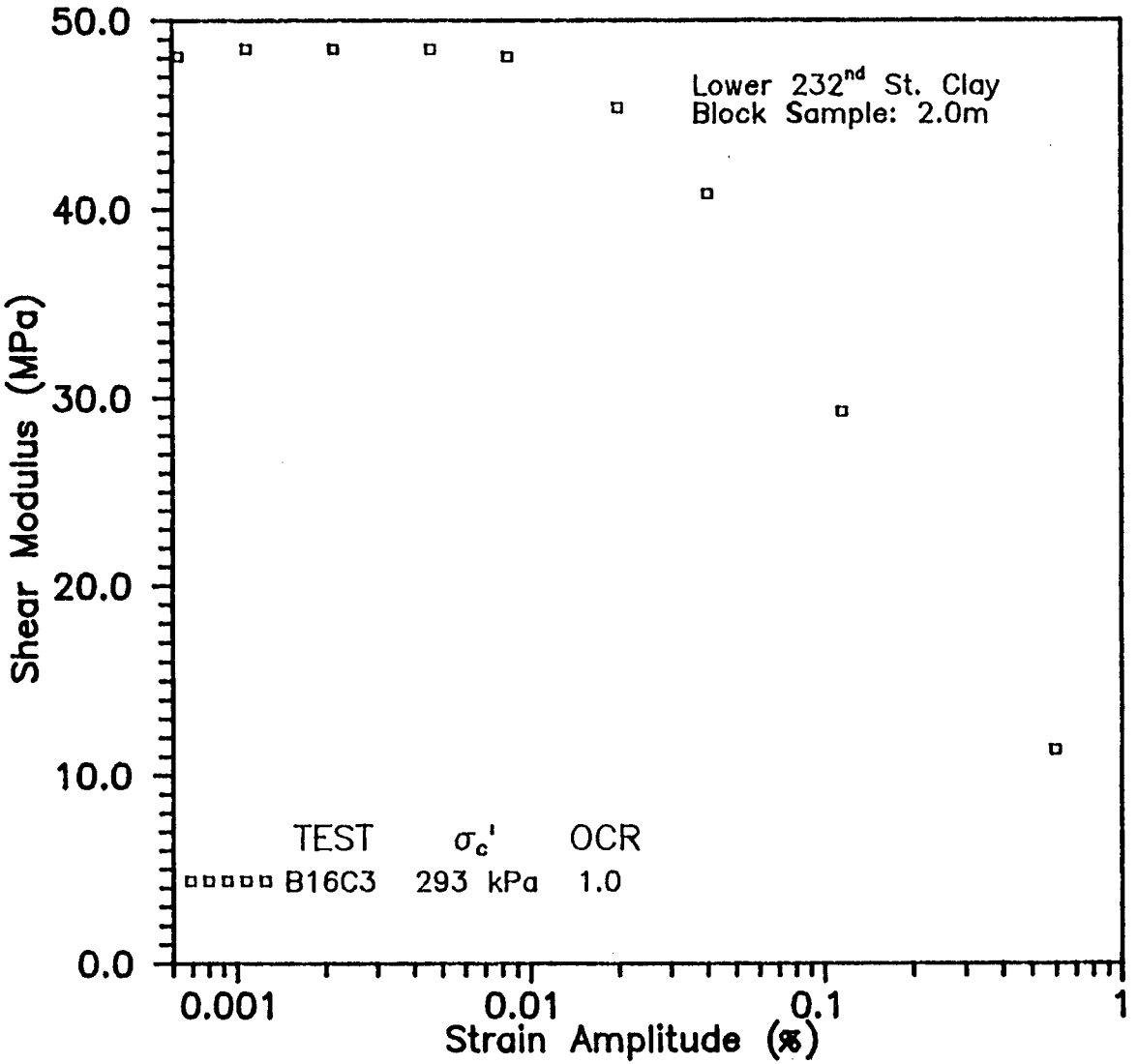
Lower 232nd St. Clay
Block Sample: 2.0m
TEST σc' OCR
B16C3 293 kPa 1.0
Shear Modulus (MPa)
50.0
40.0
30.0
20.0
10.0
0.0
0.001
0.01
0.1
1
Strain Amplitude (%)

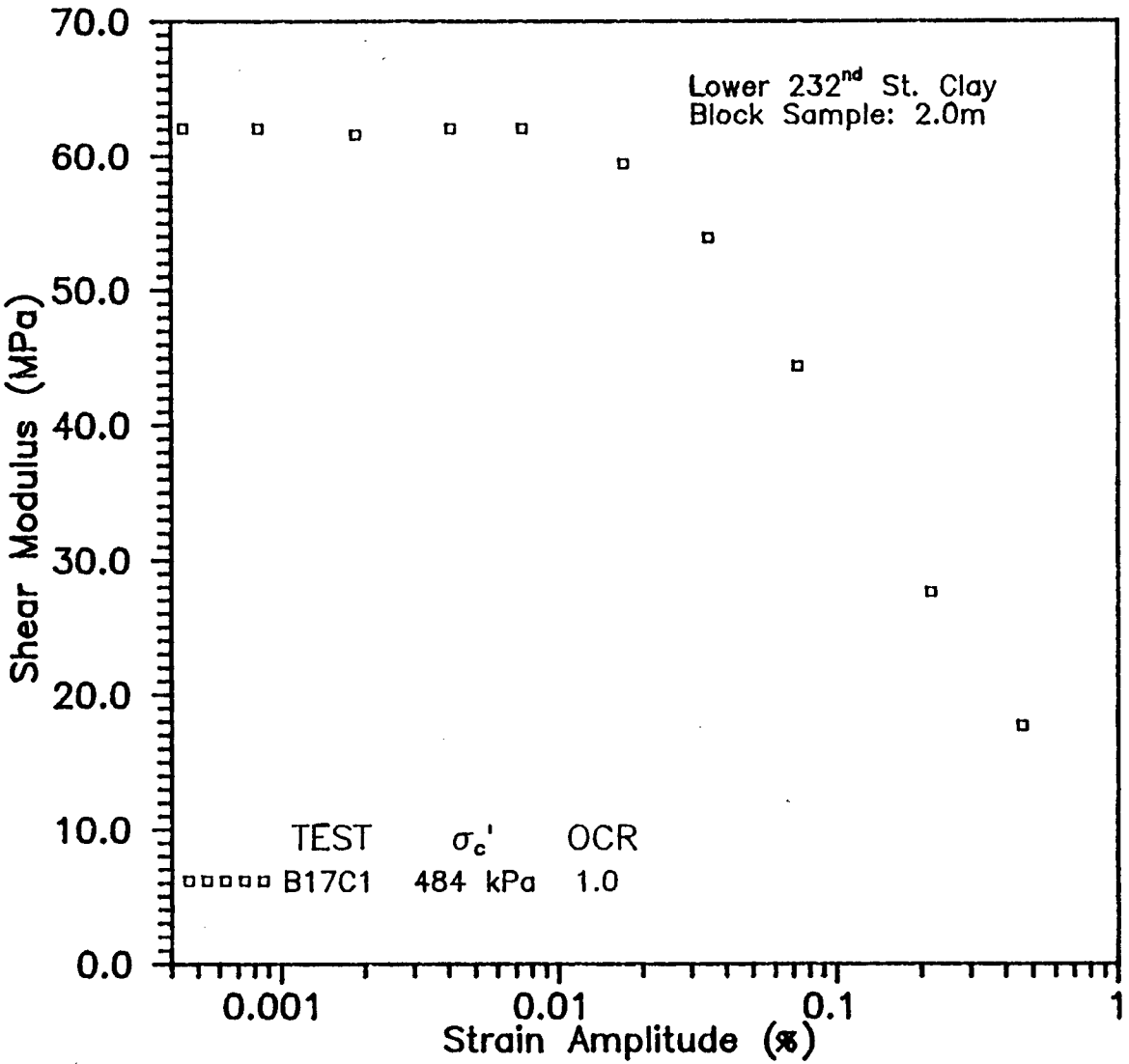
Lower 232nd St. Clay
Block Sample: 2.0m
TEST σc' OCR
B17C1 484 kPa 1.0
Shear Modulus (MPa)
70.0
60.0
50.0
40.0
30.0
20.0
10.0
0.0
0.001
0.01
0.1
1
Strain Amplitude (%)

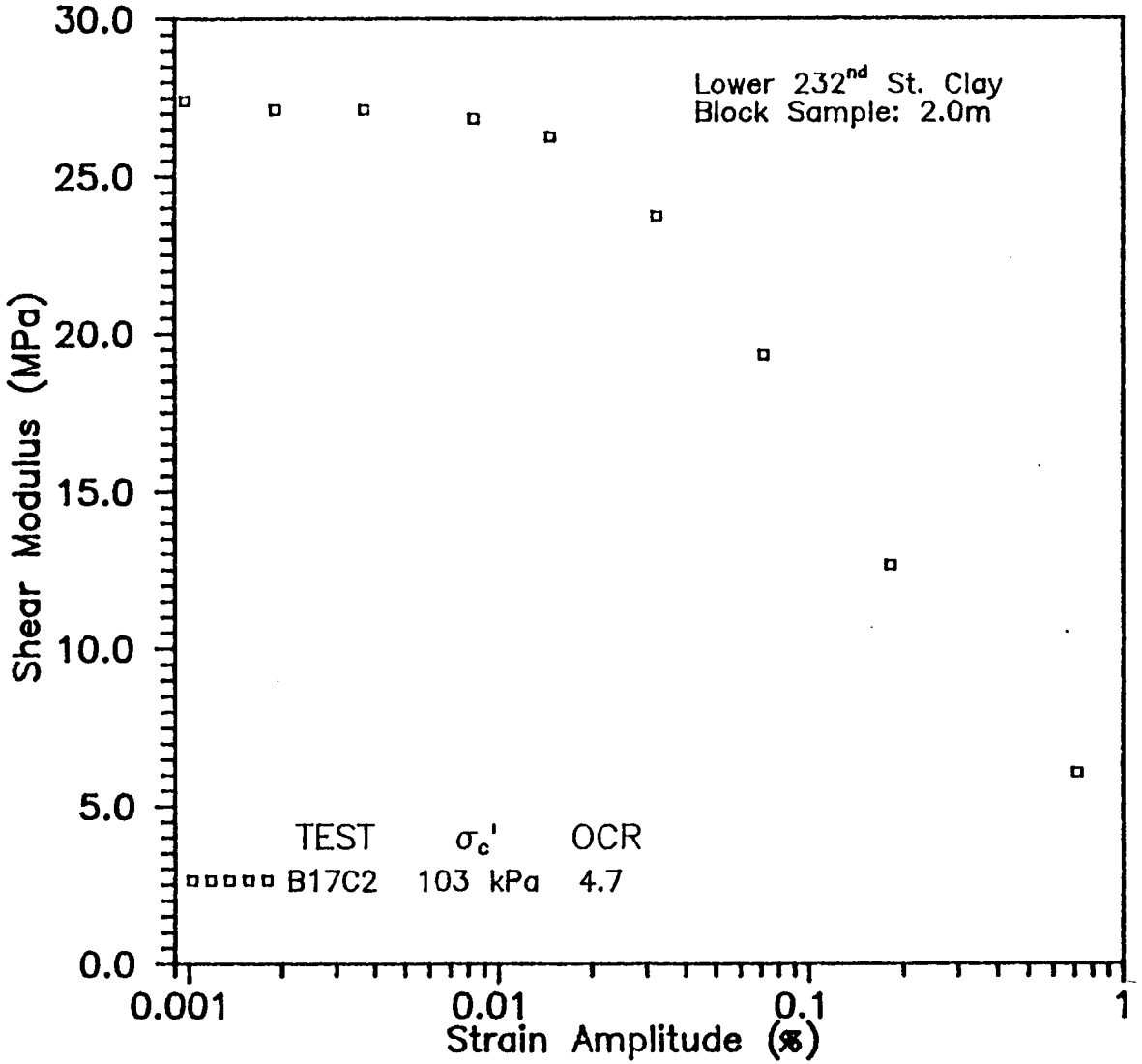
Lower 232nd St. Clay
Block Sample: 2.0m
TEST σc' OCR
B17C2 103 kPa 4.7
Shear Modulus (MPa)
30.0
25.0
20.0
15.0
10.0
5.0
0.0
0.001
0.01
0.1
1
Strain Amplitude (%)

Shear Modulus (MPa)
0.0
4.0
8.0
12.0
16.0
20.0
0.001
0.01
0.1
1
Strain Amplitude (%)
Lower 232nd St. Clay
Block Sample: 2.0m
TEST
B17C3
σc'
53 kPa
OCR
9.2

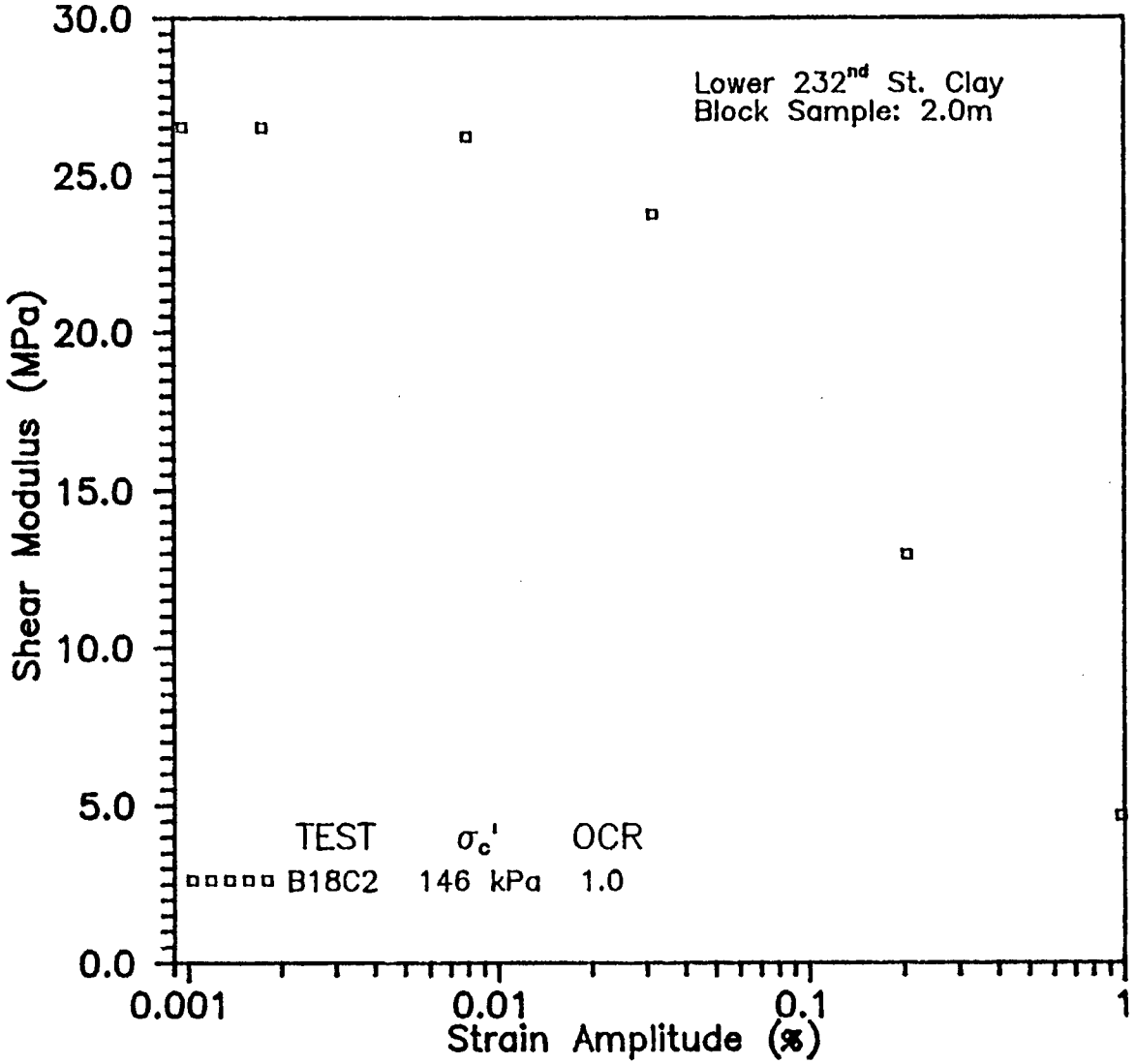
Lower 232nd St. Clay
Block Sample: 2.0m
TEST σc' OCR
B18C2 146 kPa 1.0
Shear Modulus (MPa)
30.0
25.0
20.0
15.0
10.0
5.0
0.0
0.001
0.01
0.1
1
Strain Amplitude (%)

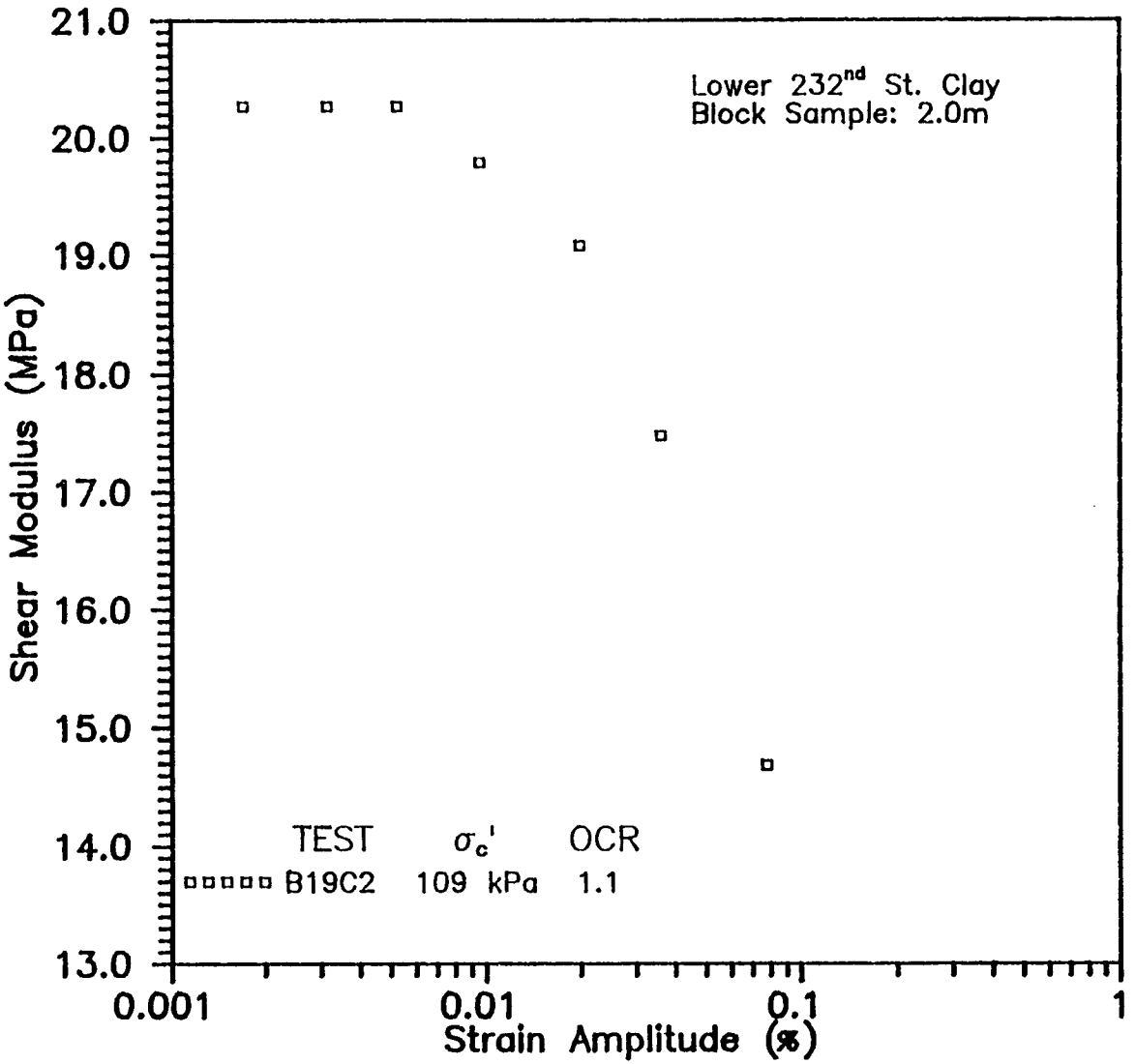
Lower 232nd St. Clay
Block Sample: 2.0m
TEST
σc'
OCR
B19C2
109 kPa
1.1
Shear Modulus (MPa)
21.0
20.0
19.0
18.0
17.0
16.0
15.0
14.0
13.0
0.001
0.01
0.1
1
Strain Amplitude (%)

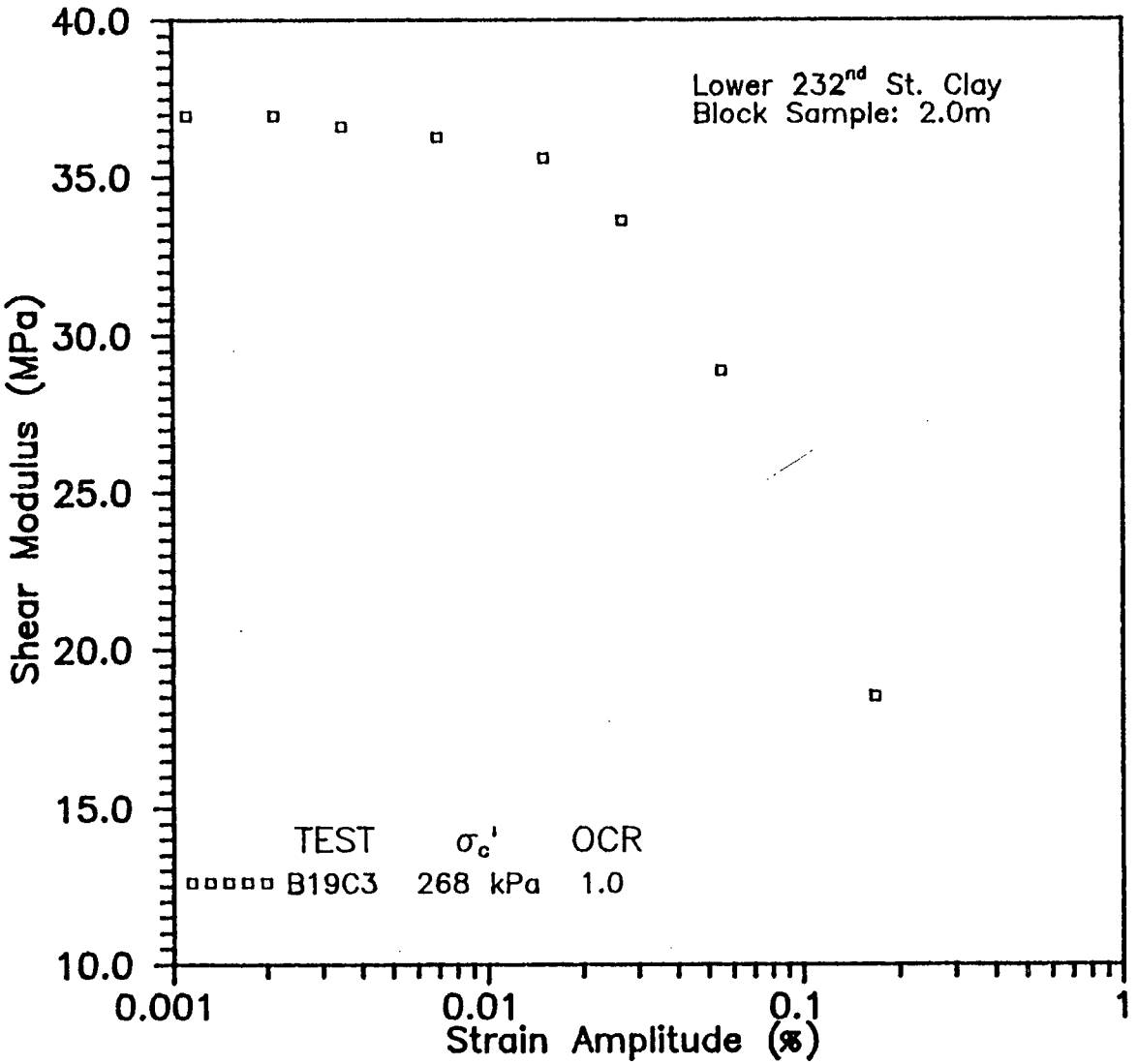
Lower 232nd St. Clay
Block Sample: 2.0m
TEST σc' OCR
B19C3 268 kPa 1.0
Shear Modulus (MPa)
40.0
35.0
30.0
25.0
20.0
15.0
10.0
0.001
0.01
0.1
1
Strain Amplitude (%)

Shear Modulus (MPa)
20.0
18.0
16.0
14.0
12.0
10.0
8.0
6.0
4.0
Strain Amplitude (%)
0.01
0.1
1
Lower 232nd St. Clay
Block Sample: 2.0m
TEST
B19C5
σc'
50 kPa
OCR
5.4

APPENDIX B:

Damping vs. Strain Curves

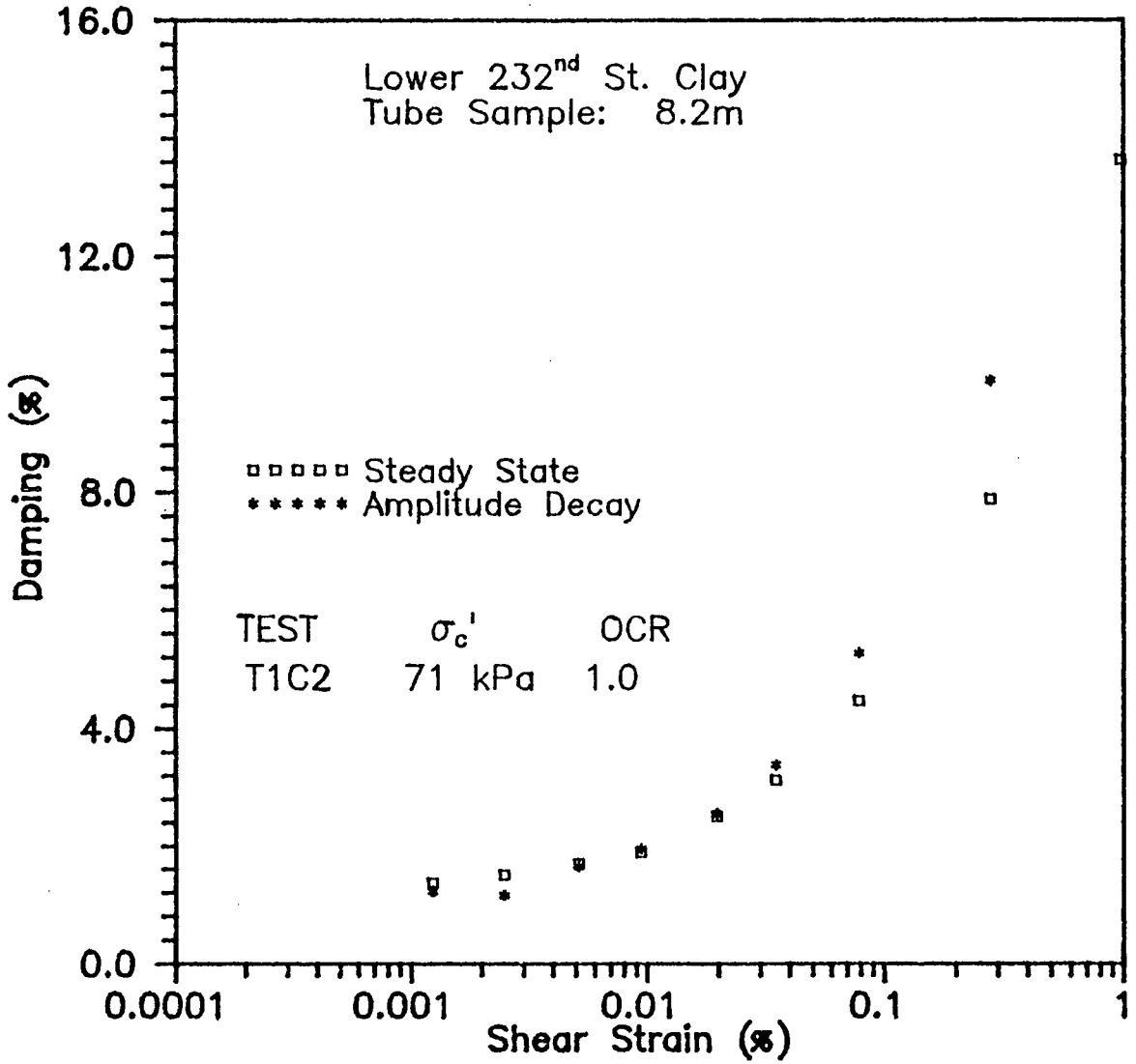
Lower 232nd St. Clay
Tube Sample: 8.2m
Steady State
Amplitude Decay
TEST σc' OCR
T1C2 71 kPa 1.0
Damping (%)
Shear Strain (%)
16.0
12.0
8.0
4.0
0.0
0.0001
0.001
0.01
0.1
1

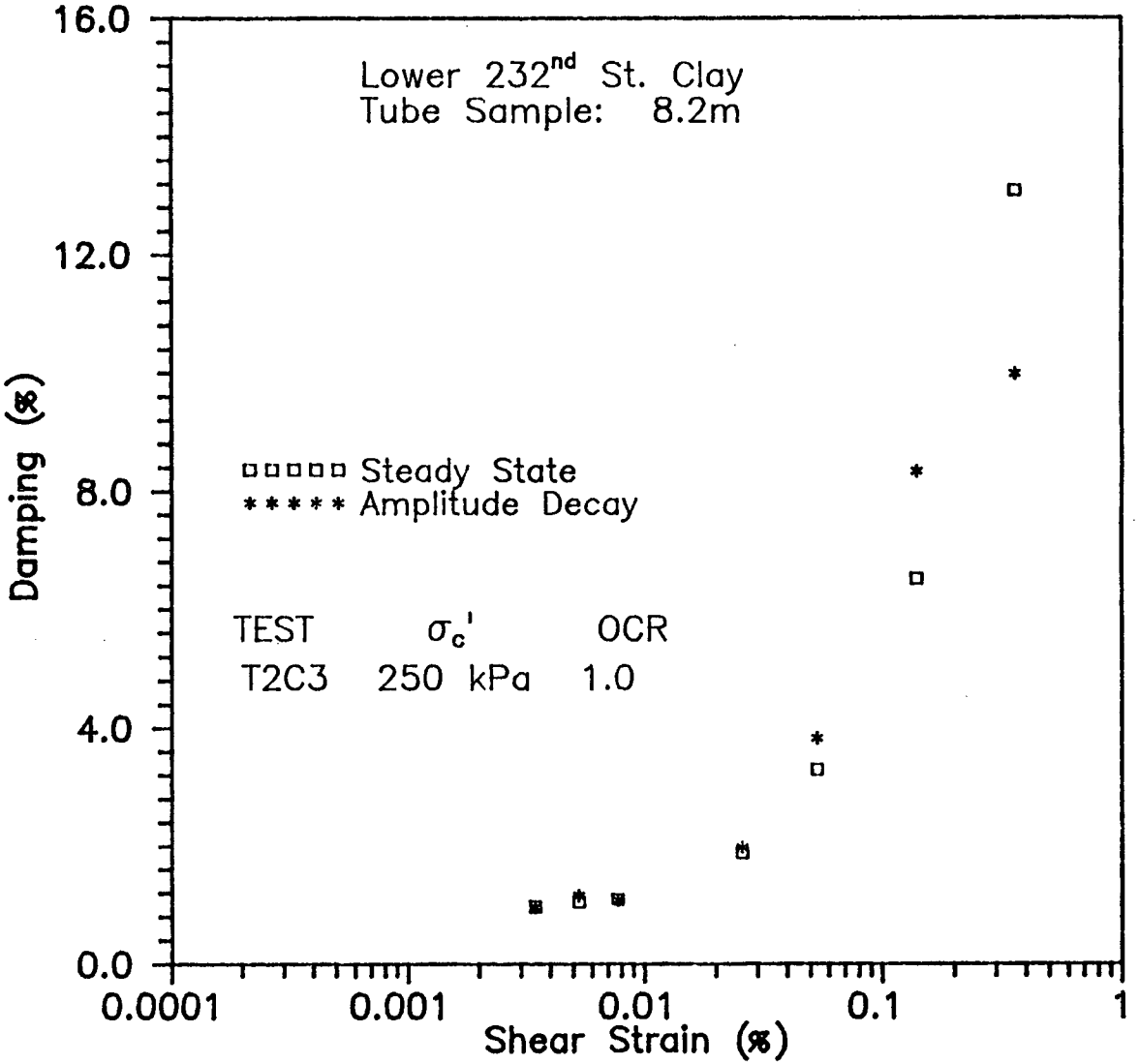
Lower 232nd St. Clay
Tube Sample: 8.2m
Steady State
Amplitude Decay
TEST σc' OCR
T2C3 250 kPa 1.0
Damping (%)
Shear Strain (%)
16.0
12.0
8.0
4.0
0.0
0.0001
0.001
0.01
0.1
1

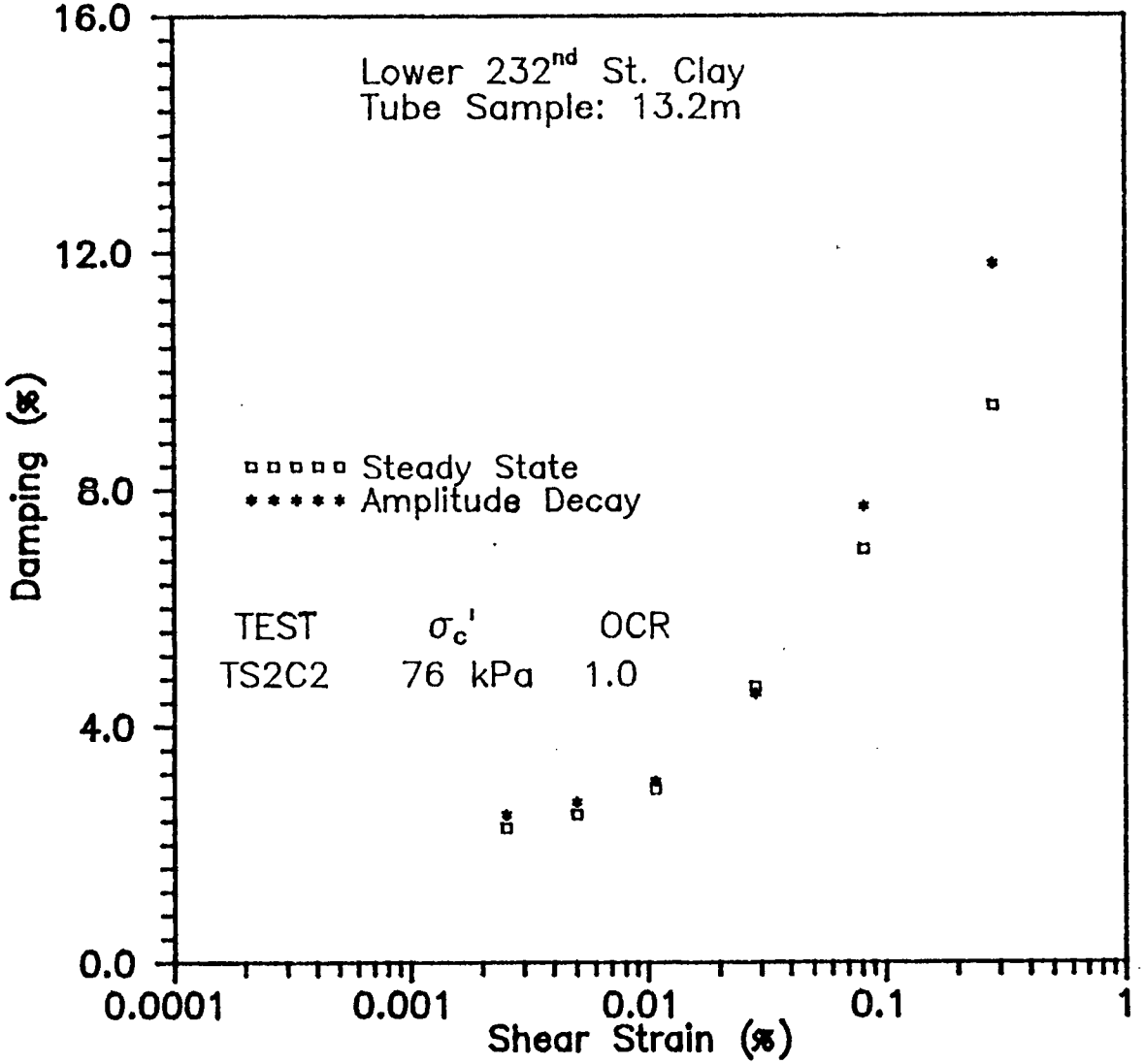
Lower 232nd St. Clay
Tube Sample: 13.2m
Steady State
Amplitude Decay
TEST
σc'
OCR
TS2C2
76 kPa
1.0
Damping (%)
Shear Strain (%)
16.0
12.0
8.0
4.0
0.0
0.0001
0.001
0.01
0.1
1

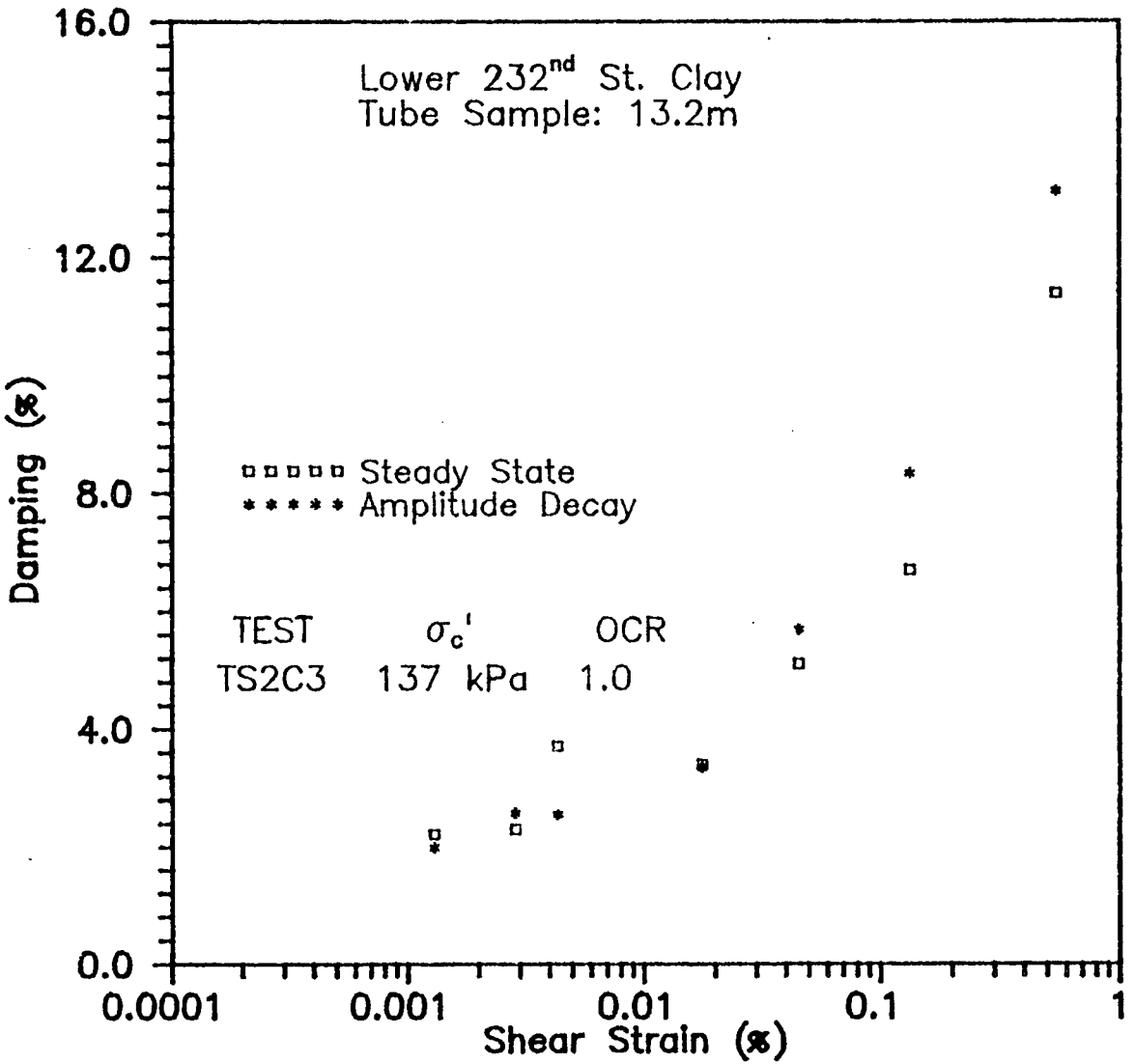
Lower 232nd St. Clay
Tube Sample: 13.2m
Steady State
Amplitude Decay
TEST σc' OCR
TS2C3 137 kPa 1.0
Damping (%)
Shear Strain (%)
16.0
12.0
8.0
4.0
0.0
0.0001
0.001
0.01
0.1
1

Lower 232nd St. Clay
Tube Sample: 13.2m
Steady State
Amplitude Decay
TEST σc' OCR
TS2C4 268 kPa 1.0
Damping (%)
16.0
12.0
8.0
4.0
0.0
0.0001
0.001
0.01
0.1
1
Shear Strain (%)

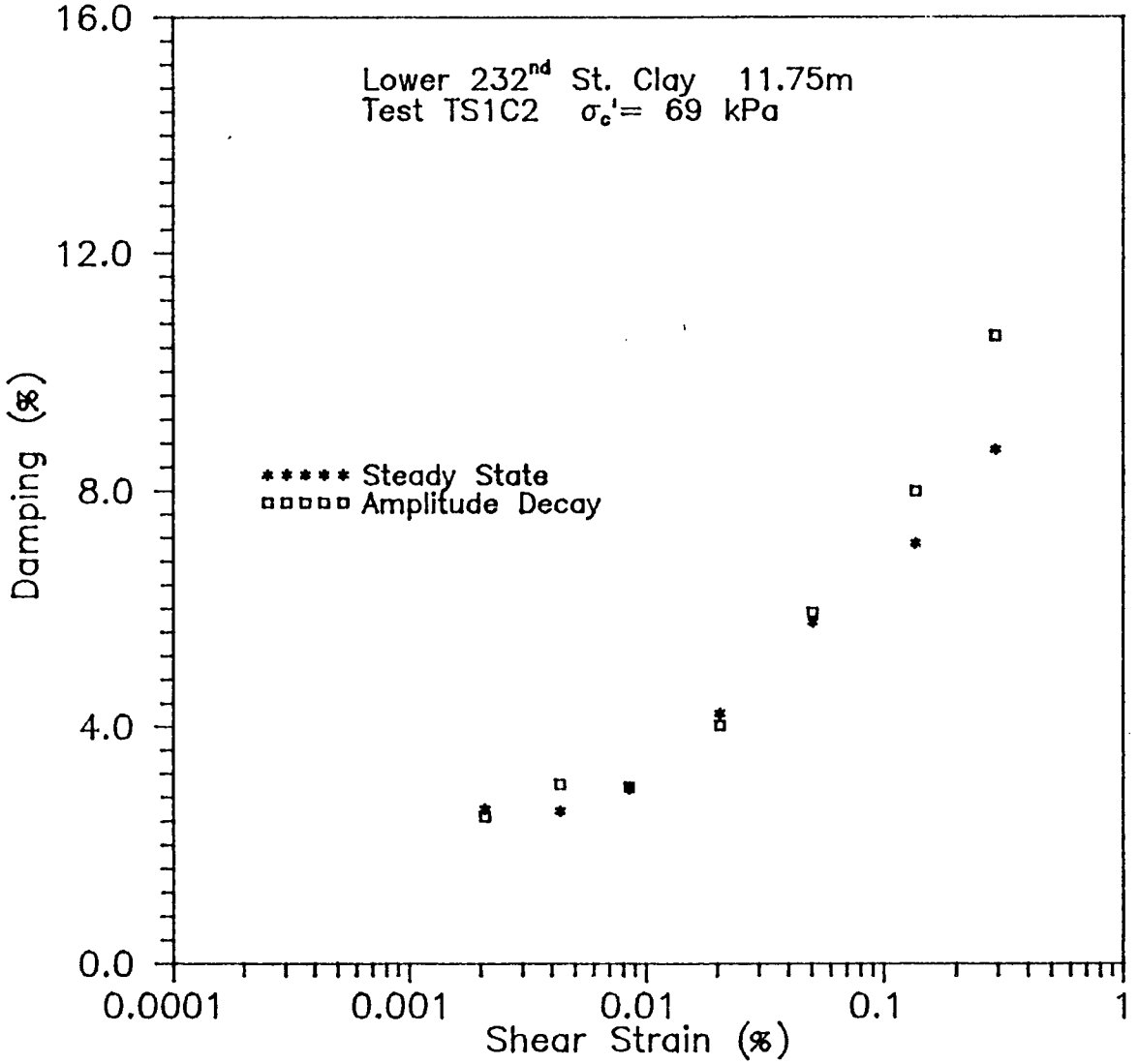
Lower 232nd St. Clay 11.75m
Test TS1C2 σc'= 69 kPa
***** Steady State
□□□□□ Amplitude Decay
Damping (%)
16.0
12.0
8.0
4.0
0.0
0.0001
0.001
0.01
0.1
1
Shear Strain (%)

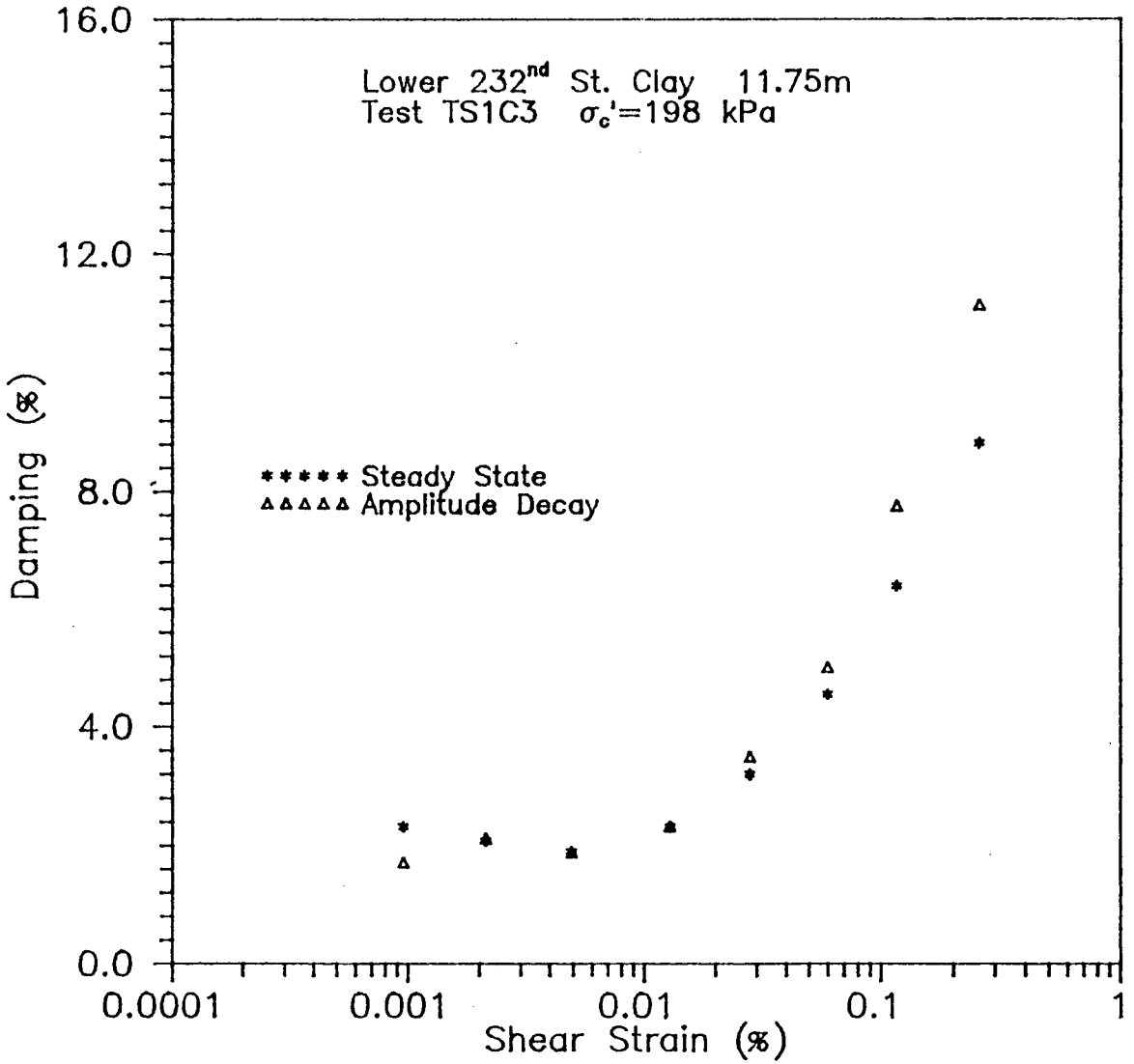
Lower 232nd St. Clay 11.75m
Test TS1C3 σc'=198 kPa
***** Steady State
ΔΔΔΔΔ Amplitude Decay
Damping (%)
16.0
12.0
8.0
4.0
0.0
0.0001
0.001
0.01
0.1
1
Shear Strain (%)

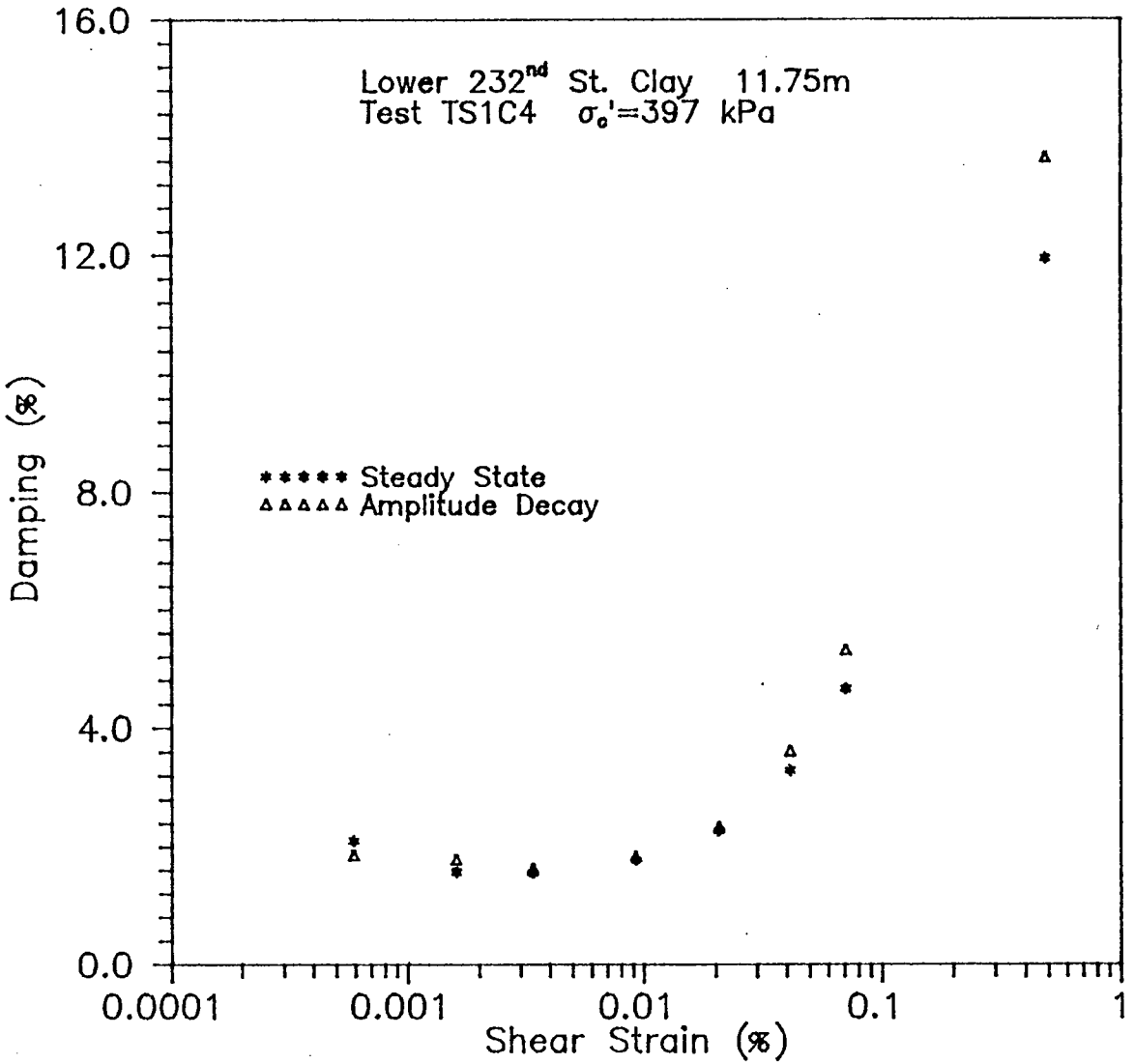
Lower 232nd St. Clay 11.75m
Test TS1C4 σo'=397 kPa
***** Steady State
ΔΔΔΔΔ Amplitude Decay
16.0
12.0
8.0
4.0
0.0
Damping (%)
0.0001
0.001
0.01
0.1
1
Shear Strain (%)

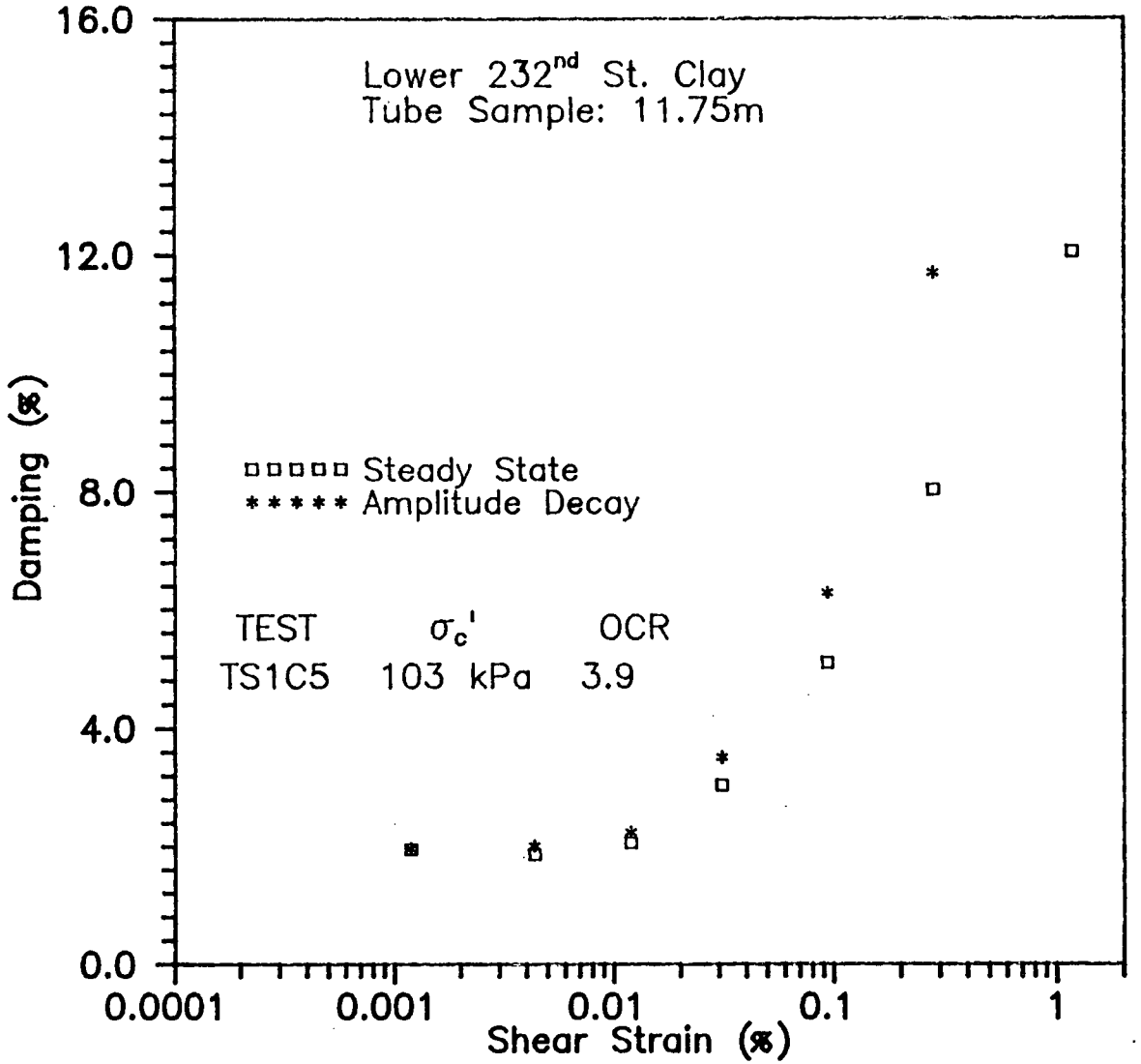
Lower 232nd St. Clay
Tube Sample: 11.75m
Steady State
Amplitude Decay
TEST σc' OCR
TS1C5 103 kPa 3.9
Damping (%)
Shear Strain (%)
16.0
12.0
8.0
4.0
0.0
0.0001
0.001
0.01
0.1
1

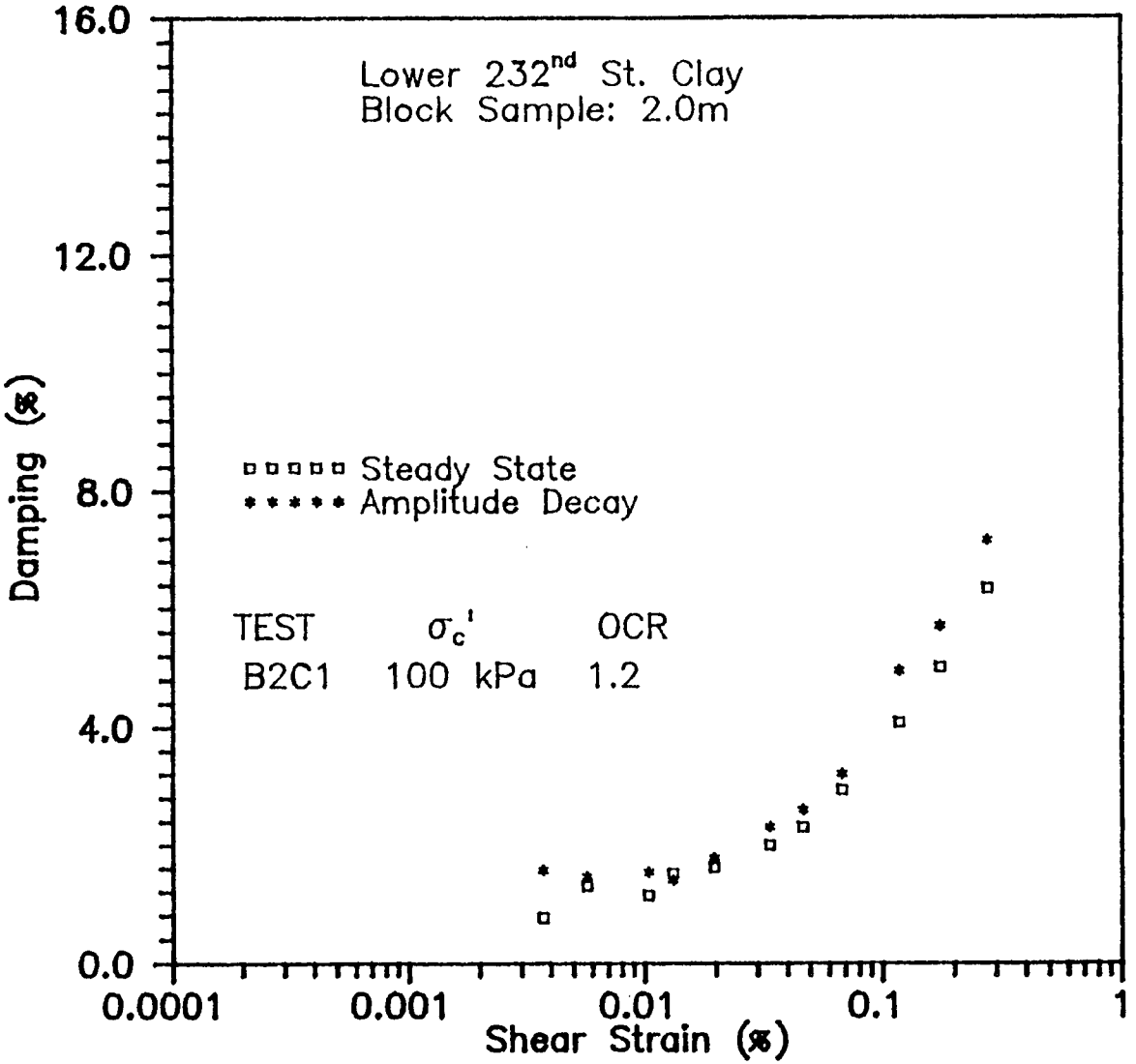
Lower 232nd St. Clay
Block Sample: 2.0m
Steady State
Amplitude Decay
TEST σc' OCR
B2C1 100 kPa 1.2
Damping (%)
Shear Strain (%)
16.0
12.0
8.0
4.0
0.0
0.0001
0.001
0.01
0.1
1

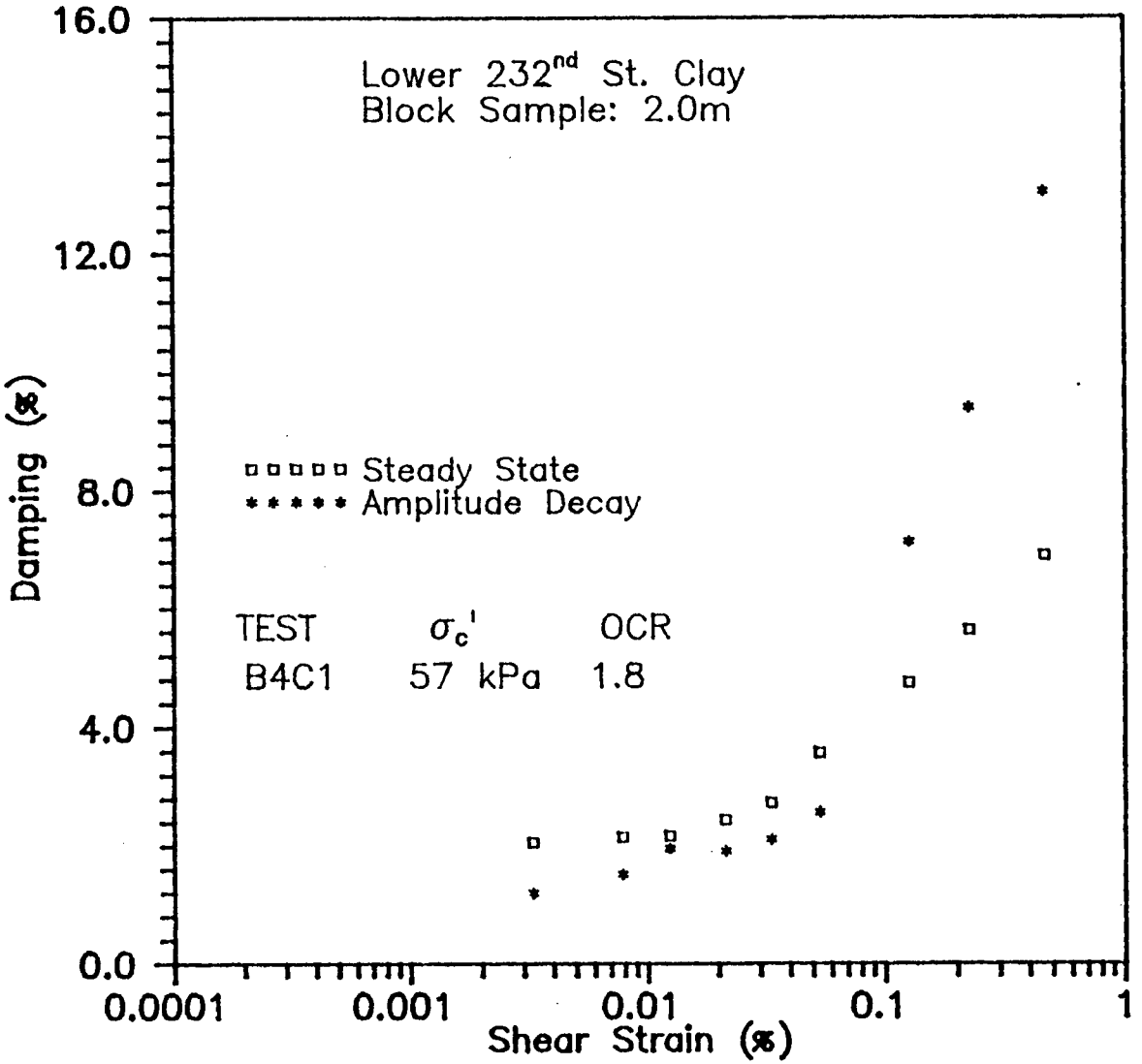
Lower 232nd St. Clay
Block Sample: 2.0m
Steady State
Amplitude Decay
TEST
σc'
OCR
B4C1
57 kPa
1.8
Damping (%)
16.0
12.0
8.0
4.0
0.0
0.0001
0.001
0.01
0.1
1
Shear Strain (%)

Damping (%)
16.0
12.0
8.0
4.0
0.0
0.0001
0.001
0.01
0.1
1
Shear Strain (%)
Lower 232nd St. Clay
Block Sample: 2.0m
Steady State
Amplitude Decay
TEST σc' OCR
B5C1 166 kPa 1.0

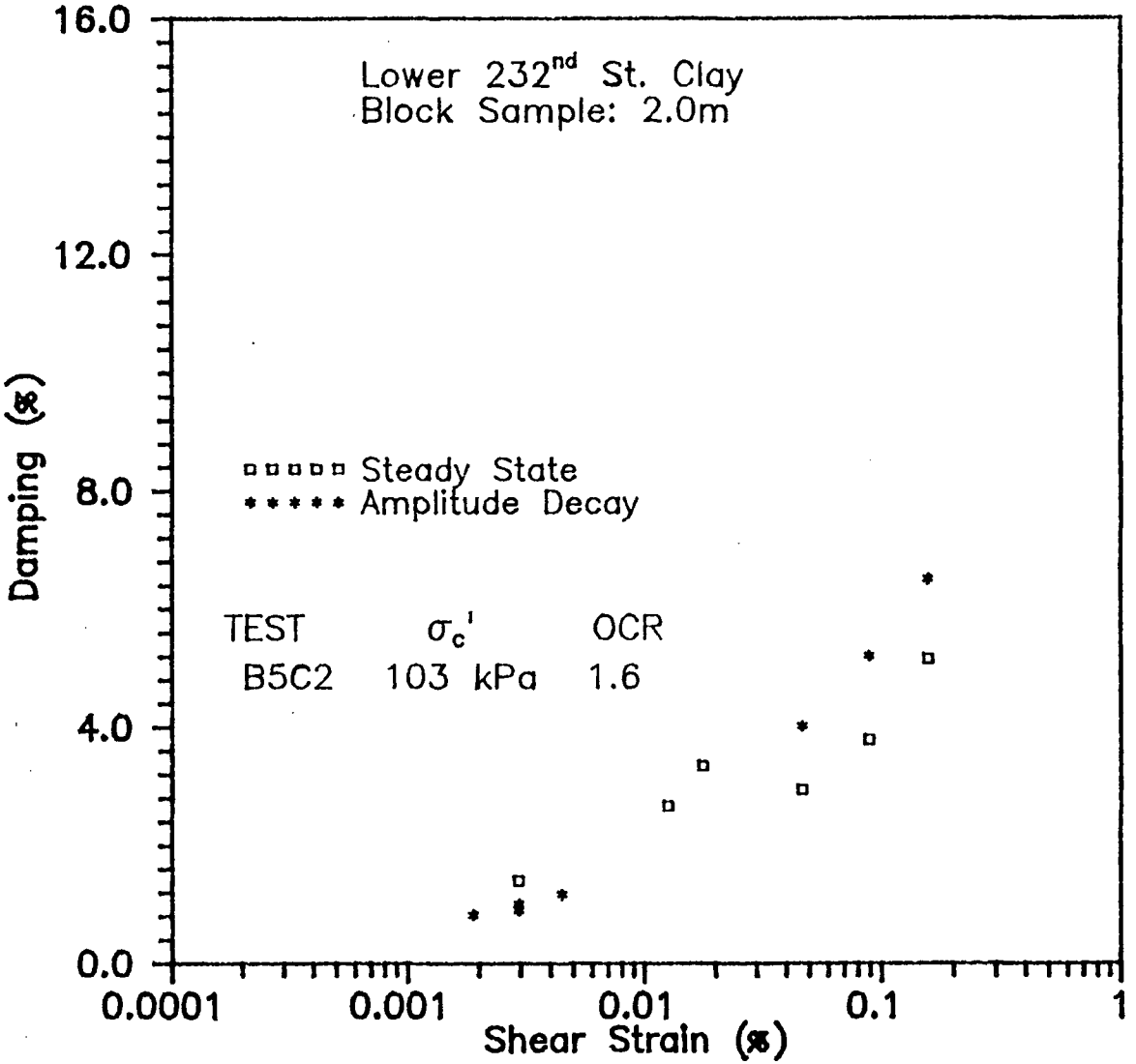
Lower 232nd St. Clay
Block Sample: 2.0m
Steady State
Amplitude Decay
TEST
σc'
OCR
B5C2
103 kPa
1.6
16.0
12.0
8.0
4.0
0.0
Damping (%)
0.0001
0.001
0.01
0.1
1
Shear Strain (%)

Lower 232nd St. Clay
Block Sample: 2.0m
Steady State
Amplitude Decay
TEST σc' OCR
B5C3 55 kPa 3.0
Damping (%)
16.0
12.0
8.0
4.0
0.0
0.0001
0.001
0.01
0.1
1
Shear Strain (%)

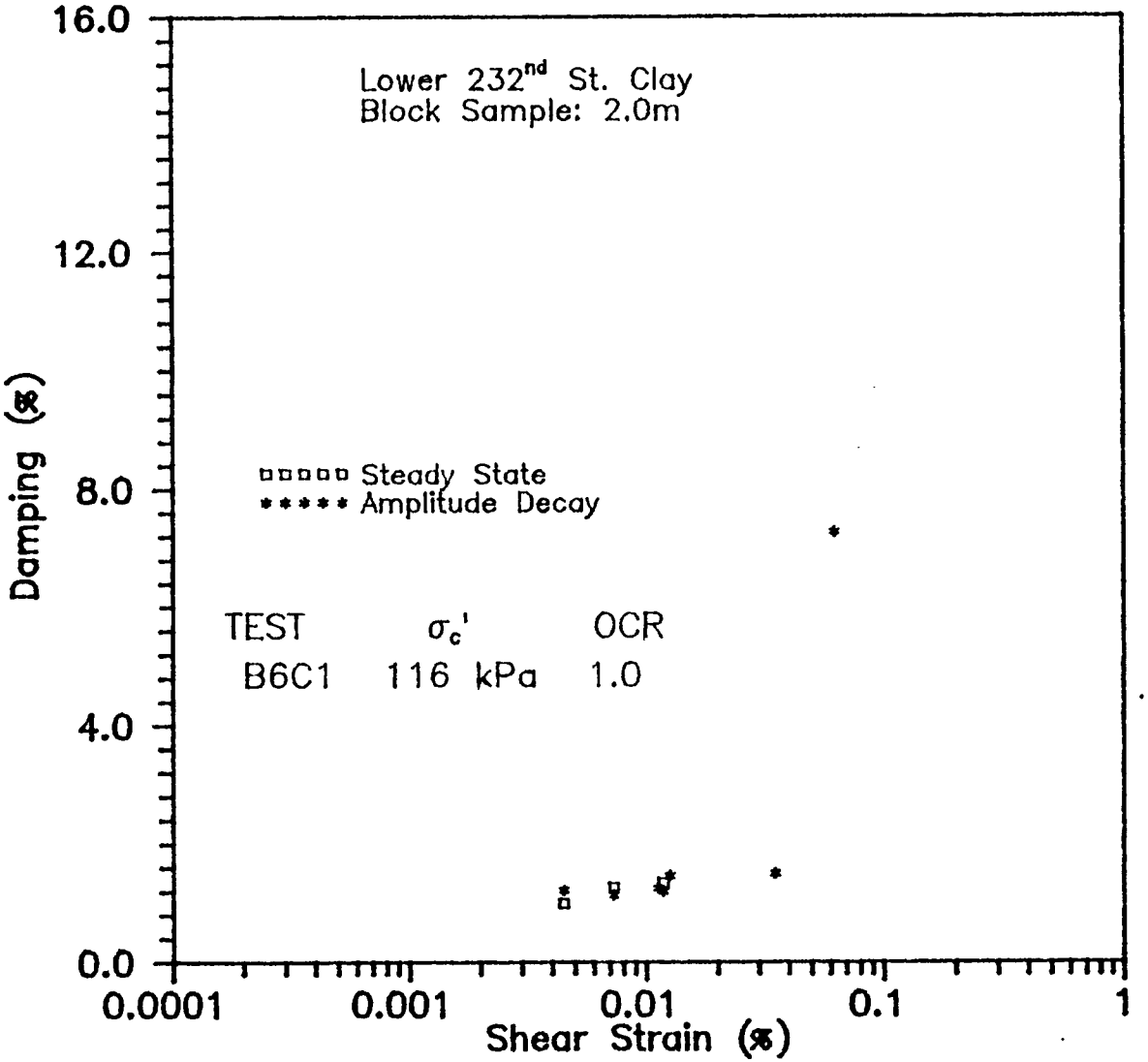
Lower 232nd St. Clay
Block Sample: 2.0m
Steady State
Amplitude Decay
TEST σc' OCR
B6C1 116 kPa 1.0
Damping (%)
16.0
12.0
8.0
4.0
0.0
0.0001
0.001
0.01
0.1
1
Shear Strain (%)

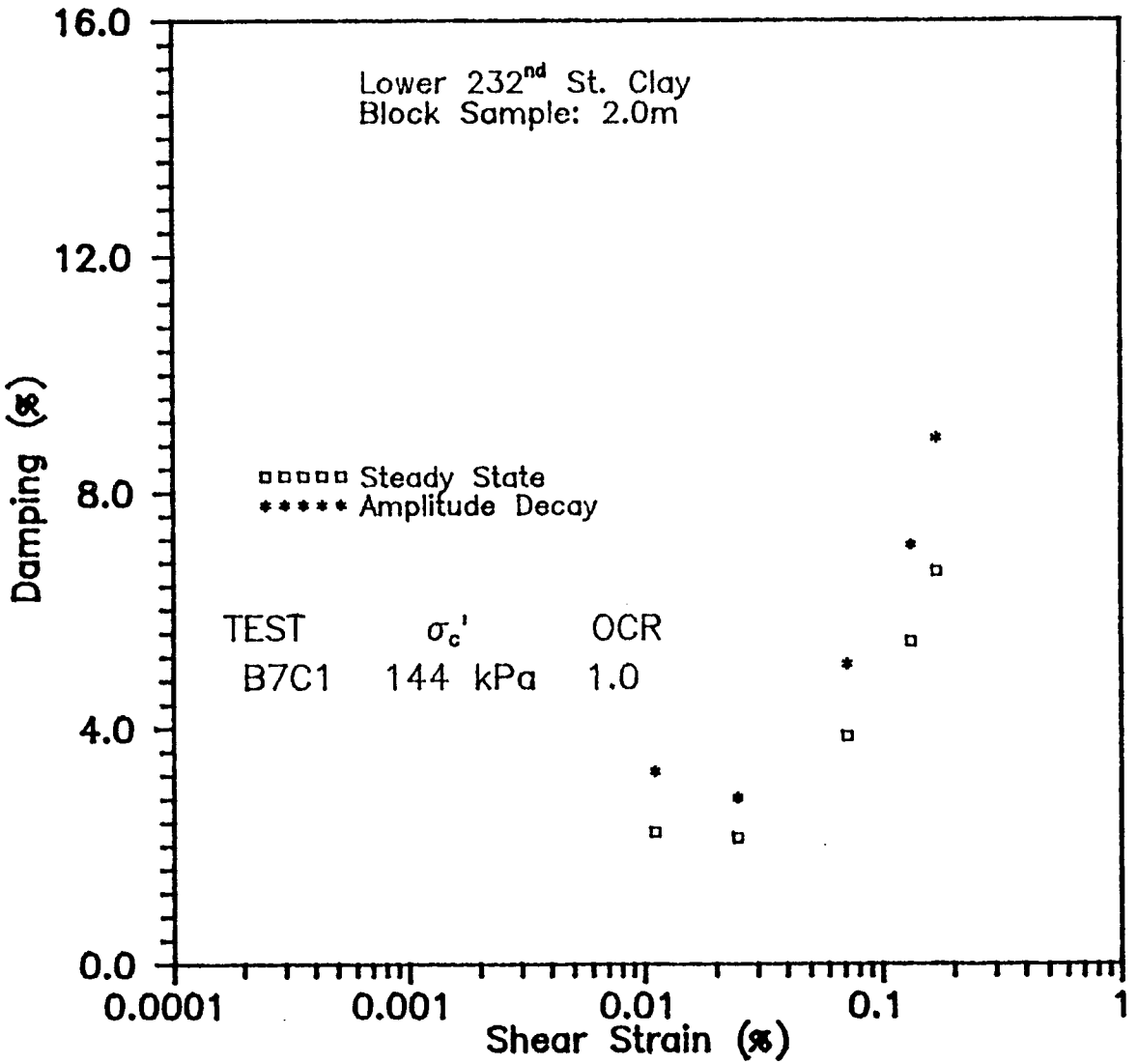
Lower 232nd St. Clay
Block Sample: 2.0m
Steady State
Amplitude Decay
TEST
σc'
OCR
B7C1
144 kPa
1.0
Damping (%)
16.0
12.0
8.0
4.0
0.0
0.0001
0.001
0.01
0.1
1
Shear Strain (%)

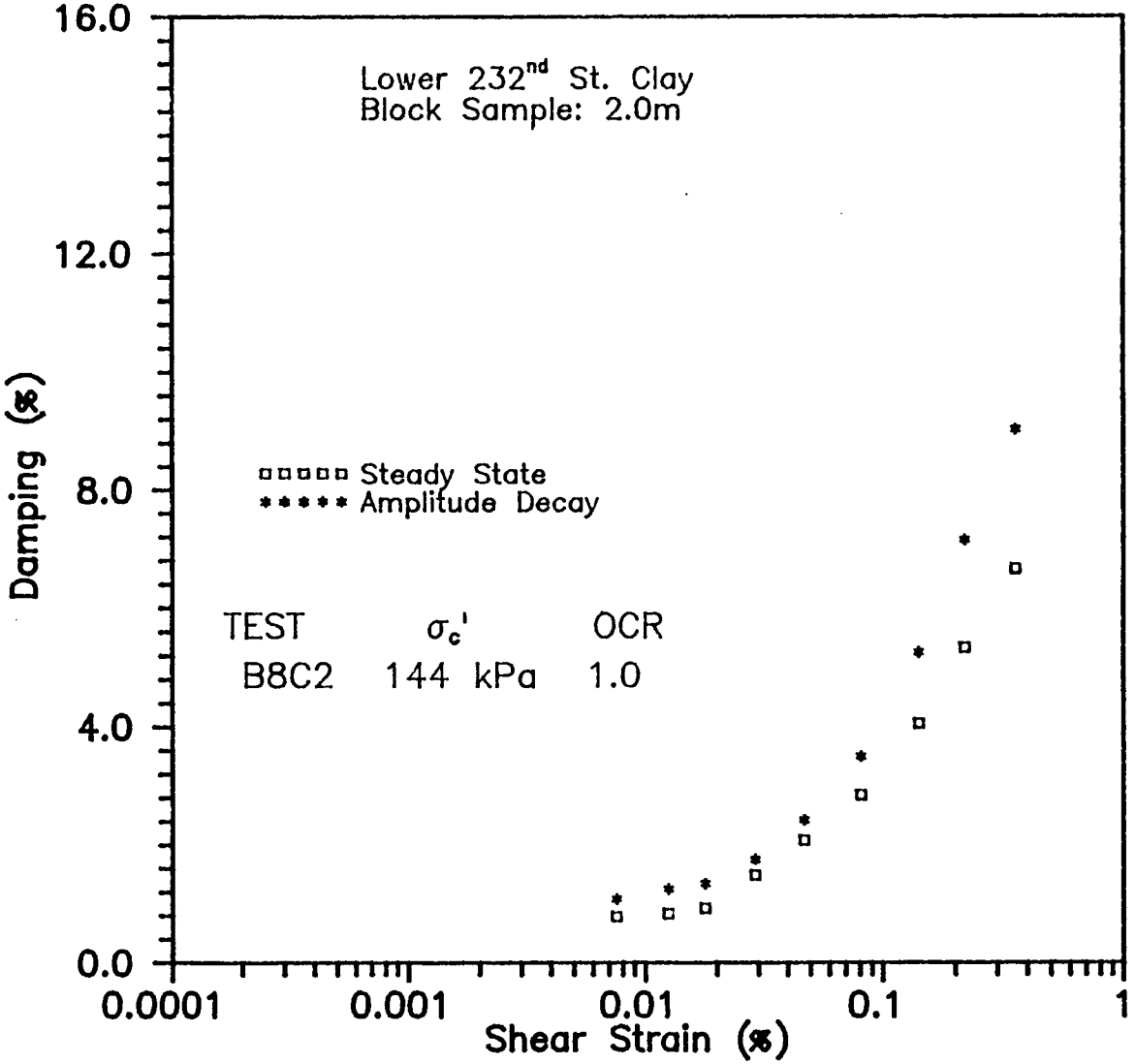
Lower 232nd St. Clay
Block Sample: 2.0m
Steady State
Amplitude Decay
TEST σc' OCR
B8C2 144 kPa 1.0
Damping (%)
Shear Strain (%)
16.0
12.0
8.0
4.0
0.0
0.0001
0.001
0.01
0.1
1

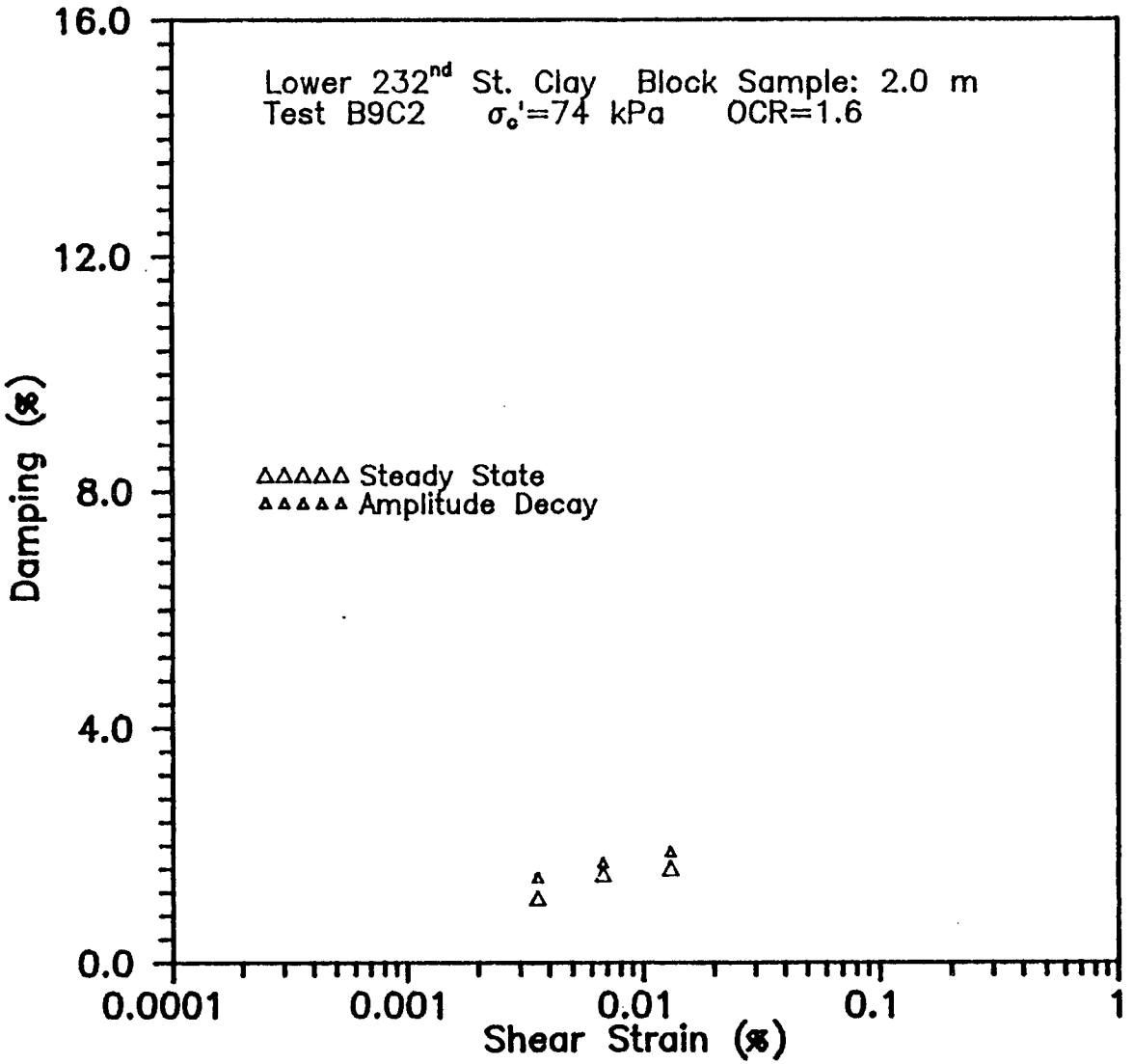
Lower 232nd St. Clay Block Sample: 2.0 m
Test B9C2 σc'=74 kPa OCR=1.6
ΔΔΔΔΔ Steady State
ΔΔΔΔΔ Amplitude Decay
16.0
12.0
8.0
4.0
0.0
Damping (%)
0.0001
0.001
0.01
0.1
1
Shear Strain (%)

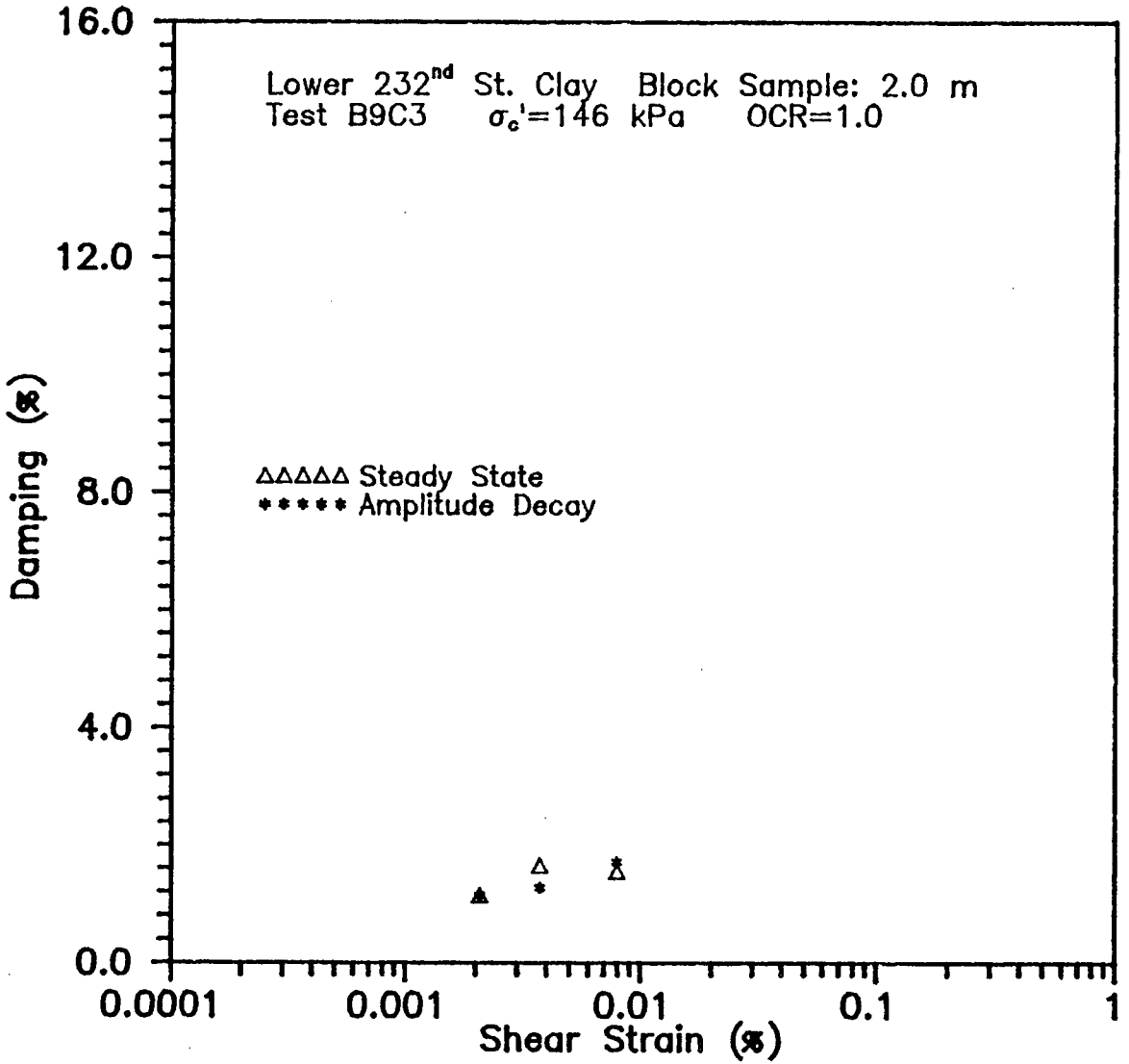
Lower 232nd St. Clay Block Sample: 2.0 m
Test B9C3 σc'=146 kPa OCR=1.0
ΔΔΔΔΔ Steady State
***** Amplitude Decay
Damping (%)
16.0
12.0
8.0
4.0
0.0
0.0001
0.001
0.01
0.1
1
Shear Strain (%)

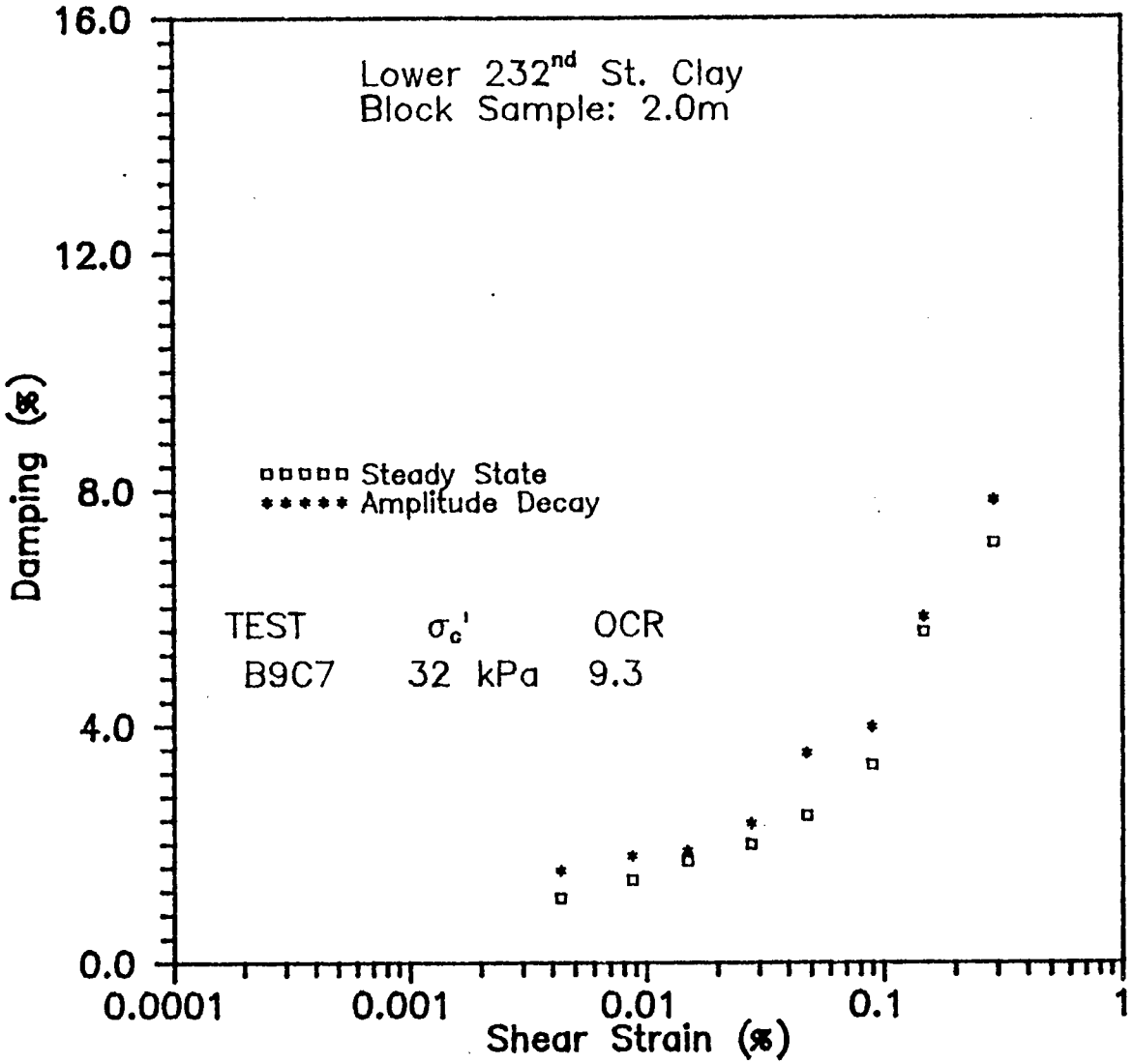
Lower 232nd St. Clay
Block Sample: 2.0m
Steady State
Amplitude Decay
TEST
B9C7
σc'
32 kPa
OCR
9.3
16.0
12.0
8.0
4.0
0.0
Damping (%)
0.0001
0.001
0.01
0.1
1
Shear Strain (%)

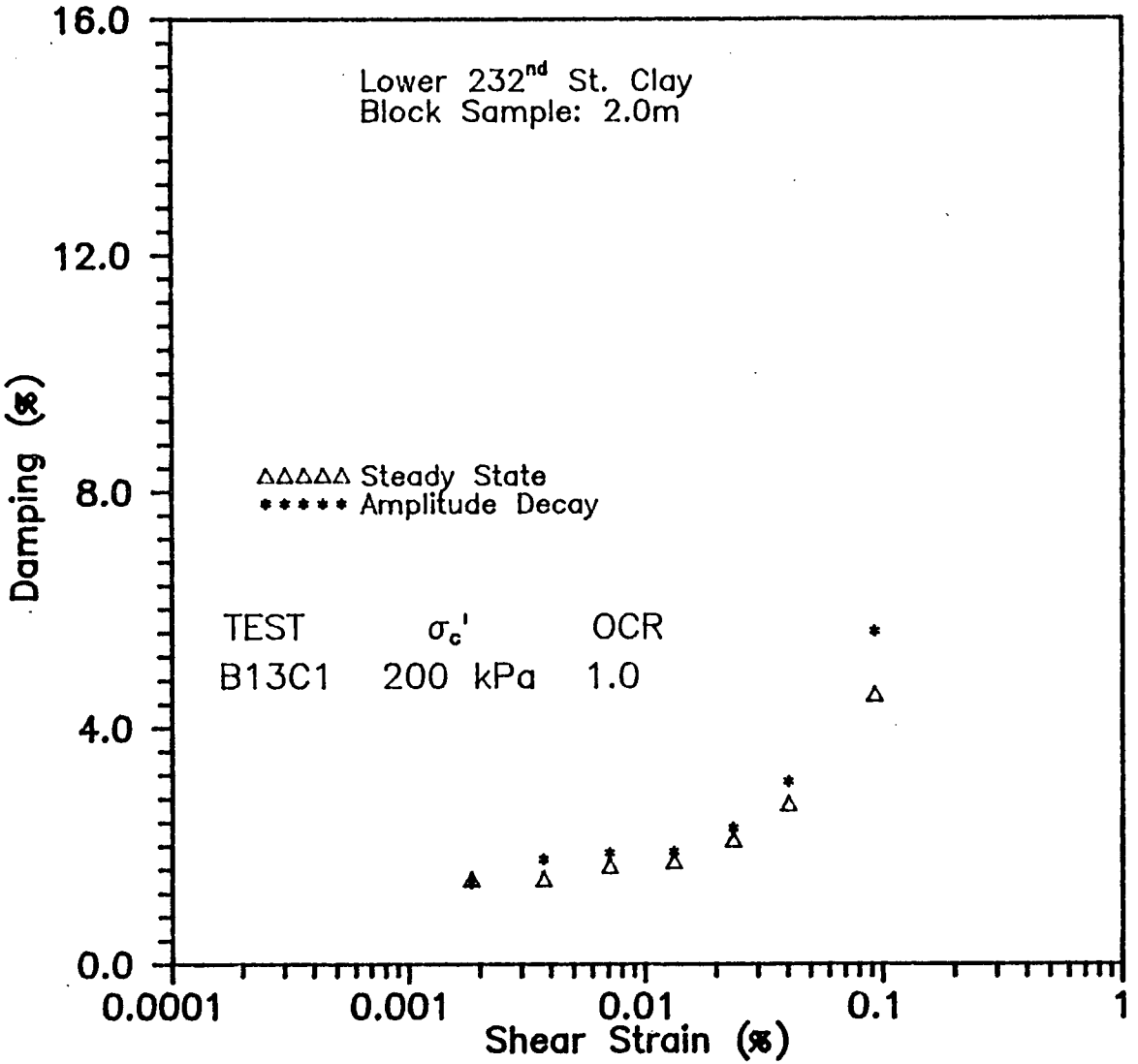
Lower 232nd St. Clay
Block Sample: 2.0m
ΔΔΔΔΔ Steady State
***** Amplitude Decay
TEST σc' OCR
B13C1 200 kPa 1.0
Damping (%)
16.0
12.0
8.0
4.0
0.0
0.0001
0.001
0.01
0.1
1
Shear Strain (%)

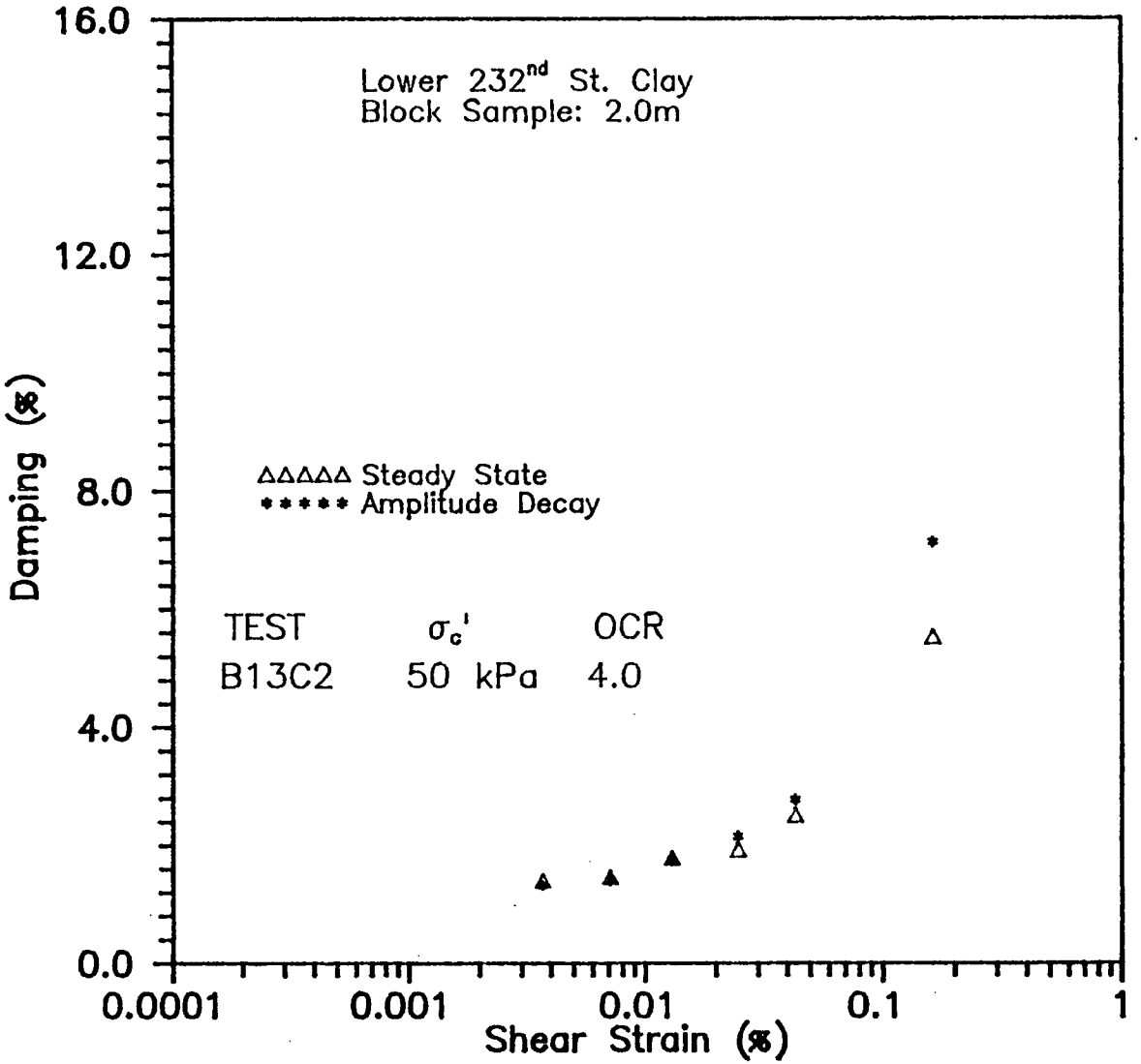
Lower 232nd St. Clay
Block Sample: 2.0m
ΔΔΔΔΔ Steady State
***** Amplitude Decay
TEST σc' OCR
B13C2 50 kPa 4.0
Damping (%)
16.0
12.0
8.0
4.0
0.0
0.0001
0.001
0.01
0.1
1
Shear Strain (%)

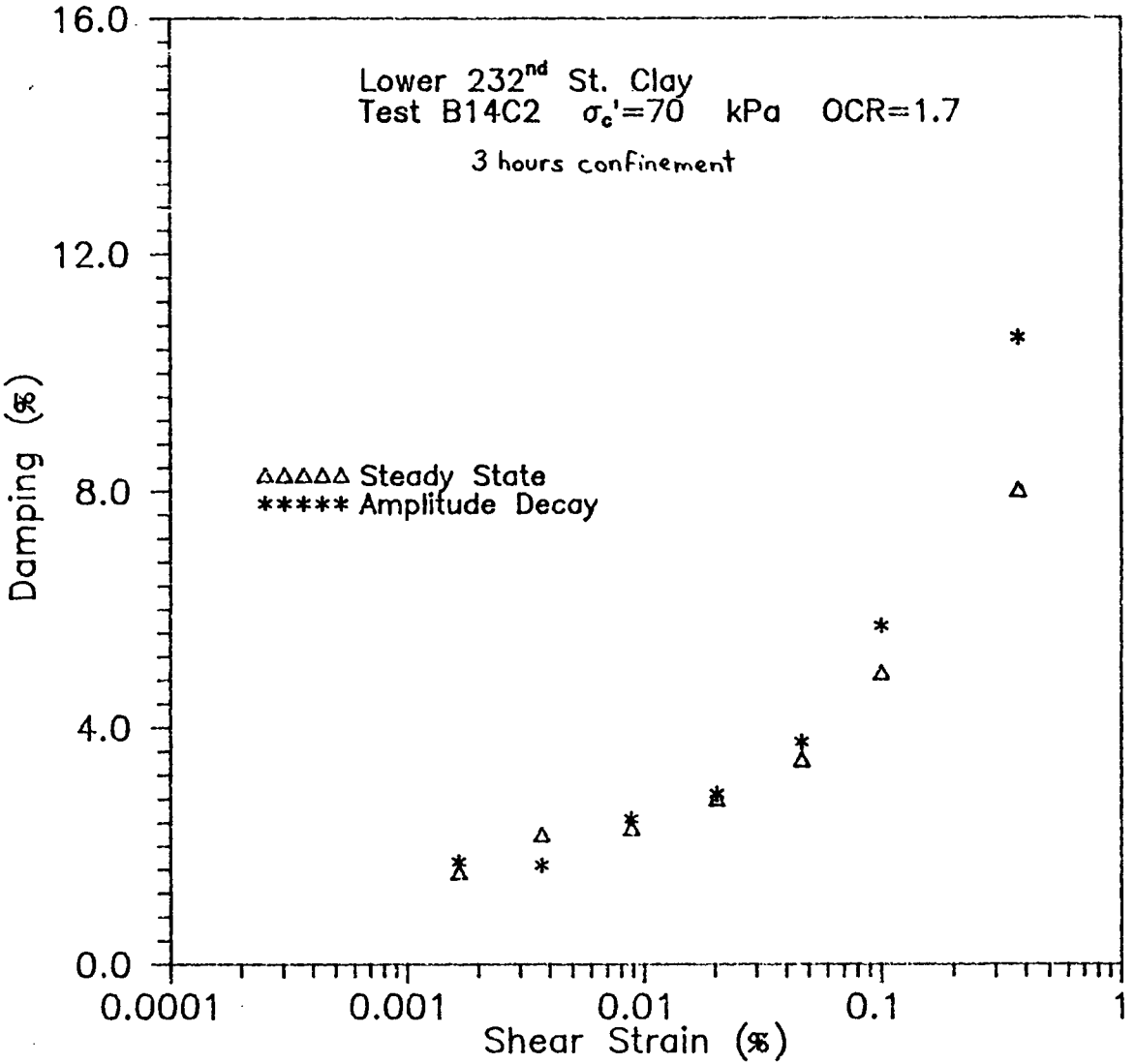
Lower 232nd St. Clay
Test B14C2 σc'=70 kPa OCR=1.7
3 hours confinement
ΔΔΔΔΔ Steady State
***** Amplitude Decay
Damping (%)
Shear Strain (%)
16.0
12.0
8.0
4.0
0.0
0.0001
0.001
0.01
0.1
1

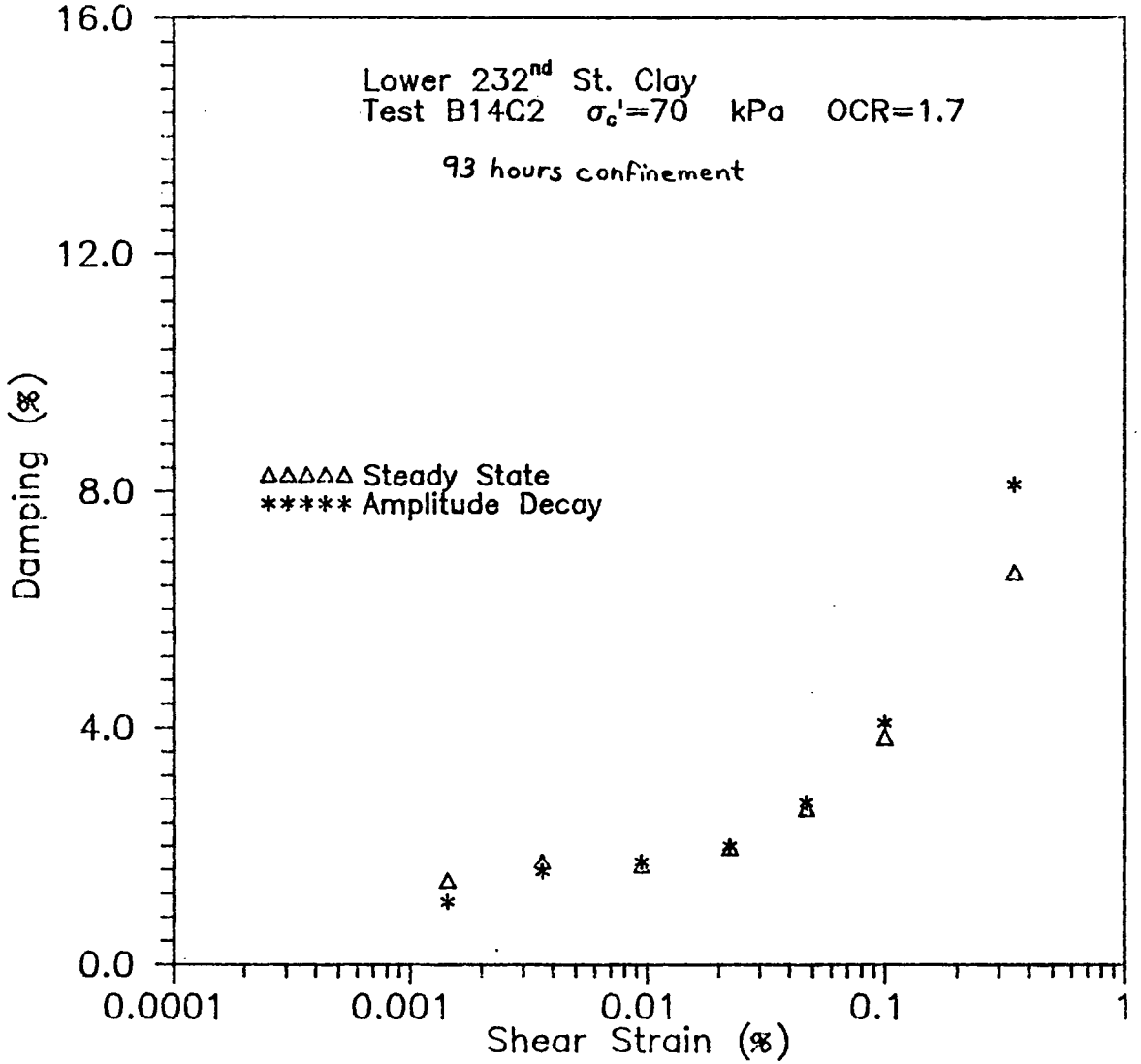
Lower 232nd St. Clay
Test B14C2 σc'=70 kPa OCR=1.7
93 hours confinement
ΔΔΔΔΔ Steady State
***** Amplitude Decay
Damping (%)
16.0
12.0
8.0
4.0
0.0
0.0001
0.001
0.01
0.1
1
Shear Strain (%)

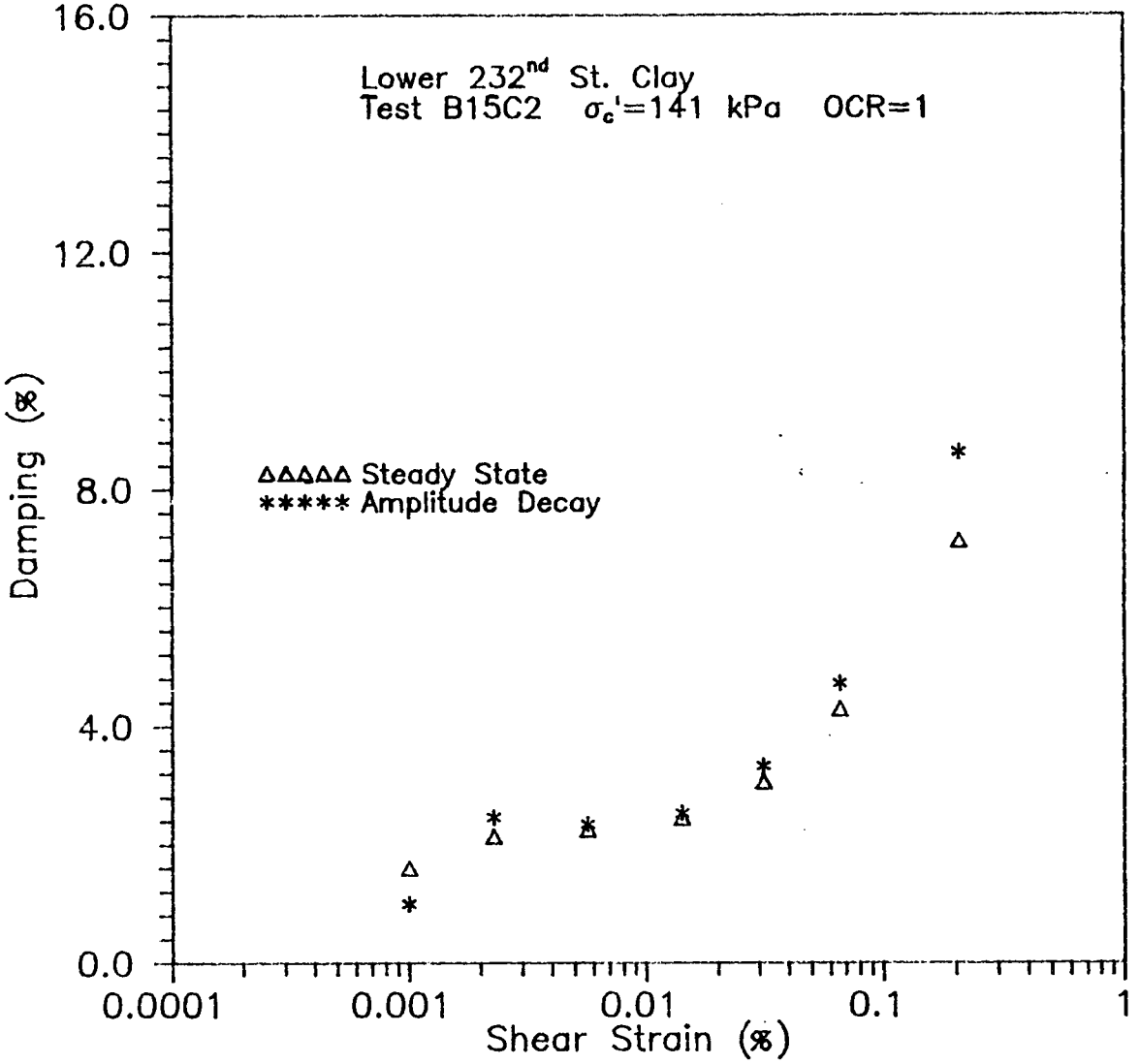
Lower 232nd St. Clay
Test B15C2 σc'=141 kPa OCR=1
ΔΔΔΔΔ Steady State
***** Amplitude Decay
Damping (%)
16.0
12.0
8.0
4.0
0.0
0.0001
0.001
0.01
0.1
1
Shear Strain (%)

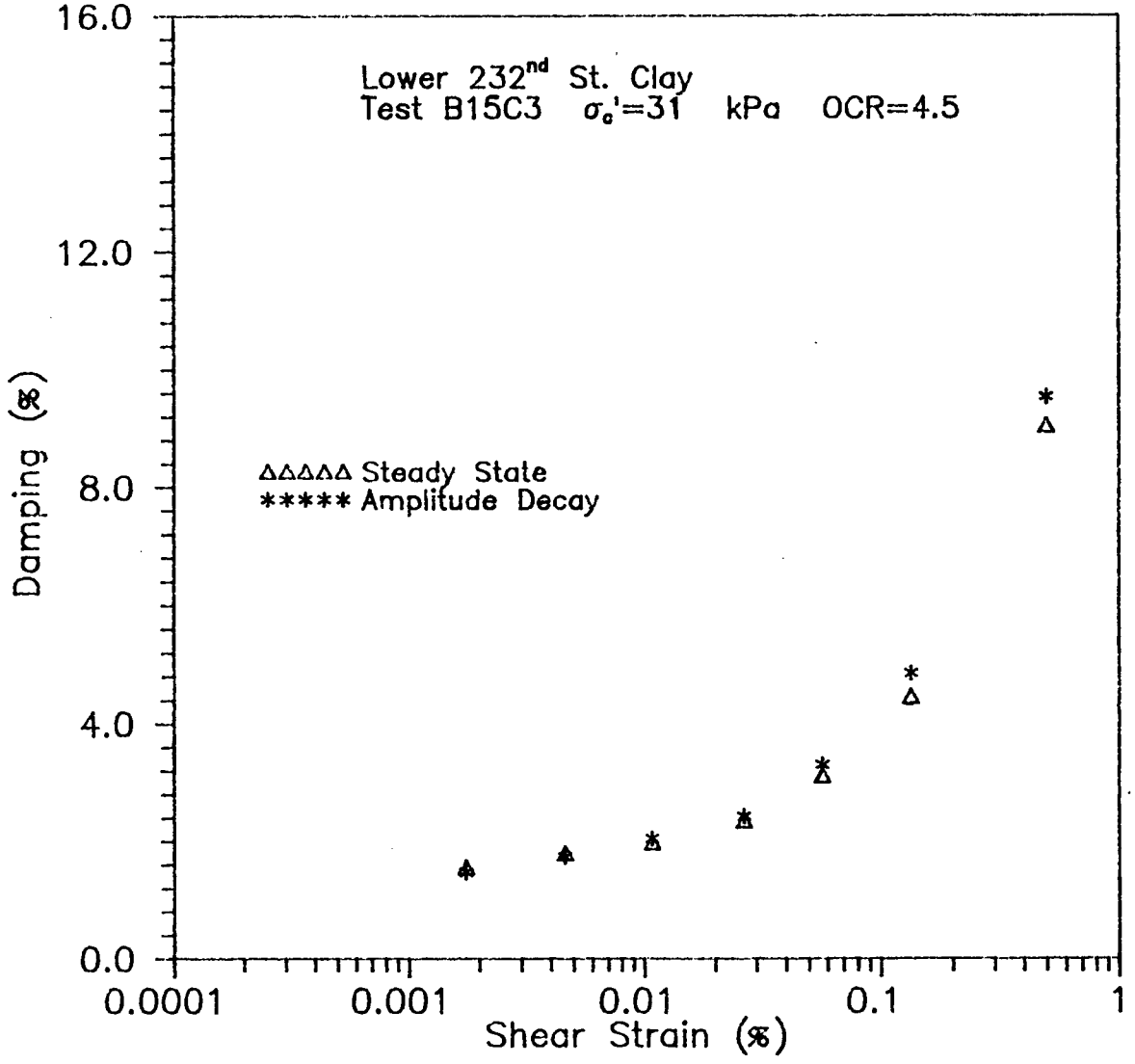
Lower 232nd St. Clay
Test B15C3 σc'=31 kPa OCR=4.5
ΔΔΔΔΔ Steady State
***** Amplitude Decay
Damping (%)
16.0
12.0
8.0
4.0
0.0
0.0001
0.001
0.01
0.1
1
Shear Strain (%)

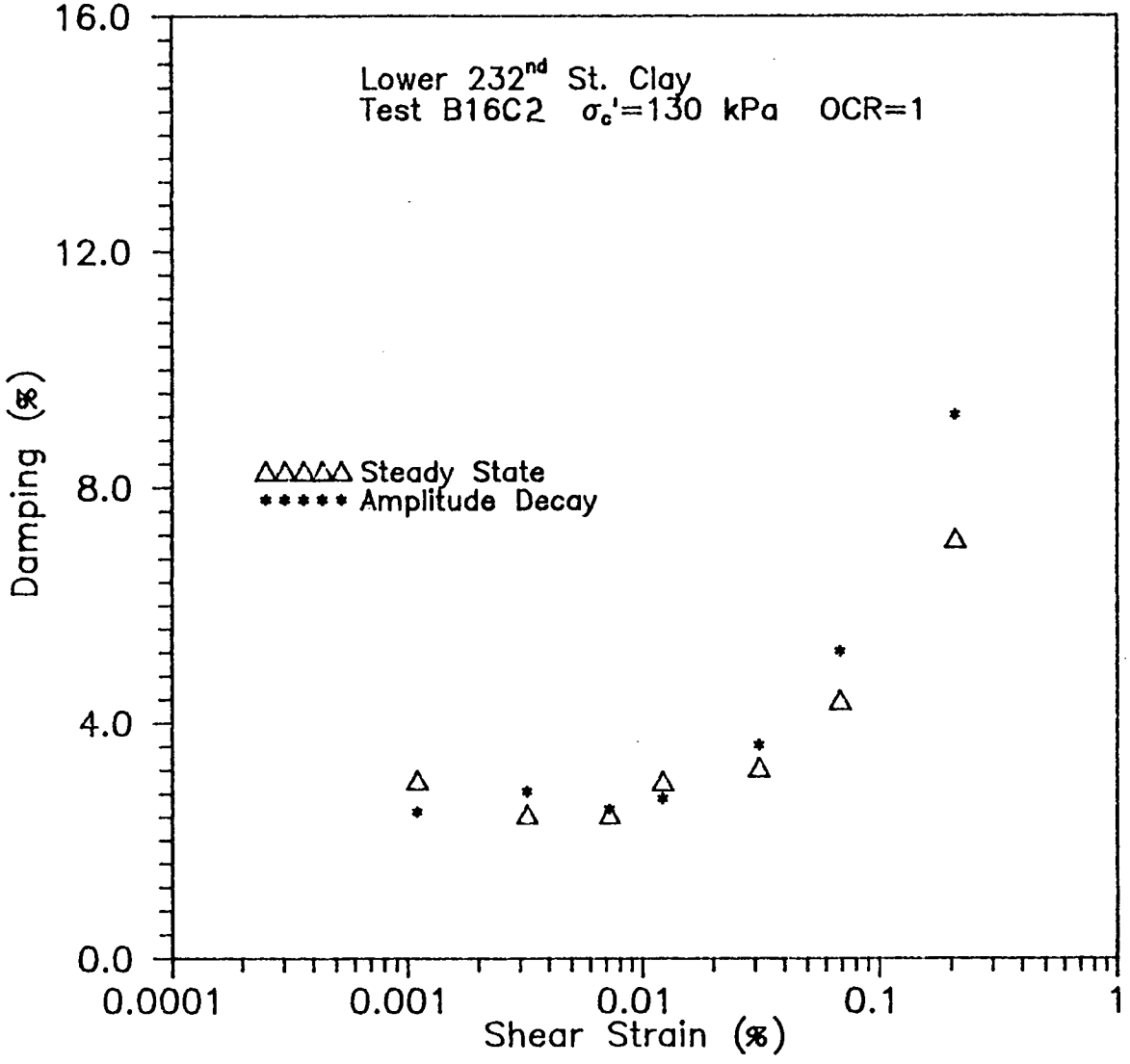
Lower 232nd St. Clay
Test B16C2 σc'=130 kPa OCR=1
Steady State
Amplitude Decay
Damping (%)
Shear Strain (%)
16.0
12.0
8.0
4.0
0.0
0.0001
0.001
0.01
0.1
1

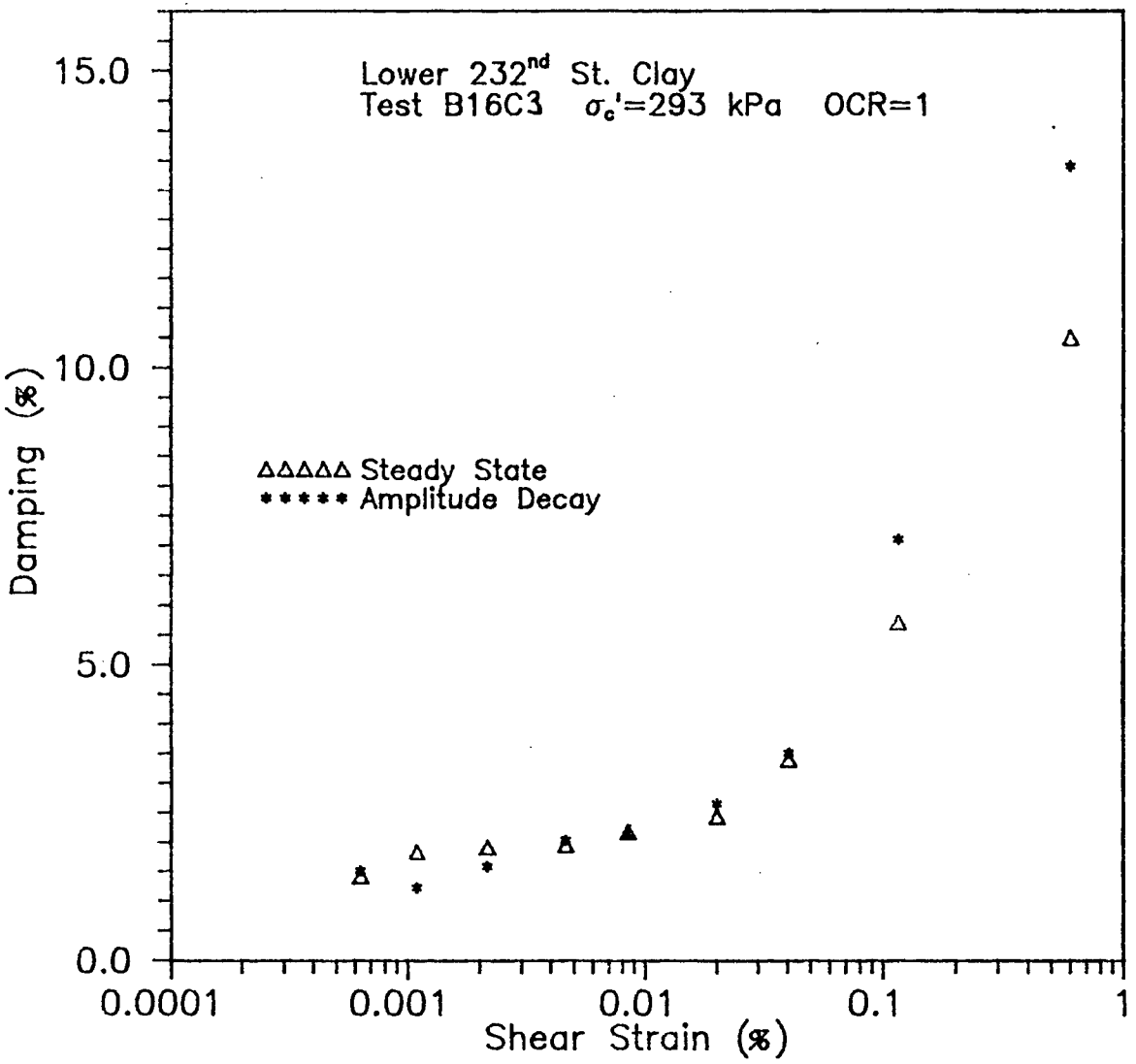
Lower 232nd St. Clay
Test B16C3 σc'=293 kPa OCR=1
ΔΔΔΔΔ Steady State
***** Amplitude Decay
Damping (%)
15.0
10.0
5.0
0.0
0.0001
0.001
0.01
0.1
1
Shear Strain (%)

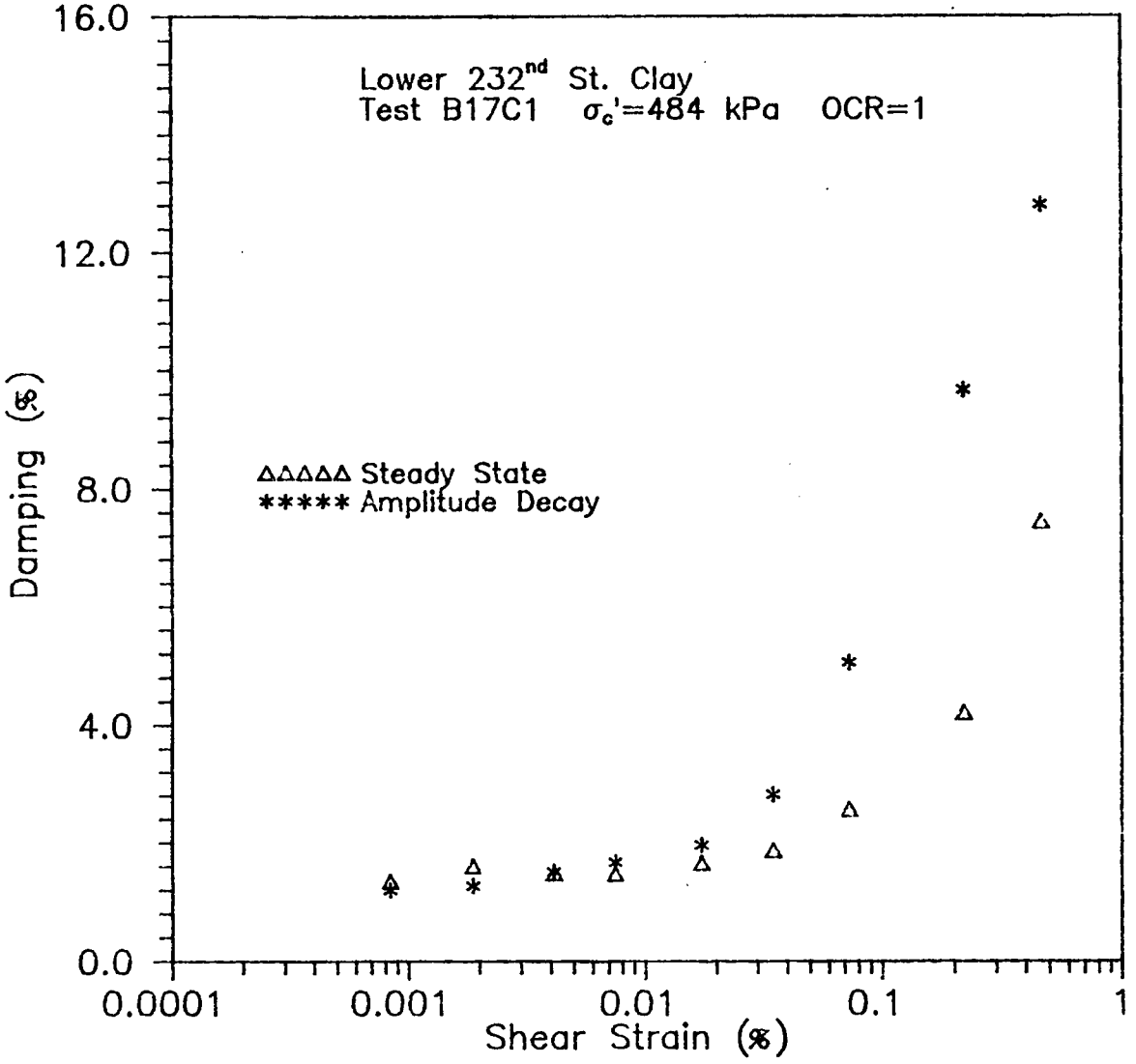
Lower 232nd St. Clay
Test B17C1 σc'=484 kPa OCR=1
ΔΔΔΔΔ Steady State
***** Amplitude Decay
Damping (%)
16.0
12.0
8.0
4.0
0.0
0.0001
0.001
0.01
0.1
1
Shear Strain (%)

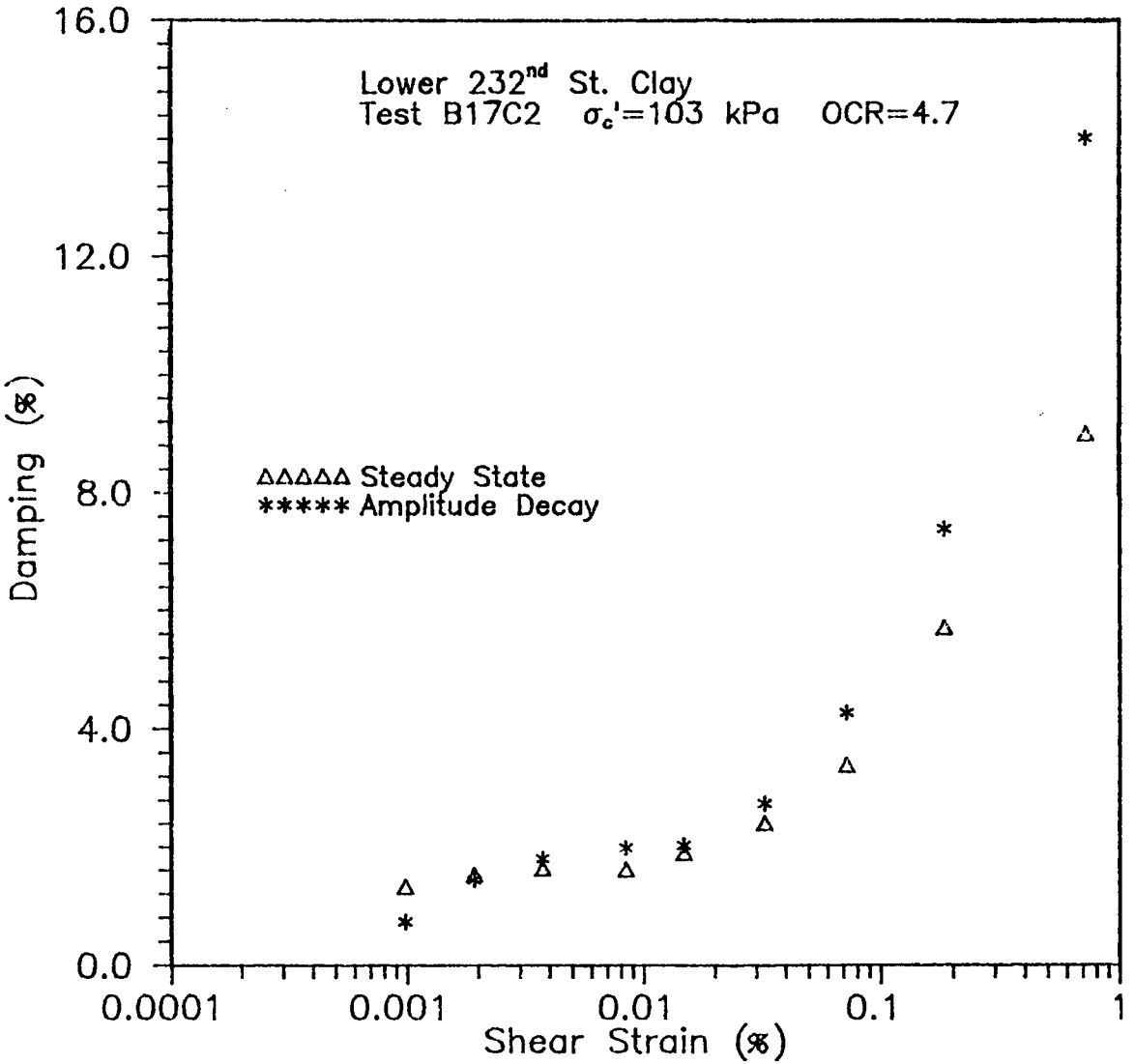
Lower 232nd St. Clay
Test B17C2 σc'=103 kPa OCR=4.7
ΔΔΔΔΔ Steady State
***** Amplitude Decay
Damping (%)
16.0
12.0
8.0
4.0
0.0
0.0001
0.001
0.01
0.1
1
Shear Strain (%)

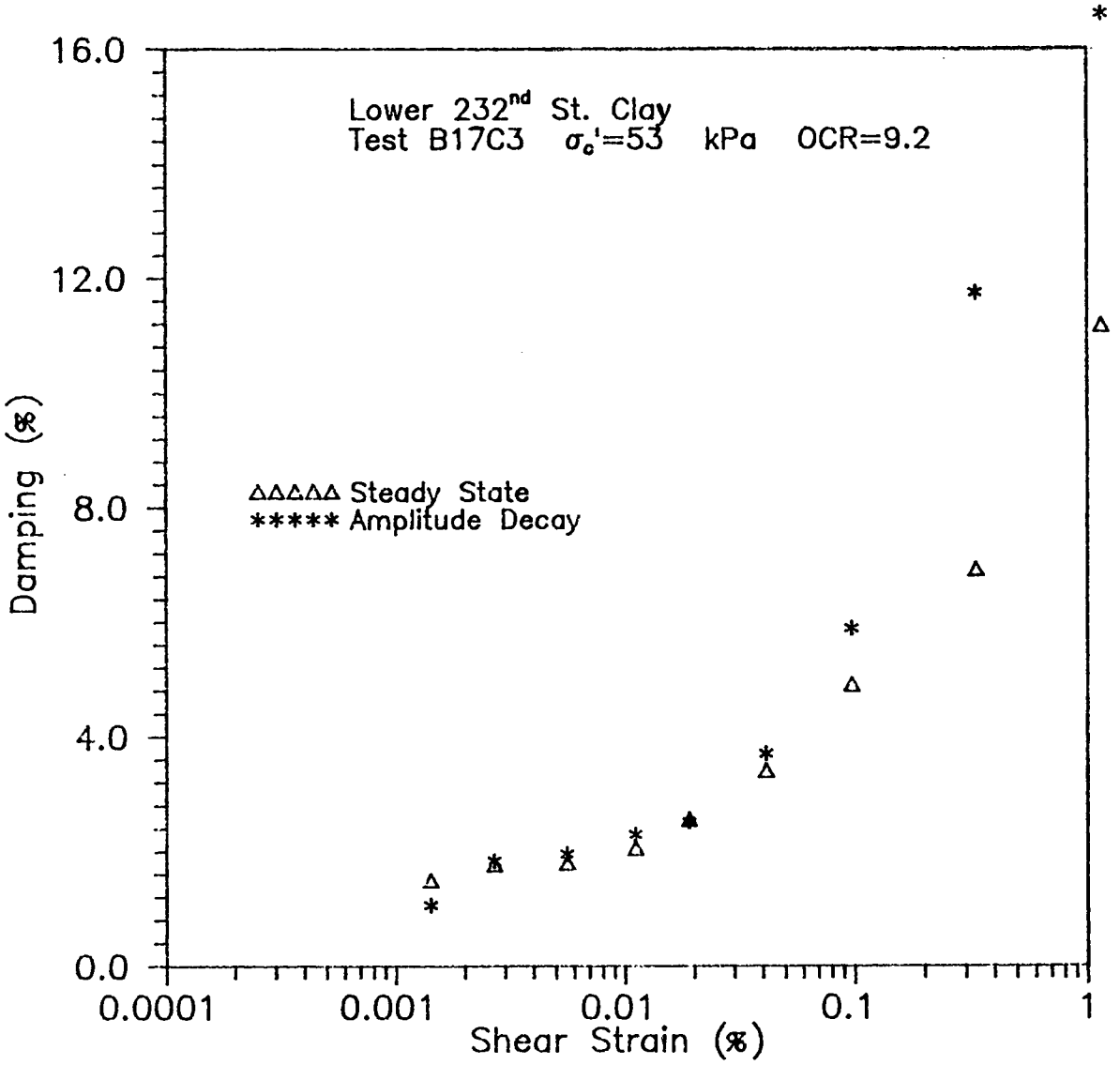
Lower 232nd St. Clay
Test B17C3 σc'=53 kPa OCR=9.2
ΔΔΔΔΔ Steady State
***** Amplitude Decay
Damping (%)
16.0
12.0
8.0
4.0
0.0
0.0001
0.001
0.01
0.1
1
Shear Strain (%)

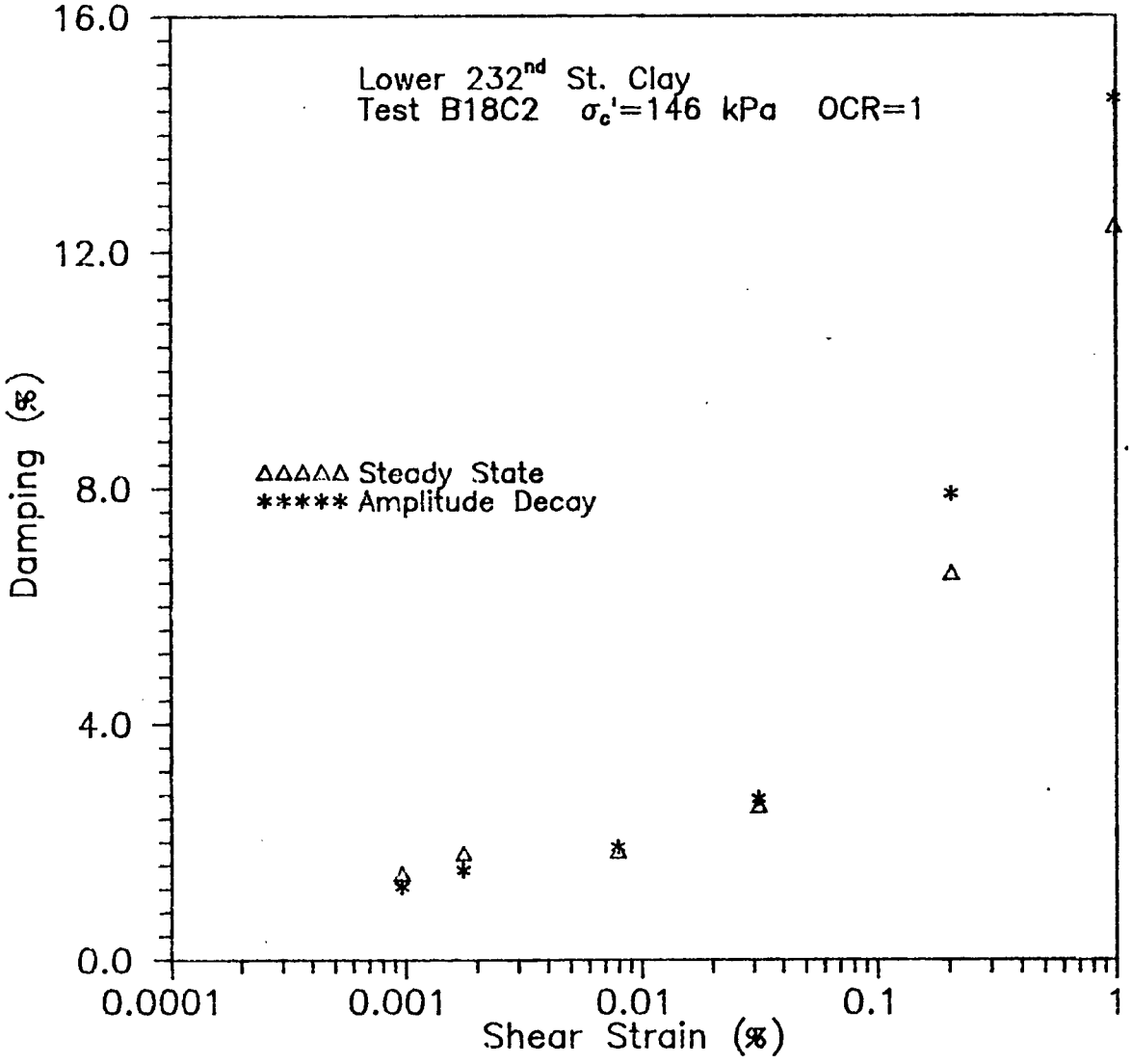
Lower 232nd St. Clay
Test B18C2 σc'=146 kPa OCR=1
ΔΔΔΔΔ Steady State
***** Amplitude Decay
Damping (%)
16.0
12.0
8.0
4.0
0.0
0.0001
0.001
0.01
0.1
1
Shear Strain (%)

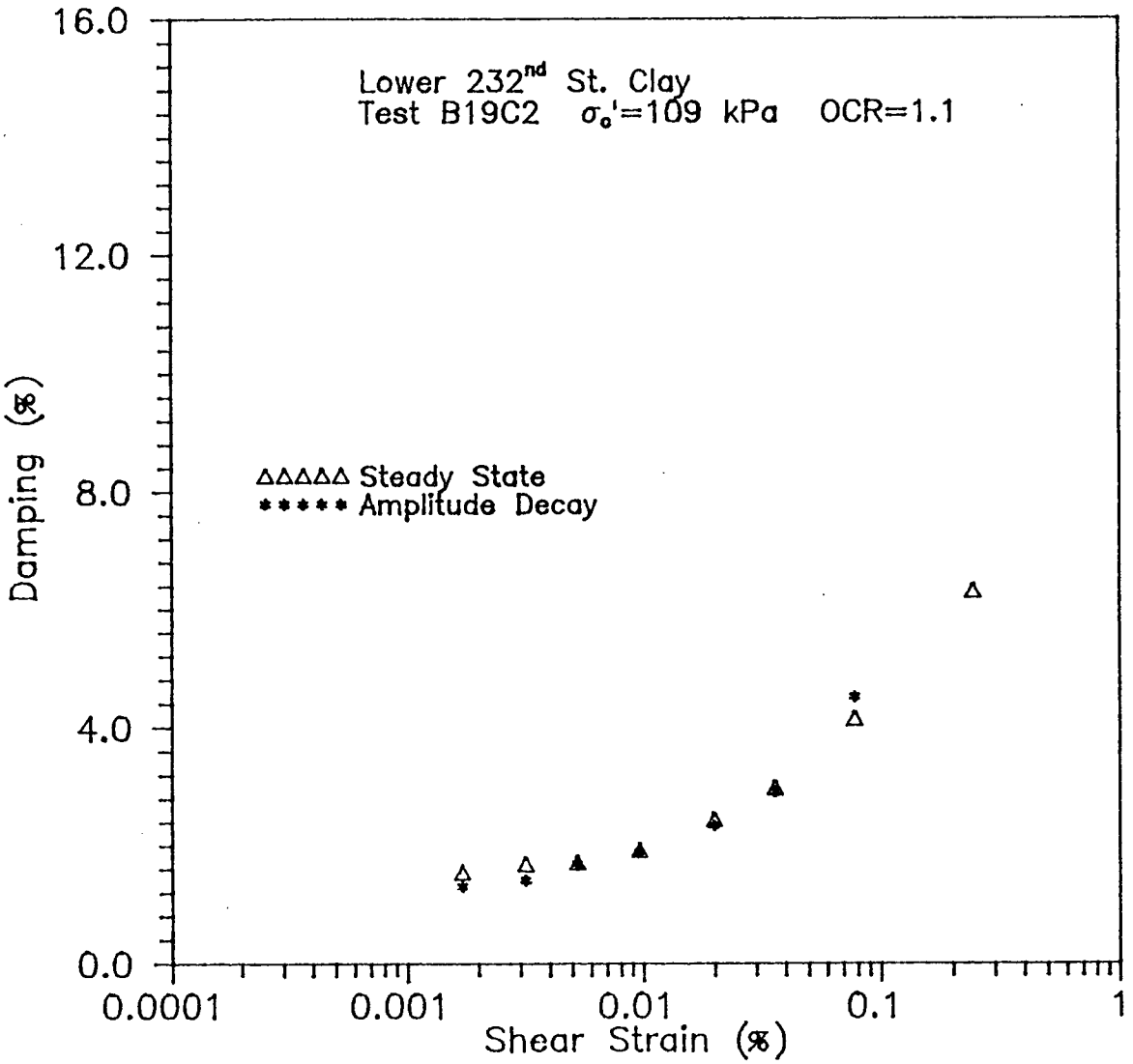
Lower 232nd St. Clay
Test B19C2 σo'=109 kPa OCR=1.1
ΔΔΔΔΔ Steady State
***** Amplitude Decay
Damping (%)
16.0
12.0
8.0
4.0
0.0
0.0001
0.001
0.01
0.1
1
Shear Strain (%)

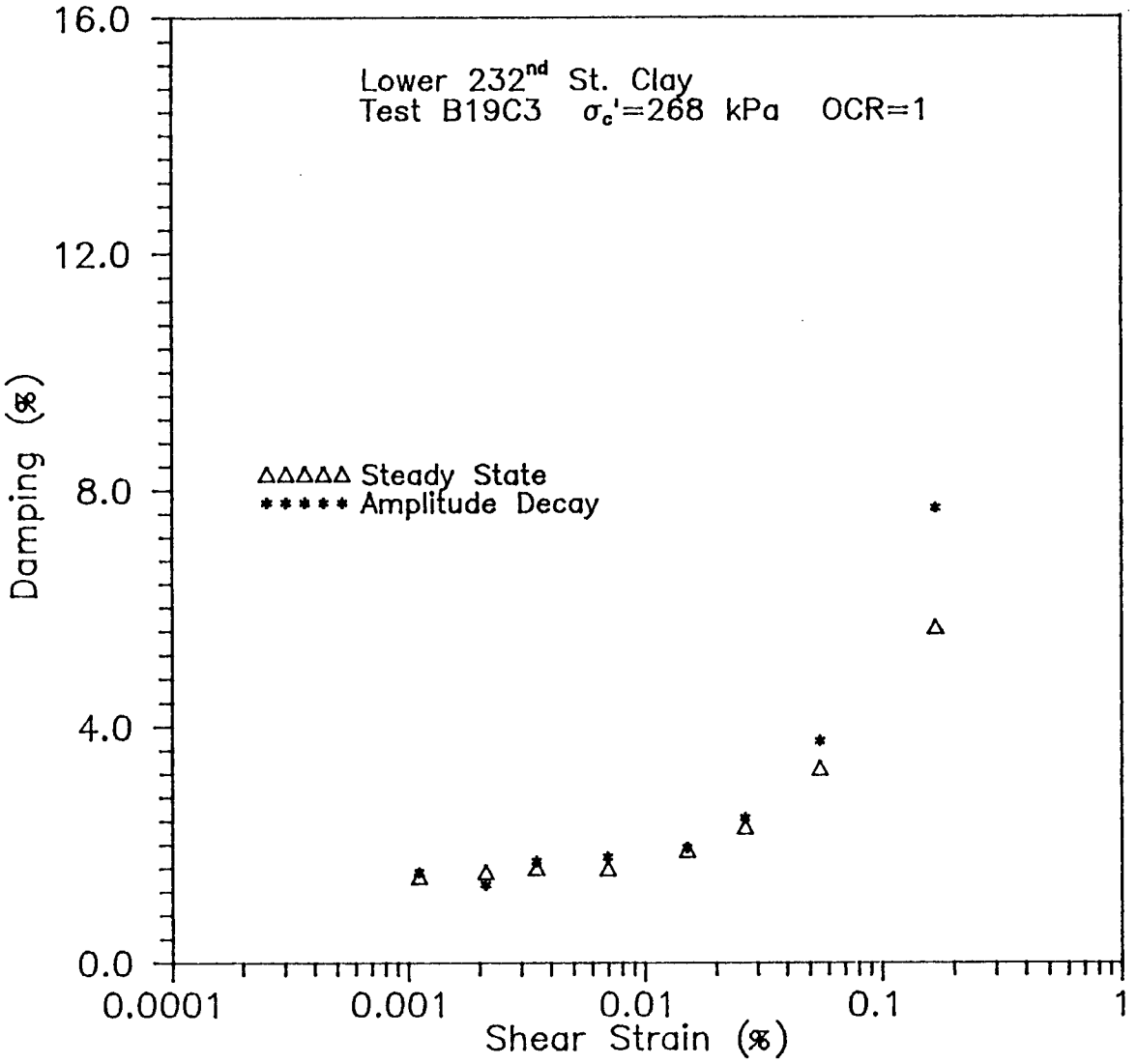
Lower 232nd St. Clay
Test B19C3 σc'=268 kPa OCR=1
ΔΔΔΔΔ Steady State
***** Amplitude Decay
Damping (%)
16.0
12.0
8.0
4.0
0.0
0.0001
0.001
0.01
0.1
1
Shear Strain (%)

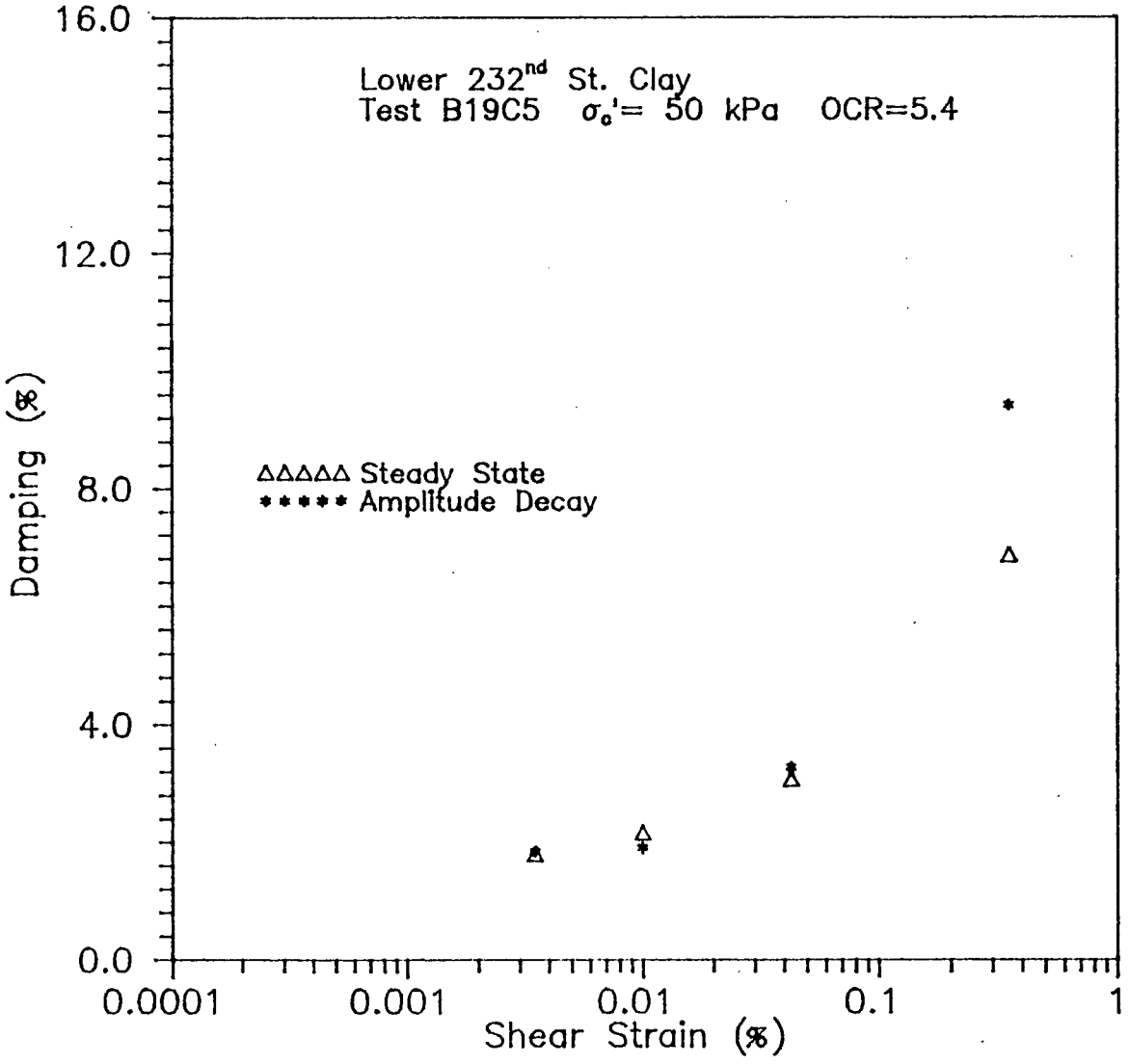
Lower 232nd St. Clay
Test B19C5 σc'= 50 kPa OCR=5.4
ΔΔΔΔΔ Steady State
***** Amplitude Decay
Damping (%)
16.0
12.0
8.0
4.0
0.0
0.0001
0.001
0.01
0.1
1
Shear Strain (%)